

DEVELOPMENT AND BIOLOGICAL INVESTIGATION OF
NOVEL [DIARYLSALENE]- AND
[SALOPHENE]PLATINUM(II) COMPLEXES WITH
TUMOUR INHIBITING PROPERTIES

Dissertation zur Erlangung des akademisches Grades
des Doktors der Naturwissenschaften (Dr. rer. nat.)

eingereicht im Fachbereich Biologie, Chemie, Pharmazie,
der Freien Universität Berlin

verlegt von
MARIA TERESITA PROETTO
aus San Carlos de Bariloche
2011

Die vorliegende Arbeit wurde von Juni 2008 bis September 2011 unter der Leitung von Prof. Dr. Ronald Gust (Institut für Pharmazie, Freie Universität Berlin) angefertigt.

1. Gutachter: Prof. Dr. Ronald Gust

2. Gutachter: Prof. Dr. Gerhard Wolber

Disputation am 27.01.2012

Dedicated to my parents, Teresita Neumann and César Proetto,
and to the memory of Guillermo Neumann

Acknowledgement

First of all, I would like to thank my supervisor Prof. Dr. Ronald Gust for giving me the invaluable opportunity to start a Ph.D., for his guidance and for trusting in my potential during all these years.

I would like to show my gratitude to Frau Veronique vom Bauer, for helping me with many different issues always in a very kind way and wearing a smile.

I would also like to thank Dr. Adelheid Hagenbach for providing the crystal structures published in this thesis, Dr. Ruth Bieda for the DNA interaction studies and Prof. Dr. Christoph Schalley group for performing the mass spectrometry analyses.

I would especially like to thank Dr. Anja Schäfer, Prof. Dr. César Proetto and Dr. Jean-Philippe Monserrat for their help and support during the writing of this dissertation.

I am truly indebted and thankful to all my colleagues, for providing me a nice work environment during the past years. In particular I would like to thank Andrey Molchanov, Elena Mazzanti, Ewelina Fogelström, Magnus Krüger, Murat Üstünel, Sandra Alscher, Sandra Meieranz, Silke Bergemann and Thomas Rudolf. Wukun Liu deserves special thanks for helping me with my research and for being such a good friend.

This thesis would not have been possible without the support and encouragement of all my people in Argentina. Although they were physically more than 11.000 km far from Berlin, they were always at my side, through the good, not so good and the winter times.

Finally, I want to thank my mother, father and brother for their patience and unconditional presence.

Table of Contents

Abbreviations	1
Introduction and aims of the project	3
1 Introduction	4
1.1 Cancer	4
1.2 Metal complexes in medicine	7
1.2.1 Platinum complexes as anticancer agents	10
1.2.2 Non-platinum metal complexes as antitumour drugs	16
1.2.2.1 Ruthenium-based compounds	16
1.2.2.2 Titanium and gallium compounds	18
2 Background and aims of the research project	20
Results and discussion	23
3 Synthesis	24
3.1 Overview of the synthesized compounds	24
3.2 Substituted [diarylsalene]platinum(II) complexes	25
3.3 Substituted [salophene]platinum(II) complexes	26
3.3.1 Complex with a different main structure	26
3.4 Overview on the synthetic route	27
3.5 Synthesis of the [diarylsalene]- and [salophene]platinum(II) complexes	28
3.5.1 Synthesis of substituted 1,2-diamino-1,2-diarylethane	28
3.5.1.1 Synthesis of <i>meso</i> -1,2-diamino-1,2-bis(2-hydroxyphenyl)ethane	28
3.5.1.2 Synthesis of <i>meso</i> -1,2-diamino-1,2-diarylethane	29
3.5.1.3 Synthesis of <i>d,l</i> -1,2-diamino-1,2-diarylethane	32
3.5.2 Synthesis of substituted phenylenediamine	33
3.5.2.1 Synthesis of 1,1,1-trimethylhydrazinium iodide	34
3.5.2.2 Synthesis of 2-fluoro-6-nitroaniline	34
3.5.2.3 Synthesis of 3-fluoro-1,2-phenylenediamine	36
3.5.3 Synthesis of the diarylsalene and the salophene ligands	36

3.5.4	Synthesis of the [diarylsalene]- and [salophene]platinum(II) complexes	37
4	Spectrometric Analysis	39
4.1	¹ H-NMR Spectroscopy	39
4.1.1	Diarylsalene and salophene ligands	39
4.1.2	[Diarylsalene]- and [salophene]platinum(II) complexes	45
4.2	Mass spectrometry	47
4.3	Atomic absorption spectroscopy	48
4.4	X-ray crystallographic studies	51
5	<i>In-vitro</i> chemosensitivity assay	57
5.1	Breast cancer cell lines	57
5.2	Crystal violet chemosensitivity assay	57
5.3	IC ₅₀ determination	59
5.3.1	Compared effect on MCF-7 and MDA-MB-231 breast cancer cells lines	60
5.3.2	[Diarylsalene]platinum(II) complexes	62
5.3.3	[Salophene]platinum(II) complexes	63
5.3.4	Conclusion on the results of the determination of IC ₅₀ values of [diarylsalene]- and [salophene]platinum(II) complexes	68
5.4	Time- and concentration-dependent cytotoxicity	69
6	Cellular accumulation	72
6.1	Cell entry mechanisms of platinum drugs	72
6.2	Cell uptake determination: method and conditions	74
6.3	Cellular accumulation of [salophene]- and [saldach]platinum(II) complexes after 6 and 24 h of drug exposure	75
6.4	Time-dependent cellular accumulation of [salophene]platinum(II) complexes	77
6.5	Efflux studies	80
6.6	Relationship between cellular accumulation and cytotoxicity	81
6.7	Conclusion on the accumulation studies	83
7	Analysis of physicochemical properties of the [salophene]platinum(II) complexes in relation to their biologic activities	84
7.1	Lipophilicity	84
7.1.1	Lipophilicity determination: procedure and results	85

7.1.2	Relationship between lipophilicity and biological properties	89
7.2	Aqueous solubility	90
7.2.1	Solubility determination: procedure and results	91
7.2.2	Relationship between solubility and biological properties	92
7.3	Conclusion on the solubility and lipophilicity results.....	93
8	DNA interaction studies of the [salophene]platinum(II) complexes	96
8.1	DNA binding modes for metal complexes	96
8.2	Interaction of the platinum(II) complexes with isolated DNA	98
8.2.1	Circular dichroism studies	98
8.2.2	Thermal denaturation studies	99
8.2.3	Viscosity measurements.....	101
8.2.4	Atomic absorption studies	102
8.3	Conclusion on the results of the interaction of the analyzed [salophene]platinum(II) complexes with isolated DNA	104
	Conclusions.....	107
9	Conclusions and outlook.....	108
	Experimental part	113
10	Materials	114
10.1	Instrumentation	114
10.2	Reactants and solutions.....	115
11	Methods	116
11.1	Structural analysis and synthesis	116
11.1.1	General considerations.....	116
11.1.2	Synthetic procedures and analytical data	116
11.1.2.1	Synthesis of <i>meso</i> - and <i>d,l</i> -3,4-bis(4-fluorophenyl)-1,6-bis(2- hydroxyphenyl)-2,5-diazahexa-1,5-diene	116
11.1.2.2	General procedure for the synthesis of <i>meso</i> - and <i>d,l</i> -3,4-diaryl-1,6- bis(2-hydroxyphenyl)-2,5-diazahexa-1,5-diene derivatives	119
11.1.2.3	Synthesis of 3'-fluoro-1,2-phenylenediamine	122
11.1.2.4	General procedure for the synthesis of <i>N,N'</i> -bis(salicylidene)-1,2- phenylenediamine and derivatives.....	123

11.1.2.5	General procedure for the synthesis of the [diarylsalene]- and [salophene]platinum(II) complexes	128
11.2	GF-AAS method	141
11.3	Cell culture tests.....	142
11.3.1	Cell lines and growth conditions	142
11.3.2	<i>In-vitro</i> chemosensitivity assays	142
11.3.3	Accumulation studies on MCF-7 cells	145
11.3.4	Drug efflux studies	148
11.4	DNA binding studies	148
11.4.1	Circular dichroism spectroscopy	148
11.4.2	Thermal denaturation studies	148
11.4.3	Viscosity measurements.....	148
11.4.4	Atomic absorption studies	149
11.5	HPLC-Lipophilicity	149
11.6	Solubility	150
Appendix.....		151
A.	Time- and concentration-dependent cytotoxicity diagrams.....	152
B.	Time-dependent cellular accumulation diagrams	156
C.	Efflux diagrams	159
D.	Summary	160
E.	Zusammenfassung	162
F.	Curriculum Vitae	164
References.....		166

Abbreviations

¹H-NMR	Hydrogen nuclear magnetic resonance
AAS	Atomic absorption spectroscopy
abs.	absolute
A_x	Absorbance at x nm
calc.	calculated
CD	Circular dichroism
c_{int}	Intracellular molar drug concentration
CT-DNA	Calf thymus DNA
d	doublet
dd	double doublet
DMF(<i>d</i>₇)	<i>N,N</i> -Dimethylformamide (Heptadeutero)
DMSO(<i>d</i>₆)	Dimethylsulfoxide (Hexadeutero)
DNA	Deoxyribonucleic acid
Eq.	Equation
ER	Estrogen receptor
ESI	Electrospray-Ionization
EtBr	Ethidium bromide
EtOH	Ethanol
FCS	Fetal calf serum
Fig.	Figure
GF	Graphite furnace
h	hour(s)
H-bond	Hydrogen-bond
HPLC	High-performance liquid chromatography
HSA	Human serum albumin
i.v.	intravenous
IC₅₀	Half maximal inhibitory concentration
J	Coupling constants
m	multiplet
m/z	Mass-to-charge ratio
min	minute(s)
MS	Mass spectrometry
obs.	observed

Abbreviations

PBS	Phosphate buffered saline
RAHBs	Resonance Assisted Hydrogen Bonds
s	singlet
t	triplet
<i>t</i>-BuOK	Potassium tertbutoxide
T_m	Melting temperature
TMS	Tetramethylsilane
TOF	Time of flight
UV	Ultraviolet
δ	Chemical shift
η	DNA viscosity

Introduction and aims of the project

1 Introduction

1.1 Cancer

Cancer, as defined by the World Health Organization (WHO), is a generic term used for a large group of diseases, in which one defining factor is the rapid creation of abnormal cells that grow beyond their usual boundaries. They can then invade adjoining parts of the body and spread to other organs¹.

The global burden of cancer has more than doubled during the past 30 years, and in 2008 alone it accounted for approximately 7.6 million deaths worldwide (around 13% of all deaths)². Due to the continued growth and ageing of the world's population, rates are projected to exceed 17 million cancer deaths by 2030³. The magnitude of the most common cancers in terms of incidence and mortality differs between the more developed (Europe, North America, Australia/New Zealand and Japan) and the less developed countries of the world. While in men prostate cancer is the most common form of cancer diagnosed in the more developed regions, lung cancer ranks first in the less developed countries. Among women, breast cancer is by far the most frequent cancer worldwide, with an estimated 26.5% and 18.8% of the total new cases diagnosed in the more and less developed regions, respectively³.

The specific treatment of a cancer depends on the type of cancer, its location and stage, as well as the general state of the patient health. The major existing therapeutic options include surgery, radiotherapy and chemotherapy. The spread of the tumour to other parts of the body (metastasis) often limits the effectiveness of treatments such as surgical excision or local ablation by radiotherapy, and defines the need for a systemic drug based approach to cancer treatment.

Antineoplastic drug treatments generally work by targeting and damaging rapidly growing cells, which is one of the main properties of most cancer cells. But, since these drugs are toxic to cancer as well as to normal fast-dividing cells of the body, side effects are commonly observed during the therapy. Classical anticancer agents are represented by the following groups of drugs⁴:

- Alkylating agents

They act by alkylating DNA bases, leading to the formation of cross-links between opposite bases in double-stranded DNA. Examples, shown in Fig. 1.1, include cyclophosphamide (nitrogen mustard), carmustine (nitrosourea) and busulfan (alkyl sulfonate).

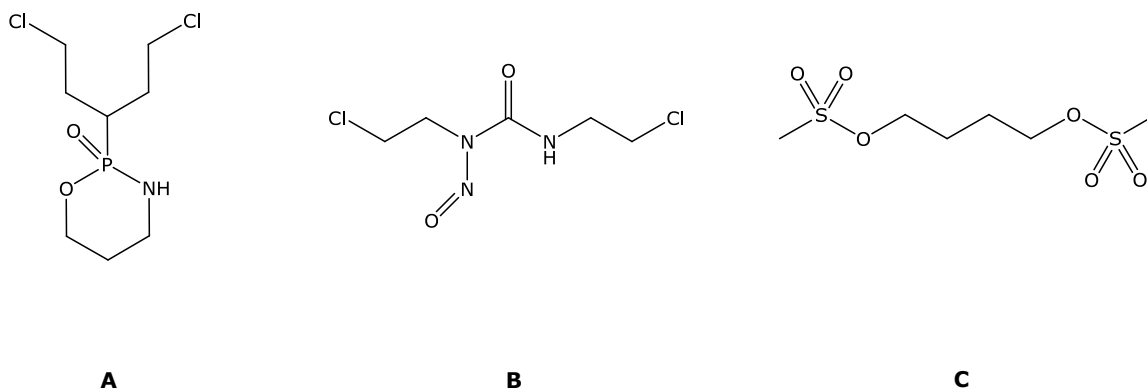


Figure 1.1 Structure of alkylating agents. **A:** cyclophosphamide, **B:** carmustine and **C:** busulfan.

- Antimetabolites

As they have a similar molecular structure to the substrates of enzymes involved in the synthesis of DNA, they can interfere with DNA production in two ways. Firstly, as structural analogues of precursors and intermediates along the synthetic chain and therefore interfering with the synthesis of purine and pyrimidine bases (folate analogues). Secondly, as “false” bases in the assembly of the DNA double helix during replication and transcription (purine, pyrimidine or nucleoside analogues). Examples are methotrexate, 6-mercaptopurine and 5-fluorouracil as folate, purine and pyrimidine analogues respectively (Fig. 1.2).

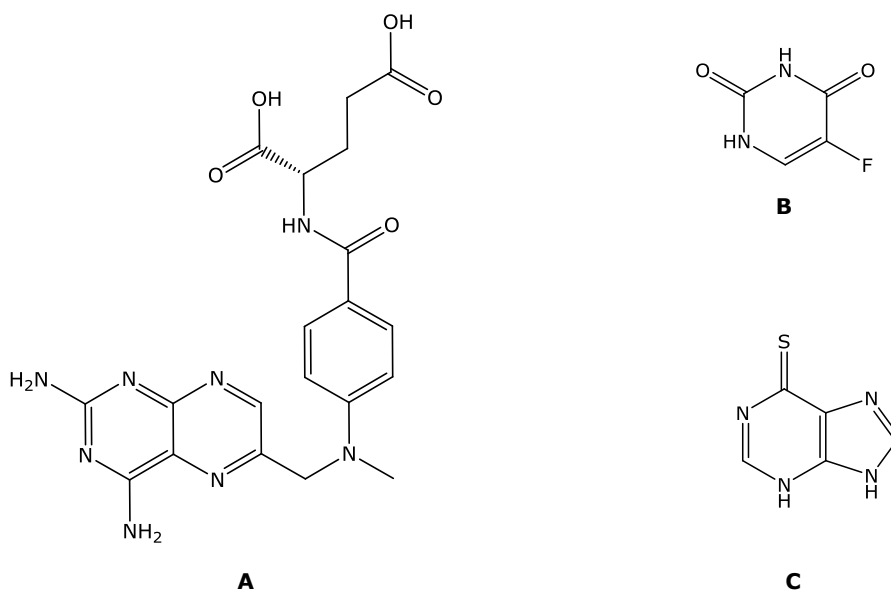


Figure 1.2 Structure of antimetabolites. **A:** methotrexate, **B:** 5-fluorouracil and **C:** 6-mercaptopurine.

- Plant alkaloids and terpenoids
 - a. Antitumour antibiotics: anthracycline antibiotics (doxorubicin) are a major class of antitumour antibiotics and present several modes of action including intercalation between DNA bases, production of free radicals and inhibition of topoisomerase II.
 - b. Inhibitors of topoisomerase: topoisomerase I and II are enzymes that induce DNA strand breaks to facilitate correct unwinding and supercoiling. Their inhibition interferes with transcription and replication of DNA. Examples of type I and II topoisomerase inhibitors are the drugs topotecan and etoposide, respectively.
 - c. Mitotic inhibitors: they target tubulins, interfering with the dynamics of the mitotic spindle. The two main examples are the vinca alkaloids (vincristine) and the taxenes (paclitaxel).
- Hormonal anticancer agents

The growth and proliferation of breast and prostate cancers can be driven by their respective classes of steroid hormones (estrogens and androgens) by binding to their cognate receptors. Therefore, these drugs modulate the level or action of the steroid hormones in the body. Some examples are tamoxifen (Fig. 1.3 **A**), which is a selective oestrogen receptor modulating agent, or flutamide (Fig. 1.3 **B**) which acts as an androgen receptor blocker and have been shown to be effective in prostate cancer treatments³.

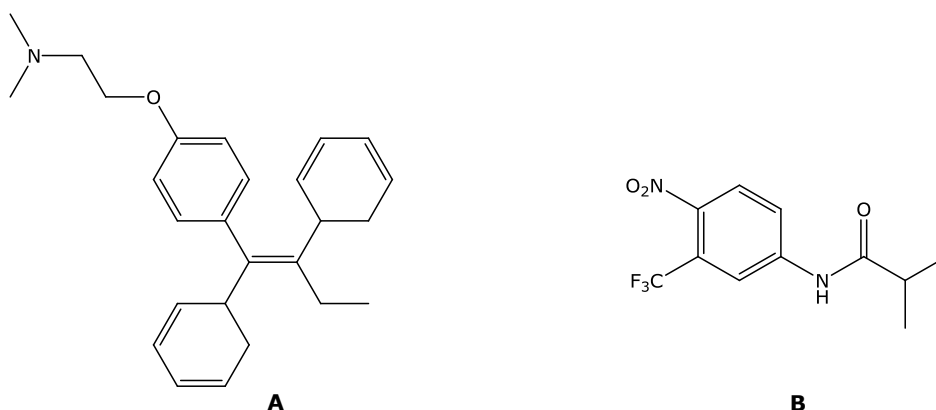


Figure 1.3 Structure of hormonal anticancer agents. **A**: tamoxifen and **B**: flutamide.

Despite all the available treatments, the high mortality of the illness reflects that it is still a major health challenge worldwide. Pharmaceutical problems in chemotherapy, such as manifestation of toxicity or drug resistance can lead to treatment failure. Moreover, cancer treatment facilities are not universally available, and life-extending treatment is often unavailable, generally for economic reasons. To stop people from dying of cancer it is necessary to find cures for the different forms of the disease or to find ways to prevent

cancer in the first place. Novel agents for cancer therapy and a worldwide implementation of prevention and early diagnosis programs are needed to overcome the current situation.

1.2 Metal complexes in medicine

Metals and their compounds have been used for medical applications for almost 5000 years. One of the earliest examples is the use of copper sulphate and alums, which were used by ancient Egyptians (3000 BC) to sterilize water. In China and Arabia gold-based preparations were used by physicians around 2500 BC. Mercury has been widely used in medicine for around 2000 years. During the Renaissance era in Europe mercury(I) chloride has been used as a diuretic, a topical disinfectant and a laxative. It is also known that mercury(II) chloride has been used in the treatment of syphilis^{5,6}.

In the 20th century, metal-based drugs began to be screened in a systematic way for their medicinal properties. A good example is arsphenamine (salvarsan), whose anti-syphilitic activity was discovered in 1909 in the laboratory of Paul Ehrlich during a survey of hundreds of newly synthesized organic arsenical compounds (see Fig. 1.4). It became the first modern chemotherapeutic agent for the treatment of syphilis, which was followed by a similar but more soluble arsenic complex (neoarsphenamine). Due to the high risk of side effects, this kind of arsenic drugs was supplanted in 1940 by penicillin.

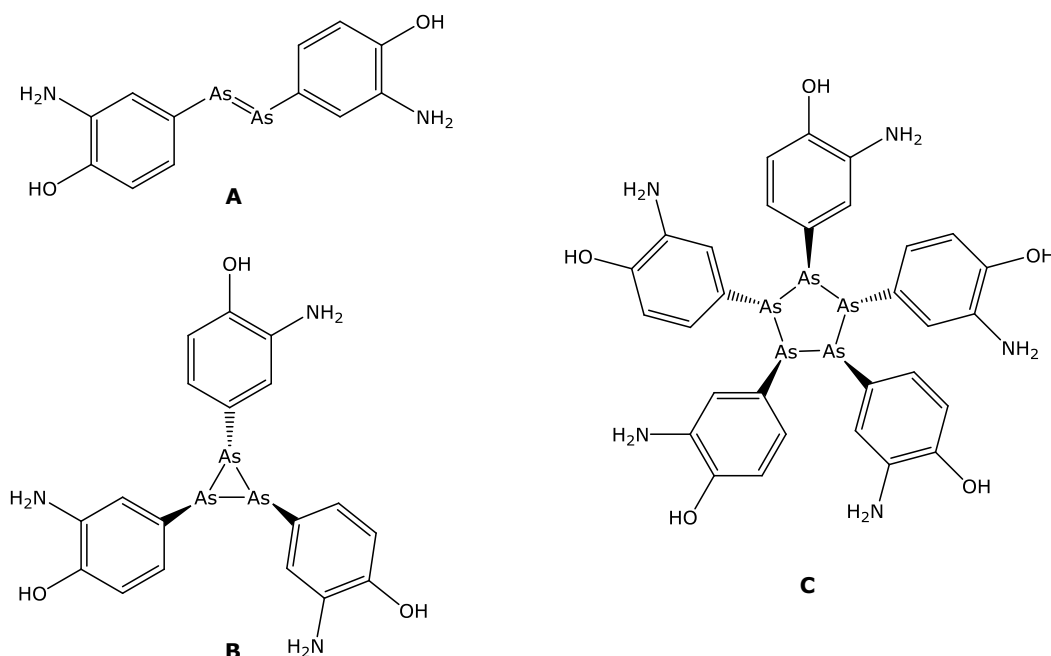


Figure 1.4 Reported structures for salvarsan. By analogue with azo compounds, Ehrlich assigned **A** to the free base of salvarsan. In 2005, studies by ESI-MS revealed that salvarsan is actually a mixture of cyclic species $(\text{RAs})_n$ with $n=3$ (**B**) and $n=5$ (**C**) as the preferred sizes⁷.

Over the past 30 years, metal compounds have become very important in medical application. Due to the particular chemical relativities of metals, their magnetic and nuclear properties and the structural variety of their ligands, nowadays medical practice has access to a variety of metal-based compounds. These metal-based agents are then introduced into a biological system with either a therapeutic or a diagnostic purpose. Listed below are some representative examples of metal-based compounds with their current medical application:

- Cisplatin is probably the best known example of a metal-containing drug. Moreover, platinum-based combination chemotherapy is still the mainstay for the treatment of solid tumours. Due to their importance in cancer therapy they are going to be described in Section 1.2.1.

- Various gold compounds are used in chrysotherapy, the treatment of rheumatoid arthritis. All are gold(I) complexes containing thiolate ligands, as for example auranofin and aurothiomalate (Fig. 1.5 **A** and **B** respectively)⁸.

- Salts of lithium, as lithium carbonate, are commonly used in the treatment of bipolar affective disorders, such as manic depression⁹.

- Sodium nitroprusside (Fig. 1.5 **C**), an iron(II) complex, is a potent vasodilatador, due to its ability to release nitric oxide. It has a number of clinical uses, such as hypertensive anaesthesia during surgery and it is used in cases of hypertensive emergencies¹⁰.

- Gallium nitrate is currently used for the treatment of cancer-related hypercalcemia¹¹.

- Silver sulfadiazine (Fig. 1.5 **D**) is a topical antibacterial agent, used as a cream for the treatment of burns. It combines the antibacterial properties of both silver and sulfadiazine¹².

- Bismuth subsalicylate is a drug used to treat a variety of gastrointestinal discomforts, including duodenal and peptidic ulcers, ulcerative colitis and diarrhoea¹³.

- Organomercury compounds are well known as antiseptical and antifungal agents. Examples are thiomersal (Fig. 1.5 **E**) and merbromin^{14,15}.

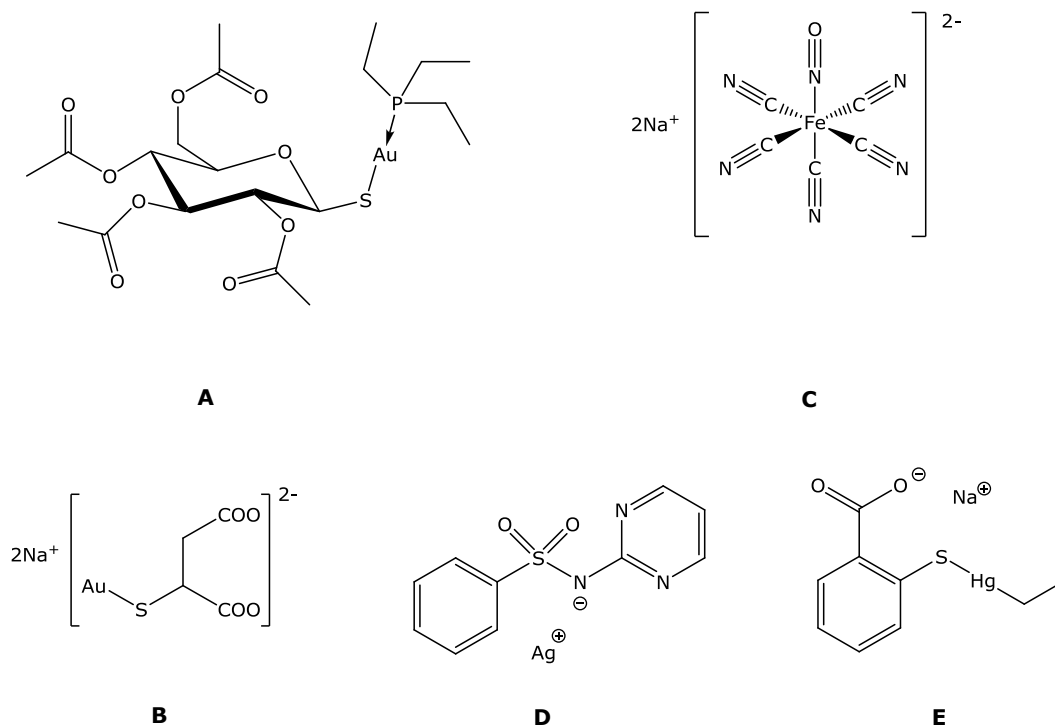


Figure 1.5 Structure of metal-based therapeutic agents. **A:** auranofin, **B:** aurothiomalate, **C:** sodium nitroprusside, **D:** silver sulfadiazine and **E:** thiomersal.

Coordination compounds also have a variety of applications in the diagnosis of illness or injury. The *in-vivo* use of metals provides a tool for non-invasive diagnostic imaging procedures.

- Metal-containing drugs are commonly used in X-ray imaging as contrast agents. These are substances that preferentially absorb X-rays, and hence when administered to a patient enter and pass through anatomic regions of interest to provide transient contrast enhancement. Although the most commonly used contrast agents are the water-soluble iodinated agents, barium sulphate suspensions (BaSO₄) are used for gastrointestinal track imaging¹⁶.

- Magnetic resonance imaging (MRI) is a non-invasive imaging technique used to visualize internal structures of the body, by measuring the nuclear magnetic resonance of nuclei atoms (inside the body). A number of different coordination compounds are used as paramagnetic MRI contrast agents. They enhance the image contrast, by incrementing the relaxation rate of interacting water protons. Then, if this paramagnetic compound enters into one tissue in preference to another, the respective image is enhanced. Therefore, these agents should have a suitable biodistribution and pharmacokinetic

behaviour combined with low toxicity. There are several gadolinium(III) complexes approved for clinical use. For example, gadobutrol (Fig. 1.6 **A**) which is used to detect and visualize areas with disrupted blood brain barrier or abnormal vascularity of the central nervous system. Manganese(II) chelates such as mangafodipir have been used as contrast agent to detect lesions of the liver.

• In nuclear medicine, radioactive nuclides can be used both for diagnosis or therapy. Among the γ -emitters nuclides being used for nuclear imaging are ^{99m}Tc , ^{111}In and ^{67}Ga . β -emitters nuclides such as ^{186}Re , ^{188}Re , and ^{89}Sr are mainly used in radiotherapy. Due to its highly interesting physical properties ^{99m}Tc is the most common used nuclide in nuclear imaging. Depending on the specific organ to be targeted, different ligands are incorporated in the coordination complex. For example, the complex ^{99m}Tc -sestamibi (Fig. 1.6 **B**) is mainly used to image the myocardium.

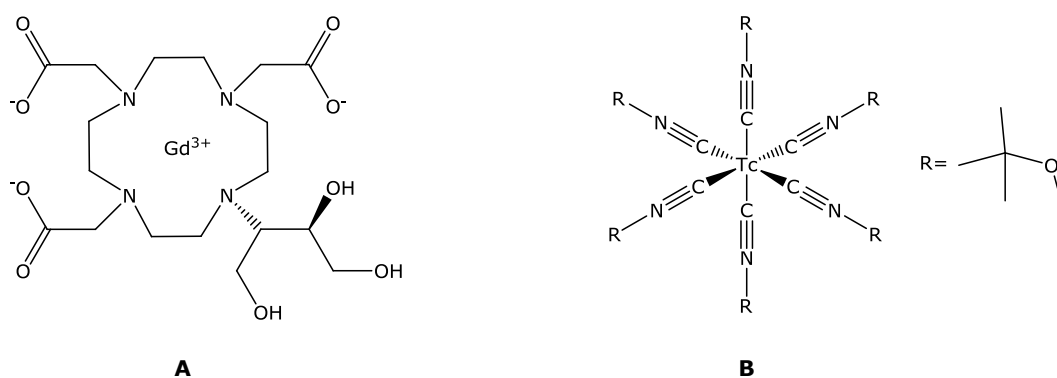


Figure 1.6 Structure of metal-based diagnostic agents. **A**: gadobutrol and **B**: ^{99m}Tc -sestamibi.

1.2.1 Platinum complexes as anticancer agents

Since the discovery of the biological activity of cisplatin (Fig. 1.7 **A**) in the early 1960s¹⁷, it has become one of the most widely used and effective antineoplastic agents. Today, more than 30 years after its approval, cisplatin still has a central role in cancer chemotherapy, especially for testicular cancer. However, its clinical applications are limited by side effects and drug resistance. In an attempt to overcome these limitations thousands of platinum compounds have been synthesized and tested for their biological activity. Only 23 platinum-based drugs entered clinical trials and two (carboplatin and oxaliplatin, see Fig. 1.7 **B** and **C** respectively) of them gained international approval, while three other (nedaplatin, lobaplatin and heptaplatin, see Fig. 1.7 **D**, **E** and **F** respectively) were regionally approved¹⁸.

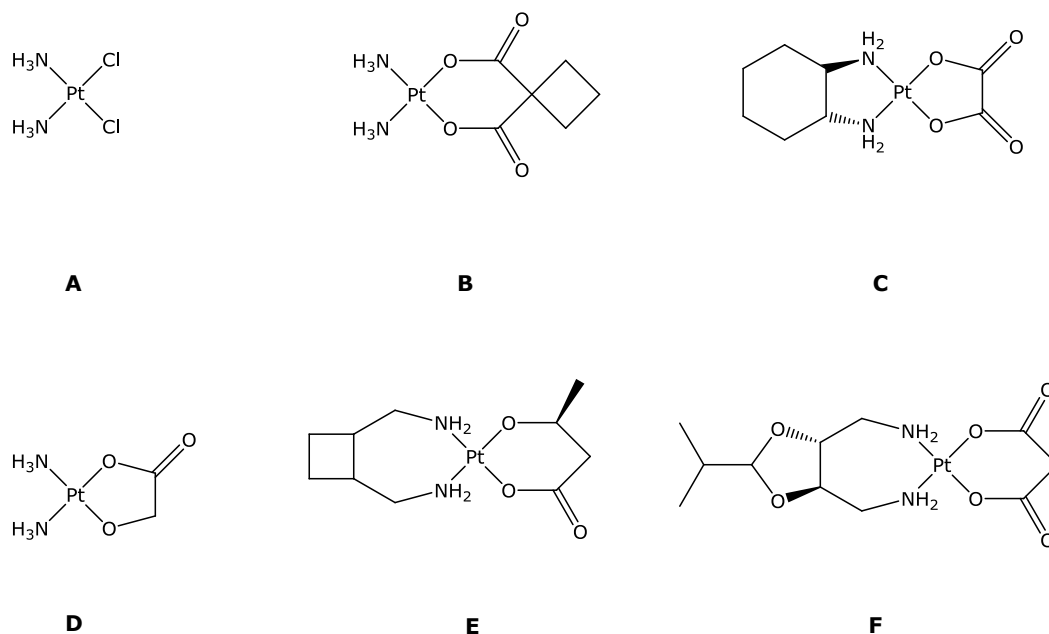


Figure 1.7 Structure of clinically approved platinum(II) complexes. **A:** *cis*-diamminedichloroplatinum(II) or cisplatin, **B:** *cis*-diammine[1,1-cyclobutanedicarboxylato]platinum(II) or carboplatin, **C:** [oxalate(2-)-*O,O'*][1*R*,2*R*-cyclohexanediamine-*N,N'*]platinum(II) or oxaliplatin, **D:** diammine[hydroxyacetato(2-)-*O,O'*]platinum(II) or nedaplatin, **E:** [2-hydroxypropanoato(2-)-*O1,O2*][1,2-cyclobutanedimethanamine-*N,N'*]platinum(II) or lobaplatin and **F:** [propanedioato(2-)-*O,O'*][2-(1-methylethyl)-1,3-dioxolane-4,5-dimethanamine-*N,N'*]platinum(II) or heptaplatin.

A list of platinum-based antitumour drugs which achieved marketing approval or entered clinical human trials is presented in Table 1.1.

Table 1.1 Platinum-based anticancer drugs which have achieved marketing approval for human use and platinum-drugs in development^{18,19}.

Indication	Approval year or approval development status	Dose-limiting toxicities	Country
Cisplatin (i.v. injection) Metastatic testicular cancer, metastatic ovarian cancer and transitional bladder cancer	1978	Nephrotoxicity, neurotoxicity	Global
Carboplatin (i.v. injection) Ovarian cancer, first line	1989	Myelosuppression	Global

Table 1.1 (cont.)

Indication	Approval year or approval development status	Dose-limiting toxicities	Country
Oxaliplatin (i.v. injection) Colorectal cancer	2002	Neurotoxicity, nausea and vomiting	Global
Nedaplatin (i.v. injection) (Non)-small cell lung cancer, oesophageal cancer, head and neck cancer	1995	Myelosuppression	Japan
Lobaplatin (i.v. injection) Chronic myelogenous leukaemia, inoperable metastatic breast cancer, small cell lung cancer	1998	Thrombocytopenia	China
Heptaplatin (i.v. injection) Gastric cancer	1999	Nephrotoxicity, intra-abdominal bleeding	Korea
Satraplatin (oral) Hormone-refractory prostate cancer	Under consideration for approval by FDA	Myelosuppression	
Picoplatin (i.v. infusion or oral) Small cell lung cancer	Phase III trial about to begin	Myelosuppression	

i.v.: intravenous, FDA: Food and Drug Administration

All these platinum complexes have the square plane geometry (see Fig. 1.7) and can be described by the general formula $cis-[PtX_2(NHR_2)_2]$, where R represents the organic non-leaving fragment and X the leaving group such as chloride or the chelated bis-carboxylate. It is worth noting that similar coordination compounds from other metals, such as Pd, did not exhibit antitumour activity. The success of platinum drugs is related to their ligand-exchange kinetics. The Pt-ligand bond in a typical coordination compound is much weaker than a covalent single or double bond. However, the ligand exchange

rate of platinum-based compounds is rather slow. The fact that platinum complexes are slow in ligand exchange reactions gives them a high kinetic stability and therefore the possibility to reach their target molecules in the cell²⁰. In addition to this, the kinetic *trans*-effect should be mentioned, which is most pronounced in square planar complexes such as platinum(II) compounds: ligands in *trans* position to the leaving group affect its rate of displacement or the strength of the bond. Besides, strong π -acceptor ligands accelerate the rate of substitution. These electronic effects also play an important role in the kinetic of substitution. It explains for example, why the voluminous chloride ions are the leaving groups and not the ammine groups, although they have a stronger *trans*-effect than the chlorides²¹. All these factors play an important role in understanding the ligand-exchange behaviour of the Pt antitumour complexes.

The cellular responses to cisplatin and platinum compounds have been widely studied²²⁻²⁵. Upon administration to the bloodstream as an intravenous injection, cisplatin is rapidly distributed and due to the high chloride concentration of the blood (~ 100 mM), it maintains a stable neutral state, although it can bind to serum proteins such as human serum albumin. Cisplatin is taken up eventually by all types of cells. Three possible mechanisms of platinum compounds accumulation have been reported: passive diffusion, uptake by copper transporters proteins (e.g. CTR1) and organic cation transporters^{26,27}. Due to the low chloride ion concentration in the cytosol ($\sim 4-12$ mM), once cisplatin enters the cells it undergoes aquation that is accompanied by the displacement of either one or both chloride ligands (mono or diaqua species)²². Although the aquated form is highly reactive to cellular components, it enters the nucleus and interacts with its main target, the DNA²⁸. It will preferably bind to the N7 position of a guanine and to a lesser extent to an adenine. This is explained, among other factors, by the strong hydrogen bonding between the ammine ligand on Pt and the O6 group guanine, which stabilizes the Pt-guanine adduct by comparison with the Pt-adenine adduct²⁹. In Fig. 1.8 the structures of monofunctional adducts of platinum at the N7 sites of adenosine (**A**) and guanosine (**B**) using the diaqua complex of cisplatin as reactant are displayed.

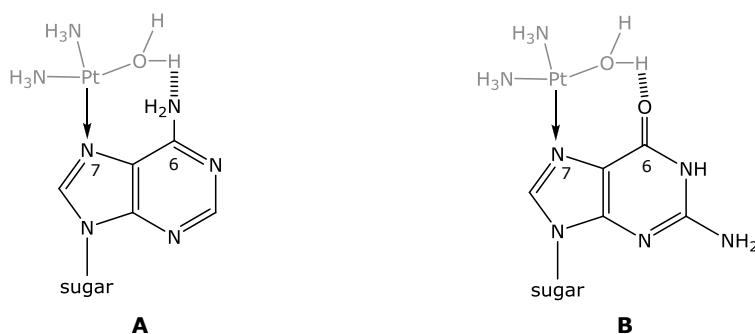


Figure 1.8 Platinum binding at the N7 sites of adenosine (**A**) and guanosine (**B**).

In both structures, the water ligand acts as a strong hydrogen-donor while the oxo and amino groups at the C6 position of the guanine and adenine rings, are hydrogen-bond acceptors. As expected, the oxo group is a much better hydrogen-bond acceptor than the amino group, which provides additional stabilization of the Pt-guanosine adduct over the adenosine one²⁹. This first monofunctional binding is a crucial step for the formation of 1,2-intrastrand cross-links with adjacent guanine bases, 1,2-d(GpG), which are reported to be the main covalent bis-adducts, followed by 1,2-d(GpA) and 1,3-d(GpNpG) intrastrand cross-links³⁰. Monofunctional adducts and interstrand cross-links are also found (see Fig. 1.9).

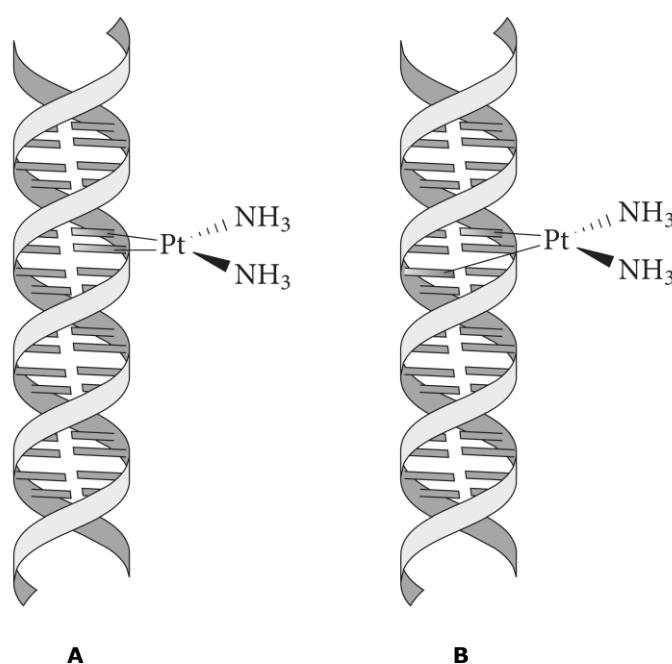


Figure 1.9 Diagram of cisplatin-DNA structures: 1,2-intrastrand cross-link (**A**) and interstrand cross-link (**B**)¹⁹.

These adducts cause distortions in the DNA, that include blending and unwinding of the double helix, which prevents replication and transcription and finally leads to cellular apoptosis^{22,25}.

Unfortunately, the use of cisplatin is restricted by severe dose-limiting side effects which arise from its lack of selectivity for tumour tissue. Moreover, the efficacy of cisplatin therapy is often limited by the emergence of resistant tumours following treatment. As the toxicity of platinum-based drugs is related to the liability of the leaving groups, a first attempt of drug-development to overcome these limitations was to obtain a less toxic analogue by incorporation of more stable leaving groups, such as bis-

carboxylates. Thus, carboplatin (Fig. 1.7 **B**) was developed as a second generation platinum analogue through the replacement of the chloride ligands of cisplatin by 1,1-cyclobutanedicarboxylate, which aquates much slower than cisplatin. As a result, carboplatin has fewer side effects than cisplatin and its low reactivity allows a higher dose to be administered¹⁸.

Oxaliplatin (Fig. 1.7 **C**), which contains a 1,2-diaminocyclohexane (DACH) carrier ligand, was the first drug capable of overcoming cisplatin resistance. While the replacement of the chloride ligands of cisplatin with the oxalate ligands reduces the severity of the side effects, the replacement of the two ammine ligands with the carrier ligand is thought to have an influence on the type of DNA-adducts that oxaliplatin generates and the way these DNA lesions are processed. These properties may be responsible for the differences in the tumour range, toxicity and mutagenicity of oxaliplatin and cisplatin³¹.

Promising platinum complexes are currently at various stages of clinical trials with close marketing approval (Fig. 1.10).

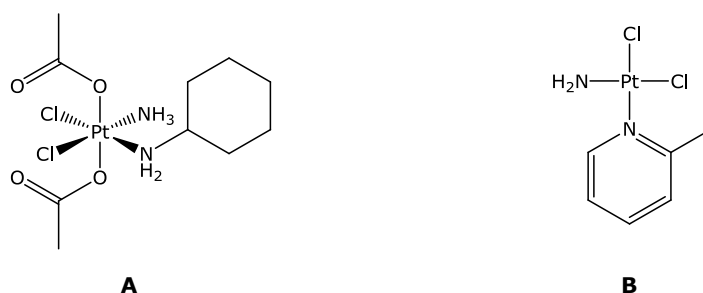


Figure 1.10 Structures of platinum complexes with close marketing approval. **A**: bis-(acetato)ammine-dichloro[cyclohexylamine]platinum(IV) or satraplatin and **B**: *cis*-ammine-dichlorido[2-methylpyridine]platinum(II) or picoplatin.

Satraplatin (Fig. 1.10 **A**) is a platinum(IV) complex, which was rationally designed to be an orally active platinum drug. Oral administration of anticancer drugs offer multiple potential advantages over the commonly i.v. platinum drugs, such as ease of administration, reduced need for office visits and elimination of the need for venous access devices and their associated complications and costs. Hence, two axial acetate groups were incorporated to the complex in order to make it more lipophilic and increase its oral bioavailability. Once in the blood satraplatin is reduced to give at least six different platinum(II) complexes. The most active and abundant metabolite is *cis*-ammine-dichlorido[cyclohexylamine]platinum(II), obtained by the metabolization of both

acetate groups. It is structurally similar to cisplatin, except for the replacement of one of the ammine ligands with a cyclohexylamine group³².

Picoplatin (Fig. 1.10 **B**) was rationally designed to reduce drug inactivation by thiol containing species such as glutathione, which is a known mechanism of platinum resistance²⁵. Thus, a bulky methylpyridine ring was introduced to provide steric hindrance to the attack of the drug by nucleophiles¹⁸. Picoplatin demonstrated ability to circumvent acquired platinum resistance, showing antitumour activity in cisplatin, carboplatin and oxaliplatin resistant cell lines^{18,33,34}.

Currently, there is another strategy in platinum cancer chemotherapy, which consists in improving the way to deliver platinum to the tumours. Therefore, delivery vehicles are being developed to transport selective the cytotoxic agent to the tumour and then reduce its side effects, while its cancer killing ability is maintained. Three of these platinum-based products (Aroplatin, Lipoplatin and ProLindac) have already entered clinical trials¹⁸.

1.2.2 Non-platinum metal complexes as antitumour drugs

As described in Section 1.2.1, platinum-based chemotherapy presents several disadvantages, particularly related with its general toxicity which leads to the undesirable side effects and with the fact that it is inactive against several cancer cell lines and metastasis cancers. This stimulated not only research of novel platinum drugs, but also of novel non platinum-containing metal species as chemotherapeutics. In this context, transition metals represent a uniquely modular system. They typically exhibit several oxidation states, which give them a large flexibility in their chemical and physical properties. Accordingly, a countless number of organic ligands can be combined with a transition metal centre, which holds them in a well defined three-dimensional structure. Thus, the characteristics of the complex can easily be modulated by a particular choice of the ligands. As a consequence, promising non platinum metal compounds have been developed and some of them have already been evaluated in Phase I and Phase II clinical trials³⁵.

1.2.2.1 Ruthenium-based compounds

In the last 30 years, a large number of ruthenium-containing agents with oxidation state II or III have been synthesized and tested for potential antitumour activity³⁶. Among them, some ruthenium(III) complexes show unique biochemical characteristics, which allow them to accumulate preferentially in neoplastic tissues rather than in normal

ones³⁷. Moreover, ruthenium remains in its relatively inactive state ruthenium(III) until it reaches the tumour site, where it converts into its active state ruthenium(II)^{36,38}.

Two ruthenium-based drugs, NAMI-A and KP1019 (Fig. 1.11 **A** and **B** respectively), have reached human clinical trials. Although these octahedral ruthenium(III) complexes have structural and chemical similarities, they demonstrated different antitumour behaviours. NAMI-A appears to reduce the metastatic potential of tumours, irrespective of the lack of a significant reduction of primary tumour growth³⁹. Even though NAMI-A can bind to DNA, this does not seem to be the source of its biological effects. It rather appears to act as an anti-angiogenic and anti-invasive agent^{40,41}. In contrast, KP1019 has shown direct cytotoxic activity in primarily tumours, and its activity against colorectal cancers is being especially investigated. The agent is thought to promote apoptosis, predominantly by the intrinsic mitochondrial pathway⁴².

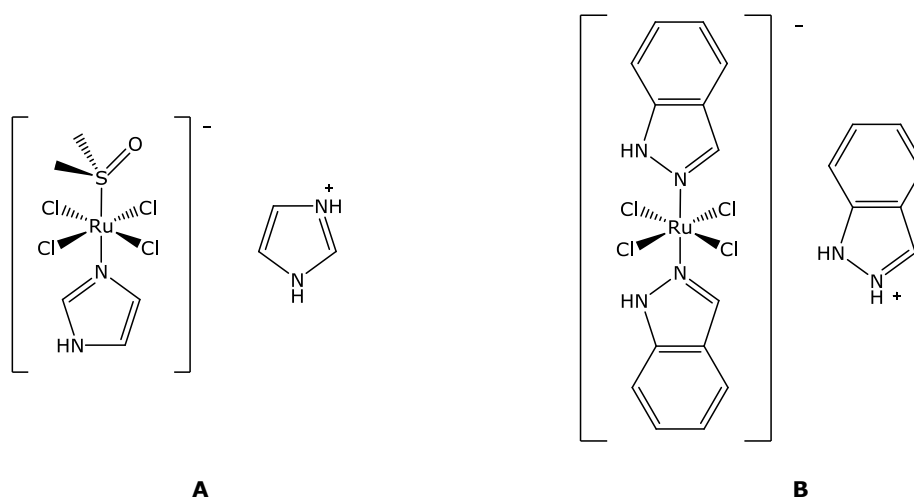


Figure 1.11 Structure of ruthenium complexes in clinical trials for cancer treatment. **A**: imidazolium [*trans*-tetrachloro(1*H*-imidazole)(*S*-dimethylsulfoxide)ruthenate(III)] or NAMI-A and **B**: indazolium [*trans*-tetrachlorobis(1*H*-indazole)ruthenate(III)] or KP1019.

More recently, Dyson *et al.* introduced a number of organometallic ruthenium(II) arenes with phosphadamantane (PTA) ligands, called RAPTAs (Fig. 1.12). Like NAMI-A, these agents are only poorly toxic towards tumour cells *in-vitro*, but have shown *in-vivo* antimetastatic activity⁴³. Particularly RAPTA-T has been shown to inhibit *in-vitro* some steps of the metastatic process and to reduce *in-vivo* the growth of lung metastases⁴⁴.

The outstanding behaviours of RAPTA-T and NAMI-A make them agents of high practical interest, since the need for effective drugs on metastatic tumours is of huge importance and only very few selective drugs with these properties have been identified.

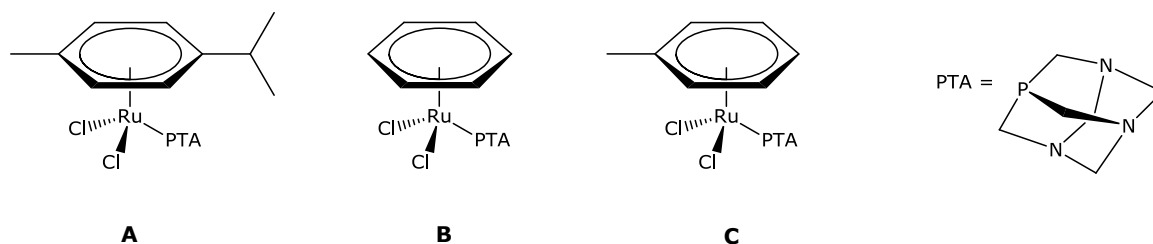


Figure 1.12 Structure of some examples of ruthenium(II)-arene PTA (RAPTA) compounds where PTA = 1,3,5-triaza-7-phospha-adamantane **A**: RAPTA-C, **B**: RAPTA-B and **C**: RAPTA-T.

1.2.2.2 Titanium and gallium compounds

Among the titanium-based drugs that have been investigated in clinical trials, budotitane (Fig. 1.13 **A**) has been the first one, and then became the first non-platinum metal compound that reached clinical testing. Unfortunately, during Phase I trials it caused no objective tumour response, with cardiac arrhythmia as dose-limiting toxicity⁴⁵.

Titanocene dichloride is an organotitanium compound (Fig. 1.13 **B**). Although it has shown promising results in clinical Phase I, its efficacy in Phase II clinical trials in patients with metastatic renal-cell carcinoma⁴⁶ or metastatic breast cancer⁴⁷ was too low to be pursued. The two main disadvantages of this type of compound that could have led to their low activity in clinical Phase II trials are their poor water solubility and their hydrolytic instability, which ultimately leads to unidentified metabolites⁴⁸. Therefore, drug development has recently been focusing on substituted titanocenes that might offer greater aqueous stability, water solubility, or cytotoxicity. In this context, a promising series of benzyl-substituted titanocenes has been introduced in 2005⁴⁹. Particularly Titanocene Y (Fig. 1.13 **C**), which contains methoxyphenyl substituents at the cyclopentadienyl rings, has been considered a novel potential anticancer drug due to its increased solubility and cytotoxicity.

Anticancer properties of gallium salts have been described for the first time in 1971 by Hart *et al.*⁵⁰ Gallium is known to interfere with DNA structure and its synthesis, it modulates the activity of enzymes and the synthesis of proteins. Moreover, it alters plasma membrane and mitochondrial functions⁵¹. Gallium nitrate, gallium chloride and gallium malonate have been investigated in clinical trials with moderate results⁵¹. More recently, a novel oral gallium(III) complex (tris(8-quinolinolato)gallium(III) or KP46) has been developed and investigated in Phase I trials. It has demonstrated cytotoxic and antihypercalcemic efficiency in preclinical tumour models and it finished Phase I trials with evidence of clinical activity in renal cell carcinoma⁵².

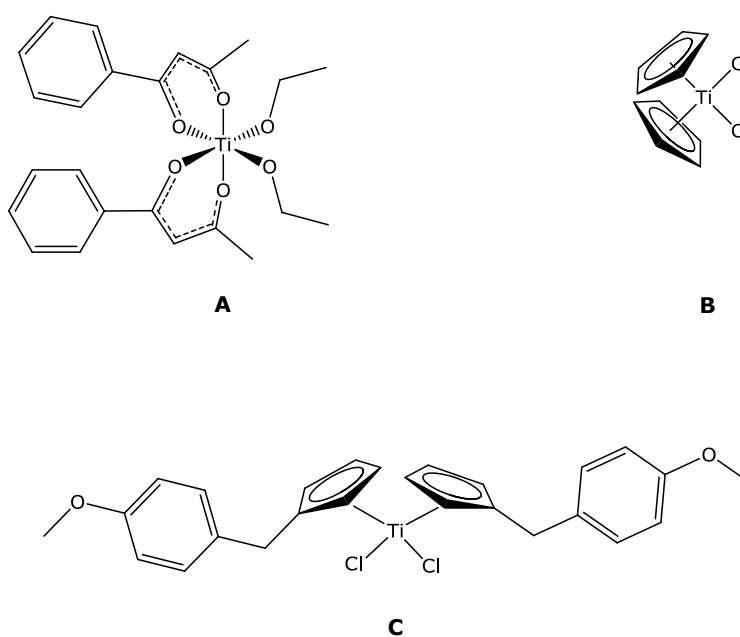


Figure 1.13 Structure of titanium complexes **A**: budotitane, **B**: titanocene dichloride and **C**: titanocene Y.

The work selected and summarized above includes all metals that have been investigated in clinical Phase I and II trials so far. Furthermore, promising results have been reported in preclinical research on other non platinum-based metal agents, such as iron, gold and cobalt compounds. Since combining drugs with different modes of action often synergizes their effects, complexes that attract great interest are those whose mode of action is different than cisplatin. Moreover, compounds with different antitumour mechanisms or specific molecular targets different to DNA, are likely to overcome the existing limitations of the current chemotherapy. Examples are ferrocene compounds that cause oxidative DNA damage^{53,54} or the inhibition of thioredoxin reductase by gold complexes^{55,56}.

2 Background and aims of the research project

The existing limitations of platinum based chemotherapy and the fact that some cancer diseases (as breast cancer) are not sensitive to platinum agents, stimulated our research in the development of novel anticancer agents combining platinum(II) as a metal center with a suitable carrier ligand. With this aim, over the past years the ligands of cisplatin have been systematically modified. The exchange of the non-leaving groups (ammine) of cisplatin by a substituted 1,2-diaminoethane backbone (e.g. 1,2-diamino-1,2-diarylethane) has resulted in a lead structure used in a great number structure-activity relationships. It was shown that appropriate functional groups as substituents in the aromatic rings could increase the cytotoxicity of the complexes. Moreover, in the diastereomeric [1,2-diamino-1,2-bis(4-fluorophenyl)ethane]platinum(II) complexes the neutral ligand has been identified as a carrier for the PtCl_2 moiety⁵⁷. These interesting results lead us to the synthesis of platinum(II) complexes bearing Schiff bases derived from 1,2-diamino-1,2-diarylethanes and substituted salicylaldehydes (Fig. 1.14). These Schiff bases (diarylsalene) containing the N_2O_2 donor set are capable of forming stable complexes with transition metal ions. It is worth noting that the influence of the configuration of the diarylsalene ligand as well as its substitution pattern on the cytotoxicity of the [diarylsalene]cobalt complexes has already been reported⁵⁸.

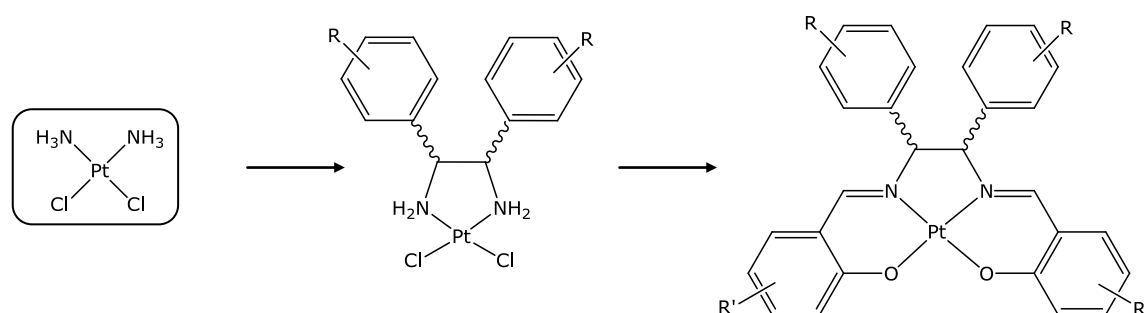


Figure 1.14 Route design of [diarylsalene]platinum(II) complexes. First (left-middle panels), the non-leaving groups of cisplatin were exchanged by a substituted 1,2-diamino-1,2-diarylethane moiety, which has been structurally developed from the synthetic estrogens diethylstilbestrol and hexestrol⁵⁹. Second (middle-right panels), Schiff bases derived from the 1,2-diamino-1,2-diarylethanes and substituted salicylaldehyde were used as chelating ligands for the platinum(II) metal centre.

Further structural modifications of cisplatin included the exchange of the ammine groups by ligands bearing the 1,2-phenylenediamine moiety (Fig. 1.15 middle). Köckerbauer and Bednarski observed the poor water stability of these complexes, which

was attributed to oxidation reactions, resulting in the formation of [*o*-benzoquinonediimine]platinum complexes and H₂O₂⁶⁰. Furthermore, they proposed that the mutagenic properties of the dichloro[*o*-phenylenediamine]platinum(II) complexes⁶¹ were associated to one or more of their oxidative decomposition products.

In analogy to the developed [diarylsalene]platinum complexes, series of *N,N'*-bis(salicylidene)-1,2-phenylenediamine ligands (salophene) containing again the N₂O₂ donor set have been synthesized and finally coordinated to the platinum(II) metal centre (Fig. 1.15). Over the past years, several metal ions in different oxidation states have been chelated with salophene ligands and investigated for their cytotoxicity. Outstanding antitumour properties have been obtained with the [salophene]iron complexes, which are up to 50-fold more active than cisplatin against MDA-MB-231 breast cancer cells⁶². Investigations on the mode of action of the [salophene]iron(III) complexes have shown that they are able to generate reactive oxygen species (ROS) and to induce apoptosis, but have demonstrated only marginal interactions with DNA⁶². Furthermore, studies on lymphoma and leukemia cells have demonstrated that cell death is induced *via* the intrinsic mitochondrial pathway⁶³. Further studies on substituted [salophene]iron(III) complexes have evidenced the influence of the position of methoxy groups at the salicylidene moiety on cytotoxicity⁶⁴. Promising results have also been obtained with a 3-methoxy substituent at the salicylidene moiety of [salophene]nickel(II) complexes, which exhibit outstanding cytotoxicity in MCF-7 breast cancer cells. In this case it has been demonstrated that the nickel(II) complex efficiently triggered the extrinsic pathway of apoptosis⁶⁵. Studies concerning [salophene]platinum(II) complexes have recently been reported by Wu *et al.*⁶⁶. They have investigated the inhibition of human oncogen *c-myc*, whose overexpression is linked to cellular proliferation in malignant tumours, by stabilizing the G-quadruplex DNA structure⁶⁷. Thus, a platinum(II) Schiff base complex bearing an amine side chain has been satisfactorily identified, after a lead optimization process, as a potent and specific *c-myc* transcription inhibitor.

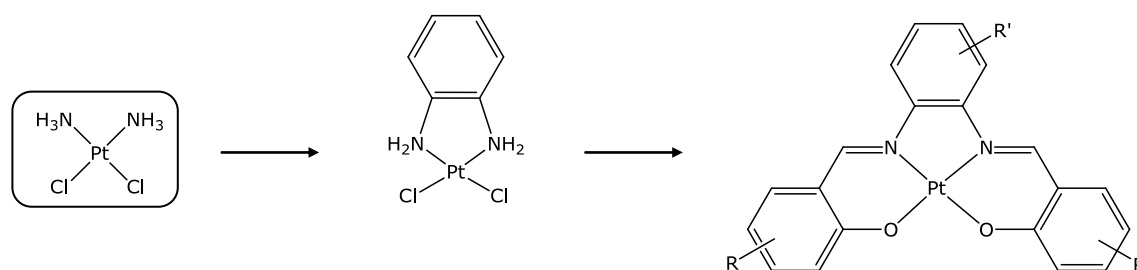


Figure 1.15 Route design of [salophene]platinum(II) complexes. First (left-middle panels), the ammine ligands of cisplatin were replaced by a 1,2-phenylenediamine moiety and second (middle-right panels), Schiff bases derived from 1,2-phenylenediamine moiety and substituted salicylaldehyde were used as chelating ligands for the platinum(II) metal centre.

On the basis of these findings, our research aimed at developing [diarylsalene]- and [salophene]platinum(II) complexes as novel anticancer agents (Section 3 and 4). **1-Pt** and **13-Pt** were designed as lead compounds of the [diarylsalene]- and [salophene]platinum(II) series respectively (see Fig. 1.16).

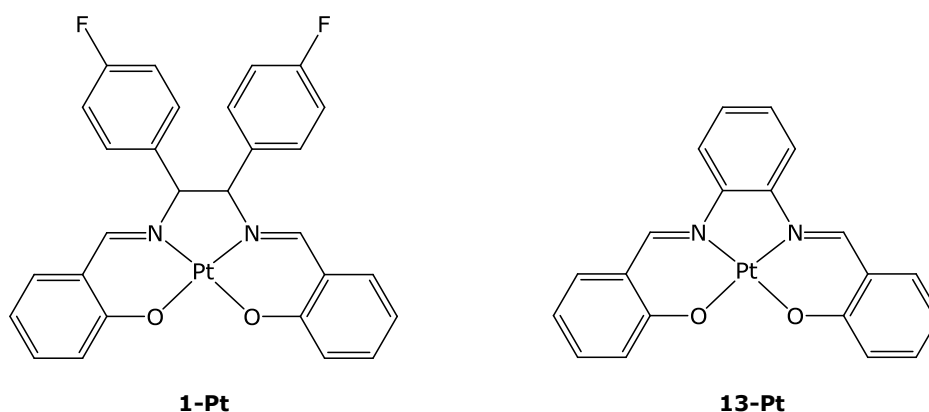


Figure 1.16 Structure of the lead compounds of the [diarylsalene]- (**1-Pt**) and [salophene]platinum(II) (**13-Pt**) series. **1-Pt** was chosen with a 4-fluoro substituted 1,2-diamino-1,2-diarylethane moiety, due to its reported carrier function.

In-vitro antitumour activities of the platinum compounds have been validated against breast cancer cell lines (Section 5) and the effect of ligand substitution (mostly with methoxy and fluorine substituents) on cytotoxicity has also been investigated. As part of an effort to understand the mechanism of cytotoxicity, and considering that DNA is commonly identified as a possible target of platinum-based agents^{22,23}, drug-DNA interactions have been evaluated (Section 8). Furthermore, cellular accumulation studies have been performed, and a possible relationship with cytotoxicity has been analyzed (Section 6). Finally, considering that physicochemical properties play a major role during early drug development, aqueous solubility and lipophilicity have been determined and have subsequently been related to their biological activities (Section 7).

Results and discussion

3 Synthesis

3.1 Overview of the synthesized compounds

Two main structures, diarylsalene and salophene, were used to provide the respective platinum complexes.

In this work, the aromatic rings present in the salicylidene moiety are called *Ar*, while the ones present in the 1,2-diarylethane (in the case of the diarylsalene structures) or in the 1,2-phenylene moiety (in the case of the salophene structures) are called *Ar'* (Fig. 3.1).

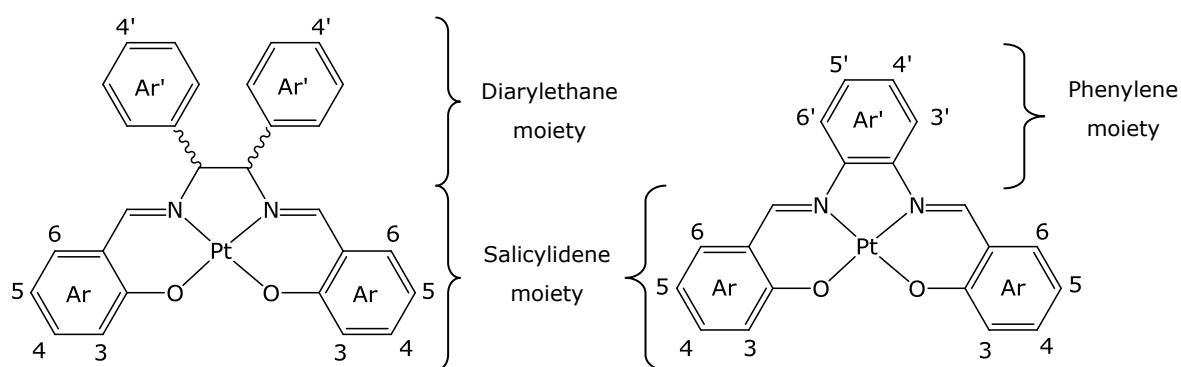


Figure 3.1 Main structure of the [diarylsalene]platinum(II) complexes (left) and the [salophene]platinum(II) complexes (right) with the numbering of the substituted positions.

In the following section a list of all synthesized complexes with their respective synthesis number is presented. Details for every compound can be found in the Experimental part (11).

3.2 Substituted [diarylsalene]platinum(II) complexes

Table 3.1 Substitution pattern present in the [diarylsalene]platinum(II) series.

Substitution pattern					Config.	Compound
R' ₄	R ₃	R ₄	R ₅	R ₆		
F	H	H	H	H	<i>meso</i>	1-Pt
F	H	H	H	H	<i>d,l</i>	2-Pt
F	H	H	NO₂	H	<i>meso</i>	3-Pt
F	OCH₃	H	H	H	<i>meso</i>	4-Pt
F	H	OCH₃	H	H	<i>meso</i>	5-Pt
F	H	H	OCH₃	H	<i>meso</i>	6-Pt
F	H	H	H	OCH₃	<i>meso</i>	7-Pt
F	F	H	H	H	<i>meso</i>	8-Pt
F	H	F	H	H	<i>meso</i>	9-Pt
F	H	H	F	H	<i>meso</i>	10-Pt
F	H	H	H	F	<i>meso</i>	11-Pt
CF₃	H	H	H	H	<i>meso</i>	12-Pt

3.3 Substituted [salophene]platinum(II) complexes

Table 3.2 Substitution pattern present in the [salophene]platinum(II) series.

Substitution pattern						Compound
R' ₃	R' ₄	R ₃	R ₄	R ₅	R ₆	
H	H	H	H	H	H	13-Pt
H	H	OCH₃	H	H	H	14-Pt
H	H	H	OCH₃	H	H	15-Pt
H	H	H	H	OCH₃	H	16-Pt
H	H	H	H	H	OCH₃	17-Pt
H	H	F	H	H	H	18-Pt
H	H	H	F	H	H	19-Pt
H	H	H	H	F	H	20-Pt
H	H	H	H	H	F	21-Pt
F	H	H	H	H	H	22-Pt
F	H	F	H	H	H	23-Pt
F	H	H	F	H	H	24-Pt
F	H	H	H	F	H	25-Pt
F	H	H	H	H	F	26-Pt
H	F	H	H	H	H	27-Pt
H	F	F	H	H	H	28-Pt
H	F	H	F	H	H	29-Pt
H	F	H	H	F	H	30-Pt
H	F	H	H	H	F	31-Pt
H	CH₃	H	H	H	H	32-Pt

3.3.1 Complex with a different main structure

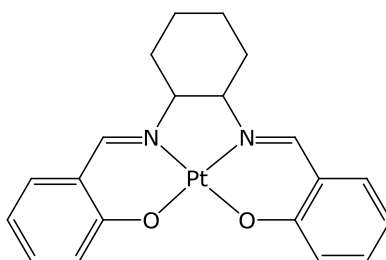


Figure 3.2 *[N,N'*-Bis(salicylidene)-*rac-trans*-1,2-cyclohexanediamine]platinum(II) (**33-Pt**).

3.4 Overview on the synthetic route

The first step of the synthesis of platinum complexes (see Section 3.5) consists of obtaining the desired diamine: 1,2-diamino-1,2-diarylethane (see Section 3.5.1) or 1,2-phenylenediamine (see Section 3.5.2), followed by preparation of the Schiff base ligands by condensation of the respective diamine with the corresponding substituted salicylaldehyde (see Section 3.5.3). Further treatment of the tetradentate ligands with the metal salt resulted in the platinum complexes (see Section 3.5.4).

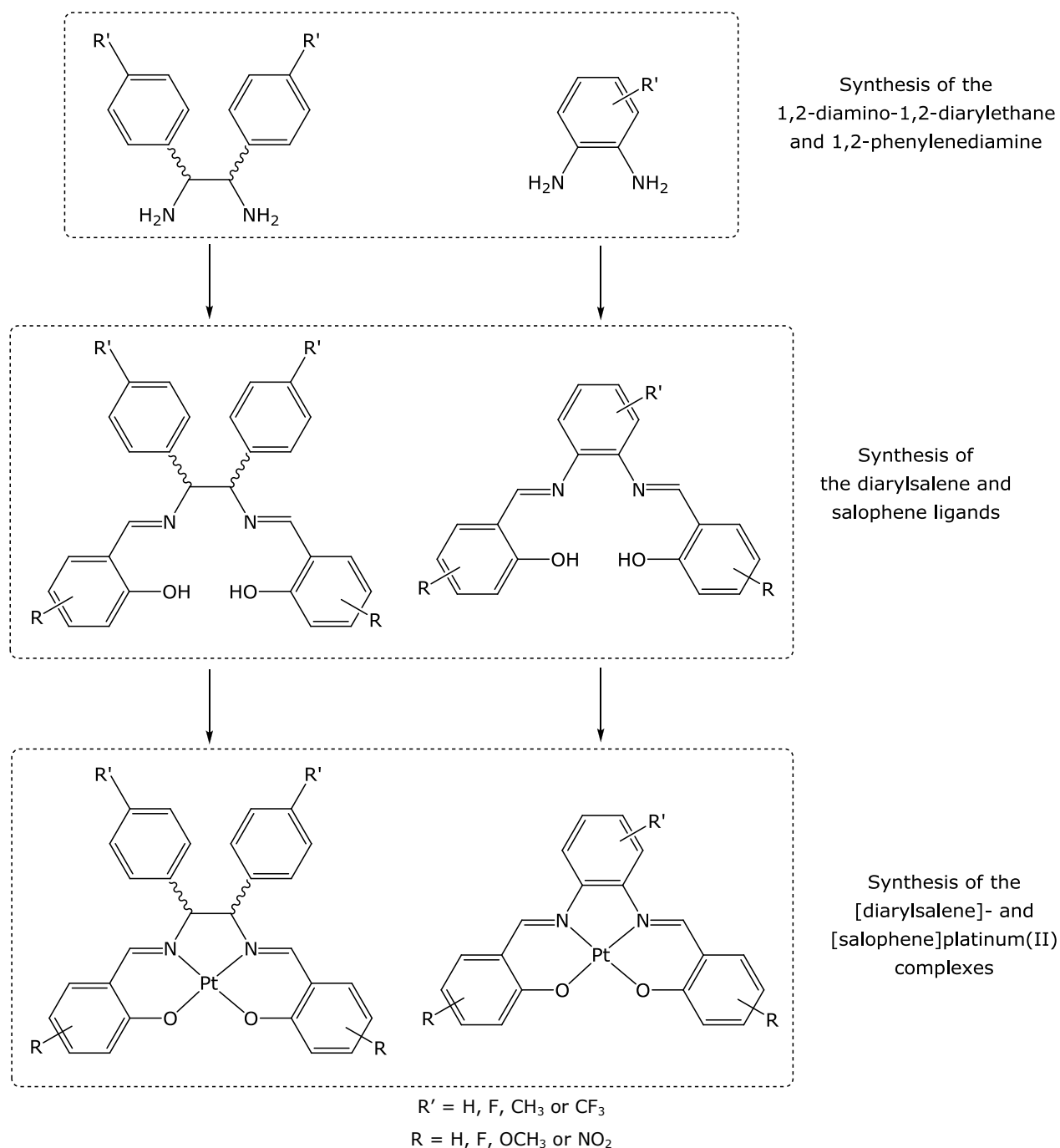


Figure 3.3 Synthesis of the Schiff base ligands and its complexes.

3.5 Synthesis of the [diarylsalene]- and [salophene]platinum(II) complexes

3.5.1 Synthesis of substituted 1,2-diamino-1,2-diarylethane

3.5.1.1 Synthesis of *meso*-1,2-diamino-1,2-bis(2-hydroxyphenyl)ethane

Over thirty years ago, Vögtle and Goldschmitt demonstrated that a diaza-Cope rearrangement reaction can be used to synthesize *meso*-configured vicinal diamines by a unified approach⁶⁸. This elegant reaction has been used to obtain the intermediate compound *meso*-1,2-diamino-1,2-bis(2-hydroxyphenyl)ethane from which the other diastereometrically pure substituted diamines are available.

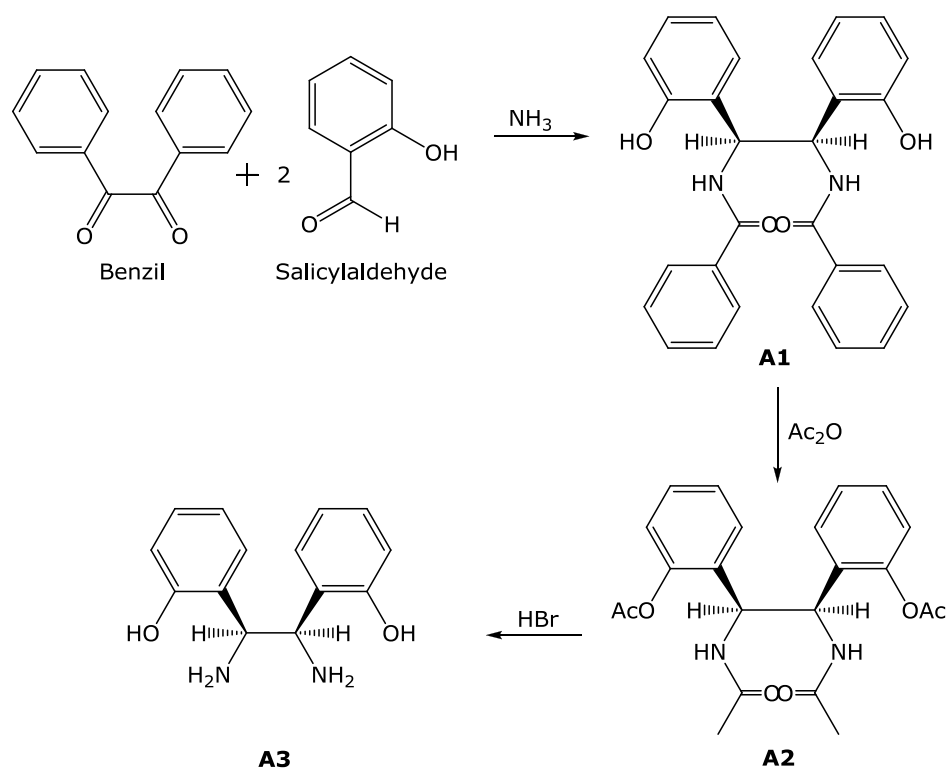


Figure 3.4 Synthesis of *meso*-1,2-diamino-1,2-bis(2-hydroxyphenyl)ethane (**A3**).

In the first step of the synthesis, ammonia was bubbled through a solution of benzil and salicylaldehyde in ethanol (Fig. 3.4). By the addition of two equivalents of the *in situ* formed salicylideneimine on benzil (**A1 α**) (Fig. 3.5), an 1,5-unsaturated diol was obtained. It suffers a [3,3]-sigmatropic rearrangement (Fig. 3.5) into a tautomer **A1 β** of the *meso*-1,2-diamino-*N,N'*-dibenzoyl-1,2-bis(2-hydroxyphenyl)ethane (**A1**). This tautomer then

leaves the rearrangement equilibrium by an irreversible proton migration, transforming into compound **A1**.

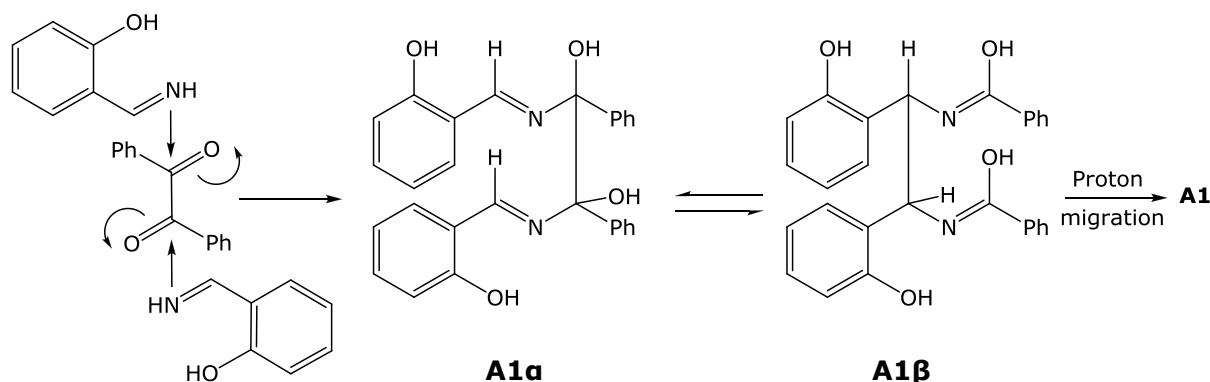


Figure 3.5 [3,3]-sigmatropic rearrangement from benzil and salicylaldehyde.

In order to understand the stereochemistry of this *meso*→*meso*-diaza-Cope rearrangement, it is necessary to take a closer look at the transition state of the reaction. The 1,5-unsaturated system has a conformation in this transition state comparable to a boat-shaped cyclohexane system with the C=N-double bond in *trans* configuration (lower energy) and the phenyl groups in equatorial position, favoring the lower energy state. This is the reason why this *meso*→*meso*-diaza-Cope rearrangement is stereoselective as long as the temperature of the reaction is kept below 120 °C⁶⁸.

In the next step, acetic anhydride is added to *meso*-1,2-diamino-*N,N'*-dibenzoyl-1,2-bis(2-hydroxyphenyl)ethane (**A1**) to obtain *meso*-*O,O',N,N'*-tetraacetyl-1,2-diamino-1,2-bis(2-hydroxyphenyl)ethane (**A2**), which will be finally hydrolyzed to *meso*-1,2-diamino-1,2-bis(2-hydroxyphenyl)ethane (**A3**) using HBr (Fig. 3.4).

3.5.1.2 Synthesis of *meso*-1,2-diamino-1,2-diarylethane

meso-1,2-Diamino-1,2-bis(4-fluorophenyl)ethane (**A4**) was synthesized by condensation of *meso*-1,2-diamino-1,2-bis(2-hydroxyphenyl)ethane (**A3**) with 4-fluorobenzaldehyde in acetonitrile (Fig. 3.6). As previously described for the synthesis of *meso*-1,2-diamino-1,2-bis(2-hydroxyphenyl)ethane (**A3**), a [3,3]-sigmatropic rearrangement is taking place.

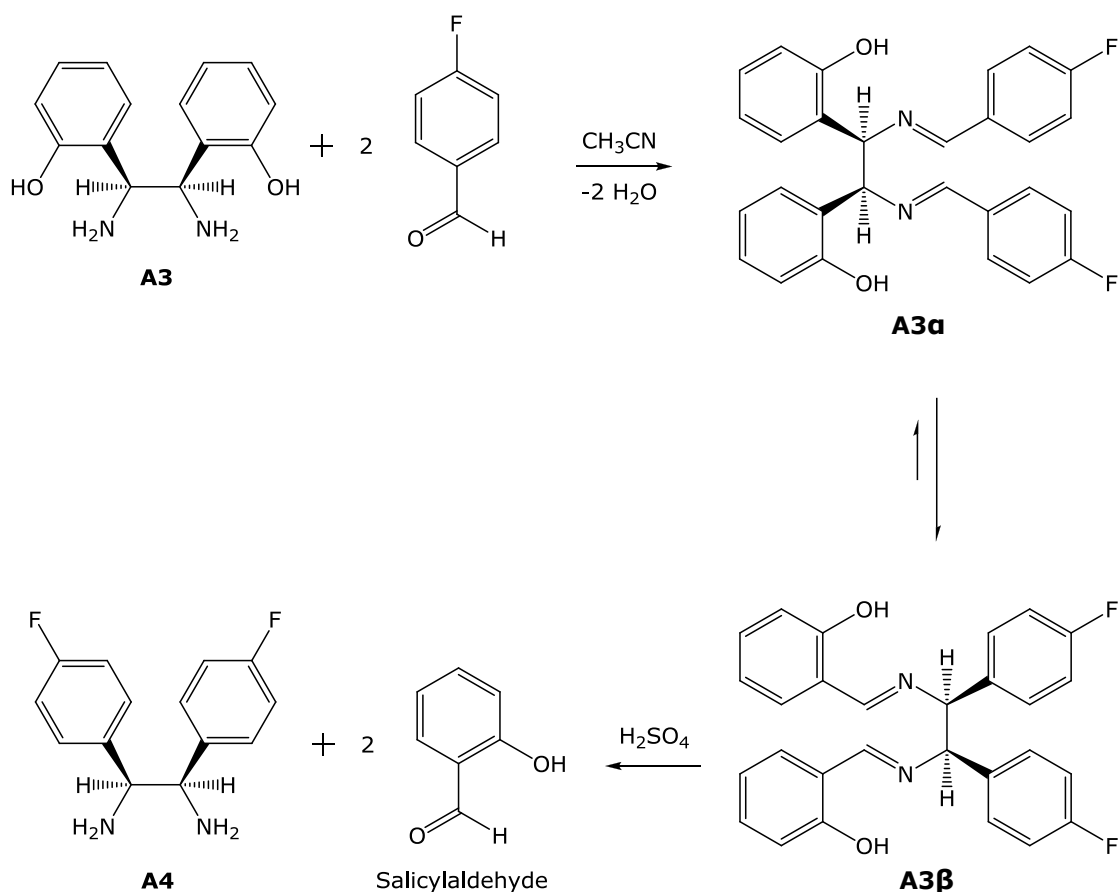


Figure 3.6 Synthesis of *meso*-1,2-diamino-1,2-diarylethane (**A4**).

Vögtle and Goldschmitt showed that the equilibrium for the [3,3]-sigmatropic shift reaction favors the formation of **A3b** over **A3a** (Fig. 3.6). Because of the “salicyl effect”, the rearrangement in this case is almost quantitative. This can be explained not only by the proton mediated catalysis of the phenolic hydroxyl groups, but also for the stronger hydrogen bonds (H-bonds) in **A3b** than in **A3a**.

Although it was suspected that internal hydrogen bonds may play a role in the selectivity⁶⁹ it was not known how much could they affect the equilibrium since both structures can form internal H-bonds (Fig. 3.7). This can be explained now by the existence of a class of unusually short, strong hydrogen bonds named Resonance Assisted Hydrogen Bonds (RAHBs)^{70,71}.

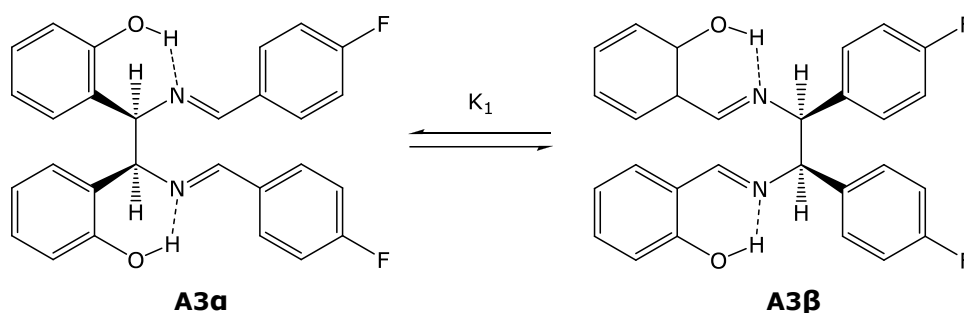


Figure 3.7 [3,3]-sigmatropic rearrangement from to **A3a** to **A3β** .

RAHB is a model of synergistic interplay between π -delocalization and H-bond strengthening. They can be reduced to the formula $\cdots\mathbf{A}=\mathbf{R}_n\mathbf{-DH}\cdots$, where **A** is the H-bond acceptor atom, **D** is the H-bond donor atom, and **R_n** is a resonant spacer of *n* atoms which form a chain of alternating single and double bonds⁷².

The intramolecular H-bonds in salicyl imines (Fig. 3.8) have been thoroughly characterized as RAHBs on the basis of crystallographic-, NMR-, IR-, and computational data^{70,71}.

According to Gilli *et al.*⁷², stabilization by resonance (in a RAHB, like in structure **A3β**) permits overpassing of the steep increase of the interatomic repulsion term when the **A \cdots D** distance is shortened and contributes to formation of a symmetrical and totally delocalized three-center four-electron covalent **A \cdots H \cdots D** bond. Such delocalization becomes a factor increasing the strength of the intramolecular H-Bond^{72,73}. This delocalization is not possible in **A3a**⁷¹.

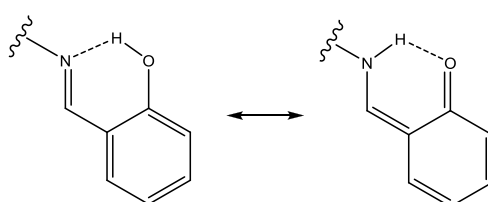


Figure 3.8 Resonance structures of **A3β**.

In order to obtain the *meso*-1,2-diamino-1,2-bis(4-fluorophenyl)ethane (**A4**), *meso*-3,4-bis(4-fluorophenyl)-1,6-bis(2-hydroxyphenyl)-2,5-diazahexa-1,5-diene (**1**) was hydrolyzed with 6 N H₂SO₄. It is important to note that to favor a quantitative reaction, the forming salicylaldehyde must be removed of the mixture by steam distillation. The free diamine can be isolated with high purity by treatment of the sulfate of *meso*-1,2-diamino-1,2-bis(4-fluorophenyl)ethane with 1 N NaOH and extraction with

dichloromethane. This is possible since the reactants that could not be hydrolyzed and the salicylaldehyde that was not removed with the steam distillation are easily soluble in alkaline solutions (Fig. 3.6).

3.5.1.3 Synthesis of *d,l*-1,2-diamino-1,2-diarylethane

While diaza-Cope rearrangements at temperatures below 120 °C remains *meso*→*meso* stereoselective, at higher temperatures (> 120 °C) a partial *meso*→*d,l* stereoisomerization takes place^{68,74}.

This high temperature stereoisomerization was used to synthesize the *d,l*-1,2-diamino-1,2-bis(4-fluorophenyl)ethane using the congeneric substituted tetraaryl diimine (**A5**) as starting material.

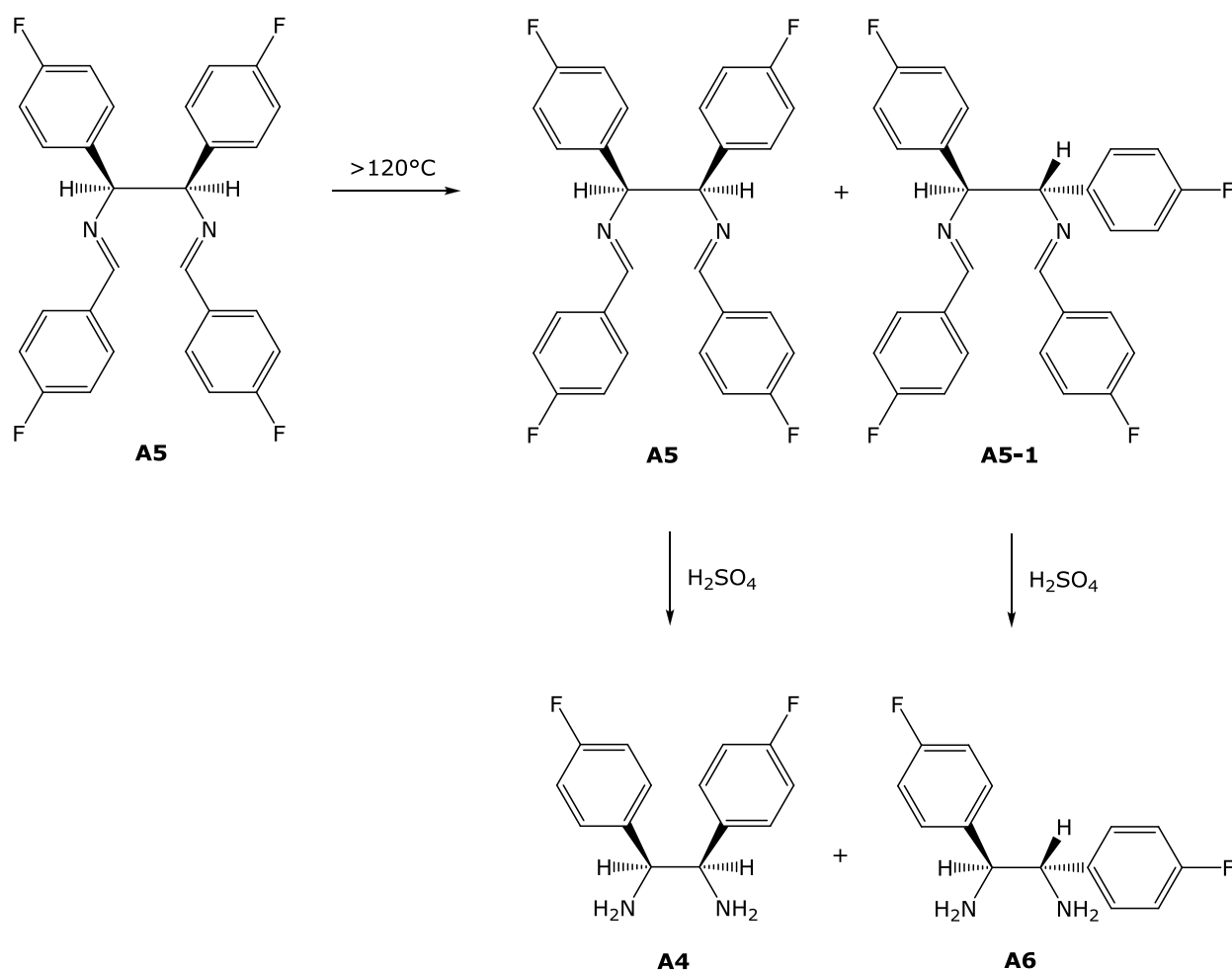


Figure 3.9 Synthesis of *d,l*-1,2-diamino-1,2-diarylethane (**A6**).

The stereomerization was performed by heating a solid sample of *meso*-1,3,4,6-tetrakis(4-fluorophenyl)-2,5-diazahexa-1,5-diene (**A5**) to 210-220 °C. Thereafter, 3 N H₂SO₄ was added and the forming 4-fluorobenzaldehyde was removed by steam distillation. The diastereomeric bases can be easily separated since the salt of the *meso*-diamine is rather soluble in hot water and the sulfate of the *d,l*-diamine precipitates as white plates (Fig. 3.9).

3.5.2 Synthesis of substituted phenylenediamine

1,2-Phenylenediamine and 4-fluoro-1,2-phenylenediamine were commercially available and used without further purification in the synthesis of the respective ligands. In the case of the 3-fluoro-1,2-phenylenediamine, the synthesis involved three steps.

The main reaction was the introduction of an amine nucleophile into an electrophilic aromatic ring *via* vicarious nucleophilic substitution (VNS) of hydrogen. VNS reactions are a special case of nucleophilic aromatic displacement of hydrogen (S_N^H) reactions in π -deficient aromatic compounds^{75,76} (Fig. 3.10).

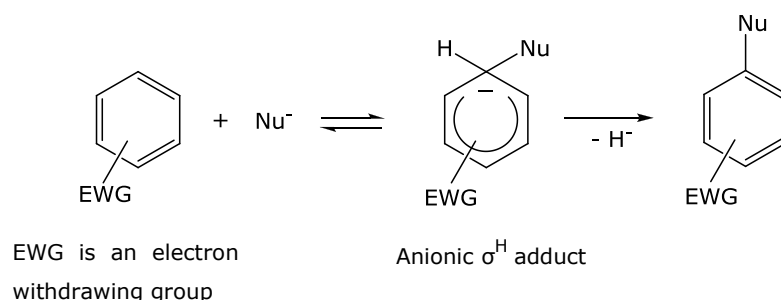


Figure 3.10 Nucleophilic aromatic substitution of hydrogen.

The anionic σ^H adducts, which are derived from a nucleophilic attack on unsubstituted carbon of an aromatic ring, presents difficulties associated with elimination of the hydrogen with a pair of electrons (a hydride ion). In the case of the VNS reactions this step is mediated by an auxiliary group (a nucleophile) that facilitates the elimination of hydrogen as a proton^{75,76}. In this work, 1,1,1-trimethylhydrazinium iodide (TMHI) has been used as VNS reagent for the introduction of an amino group into nitroaromatic substrates⁷⁷.

3.5.2.1 Synthesis of 1,1,1-trimethylhydrazinium iodide

The preparation of quaternized hydrazine halides, including TMHI, has been previously reported^{78,79}. These compounds can be prepared by the reaction of 1,1-disubstituted hydrazine with an alkyl halide (Fig. 3.11).

The alkylation generally occurs at the more substituted nitrogen, provided steric effects do not interfere. When an alkyl halide free of electron acceptor or bulky groups is used, the hydrazine becomes more basic upon substitution, which facilitates further alkylation⁸⁰.

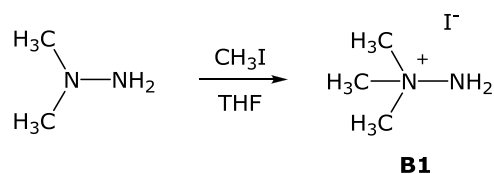


Figure 3.11 Synthesis of 1,1,1-trimethylhydrazinium iodide (TMHI).

In this case, methyl iodide reacts with 1,1-dimethylhydrazine in THF to give the desired 1,1,1-trimethylhydrazinium iodide (**B1**) as white pellets.

3.5.2.2 Synthesis of 2-fluoro-6-nitroaniline

As mentioned, 2-fluoro-6-nitroaniline has been synthesized using a VNS hydrogen reaction with an amine nucleophile (TMHI) as reagent. These reagents are of the common form of XNH_2 , where X is an auxiliary group capable of stabilizing a negative charge. The anionic σ^{H} adducts formed *via* addition of such nucleophiles to nitroaromatic rings undergo base induced β -elimination of HX to give anionic products, which upon protonation, leads to rearomatization of the σ -intermediate adduct⁷⁶. TMHI (or its corresponding ylide, which may be produced upon reaction with strong base) as nucleophilic reagent is sufficiently nucleophilic to attack nitro-substituted aromatic rings with the neutral trimethylamine as efficient leaving group⁷⁷.

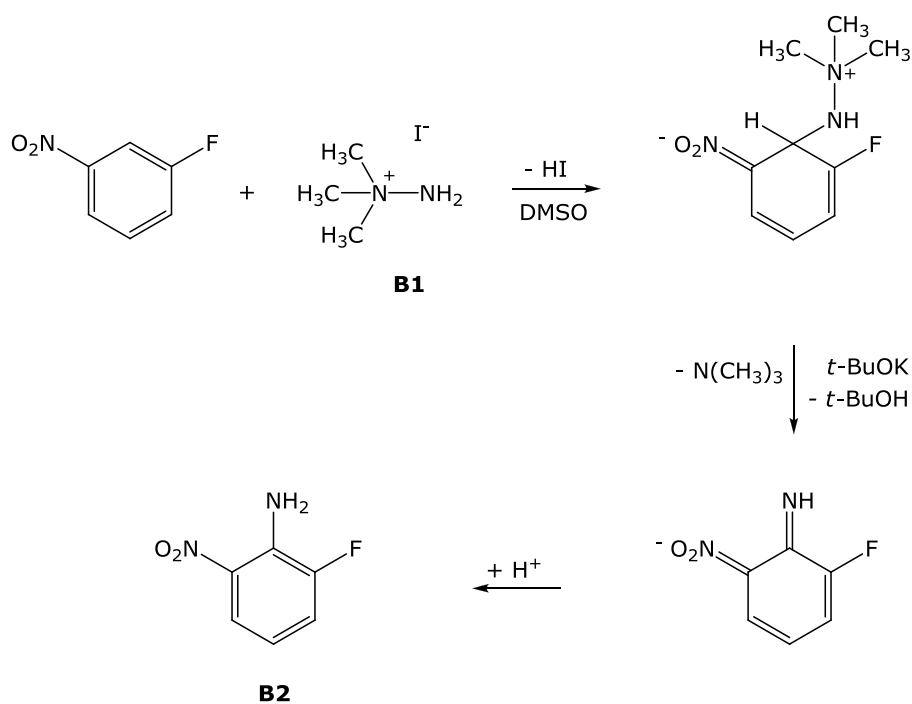


Figure 3.12 Synthesis of 2-fluoro-6-nitroaniline (**B2**).

TMHI was dissolved in a solution of 3-fluoro-nitrobenzene in dry DMSO, and solid alkoxide base was added upon stirring. The reaction was quenched with HCl, followed by an extraction of the remaining solution (Fig. 3.12).

As amination occurs at the *ortho* and *para* position to the nitro group (Fig. 3.13), the 2-fluoro-6-nitroaniline (**a**) must be separated from the isomers **b** and **c** by silica gel chromatography.

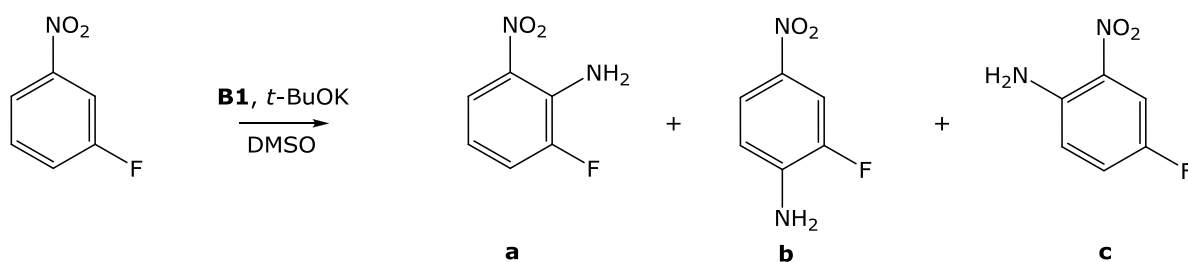


Figure 3.13 Amination of 3-fluoro-nitrobenzene with TMHI (**a**: 2-fluoro-6-nitroaniline; **b**: 2-fluoro-4-nitroaniline and **c**: 4-fluoro-2-nitroaniline).

3.5.2.3 Synthesis of 3-fluoro-1,2-phenylenediamine

Bellamy and Ou reported in 1984 the selective reduction of aromatic nitro compounds with stannous chloride in a non acidic and non aqueous medium⁸¹.

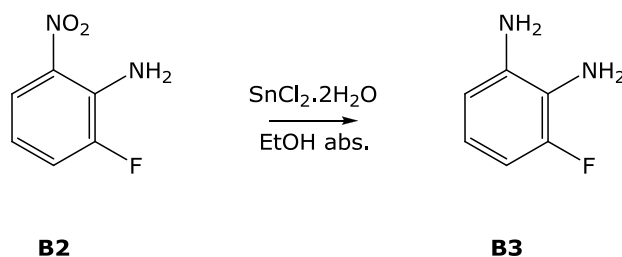


Figure 3.14 Reduction of 2-fluoro-6-nitroaniline into 3-fluoro-1,2-phenylenediamine.

A mixture of one equivalent of 2-fluoro-6-nitroaniline (**B2**) and 5 equivalents of SnCl₂·2H₂O in absolute ethanol was heated under nitrogen atmosphere. After 30 min (completion of reaction) the solution was allowed to cool down to room temperature and poured on ice. The pH was made slightly basic before extraction with ethyl acetate. After evaporation of the solvent 3-fluoro-1,2-phenylenediamine (**B3**) remained as a black solid (Fig. 3.14).

3.5.3 Synthesis of the diarylsalene and the salophene ligands

The compounds used as ligands are Schiff bases⁸². They have the general formula Ar-CH=N-R and were prepared by the condensation of diamine (1,2-diamino-1,2-diarylethane or 1,2-phenylenediamine) with two equivalents of substituted salicylaldehyde. In these kind of compounds, the unsaturated -CH=N- bond permits π -electronic coupling between the acidic and the basic centers of the molecule. As described earlier, they present two asymmetric intramolecular hydrogen bonds formed between the oxygen and the nitrogen atoms. Additionally, these hydrogen bonds form planar six-membered chelate rings. For these reasons they are called pseudoaromatic chelate rings⁸³.

In the case of the synthesis of the diarylsalene ligands, the diamine was dissolved in absolute acetonitrile with two equivalents of the substituted salicylaldehyde. The reaction mixture was stirred at reflux for 4 h, cooled down, and the resulting precipitate was collected (Fig. 3.15).

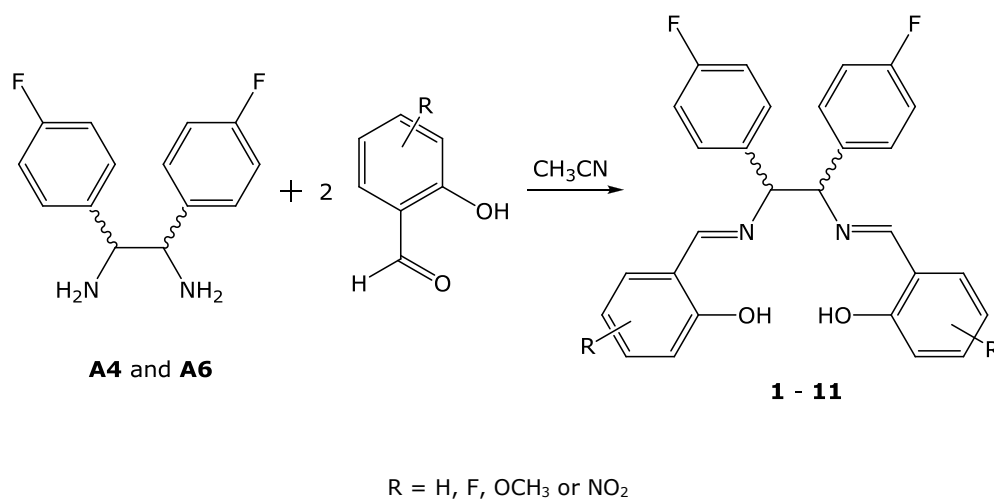


Figure 3.15 Synthesis of the diarylsalene ligands.

The synthesis of the salophene ligands proceeds in the same fashion as was described for the diarylsalene ligands with the exception of ethanol being used as solvent (Fig. 3.16).

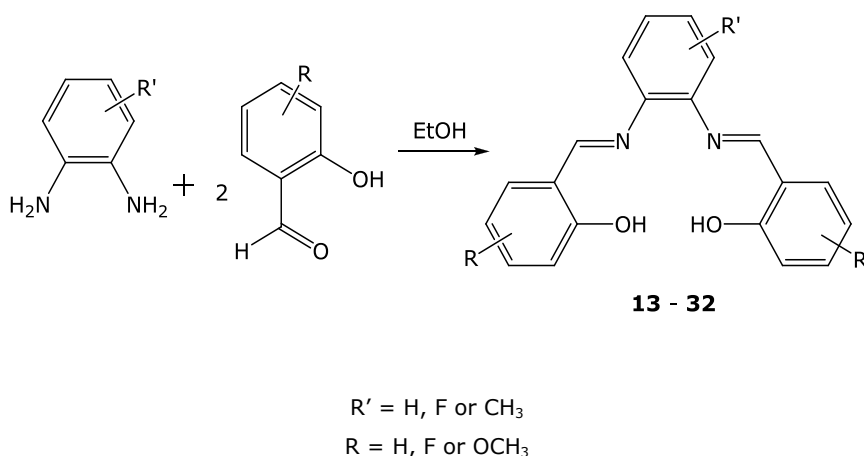


Figure 3.16 Synthesis of the salophene ligands.

3.5.4 Synthesis of the [diarylsalene]- and [salophene] platinum(II) complexes

The [diarylsalene]platinum(II) and the [salophene]platinum(II) complexes were synthesized as previously described by Tong *et al.*⁸⁴. They were obtained from the gently heated reaction mixture of the tetradentate ligands, potassium carbonate and potassium tetrachloroplatinate(II) in DMSO (Fig. 3.17).

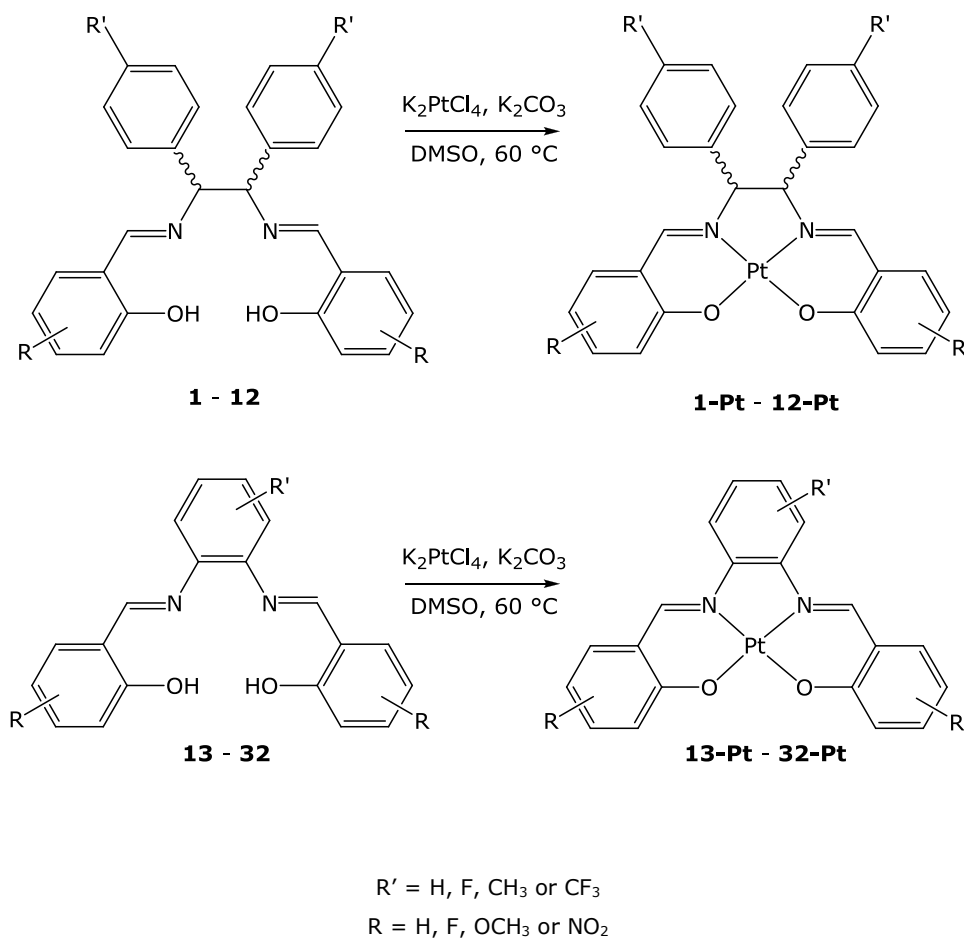


Figure 3.17 Synthesis of the platinum(II) complexes.

Platinum is one of the late row transition metals and forms with ligands containing the N_2O_2 donor center diamagnetic neutral Schiff base complexes. The two positive charges of the original platinum(II) ion are cancelled by the two negative charges supplied by the alkoxides. These complexes have planar square molecular geometry (see the two structures on the left of Fig. 3.17).

4 Spectrometric Analysis

4.1 $^1\text{H-NMR}$ Spectroscopy

The structural characterization of the ligands and platinum complexes reported in this work was performed using $^1\text{H-NMR}$ spectroscopy. All ^1H spectra were referenced against TMS (tetramethylsilane).

4.1.1 Diarylsalene and salophene ligands

In the case of the diarylsalene ligands, there is a free rotation about the central C-C bond. This leads to three staggered conformations: two structures with a *gauche* and one with an *anti* conformation. Previous crystallographic studies showed that the substituted 3,4-diphenyl-1,6-bis(2-hydroxyphenyl)-2,5-diazahexa-1,5-diene in *meso* configuration has an *anti* conformation⁷⁰.

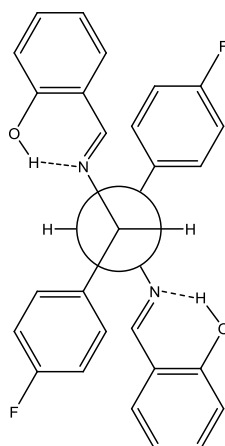


Figure 4.1 Newman projection of **1** in the *anti* conformation.

In this *anti* conformation (Fig. 4.1), the azomethine protons (NCH) are in the region above the aryl groups, and suffer a shielding effect that reflects upfield of the signals of the above mentioned protons. This effect was used to characterize the *meso* and *d,l* structures. The azomethine protons in *meso*-3,4-bis(4-fluorophenyl)-1,6-bis(2-hydroxyphenyl)-2,5-diazahexa-1,5-diene (**1**) show a chemical shift δ [ppm] of 8.45 against 8.56 in the *d,l*-3,4-bis(4-fluorophenyl)-1,6-bis(2-hydroxyphenyl)-2,5-diazahexa-1,5-diene (**2**) (see Fig. 4.2).

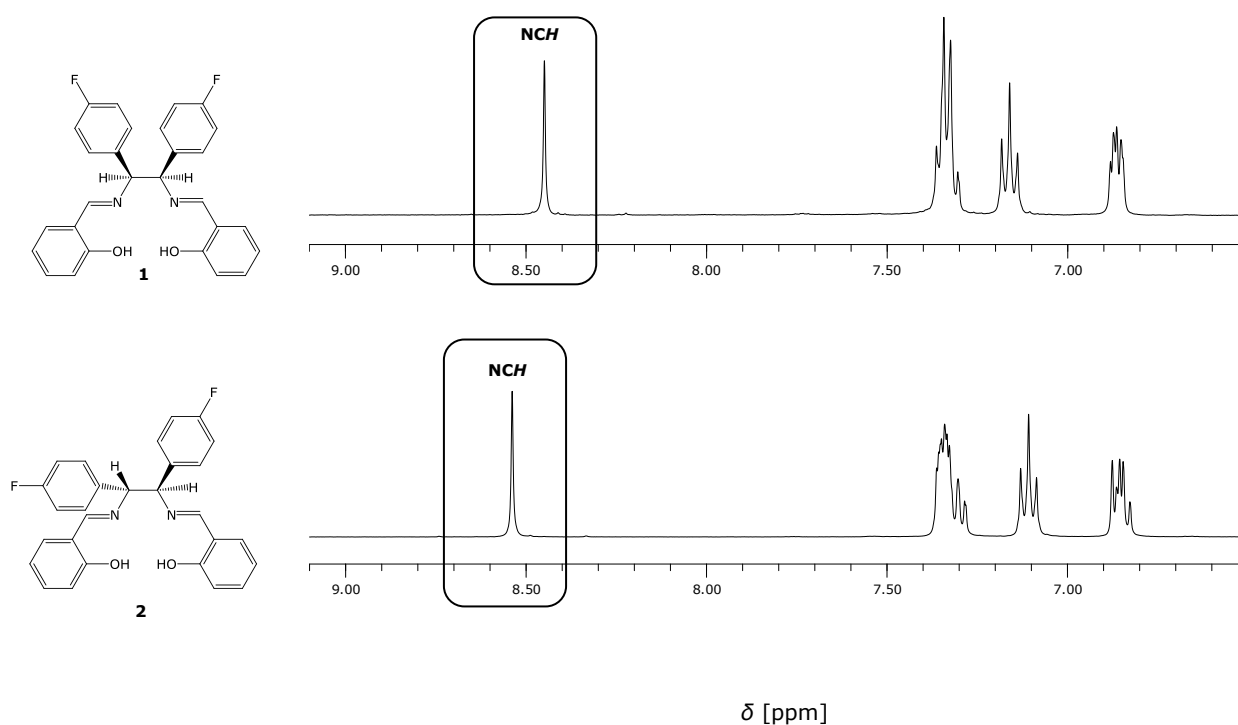


Figure 4.2 ^1H -NMR spectra of the ligands **1** (above) and **2** (below) in $\text{DMSO-}d_6$. Remarked are the peaks corresponding to the azomethine protons in both cases.

While the resonance of the azomethine proton was nearly identical for all the diarylsalene ligands ($\delta = 8.30 - 8.70$), the position (*ortho*, *meta* or *para*), much more than the kind ($-\text{F}$, $-\text{OCH}_3$ or $-\text{NO}_2$) of substituent located in the salicylidene moiety, affected the OH signals ($\delta = 12.60 - 14.30$). It is important to emphasize that the resonance of the OH group is downfield-shifted relative to the signal for phenolic protons of regular H-bonds⁷⁰. This paramagnetic shift is as expected for Resonance-Assisted Hydrogen Bonds (RAHBs)^{70,71} (see Section 3.5.1.2).

Substituents ($-\text{F}$ or $-\text{OCH}_3$) located in *ortho* or *para* position shifted the OH signal to a higher field (**6**: $\delta = 12.41$) compared to that of the *meta* derivatives (**7**: $\delta = 13.97$) (Fig. 4.3). It is possible to compare the effect of fluorine and methoxy substitution for each position (Fig. 4.3: ligands **6** and **10**). We can observe that an electron donating substituent like the methoxy group has a more pronounced shielding effect on the OH proton, causing a larger diamagnetic shift (**6**: $\delta = 12.41$), compared to the fluoro substituted analog (**10**: $\delta = 12.68$).

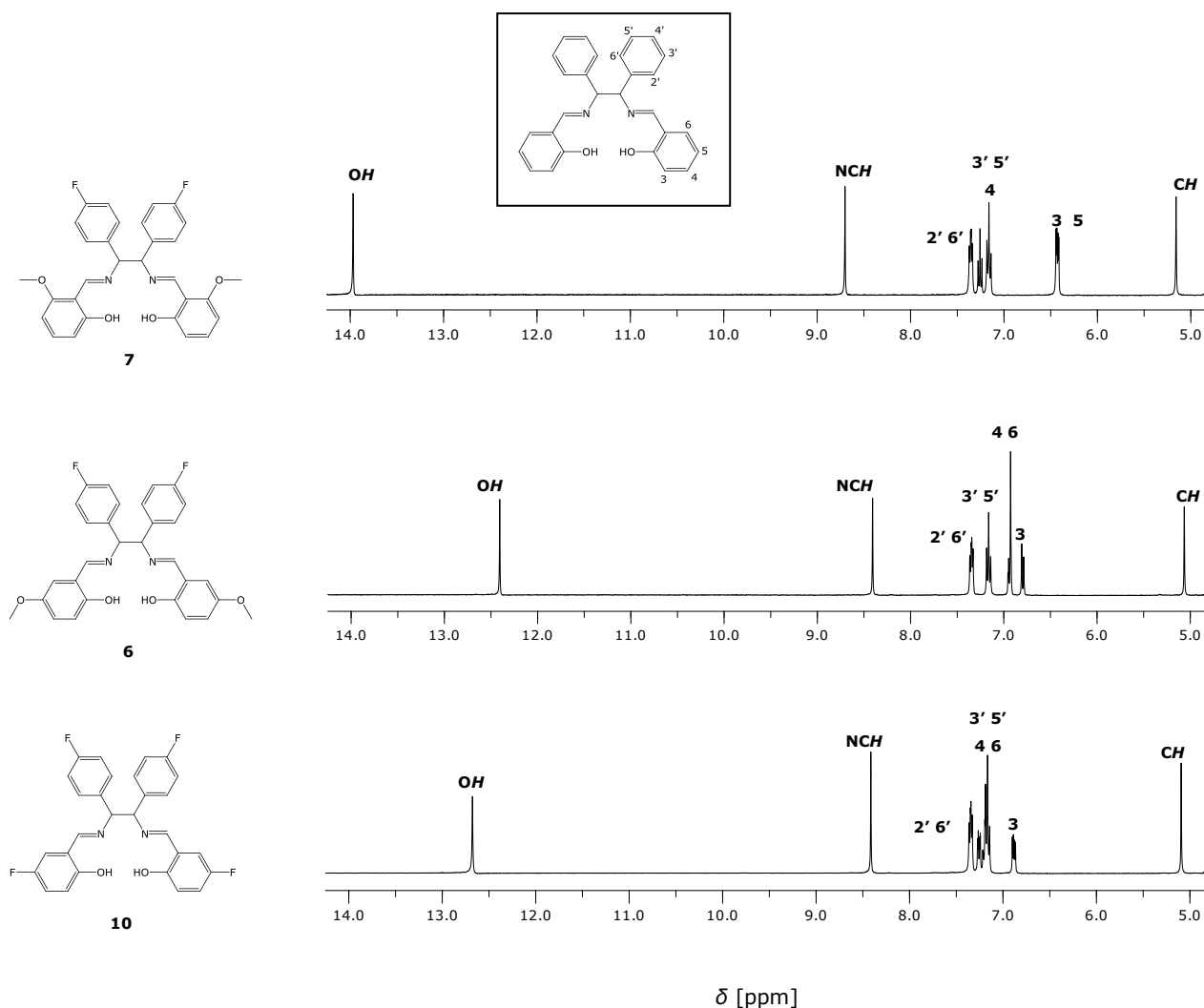


Figure 4.3 ¹H-NMR spectra of the ligands **7** (above), **6** (middle) and **10** (below) in DMSO-*d*₆. The main structure of the diarylsalene ligands with the numbering of the different positions is shown in the inset.

The OH signal reaches $\delta = 14.22$ if the compound is substituted at the *para* position with a strong electron-withdrawing group like the -NO₂ group (**3**). In this case, the signal was shifted downfield even though the substituent was in the *para* position.

As expected, similar chemical shift of the OH signal is seen in the spectra of salophene ligands, since they have similar substitution pattern on the salicylidene moiety. These observed shifts might be the consequence of changes of the electron density in oxygen, which produces RAHBs of different strength.

The resonance signals of the phenylene moiety, in the case of the salophene ligands, and the diarylethane moiety, in the case of the diarylsalene ligands, appear in the same region irrespective of the substituent located at the salicylidene. This indicates that the electron density within the aromatic rings is not significantly affected.

It is known that proton signals in the ^1H -NMR spectra are not only split by other protons but are also by other NMR-active nuclei that are nearby in the bonding network^{85,86}. In this work long-range (> 3 bonds) couplings with ^{19}F (J_{HF}) were often observed on fluorinated salicylidene moieties. A special phenomenon was observed on the ^1H -NMR spectra of the salophene compounds bearing a fluorine in position R'_3 (**22**, **23**, **24**, **25**, **26** and the respective complexes). A coupling arising because of the spatial approaching interacting nuclei ^1H (NCH) and ^{19}F ($\text{R}'_3 = \text{F}$) was found in these kind of compounds. As an example of this effect it is shown in Fig.4.4 the spectrum of **22** ($\text{R}'_3 = \text{F}$, $\text{R}'_4 = \text{H}$).

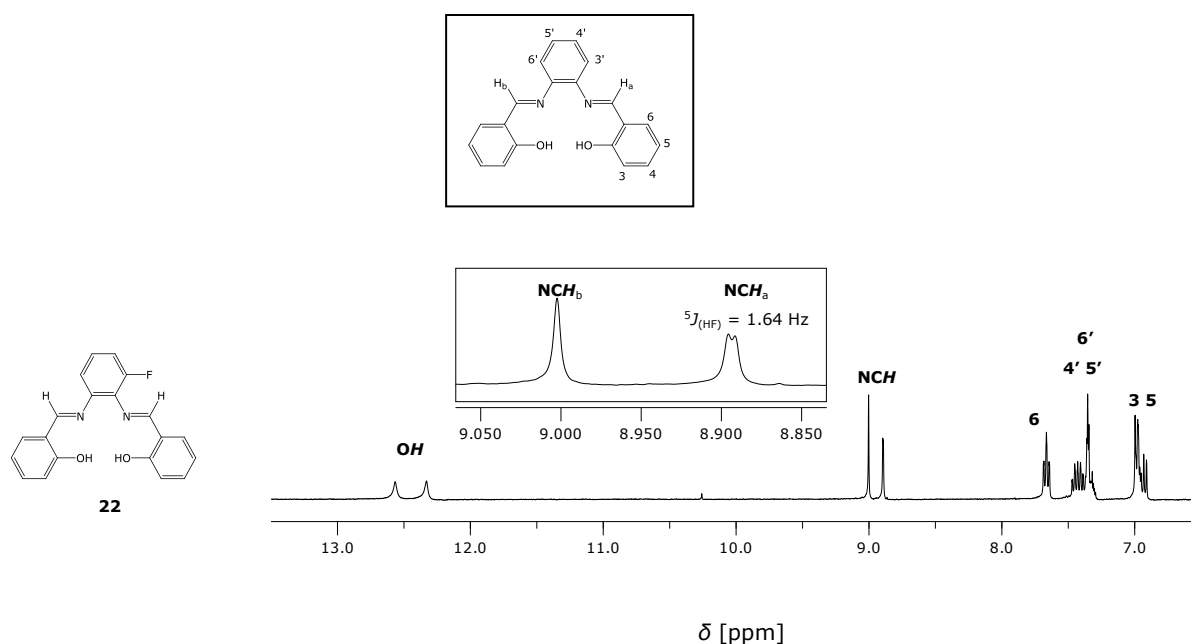


Figure 4.4 ^1H -NMR spectrum of **22** in $\text{DMSO-}d_6$. Zoom is made over the peaks corresponding to the azomethine protons. The main structure of the salophene ligands with the numbering of the different positions is shown in the inset above the spectrum.

Comparing the spectrum of **22** (Fig. 4.4) with the ones of **13** and **27** (Fig. 4.5, above and below respectively) it can be clearly deduced that the coupling of H_a in compound **22**, is due to a spin-spin interaction with the ^{19}F present in position R'_3 of the phenylene moiety. In compound **13**, the molecule is symmetric and the NCH protons appear as one singlet, while in compound **27** they appear as two singlets due to asymmetry generated by the fluorine on position R'_4 . Moreover, in **22** the azomethine protons are present as a singlet (H_b) and a doublet (H_a) with a coupling constant $^5J_{(\text{HF})} = 1.64$ Hz.

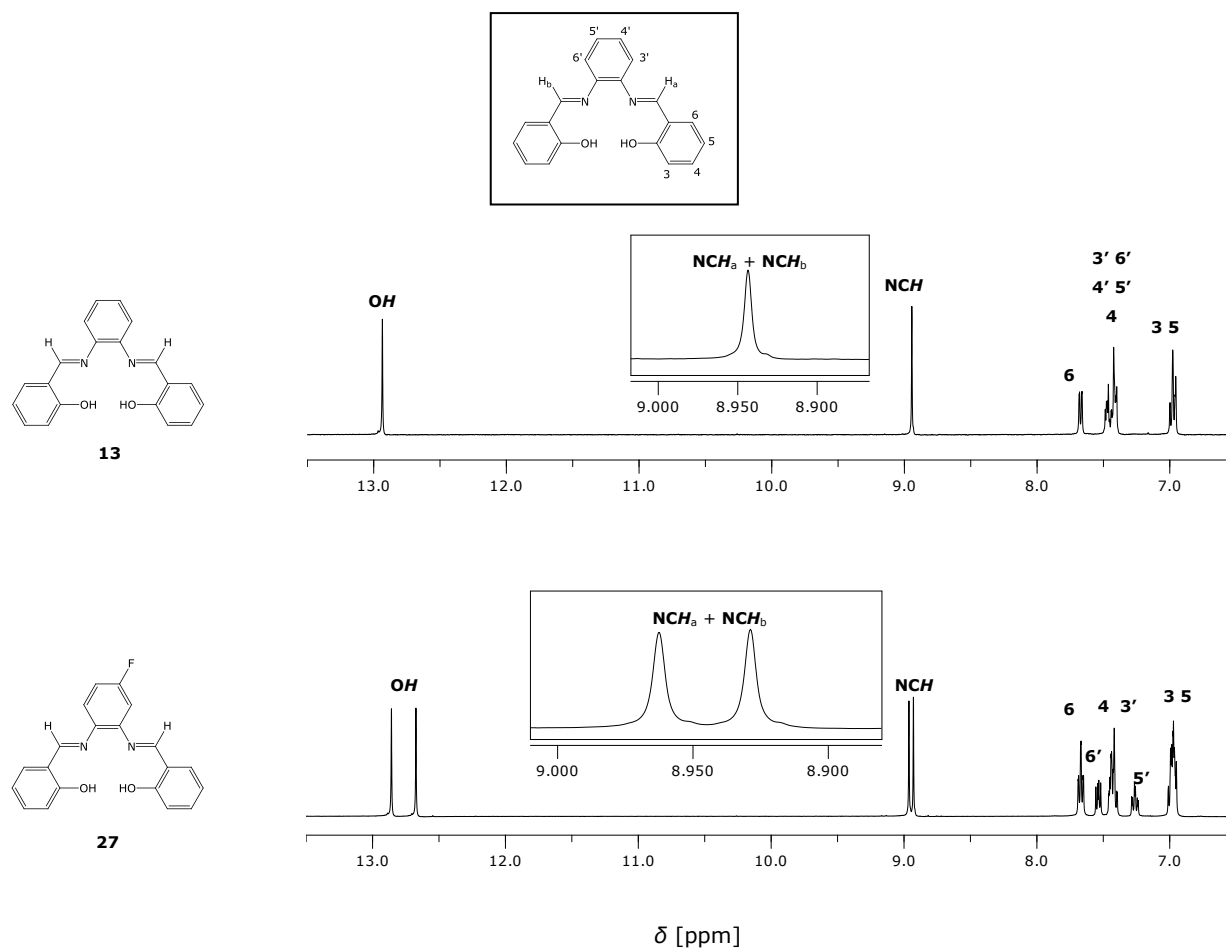


Figure 4.5 The same as for Fig. 4.4, but for **13** (above) and **27** (below).

Through-space nuclear spin-spin coupling between nuclei belonging to molecular fragments which are proximate in space is a well documented phenomena and has been intensely experimentally and theoretically studied^{87,88}. Comparing the spectra of compounds **21**, **26** and **31** (Fig. 4.6 above, middle and below respectively) further information on the ^1H - ^{19}F coupling could be deduced. In these compounds, fluorine as substituent was introduced in position R_6 of the salicylidene moiety. This could supposedly generate spin-spin coupling between the fluorine and the azomethine protons, since there are four bonds between the two nuclei ($^4J_{(\text{HF})}$). Contrary to this, in the spectrum of compound **21** (Fig. 4.6 above) the NCH protons appear as one singlet and in the spectrum of **31** (Fig. 4.6 below) as two singlets due to asymmetry generated by the fluorine on position R'_4 , as in the spectrum of compound **27** (Fig. 4.5 below). Surprisingly, by the introduction of a fluorine in position R'_3 of the phenylene moiety (**26**, Fig. 4.6 middle) the NCH protons appear, overlapped with each other, as a singlet (H_b) and a doublet (H_a).

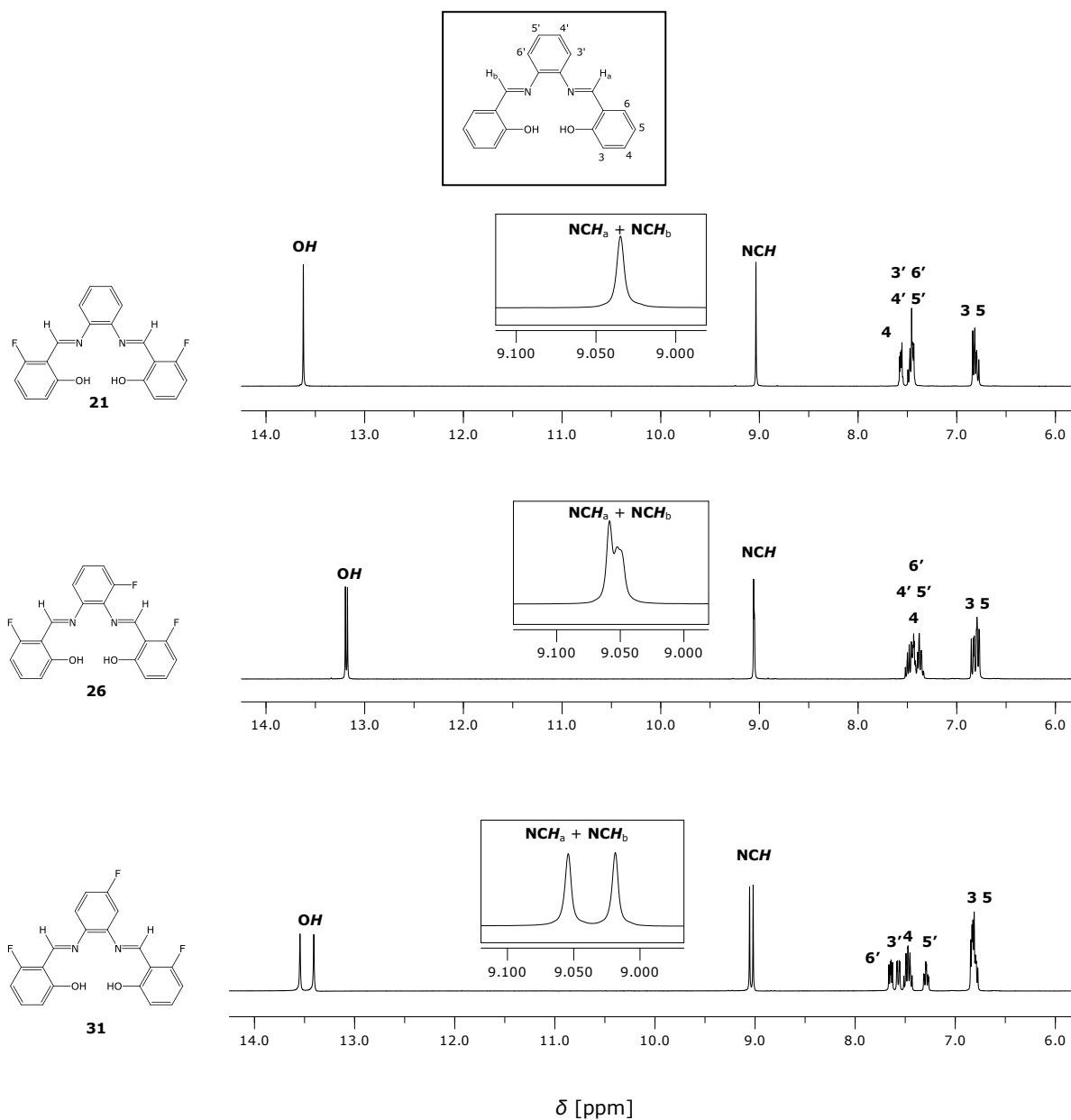


Figure 4.6 The same as for Fig. 4.4, but for **21** (above), **26** (middle) and **31** (below).

This data suggests that in compounds **22** and **26** there is a coupling arising because of spatial approaching of the NCH proton and the R'_3 fluorine, in view of the fact that this effect can be seen in these cases (**22** and **26**) but not in the spectra of **21** and **31**, even though the number of bonds between the possible interacting nuclei is four instead of five (Fig. 4.7).



Figure 4.7 Molecular structure of **21** and **22**. Marked in a circle are the possible interacting ^1H - ^{19}F nuclei, the numbering corresponds to the bonds between them.

4.1.2 [Diarylsalene]- and [salophene]platinum(II) complexes

The coordination of diarylsalenes and salophenes with platinum(II) and the building of a square-planar chelate⁸⁹ complex led to changes in the ^1H -NMR spectra allowing the characterization of the molecule.

The resonance signal of the phenolic OH groups completely disappeared in all cases upon coordination. This confirms the bonding of oxygen to the metal ions (C–O–M). The resonance signal of the aromatic protons, as well as the signal of the azomethine proton shifted in different directions (Figs. 4.8 and 4.9). The aromatic protons of the salicylidene moiety, in most of the complexes, were shifted to higher field. H₅, as an exception appeared at lower field.

In the case of the [diarylsalene]platinum(II) complexes the resonance signals of the diarylethane moiety and the azomethine proton suffered a diamagnetic shift ($\Delta \delta < 0$), while the ones at the ethane bridge suffered a paramagnetic shift ($\Delta \delta > 0$) (Fig. 4.8).

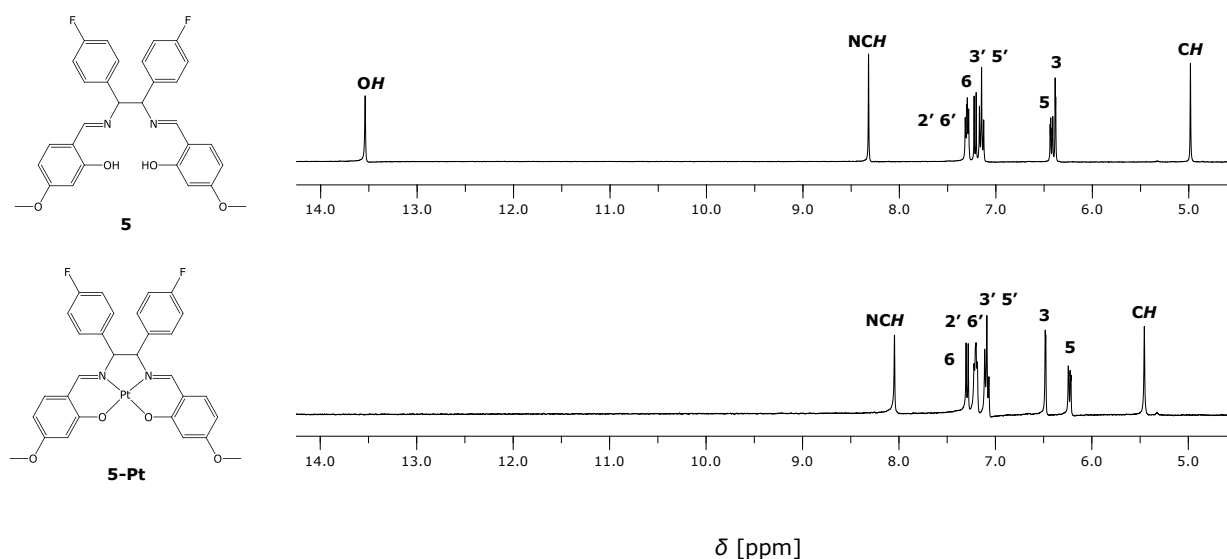


Figure 4.8 ^1H -NMR spectra of **5** and **5-Pt** in $\text{DMSO}-d_6$.

A different pattern of shifts could be seen in the [salophene]platinum(II) complexes: while the signals of H'₄ and H'₅ in the phenylene moiety were not significantly affected upon coordination. H'₃, H'₆ and the azomethine proton were characteristically shifted about $\Delta \delta = 1$ (from 7.3 - 7.6 to 8.2 - 8.5) (Fig. 4.9).

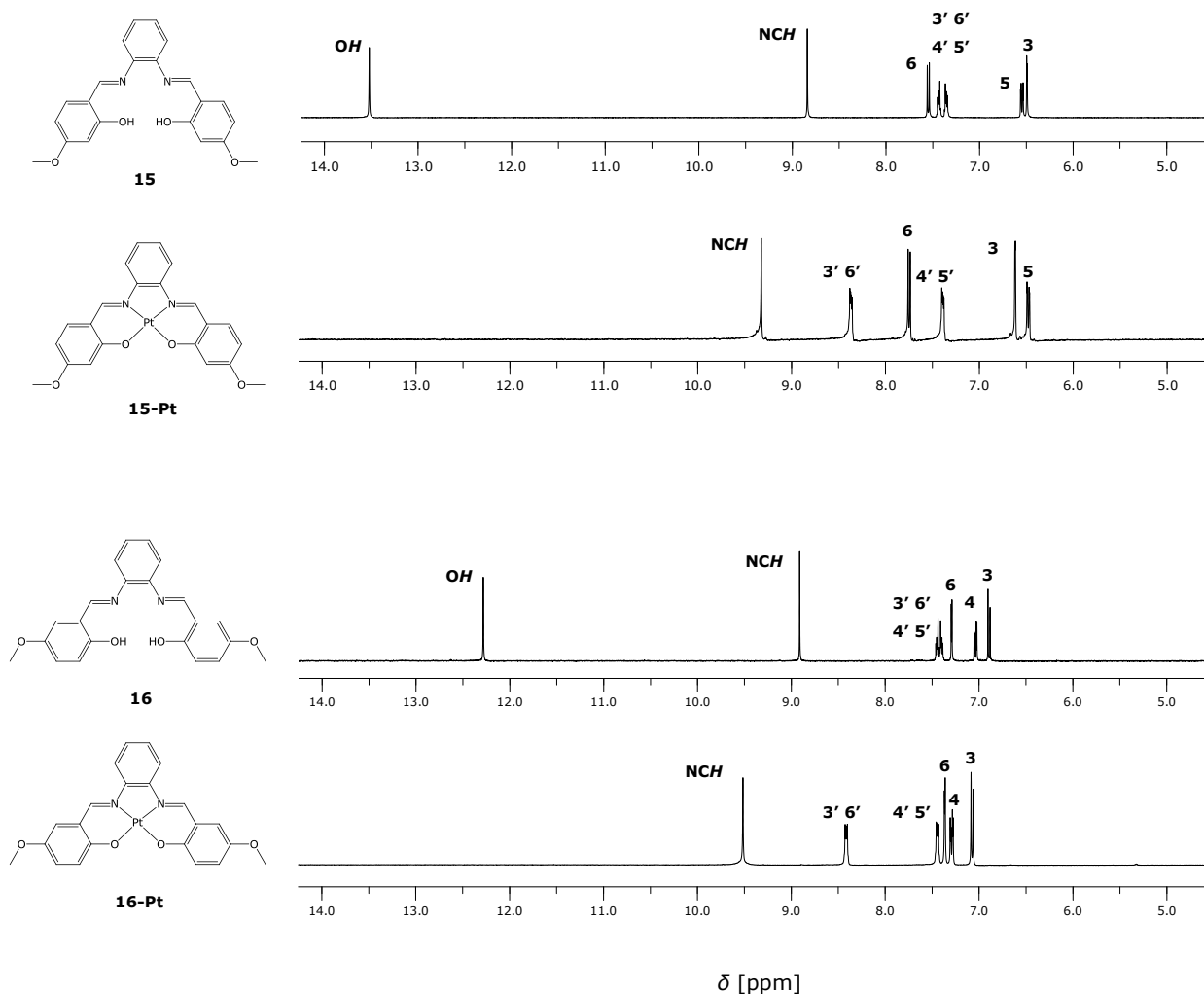


Figure 4.9 ¹H-NMR spectra of **15**, **15-Pt**, **16** and **16-Pt** in DMSO-*d*₆.

The observed paramagnetic shift in the azomethine proton of the [salophene]platinum(II) complexes might be the consequence of anisotropy⁹⁰ associated to the phenylene ring. Upon coordination this structure becomes almost planar (see Section 4.4) which means that the position of the azomethine proton is in the same plane and at the edge of the aromatic ring. It is well known that in the external (B_0) magnetic field, the π -electrons of an aromatic ring circulate and generate a supporting paramagnetic field at the edge of the ring. This produces a characteristic deshielding effect that leads to the downfield shifting of the azomethine protons. Moreover, this effect could explain also the resonance of protons on aromatic rings at unexpectedly low fields.

The [diarylsalene]platinum(II) complexes are non-planar structures. The rings from the diarylethane moiety can rotate around the C-C single bond of the benzyl group and the C of the ethane bridge have sp^3 hybridization, which leads to a tetrahedral geometry. On the other hand, the rings of the diarylethane moiety are in β position⁹¹ to the azomethine group while in the [salophene]platinum(II) complexes the phenylene ring is in α position. Consequently, the azomethine proton might be not in the deshielding region caused by the aromatic rings of the diarylethane moiety. Furthermore, we can observe a differential diamagnetic shift of the azomethine proton of the [diarylsalene]platinum(II) complexes.

4.2 Mass spectrometry

High resolution mass spectrometry was used to identify the composition (from exact mass determination) and the purity of the platinum complexes.

Electrospray-Ionization (ESI) in positive voltage mode was used as the ionization method. ESI is a gentle ionization process and typically yields "Quasi molecule ions" with little or no fragmentation. The platinum complexes are neutral (M). Therefore, they ionize by aggregation with a solution cation (X^+) to give detectable $[M+X]^+$ positive ions. TOF (Time of Flight) detector was used for analysis.

Here, as an example, is the mass spectra of **32-Pt**. It can be recognized by the typical signal for the ions $[M+X]^+$ and $[2M+X]^+$ (Figs. 4.10, 4.11 and 4.12).

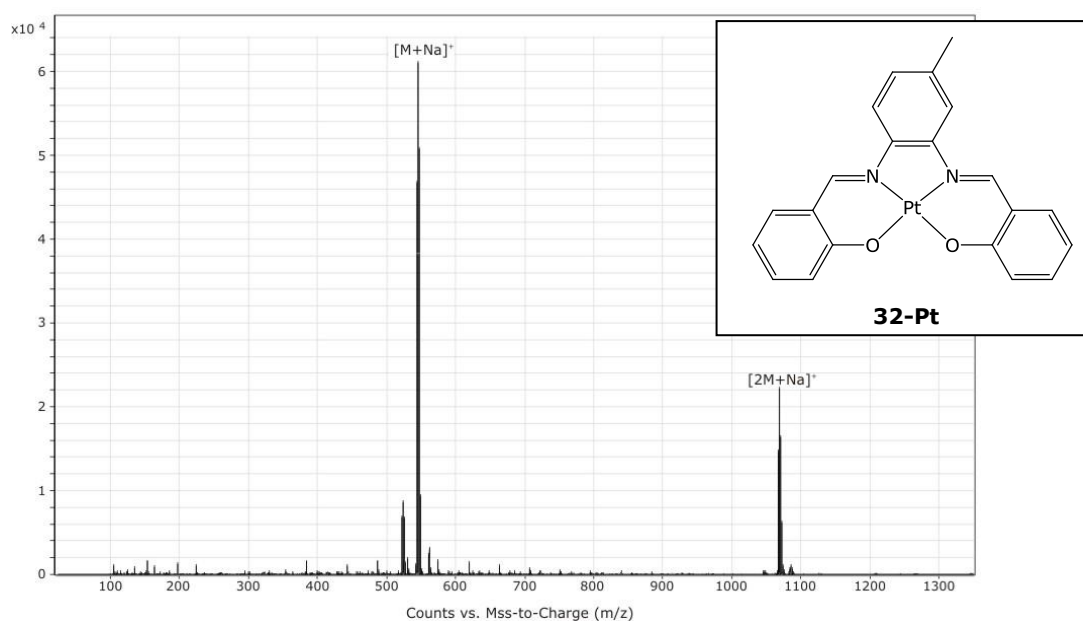


Figure 4.10 Typical mass spectrum of the platinum(II) complexes. It is shown in the inset the molecular structure of the complex **32-Pt**.

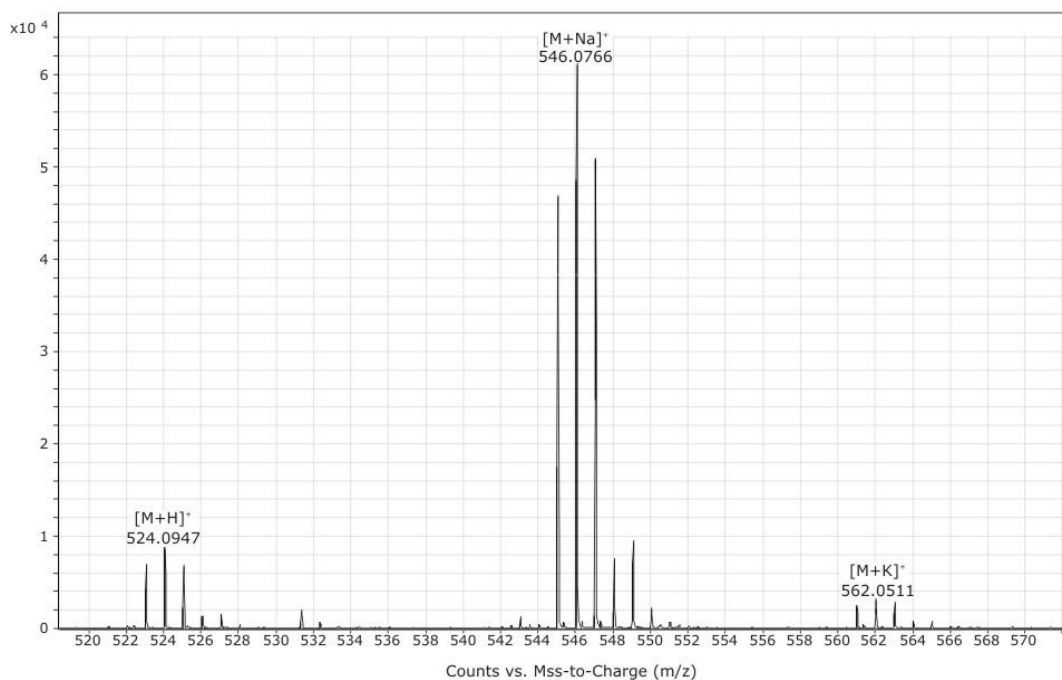


Figure 4.11 Zoom of Figure 4.10.

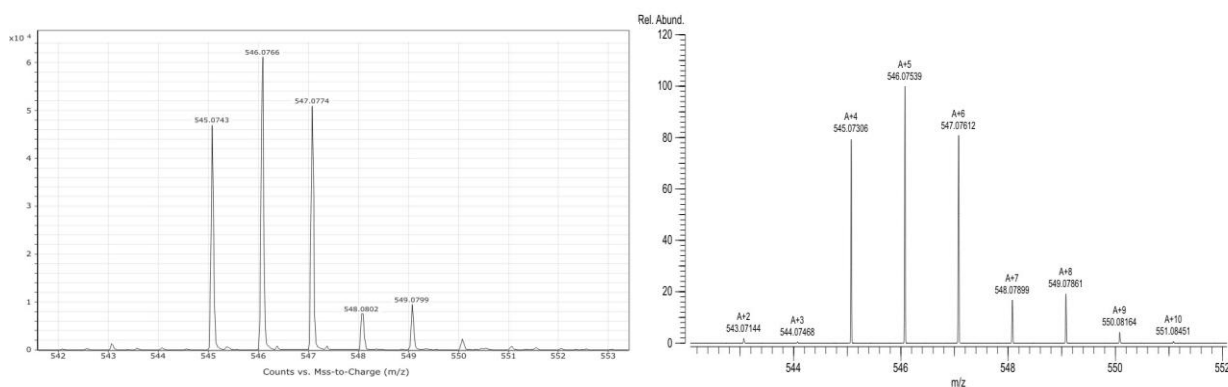


Figure 4.12 Experimental (left) and calculated (right) isotopic distribution for $[M+X]^+$, in this case $[C_{21}H_{16}N_2O_2Pt+Na]^+$.

4.3 Atomic absorption spectroscopy

Atomic absorption spectroscopy (AAS) is a universal procedure that uses the absorption of light for the identification of metallic elements and metalloids present at both low and high concentrations (between 1 and 0.005 ppm). In case of platinum the typical detection limit is 0.098 ppm⁹².

Therefore, this technique is appropriate for the determination of cellular uptake of the synthesized platinum complexes (Section 6), their solubility in culture medium (Section 7) and their DNA binding (Section 8).

An important advantage of using this method is that the identity of the individual elements can be determined in the presence of each other without prior separation. The electrons of the atoms in the atomizer are promoted to higher energy levels for a short period of time by absorbing a discrete quantity of energy (light of a defined wavelength). This amount of energy (or wavelength) is specific to a particular electronic transition in a given element. This allows selectivity and enables analytical determination of complex metal samples.

In this work, a graphite furnace (GF) was used to vaporize the samples. This technique consists in the injection of the samples into the GF, which can be then electrothermally heated following a temperature program, in order to vaporize and atomize the analyte. The used temperature program consists in four stages:

1. Drying (removal of the solvent)
2. Pyrolysis (thermal pre-treatment in order to remove matrix components that are more volatile than the chemical compounds of the analyte)
3. Atomization (Generation of atoms in the ground state)
4. Cleaning (removal of residual matrix or analyte)

With the purpose of obtaining an efficient separation and atomization of the platinum-containing samples, it is important to optimize the temperature program, which means to select for each stage the heating rate and the holding time. This is illustrated in Fig. 4.13, which shows the different stages of the temperature program.

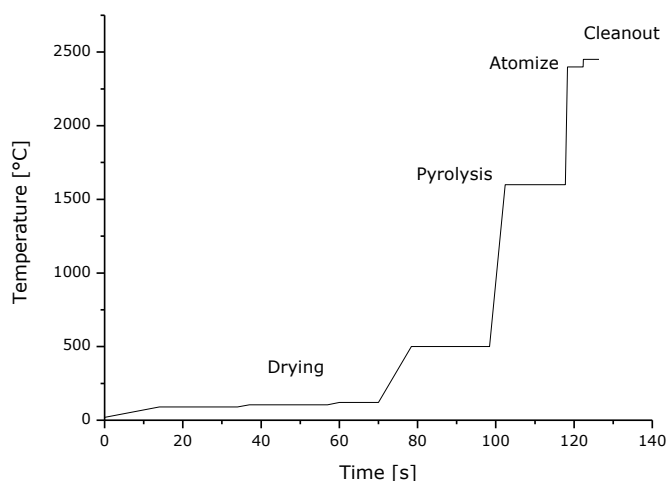


Figure 4.13 GF-AAS temperature program, used for the platinum determination in the analyzed samples.

The optimized temperature program was kindly provided by the college Ewelina Fogelström, who works with similar platinum-containing samples.

Atomic absorption like the majority of analytical techniques is only relative and requires careful calibration. Using Beer's law, which states that the absorbance of an absorbing species is proportional to its concentration, it is possible to obtain a calibration graph plotting the absorbance versus the concentration. A common method to measure platinum concentrations consists on the construction of a calibration curve using a *ready-to-use* platinum standard for AAS (in this case Hexachloroplatinic(IV) acid solution) (Fig. 4.14). Afterwards, the concentration of the unknown solution is read off the calibration graph. This procedure can be used as long as the absorbing samples have all the same absorption coefficient⁹², calculated from the slope of the calibration curve when the path length in the absorbing medium is constant. Technically, as the platinum concentration in the samples is measured from its atomic vapour, it should be possible to calculate the concentration of different platinum complexes using a same calibration curve, obtained from a standard platinum solution as above mentioned. To corroborate this, two calibration curves were made: one with the platinum standard and other one with **18-Pt** (Fig. 4.14).

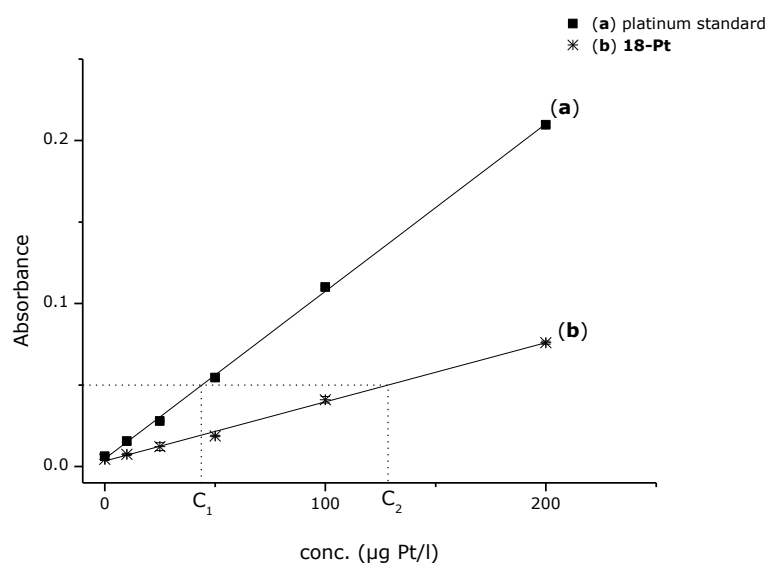


Figure 4.14 Calibration curve obtained from the platinum standard solution (a) and with **18-Pt** (b).

By interpolation of a given absorbance with the calibrations curves ((a) and (b)), different concentrations (C_1 and C_2) for the same sample are obtained. Therefore, in this work each compound was measured against its own calibration curve.

The response obtained in the AAS for an analyte could be reduced by many causes. Since the concentration of the analyte element is considered to be proportional to the ground state atom population in GF, any factor that affects the ground state population

of the analyte element can be classified as an interference. They can be divided into chemical, ionization, physical and background absorptions interferences. It is difficult to determine the cause of the difference in the slope of the calibration curves of Fig. 4.14. Nevertheless, the most probable interferences in the measured samples are:

- Chemical interferences, related with the formation of stable compounds that are not completely atomized at the temperature of GF. Normally, this problem could be solved by increasing the atomization temperature. Unfortunately, the used temperature (2400-2450 °C) was already very high (higher temperatures can produce structural problems in the GF).
- Physical interferences, related with the amount of sample that reaches the GF. Adsorption of the complexes onto the wall of the sample containers will lead to reduced levels in the graphite tube.

The detailed GF-AAS method can be found in the Experimental section (11).

4.4 X-ray crystallographic studies

A "crystal" is a solid object in which a basic pattern of atoms is repeated over and over in all three dimensions. About 95% of all solid materials can be described as crystalline. They are based on a three dimensional lattice which scatters radiation with a wavelength in the vicinity of interatomic distances. The process by which this radiation, without changing its wavelength, is converted through interference with the lattice to a vast number of observable "reflections" with characteristic directions in the space is called *X-ray diffraction*. The method by which the directions and the intensities of these reflections are measured, and the ordering of the atoms in the crystal deduced from them, is called *X-ray structure analysis*.

To solve a crystal structure means to determine the precise spatial arrangements of all the atoms in the chemical compound in the crystalline state. This knowledge gives access to a large range of information, including connectivity, conformation, and accurate bond length and angles. In addition, it implies the stoichiometry, the density, the symmetry and the three dimensional packing of the atoms in the solid.

In this work, the crystal structures of **10-Pt** and **16-Pt**, shown in Fig. 4.15 together with the numbering scheme for the atoms, have been determined as examples for the [diarylsalene]- and [salophene]platinum(II) complexes respectively. As they present

many common features they will be discussed together. A summary of crystal data, experimental details and refinement methods are given in Table 4.1.

Table 4.1 Crystal data and structure refinement for **10-Pt** and **16-Pt**.

	10-Pt	16-Pt
Empirical formula	C ₂₈ H ₁₈ F ₄ N ₂ O ₂ Pt	C ₂₂ H ₁₈ N ₂ O ₄ Pt
M_r	685.53	569.47
Crystal system	Monoclinic	Monoclinic
Space Group	P21/n	P21/n
a (Å)	12.075(2)	13.739(5)
b (Å)	18.559(2)	7.785(5)
c (Å)	11.839(2)	17.102(5)
α (°)	90.000(5)	90.000(5)
β (°)	107.270(10)	99.448(5)
γ (°)	11.839(2)	90.000(5)
V (Å ³)	2533.5(7)	1825.2(14)
Z	4	4
ρ_{calcd} (g cm ⁻³)	1.860	2.065
μ (MoK α) (mm ⁻¹)	5.602	7.721
$F(000)$	1372	1088
Crystal size (mm ³)	0.16 x 0.12 x 0.10	0.16 x 0.02 x 0.02
Reflections collected	14473	16550
Independent reflections	6755 ($R_{\text{int}} = 0.1085$)	4891 ($R_{\text{int}} = 0.0733$)
Absorption correction	Integration	Integration
Max. and min. transmission	0.6083 and 0.4751	0.7625 and 0.4817
Refinement method	Full-matrix least-squares on F^2	Full-matrix least-squares on F^2
Data/restraints/parameters	6755 / 0 / 346	4891 / 0 / 263
Goodness of fit on F^2	0.670	0.921
Final R indices [$I > 2\sigma(I)$]	$R_1 = 0.0428$, $wR_2 = 0.0601$	$R_1 = 0.0584$, $wR_2 = 0.1412$
R indices (all data)	$R_1 = 0.1560$, $wR_2 = 0.0757$	$R_1 = 0.0900$, $wR_2 = 0.1613$
Largest diff. peak and hole (eÅ ⁻³)	1.656 and -1.723	1.793 and -3.160

Important bond lengths and angles are given in Table 4.2 together with their estimated standard deviations.

Table 4.2 Selected bond length (Å) and bond angles (°) for **10-Pt** and **16-Pt**.

	10-Pt	16-Pt
Pt(1)-N(1)	1.922(7)	1.980(8)
Pt(1)-N(2)	1.932(7)	1.964(8)
Pt(1)-O(1)	1.959(6)	2.009(7)
Pt(1)-O(2)	2.022(6)	2.017(7)
N(1)-C(8)	1.277(10)	1.301(11)
N(1)-C(9)	1.511(9)	1.437(12)
N(2)-C(14)	1.499(11)	1.413(13)
N(2)-C(15)	1.282(10)	1.313(12)
O(1)-C(1)	1.317(10)	1.311(11)
O(2)-C(21)	1.317(9)	1.303(11)
N(1)-Pt(1)-N(2)	85.4(3)	82.9(3)
N(1)-Pt(1)-O(1)	94.9(3)	96.1(3)
N(1)-Pt(1)-O(2)	178.8(3)	178.9(3)
N(2)-Pt(1)-O(1)	179.1(3)	178.4(3)
N(2)-Pt(1)-O(2)	93.9(3)	96.1(3)
O(1)-Pt(1)-O(2)	85.0(3)	85.9(2)

The crystal structure shows that in **10-Pt** and **16-Pt** complexes, the deprotonated Schiff base ligand (**10** and **16** in this case) is four-coordinated with the platinum(II) ion as a tetradentate chelating agent coordinating *via* the azomethine nitrogen and the oxygen atom of the hydroxyl group. The platinum atom resides in a square-planar geometry. The bond angles at the platinum atom (N1-Pt1-N2, N1-Pt1-O1, N2-Pt1-O2 and O1-Pt1-O2) lie in the range of 82.9-96.1 °. The average Pt-N distances of 1.927 and 1.972 Å for **10-Pt** and **16-Pt**, respectively, resemble those reported for similar platinum(II) Schiff base complexes⁹³. The mean Pt-O distances of **10-Pt** and **16-Pt** are 1.991 and 2.013 Å respectively, which are also comparable to those reported for **13-Pt** (1.994 Å)⁹³ and those platinum complexes bearing tetradentate bis(salicylidene)-1,2-diaminoethane ligands, [*N,N'*-bis(salicylidene)-1,2-diaminoethane]platinum(II) (2.004 Å)⁹⁴ and [*N,N'*-bis(salicylidene)-1,1,2,2-tetramethyl-1,2-diaminoethane]platinum(II) (1.986 Å)⁹⁵. As well, distances N(1)-C(8) 1.277(10) Å and N(2)-C(15) 1.282(10) Å for **10-**

Pt and N(1)-C(8) 1.301(11) Å and N(2)-C(15) 1.311(12) Å for **16-Pt**, are indicative of a typical imine bond^{94,95}.

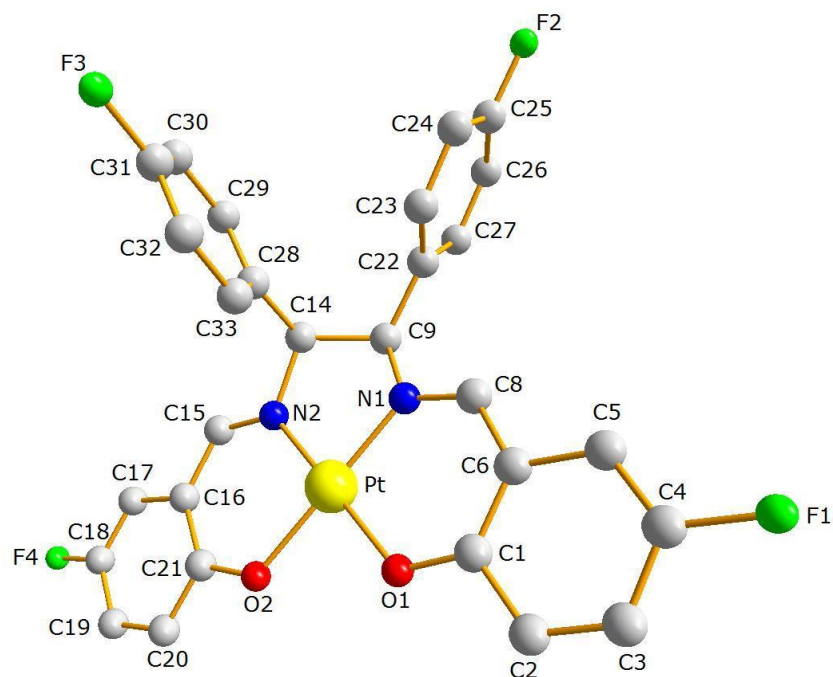
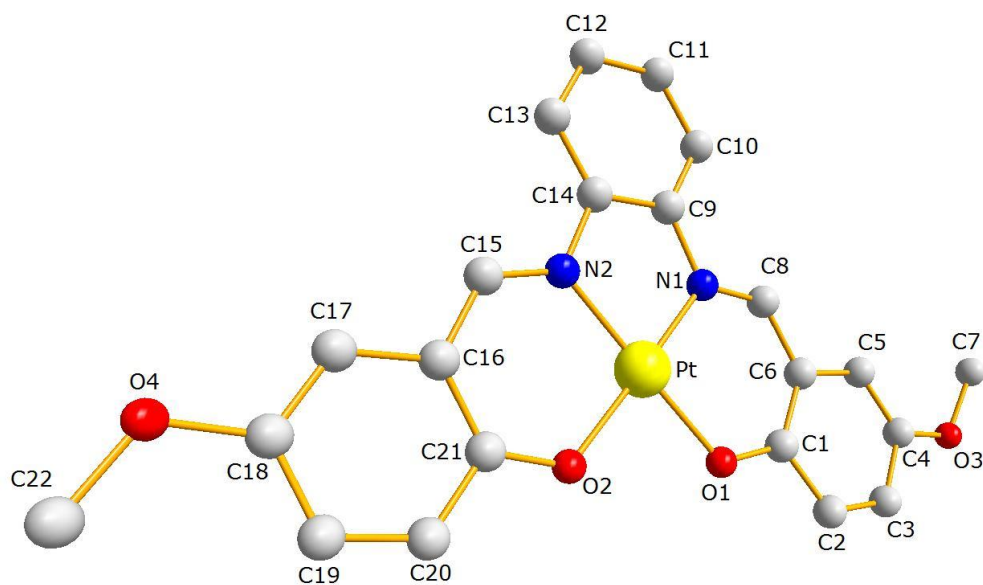
A**B**

Figure 4.15 Perspective views of the complex **10-Pt** (A) and **16-Pt** (B). The hydrogen atoms are omitted for clarity.

Concerning the crystal packing of **10-Pt** and **16-Pt**, several similarities, as well as marked differences were observed. Molecules seem to be arranged, in both cases, in a head-to-tail fashion with intermolecular π - π stacking interactions mainly between the salicylidene moieties (see Figs. 4.16 and 4.17).

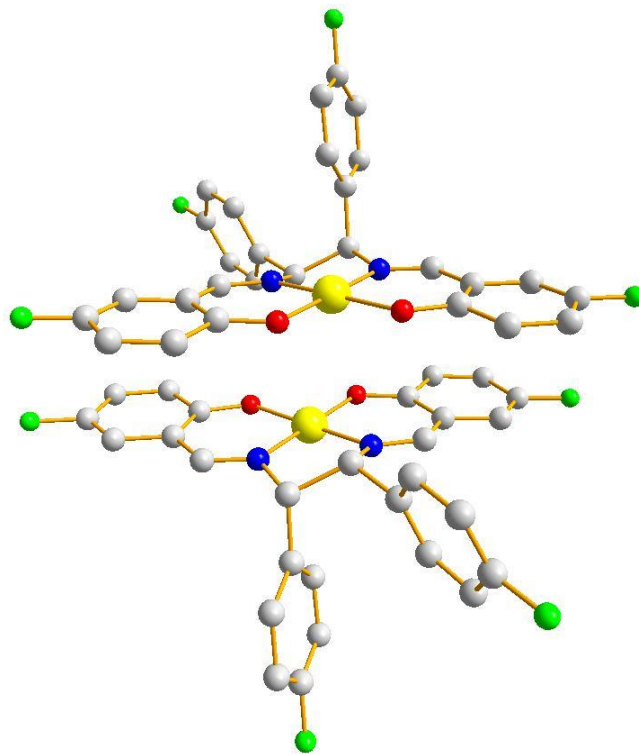


Figure 4.16 Crystal packing diagram of **10-Pt**, where complexes are arranged in pairs and in a head-to-tail fashion.

The crystal packing of **10-Pt** consisted of head-to-tail arranged pairs, as showed in Fig. 4.16. Moreover, probably due to the bulky nature of the diarylethane moiety and the considerable size of the [diarylsalene]platinum(II) derivatives, the unit cell of the monoclinic crystal lattice of **10-Pt** is rather large (as compared with **16-Pt**, see below), with a volume of 2533.5 \AA^3 . A different situation was observed for the crystal packing of the [salophene]platinum(II) derivative, **16-Pt**. Although it presented also the head-to-tail fashion (Fig. 4.17 **A**), as similarly observed for **10-Pt** and for [salophene]platinum(II) complexes reported in literature⁹³, the less bulky character of the molecule led to a smaller and more compact unit cell, with a volume of 1825.2 \AA^3 . Furthermore, complexes seem to be arranged in a zigzag chain formed from intermolecular π - π stacking interactions, not only between salicylidene, but also between salicylidene and phenylene moieties (Fig. 4.17 **B**).

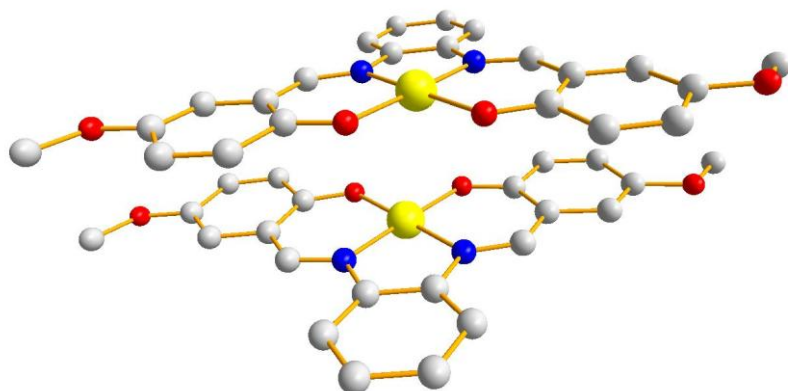
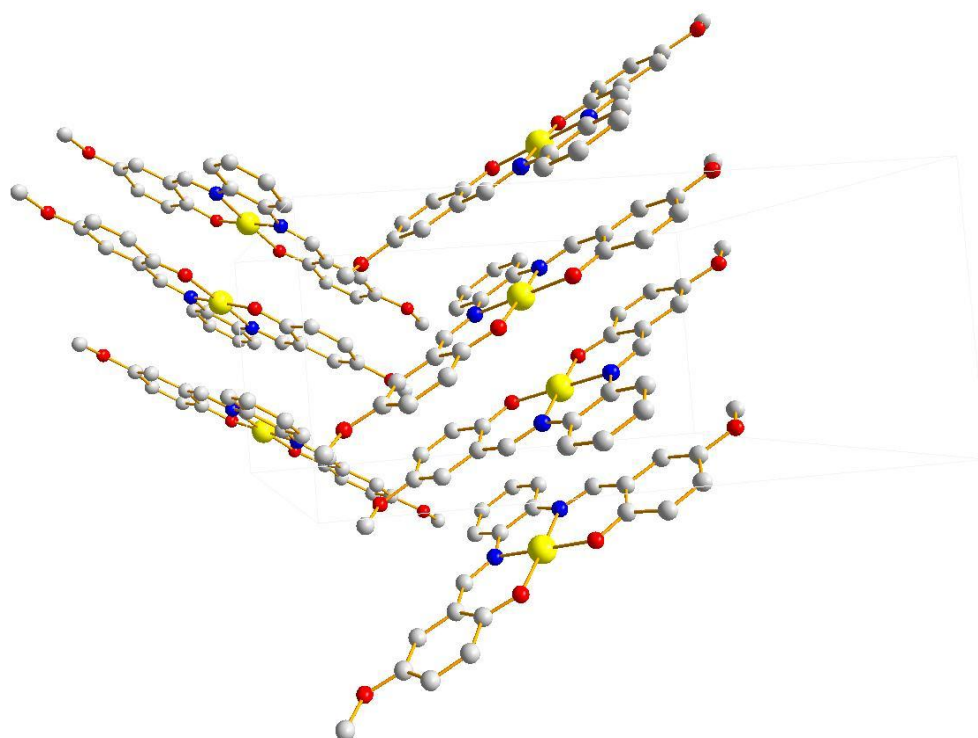
A**B**

Figure 4.17 Crystal packing diagram of **16-Pt**. **A**: complexes arranged in a head-to-tail fashion. **B**: zigzag chain formed from intermolecular interactions.

5 *In-vitro* chemosensitivity assay

5.1 Breast cancer cell lines

In-vitro studies on the cytotoxicity and antiproliferative effects of the platinum complexes on cultured breast cancer cells are the most important parameters within the established screening procedures.

Initially, the platinum complexes were tested on both MCF-7 and MDA-MB-231 breast cancer cells to determine possible selective effects. MCF-7 is a breast cancer cell line that was isolated from an *in situ* carcinoma of a 69-year-old Caucasian woman in 1970. MCF-7 cells are useful for *in-vitro* breast cancer studies because the cell line has retained several ideal characteristics particular to the mammary epithelium. These include the ability for MCF-7 cells to process estrogen, in the form of estradiol, *via* estrogen receptors. This makes the MCF-7 cell line an estrogen receptor (ER) positive cell line⁹⁶. MDA-MB-231 is a breast cancer cell line, derived from a metastatic carcinoma, obtained from a 51-year-old patient in 1973. Among other characteristics, this cell line is ER negative. Comparing the effect of the platinum complexes on both cell lines, a possible interaction of the compounds with the estrogen receptor could be evaluated.

5.2 Crystal violet chemosensitivity assay

The *in-vitro* testing of the substances for antitumor activity in adherent growing cell lines was carried out on exponentially dividing human cancer cells according to a previously published microtiter assay^{97,98}. It consist in a computer technique which allows the registration of growth curves of cells in monolayer cultures by large scale spectrophotometric measurement after crystal violet staining using 96-well microtitration plates. This technically easy microtitration assay gives access to large sets of data in short time, providing results of high statistical significance. The method, particularly developed for the *in-vitro* evaluation of the activity of potential anticancer drugs, gives the desirable features of simplicity, reproducibility and sensitivity.

Fig. 5.1 shows a schematic description of the experimental procedure to be followed during the assay.

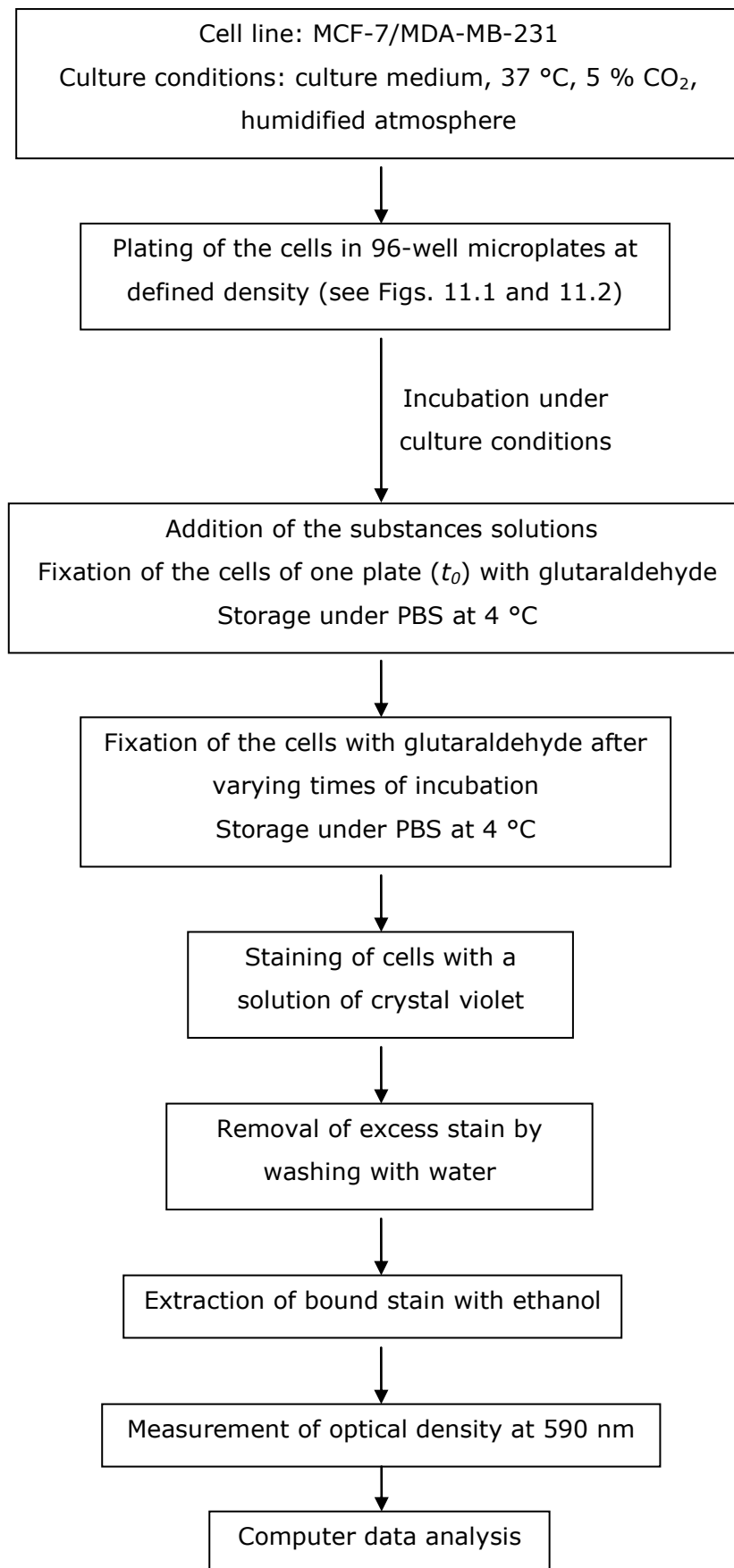


Figure 5.1 Experimental procedure of the crystal violet assay.

The activity of the complexes is expressed as corrected T/C_{corr} (%) value according to Eq. 5.1

$$\text{Cytostatic effect: } T/C_{corr} (\%) = [(T - C_0)/(C - C_0)] \times 100 \quad \text{Eq. 5.1}$$

where T (test) and C (control) are the optical densities at 590 nm of the T and C crystal violet extract of the cells in the wells (i.e., the chromatin-bound crystal violet extracted with 70% ethanol), with C_0 being the density of the cell extract immediately before treatment. As a control or blank the solvent employed to prepare the compound solution in the same concentration is used. In order to obtain the T/C_{corr} (%) value, the optical density at the time ($t = 0$) when the respective test compound was added (C_0) is subtracted from the optical density of the test (T) and control system (C), dividing afterwards the two values. That means that in this case it is possible to quantify cytostatic effects.

In case of a cytotoxic effect, the density of cell extract in the test system is lower than in the control system and the effect has to be directly calculated from the density of cell extract at $t = 0$ (C_0). We get then τ (%) values, calculated by Eq. 5.2

$$\text{Cytotoxic effect: } \tau (\%) = [(T - C_0)/C_0] \times 100 \quad \text{Eq. 5.2}$$

In this work, every negative influence produced by a compound on the rate of growth of the cells is called "cytotoxic effect".

5.3 IC₅₀ determination

A widely used form to describe antiproliferative / cytotoxic drug effects is the IC₅₀ value, which is defined as the concentration that reduces the growth of the cell biomass by 50%, in this work, after 96 hours of incubation. It represents the mean value of two independent experiments. Each experiment's IC₅₀ endpoint was estimated from fitting a sigmoid function with OriginPro 7.5G to the measured cytotoxic effects (responses) of the compound at a range of concentrations (in logarithmic scale), which constitute the concentration-effect curve. Afterwards, the sigmoid curve allowed the interpolation of the IC₅₀ value. As an example in Fig. 5.2 the concentration-effect curve of **23-Pt** and the interpolation of the IC₅₀ value is shown.

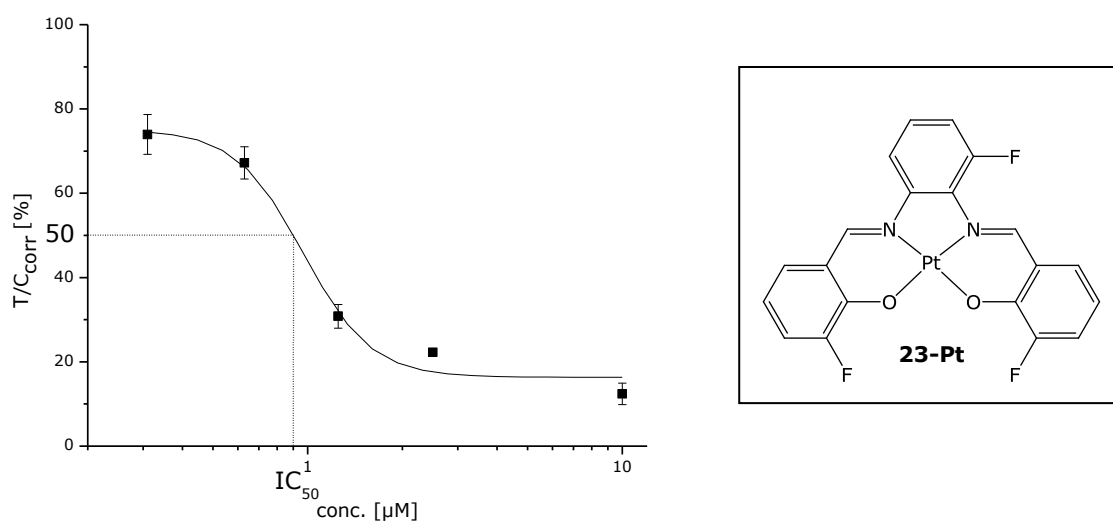


Figure 5.2 Left: Experimental concentration-effect curve (black dots) of **23-Pt**. The IC_{50} value was estimated by interpolation in the sigmoid concentration- fitted curve. Right: molecular structure of the complex **23-Pt**.

The IC_{50} was determined for all ligands and complexes up to a concentration of 20 μM . Higher values of IC_{50} were expressed as $IC_{50} > 20 \mu\text{M}$, assuming that the compound is not cytotoxic in the tested range of concentrations. In the all figures this situation is presented as an open bar.

In all the experiments cisplatin was used as a positive control.

5.3.1 Compared effect on MCF-7 and MDA-MB-231 breast cancer cells lines

As mentioned before, initially, the platinum complexes were tested *in-vitro* for growth inhibition activity on both hormone dependent MCF-7 and hormone independent MDA-MB-231 breast cancer cells, to determine a possible selective effect. In Fig. 5.3 the antiproliferative effects on both cell lines of three complexes (**12-Pt**, **1-Pt** and **13-Pt**) are shown as an example for all the complexes.

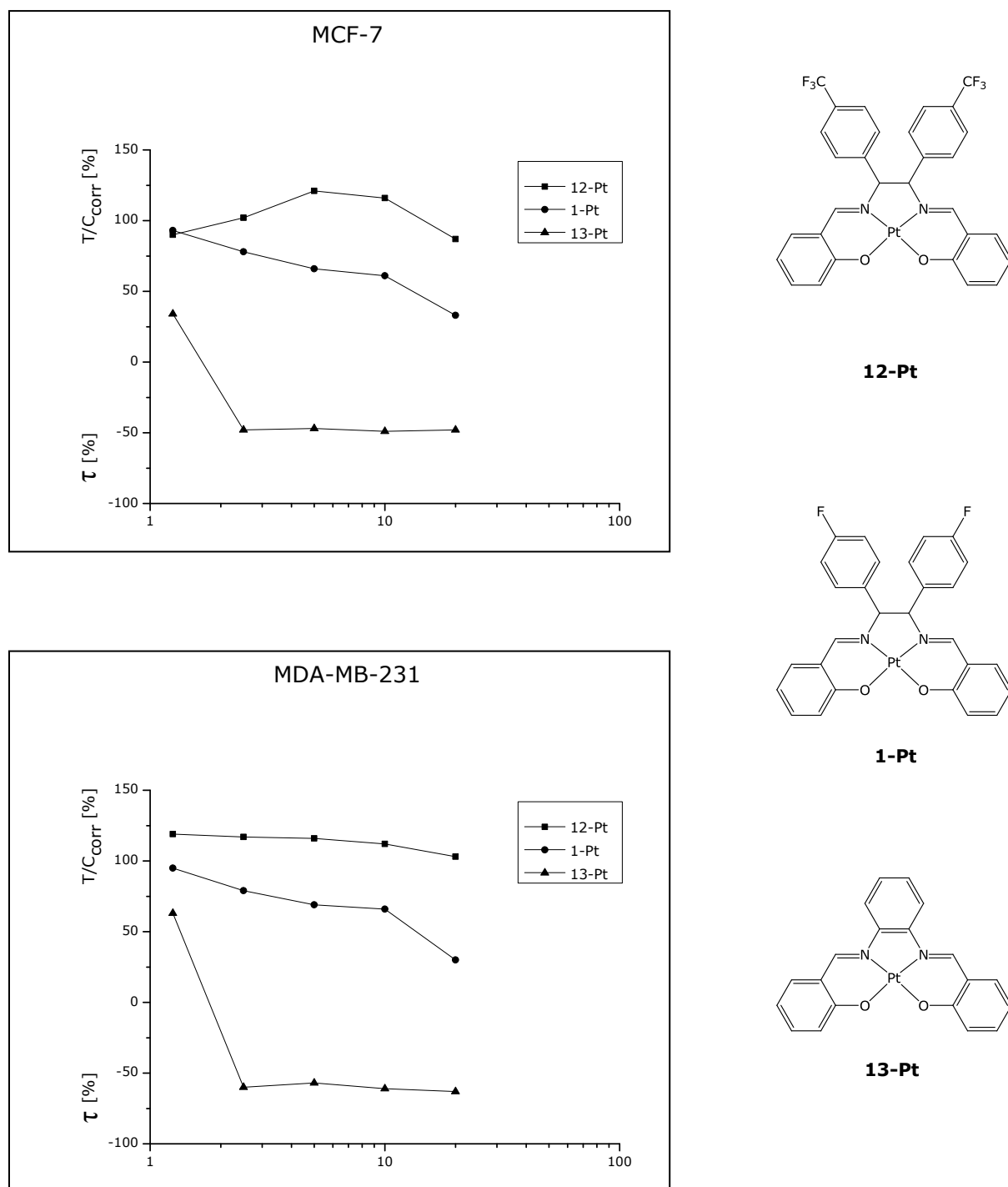
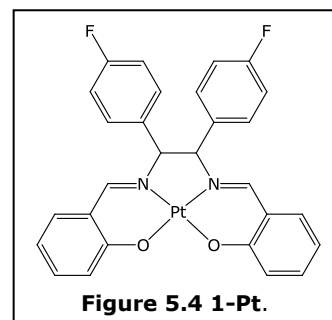


Figure 5.3 Antiproliferative effects of the platinum(II) complexes **12-Pt**, **1-Pt** and **13-Pt** on the MCF-7 (above) and MDA-MB-231 (below), and their molecular structure (right).

As it can be seen on Fig. 5.3 none of the three platinum complexes showed a marked difference in its antitumor activity on both test models. As a consequence we can assume that their action is not mediated by the ER system. We concluded that it was irrelevant to test on both cell lines, therefore the remaining antiproliferative test were carried out only on MCF-7 cells.

5.3.2 [Diarylsalene]platinum(II) complexes

The lead substance in the group of [diarylsalene]platinum(II) complexes is **1-Pt** (Fig. 5.4) with an IC_{50} value of $7.6 (\pm 2.9) \mu M$. In order to increase the cytotoxic effect, variations on the lead structure were carried out and tested for cytotoxicity.



Unfortunately, variations of the 1,2-diamino-1,2-diarylethane moiety like in complex **2-Pt** (*d,l* configuration of the ligand) or **12-Pt** (exchange of fluorine substituent for trifluoromethyl) led to loss of the cytotoxic effects ($IC_{50} > 20 \mu M$).

Variations on the salicylidene moiety produced changes on the activity of the compounds, depending on the substituent and its position on the phenolic ring.

The introduction of a methoxy group (independent of the position of the substituent on the ring) (**4-Pt**, **5-Pt**, **6-Pt** and **7-Pt**) gave inactive complexes in the tested concentrations. The impact of the incorporation of a fluorine substituent produced instead complexes with different values of IC_{50} depending on the position of the substituent on the ring (Table 5.1 and Fig. 5.5).

Table 5.1 Main structure of the [diarylsalene]platinum(II) complexes and substitution pattern of **1-Pt**, **8-Pt**, **9-Pt**, **10-Pt** and **11-Pt**.

Structure	Compound	Substitution
	1-Pt	---
	8-Pt	$R_3 = F$
	9-Pt	$R_4 = F$
	10-Pt	$R_5 = F$
	11-Pt	$R_6 = F$

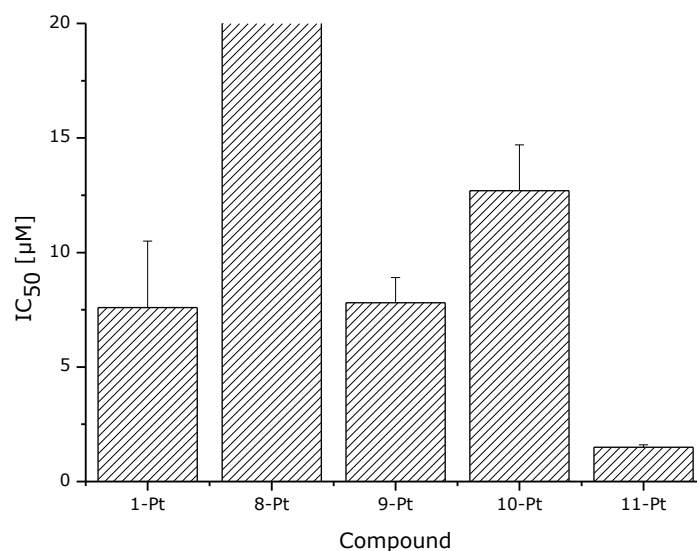


Figure 5.5 IC₅₀ values of [diarylsalene]platinum(II) complexes with non- (**1-Pt**) or fluoro-substituted salicylidene moiety (**8-Pt**, **9-Pt**, **10-Pt** and **11-Pt**)⁹⁹.

As it can be seen in Fig. 5.5, the position of the fluorine substituent on the salicylidene moiety has a huge impact on cytotoxicity. While the incorporation of a R₃ = F group (**8-Pt**) led to a complex with no relevant influence in the tumour cell growth, the shift of the fluorine substituent from the R₃- into the R₆-position (**11-Pt**) increased the antiproliferative effects enormously (IC₅₀ ~ 1 µM). Complexes **9-Pt** (R₄ = F) and **10-Pt** (R₅ = F) presented low inhibitory effects on the growth of MCF-7 cells.

5.3.3 [Salophene]platinum(II) complexes

The lead compound in the group of [salophene]platinum(II) complexes is the unsubstituted [*N,N'*-bis(salicylidene)-1,2-phenylenediamine]platinum(II) derivative (Fig. 5.6 left: **13-Pt**) It was tested on MCF-7 cells for cytotoxicity displaying an IC₅₀ value of 1.1 (± 0.2) µM. In this case also, the main structure was modified by the exchange of the aryl bridge by a cyclohexane ring ([saldach]platinum(II)), obtaining **33-Pt** (Fig. 5.6 right).

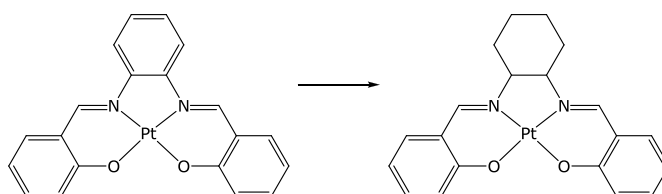


Figure 5.6 Change of the main structure from **13-Pt** (left) to **33-Pt** (right).

As this modification decreased the activity of the complex ($IC_{50} > 20 \mu M$), the original structure was maintained and different substituted derivatives were synthesized and tested.

In the first group of derivatives a methoxy group was incorporated in the salicylidene moiety. With the exception of the derivative with the methoxy group in position R_4 (**15-Pt**) which had an IC_{50} value of $1.8 (\pm 0.7) \mu M$, the introduction of a methoxy group in position R_3 (**14-Pt**), R_5 (**16-Pt**), and R_6 (**17-Pt**) led to complexes with $IC_{50} > 20 \mu M$.

The second group of derivatives, bearing a fluorine as substituent in the salicylidene moiety, presents a different IC_{50} pattern than the compounds with the methoxy substituent.

Table 5.2 Main structure of the [salophene]platinum(II) complexes and substitution pattern of **13-Pt**, **18-Pt**, **19-Pt**, **20-Pt** and **21-Pt**.

Structure	Compound	Substitution
	13-Pt	---
	18-Pt	$R_3 = F$
	19-Pt	$R_4 = F$
	20-Pt	$R_5 = F$
	21-Pt	$R_6 = F$

The difference in antitumor potency in the fluoro-substituted compounds can easily be seen in Fig. 5.7, which depends on the position of the fluorine substituent. While **20-Pt** ($R_5 = F$) caused low growth inhibitions effects ($IC_{50} \sim 10 \mu M$), a shift of the fluorine substituent from position R_5 to R_4 (**19-Pt**) or R_6 (**21-Pt**) terminated the activity at the tested concentrations. A shift to position R_3 instead, led to an analogue (**18-Pt**) more active than the lead compound and 10-fold more cytotoxic than **20-Pt** (Table 5.2).

The [salophene]platinum(II) complexes containing a methoxy group as substituent showed (with exception of **15-Pt**) no cytotoxicity in the tested concentrations. By contrast, [salophene]platinum(II) complexes bearing fluorine substituents exhibited relevant antiproliferative effects. Therefore, further experiments were designed in order to evaluate the effect on the cytotoxicity of the insertion of another fluorine, but in the phenylene moiety. The two possible positions on the phenylene moiety were substituted separately, combined with a non- or fluoro-substituted salicylidene moiety.

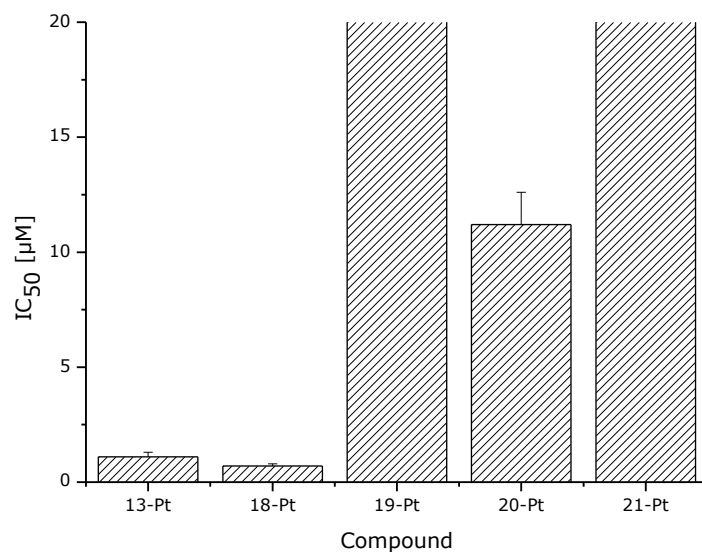


Figure 5.7 IC₅₀ values of [salophene]platinum(II) complexes with non- (**13-Pt**) or fluoro-substituted salicylidene moiety (**18-Pt**, **19-Pt**, **20-Pt** and **21-Pt**).

In Fig. 5.8 the influence of a fluoro-substitution on position R₃ of the phenylene moiety with non- (**22-Pt**) or fluoro-substituted salicylidene moiety (**23-Pt**, **24-Pt**, **25-Pt** and **26-Pt**) is shown.

Table 5.3 Main structure of the platinum(II) complexes containing 3'-substituted salophene moiety and substitution pattern of **22-Pt**, **23-Pt**, **24-Pt**, **25-Pt** and **26-Pt**.

Structure	Compound	Substitution
	22-Pt	---
	23-Pt	R ₃ = F
	24-Pt	R ₄ = F
	25-Pt	R ₅ = F
	26-Pt	R ₆ = F

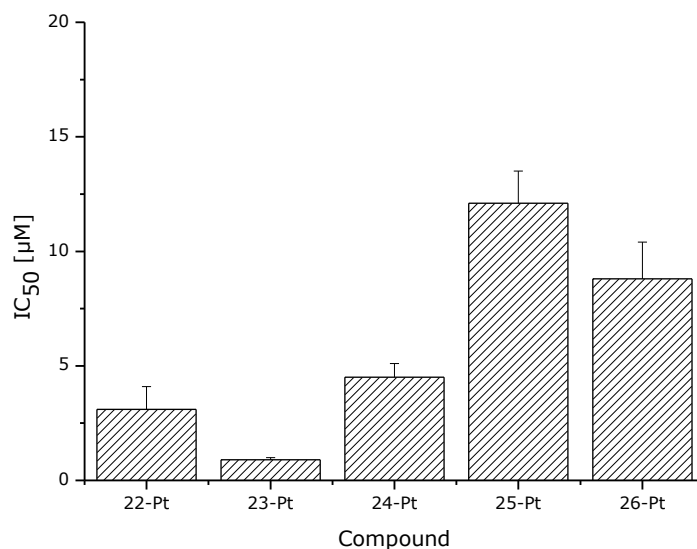


Figure 5.8 IC₅₀ values of [salophene]platinum(II) complexes with R₃ = F and non- (**22-Pt**) or fluoro-substituted salicylidene moiety (**23-Pt**, **24-Pt**, **25-Pt** and **26-Pt**).

The five complexes with R₃ = F, revealed growth inhibitory effects, which increased in the following order: **25-Pt** (R₅ = F) < **26-Pt** (R₆ = F) < **24-Pt** (R₄ = F) < **22-Pt** < **23-Pt** (R₃ = F). By contrast, most of the complexes bearing R₄ = F (**28-Pt**, **29-Pt** and **30-Pt**), had no significant toxicity. As exceptions, **27-Pt** and **31-Pt** (R₆ = F) (Table 5.4) presented strong antiproliferative effects (IC₅₀ ~ 1 µM) (Fig. 5.9).

Table 5.4 Main structure of the platinum(II) complexes containing 4'-substituted salophene moiety and substitution pattern of **22-Pt**, **23-Pt**, **24-Pt**, **25-Pt** and **26-Pt**.

Structure	Compound	Substitution
	27-Pt	---
	28-Pt	R ₃ = F
	29-Pt	R ₄ = F
	30-Pt	R ₅ = F
	31-Pt	R ₆ = F

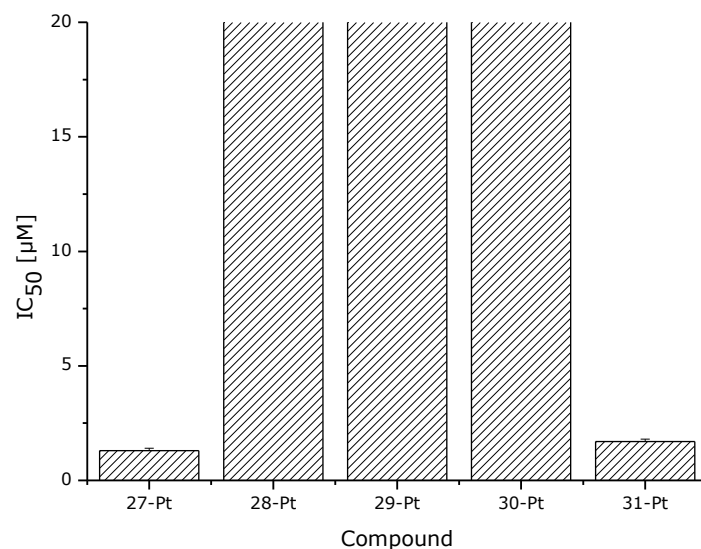


Figure 5.9 IC₅₀ values of [salophene]platinum(II) complexes with R'₄ = F and non- (**27-Pt**) or fluoro-substituted salicylidene moiety (**28-Pt**, **29-Pt**, **30-Pt** and **31-Pt**).

It is interesting to compare the effect of incorporation of fluorine in the phenylene moiety on the cytotoxicity for each substituted position of the salicylidene moiety.

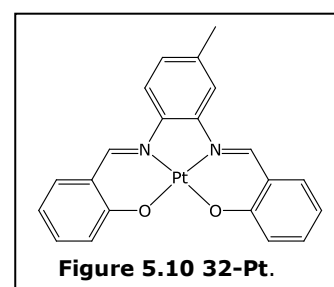
Table 5.5 IC₅₀ values of fluoro-substituted [salophene]platinum(II) complexes.

Structure	R' ₃	R' ₄	IC ₅₀ (µM)	Structure	R' ₃	R' ₄	IC ₅₀ (µM)
	H	H	1.1 ± 0.2		H	H	11.2 ± 1.4
	F	H	3.1 ± 1.0		F	H	12.1 ± 1.4
	H	F	1.3 ± 0.1		H	F	> 20.0
	H	H	0.7 ± 0.1		H	H	> 20.0
	F	H	0.9 ± 0.1		F	H	8.8 ± 1.6
	H	F	> 20.0		H	F	1.7 ± 0.1
	H	H	> 20.0				
	F	H	4.5 ± 0.6				
	H	F	> 20.0				

From Table 5.5 it is difficult to get a conclusion about the influence of fluorine substituents on the antiproliferative effects of [salophene]platinum(II) complexes.

However it is obvious that neither a fluoro-substituted salicylidene moiety nor a fluoro-substituted phenylene moiety caused a big increase on the cytotoxicity of the complexes. The only complexes that presented a IC_{50} value lower than the unsubstituted [salophene]platinum(II) complex (**13-Pt**) are **18-Pt** ($R_3 = F$) and **23-Pt** ($R'_3 = F, R_3 = F$), but the shift of the fluorine substituent from position R'_3 to R'_4 in **28-Pt** ($R'_4 = F, R_3 = F$) gave an inactive complex. It means that in the $R_3 = F$ substituted complexes the growth inhibitory effects increase in the following order: **28-Pt** ($R'_4 = F, R_3 = F$) \ll **23-Pt** ($R'_3 = F, R_3 = F$) $<$ **18-Pt** ($R_3 = F$). In contrast to this, the growth inhibition of the $R_6 = F$ substituted complexes increased in the following order: **21-Pt** ($R_3 = F$) $<$ **26-Pt** ($R'_3 = F, R_3 = F$) $<$ **31-Pt** ($R'_4 = F, R_3 = F$). On the other hand, in the $R_4 = F$ substituted complexes, the only complex which showed activity was **24-Pt** ($R'_3 = F, R_4 = F$).

The last compound which was tested for antitumor activity was **32-Pt**. As a difference with the lead structure of the group (**13-Pt**), it is substituted with a methyl group in position R'_4 (Fig. 5.10). It showed very promising results with an IC_{50} value of $0.8 (\pm 0.1) \mu M$.



5.3.4 Conclusion on the results of the determination of IC_{50} values of [diarylsalene]- and [salophene]platinum(II) complexes

At this point of the work it was demonstrated that the cytotoxicity of the complexes has high dependence on the structure of the tested compounds. Therefore, it is necessary to make a short summary of the most important conclusions.

- The [salophene]platinum(II) complexes were, in the tested concentration range, more cytotoxic than the [diarylsalene]platinum(II) complexes.
- Modifications on the main structure of the lead compounds on both groups of complexes did not produce increase on the antiproliferative effects.
- Complexes which are fluoro-substituted presented habitually higher toxicity than the methoxy-substituted complexes.
- The position of the fluorine substituent on the salicylidene moiety has not the same influence in all the complexes.

- The introduction of substituents (fluorine, methoxy or methyl) on the salophene complexes produced only in some cases a marginal increment of the cell growth inhibitory effects, compared to the unsubstituted complex.
- The [salophene]platinum(II) complexes bearing three fluorine substituents were rarely more active than the compounds bearing two fluorine substituents.
- Collectively, salophene complexes with $R'_3 = F$ were more active than $R'_4 = F$ substituted complexes.

5.4 Time- and concentration-dependent cytotoxicity

In Section 5.3 the IC_{50} values after a period of drug exposure of 96 h were discussed. Although for the preliminary large-scale screening a single-end-point, like IC_{50} determination, was sufficient, for more detailed investigations of drug action a kinetic assay procedure is preferable because it provides unambiguous information concerning differential sensitivity. In addition, potential development of resistance is readily observed from one single experiment. On the other hand, it is known that for some platinum complexes longer exposure periods can lead to more pronounced antiproliferative properties. It was demonstrated for cisplatin and carboplatin that incubation of 200 h can lead to higher cytotoxic effects than incubation up to 100 h¹⁰⁰. Therefore, for the substances with IC_{50} values $< 20 \mu\text{M}$ a time- and concentration-dependent cytotoxicity assay was performed. Various times of incubation for five different end-points (48, 72, 96, 120, and 144 h) were tested and five different concentrations were chosen for each complex as well, according to the IC_{50} value.

For the different values of T/C_{corr} and τ values, the following kind of effects were assigned

$T/C_{corr} > 80\%$	non antiproliferative effect
$80\% > T/C_{corr} \geq 20\%$	antiproliferative effect
$20\% > T/C_{corr} > 0\%$	cytostatic effect
T/C_{corr} or $\tau < 0\%$	cytotoxic effect

In contrast to cisplatin, which reached its maximum effect toward the end of the test (see Fig. 5.11), the onset of antiproliferative effect of most of the complexes was

observed earlier and remained almost constant during the test period. As an example the time-response curve of **18-Pt** is shown in Fig. 5.11.

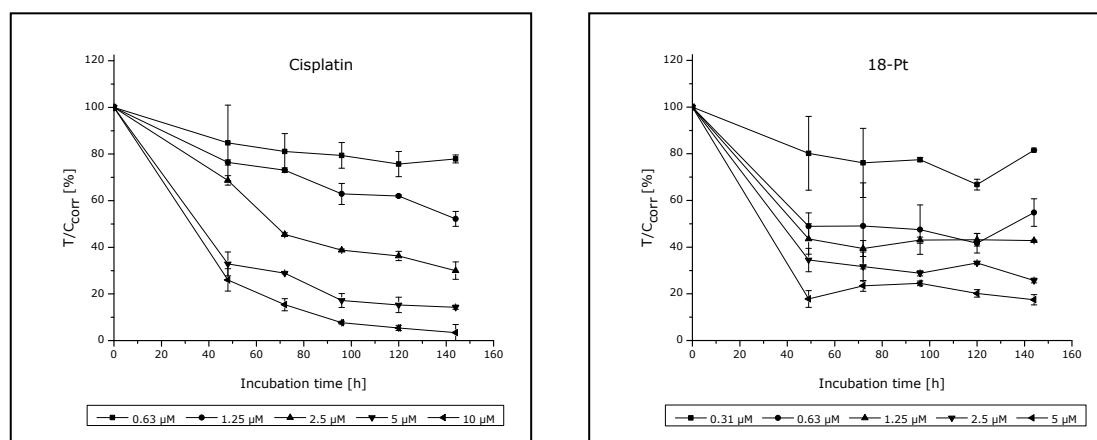


Figure 5.11 Time-activity curve of the antiproliferative effect of cisplatin (left) and **18-Pt** (right) on human MCF-7 breast cancer cell line, for five different concentrations at five different times.

The unsubstituted [salophene]platinum(II) (**13-Pt**) showed an unusual time response curve. After a reduction of the cell growth of about 100% at concentrations over 2.5 μ M, a fast onset of proliferation was observed and the cell population recovers after initial damage. Other compounds like the unsubstituted [diarylsalene]platinum(II) (**1-Pt**) showed this effect towards the end of the test (see Fig. 5.12). Because exponential cell growth is guaranteed for at least 250 h of incubation, the rise of the growth curve can be explained by the development of drug resistance⁹⁷.

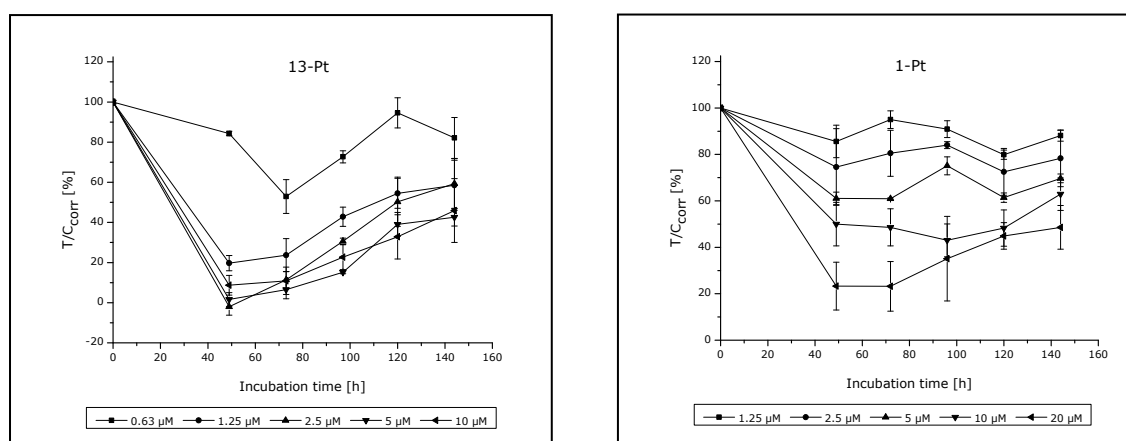


Figure 5.12 Time-activity curve of the antiproliferative effect of **13-Pt** (left) and **1-Pt** (right) on human MCF-7 breast cancer cell line, for five different concentrations at five different times.

Another atypical time-activity curve presented the compounds **22-Pt** and **26-Pt**. They showed a cisplatin-like curve reaching the maximum effect toward the end of the test (see Fig. 5.13).

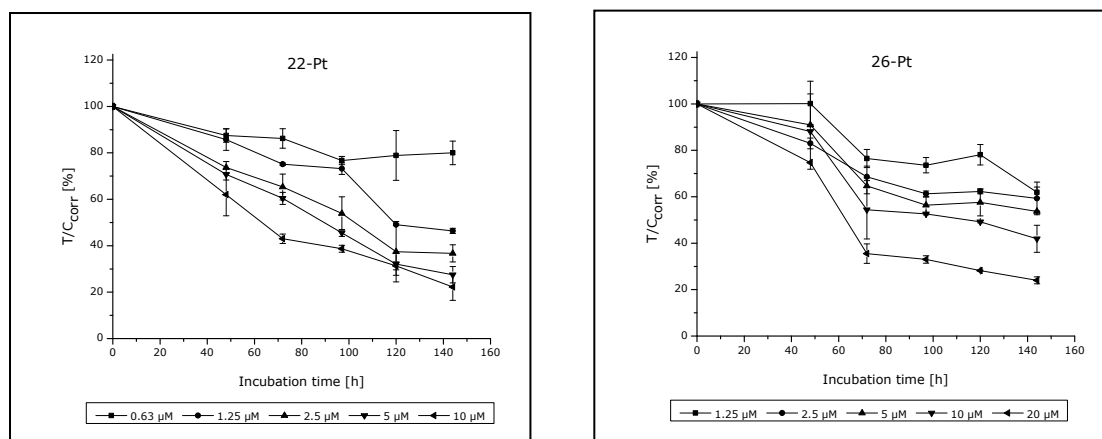


Figure 5.13 Time-activity curve of the antiproliferative effect of **22-Pt** (left) and **26-Pt** (right) on human MCF-7 breast cancer cell line, for five different concentrations at five different times.

If we look closely at the time-response curves in Figs. 5.12 and 5.13, we can confirm that a single-end-point determination like the IC_{50} determination does not give exact information about the differential sensitivity. For example complex **22-Pt** (Fig. 5.13 left) had a $T/C_{corr} = 73\%$ (concentration = $1.25 \mu\text{M}$, after 96 h incubation), but it displayed its maximum activity at 144 h with a reduction of the cell growth of about 50%. If we compare now the IC_{50} value obtained at 96 h ($3.1 \mu\text{M}$) with the one at 144 h ($1.3 \mu\text{M}$), they are both still in a same range of concentration. Therefore, to compare IC_{50} values it is possible to choose one incubation time for all complexes, in this case 96 h.

In the Appendix the time-response curves for all the complexes with an IC_{50} value below $20 \mu\text{M}$ are presented.

6 Cellular accumulation

Transport of platinum compounds across cancer cell membrane is the first step towards a cytotoxic effect. Therefore, reduced antiproliferative effects can be linked to decreased drug accumulation, which may be due to increased efflux, reduced uptake or even a combination of both processes¹⁰¹.

In the “*In-vitro* chemosensitivity assay” section (Section 5), the [diarylsalene]- and [salophene]platinum(II) complexes cytotoxicity was described. As mentioned before, the nature and position of the substituents on the complexes showed significant influence on the growth inhibition effects of the complexes. Only by shifting the position of substituents in the phenylene or salicylidene moiety, as for example complexes **19-Pt** ($R_4 = F$) and **18-Pt** ($R_3 = F$) shown in Fig. 6.1, the IC_{50} dropped from values greater than 20 μM to 0.7 μM .



Figure 6.1 Molecular structure of **19-Pt** (left) and **18-Pt** (right).

In this context, penetration of the platinum complexes in tumour cells could be a critical factor to understand the differences in cytotoxicity present in this series of [salophene]platinum(II) complexes.

6.1 Cell entry mechanisms of platinum drugs

Since reduced intracellular platinum accumulation is believed to be one of the mechanisms involved in the resistance to platinum-based chemotherapy, the uptake and efflux of platinum drugs has been extensively studied^{27,101,102}. The precise mechanism by which platinum complexes enter cells is unclear; however evidence supports the involvement of both passive diffusion and carrier mediated mechanisms.

- Passive diffusion as cell entry mechanism

If given enough time, essentially any molecule will diffuse across a lipid bilayer down its concentration gradient. The rate at which this phenomenon occurs depends on the size of the molecule and its lipophilicity. For many years it had been taken for granted that cisplatin enters cells largely by passive diffusion. Early studies revealed the platinum concentration to be the rate-limiting factor for drug accumulation inside cells, and the uptake was not saturable¹⁰³. In addition, cellular entry of cisplatin was not inhibited by its structural analogues, such as transplatin and carboplatin¹⁰¹.

- Facilitated cellular uptake

Evidence for a role of active transporters in the uptake and efflux of cisplatin and other platinum compounds has already been reported¹⁰¹. For example, Dornish *et al.* carried out multiple studies and demonstrated that reactive aldehydes inhibit cisplatin accumulation in cells, presumably by forming Schiff bases with membrane proteins^{104,105}. Recently, it has also been demonstrated that there is a direct link between copper transporters and the uptake and efflux of platinum compounds¹⁰⁶. In addition to copper transporters, the facilitated delivery of platinum compounds into cells has also been associated with the presence of organic cation transporters (OCTs)¹⁰⁷.

From this information, it is now clear that platinum drugs enter the cell through multiple routes, including both passive and active mechanisms. Moreover, each of these cell-entry pathways is likely to influence the cellular accumulation of a platinum compound differently, depending on its chemical composition and structure. Additional work is needed to fully understand how the platinum cellular concentration is influenced by passive diffusion, copper homeostasis proteins, OCTs, and other, as yet unidentified transporters.

It was already demonstrated that the ligands on the platinum atom and their structure can have influence on the uptake of the complex. For example, Reile *et al.* observed that platinum complexes bearing a 1,2-diamino-1,2-diarylethane moiety as non-leaving groups, were enriched 20- and 10-fold in MCF-7 breast cancer cells, while the intra- and extracellular concentration of cisplatin remained similar. This effect was attributed to the carrier function of the diamine ligand^{100,108}. The second example concerns 1,2-cyclohexanediamine (DACH) isomers, also tethered to the platinum(II) scaffold, as carrier ligands. Zou *et al.* proposed a chirality selectivity in the uptake of these complexes by human erythrocytes, due to interactions between the chiral platinum complexes and the head groups of the erythrocyte membrane phospholipid molecules¹⁰⁹.

6.2 Cell uptake determination: method and conditions

The cellular concentration of the compounds in MCF-7 cells was determined as previously published¹⁰⁰. Briefly, cells were incubated with drug-containing medium. Afterwards, the platinum content (pmol) of isolated cells was measured and related to the protein content (μg), which can be determined by the Bradford method¹¹⁰. As the platinum associated to the cells after incubation is small, it is important for the platinum measurement to use a technique with a low detection limit. On the basis of its high analytical selectivity and its low detection limit, AAS provided a convenient tool for the detection of platinum in the cellular extract (see Section 4.3).

The intracellular molar drug concentration (c_{int}) can be estimated from the pmol/ μg value as previously described¹⁰⁰ (see Table 6.1), according to Eq. 6.1.

$$c_{\text{int}} (\mu\text{M}) = [(\text{pmol Pt}/\mu\text{g protein}) / 8.85 \text{ pL/ng}] \times 1000 \quad \text{Eq. 6.1}$$

Table 6.1 Mean values of the parameters for the calculation of the intracellular platinum concentration, from ref. 100.

Cell line	Cell diameter (μm)	Cell volume (pL)	Protein mass per cell (pg)	Protein content of a cell (pL/ng)
MCF-7	15.38 ± 1.64	1.92 ± 0.55	217.1 ± 73.0	8.85

The cellular uptake is also commonly expressed as a dimensionless accumulation grade, dividing c_{int} by the concentration used in the extracellular medium.

The optimal extracellular drug concentration for the uptake determination was analyzed. On the one hand, using high concentrations of platinum complexes ($10 \mu\text{M}$) favours the influx process and provides higher c_{int} , and so it is possible to work with a reduced amount of cells, staying above the platinum detection limit for AAS. On the other hand, it can lead to decrease in the cellular biomass due to cytotoxic effects. Moreover, if the compound has low aqueous solubility, drug may remain undissolved and thus, the real extracellular drug concentration and the substance capable of being taken up will decrease. Hence, the cellular uptake of **18-Pt** and **19-Pt** (Fig. 6.1) was determined after 6 h incubation with an extracellular drug concentration of 0.15 and $10 \mu\text{M}$, respectively. **18-Pt** showed comparable accumulation grades at both concentrations: $7.7 (\pm 0.8)$ at $0.15 \mu\text{M}$ and $6.2 (\pm 1.1)$ at $10 \mu\text{M}$ extracellular concentration. On the contrary, **19-Pt** displayed accumulation grades of $26.6 (\pm 2.6)$ and $14.0 (\pm 0.6)$, at 0.15 and $10 \mu\text{M}$ respectively. Taking into account that **19-Pt** presents reduced aqueous solubility (lower

than **18-Pt**, see Section 8.2) and high lipophilicity (greater than **18-Pt**, see Section 7.1) it is predictable that at a concentration of 10 μM some substance is going to remain undissolved. When dividing c_{int} by the overestimated extracellular concentration (10 μM) the accumulation grade is then underestimated. This is probably the case of **19-Pt** where the accumulation grade at 10 μM was almost the half than at 0.15 μM .

In order to avoid future underestimations, the accumulation grade was determined always at a drug concentration below the determined aqueous solubility limit. The chosen concentrations were 0.15 or 0.3 μM , depending on the assay to be carried out.

6.3 Cellular accumulation of [salophene]- and [saldach] platinum(II) complexes after 6 and 24 h of drug exposure

MCF-7 human breast cancer cells were incubated for 6 and 24 h with the respective [salophene]platinum(II) complexes and **33-Pt**, at a concentration of 0.15 μM . In Table 6.2 the cell-associated platinum values expressed as accumulation grade are listed.

Table 6.2 Accumulation grade of platinum(II) complexes in MCF-7 cells after 6 and 24 h of incubation.

Compound	Substitution pattern	Accumulation grade	
		6 h	24 h
13-Pt	-	30.8 \pm 4.7	11.2 \pm 1.6
14-Pt	R ₃ = OCH ₃	12.2 \pm 1.6	6.7 \pm 0.1
15-Pt	R ₄ = OCH ₃	21.5 \pm 0.4	12.4 \pm 0.2
16-Pt	R ₅ = OCH ₃	16.4 \pm 5.6	10.0 \pm 0.5
17-Pt	R ₆ = OCH ₃	22.0 \pm 0.7	20.3 \pm 2.5
18-Pt	R ₃ = F	7.7 \pm 0.8	11.0 \pm 3.6
19-Pt	R ₄ = F	26.6 \pm 2.6	15.5 \pm 2.7
20-Pt	R ₅ = F	15.9 \pm 2.2	11.7 \pm 4.8
21-Pt	R ₆ = F	9.0 \pm 1.8	10.6 \pm 5.0

Table 6.2 (cont.)

Compound	Substitution pattern	Accumulation grade	
		6 h	24 h
22-Pt	R' ₃ = F	17.1 ± 1.0	14.2 ± 1.8
23-Pt	R' ₃ = F, R ₃ = F	20.5 ± 1.5	23.3 ± 2.7
24-Pt	R' ₃ = F, R ₄ = F	20.5 ± 2.2	22.2 ± 0.4
25-Pt	R' ₃ = F, R ₅ = F	26.4 ± 1.2	20.0 ± 2.0
26-Pt	R' ₃ = F, R ₆ = F	10.6 ± 0.8	17.5 ± 1.1
27-Pt	R' ₄ = F	17.6 ± 1.8	11.6 ± 4.3
28-Pt	R' ₄ = F, R ₃ = F	8.9 ± 1.7	8.4 ± 0.7
29-Pt	R' ₄ = F, R ₄ = F	12.9 ± 0.8	23.4 ± 3.7
30-Pt	R' ₄ = F, R ₅ = F	19.1 ± 1.9	18.0 ± 4.7
31-Pt	R' ₄ = F, R ₆ = F	27.9 ± 2.0	18.9 ± 1.7
32-Pt	R' ₄ = CH ₃	16.9 ± 0.7	17.6 ± 1.7
33-Pt	saldach	12.2 ± 2.3	6.6 ± 0.1

As mentioned before, the accumulation grade of a drug is the intracellular concentration of the drug divided by the concentration in the extracellular medium. Therefore, an accumulation grade of 1 means that the intra- and extracellular drug concentration is the same. In these experiments, the cellular concentration of all the tested platinum complexes exceeded the extracellular ones at least 6-fold, reaching in some cases a difference up to 30-fold. The uptake of the platinum(II) complexes was modified by the nature and the position of the incorporated substituents. If the results of a short (6 h) drug exposure are compared with a long (24 h) one, three possible situations were observed: the accumulation remained similar such as in the case **28-Pt**, after 6 h exposure the accumulation was reduced like in the case of **13-Pt**, or after 6 h exposure the accumulation was increased, as observed for **29-Pt**. Such behaviour could be explained by differences in the efflux rates of the platinum(II) complexes.

It is worth noting, that the complex which presented the highest intracellular concentration was the unsubstituted [salophene]platinum(II) complex (**13-Pt**). Therefore, it can be concluded that the introduction of substituents reduces the cellular uptake of the platinum(II) complexes.

6.4 Time-dependent cellular accumulation of [salophene]platinum(II) complexes

The uptake of platinum(II) complexes after 6 and 24 h appeared to be time-dependent in most of the cases. Thus, it was necessary to analyze how the complexes are taken up in the cells in more detail. Therefore, the enrichment was determined at 7 different drug exposure times and over a period of 24 h for all the [salophene]platinum(II) complexes which had IC_{50} values lower than $20 \mu\text{M}$. The chosen concentration in this case was $0.3 \mu\text{M}$, twice the concentration used in the previous assay. This was in order to be able to detect platinum in the cell pellets, even at short drug exposure times, and at the same time ensuring the aqueous solubility of the complexes and avoiding a decrease in the cellular biomass due to cytotoxic effects.

Almost all complexes were taken up to maximum levels within 2-6 h, although in most cases there are significant differences between the highest platinum contents observed for the tested compounds (Fig. 6.2).

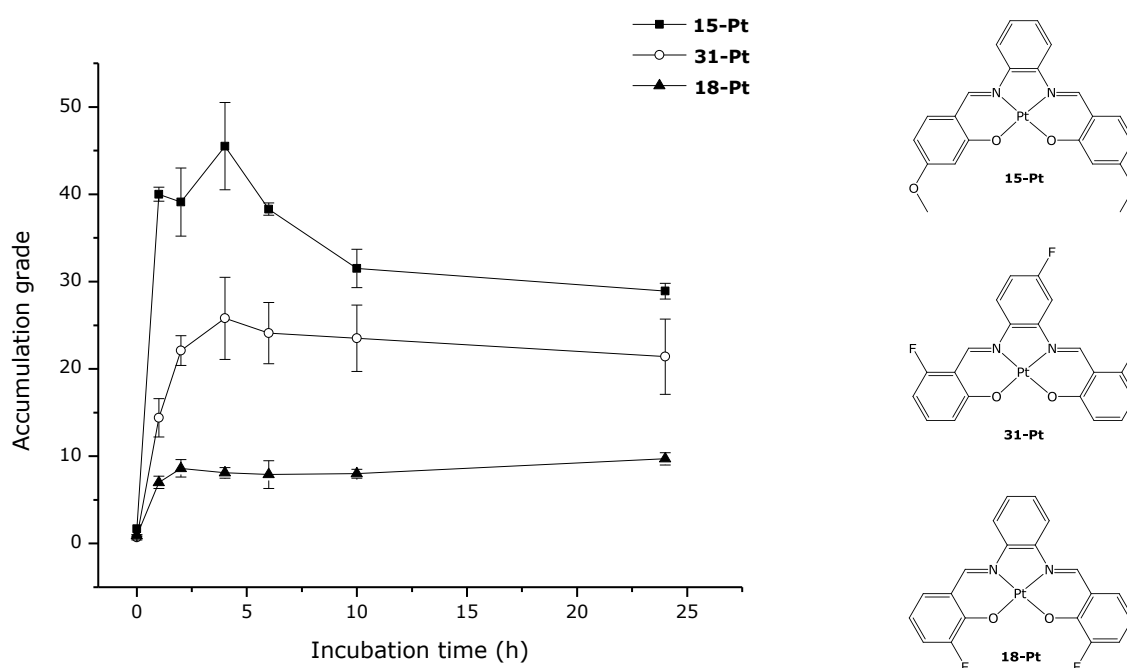


Figure 6.2 Time-dependent accumulation of $0.3 \mu\text{M}$ of **15-Pt** (■), **18-Pt** (▲) and **31-Pt** (○) in MCF-7 cells, and their molecular structure (right).

In Fig. 6.2 three examples of compounds which are taken up until different maximum levels are presented. While **18-Pt** presented a accumulation grade lower than 10 during

the whole exposure time, **31-Pt** reached after 4 h incubation an accumulation grade of 25.7 (\pm 4.7) which was only a slight decreased after longer drug exposure. The accumulation kinetic of **18-Pt** and **31-Pt** suggest the presence of a saturable system of cellular uptake. In contrast to **31-Pt** and **18-Pt** which presented after 4 h exposure nearly a linear graph, **15-Pt** accumulated fast and reached at 6 h a maximum of 45.5 (\pm 5.0)-fold enrichment compared to the cell culture medium. However, towards the end of the test the intracellular concentration was reduced to 28.9 (\pm 0.9)-fold. This could be due to a multifactorial process and can occur through several mechanisms, such as increased drug efflux and decreased drug transport into the cell. It has also been suggested that the plateau seen in many uptake profiles is due to damage of the membrane functionality, as the result of extensive platination¹⁰⁸.

In Fig. 6.3 the accumulation grade of **26-Pt** and **27-Pt** are plotted against the incubation time.

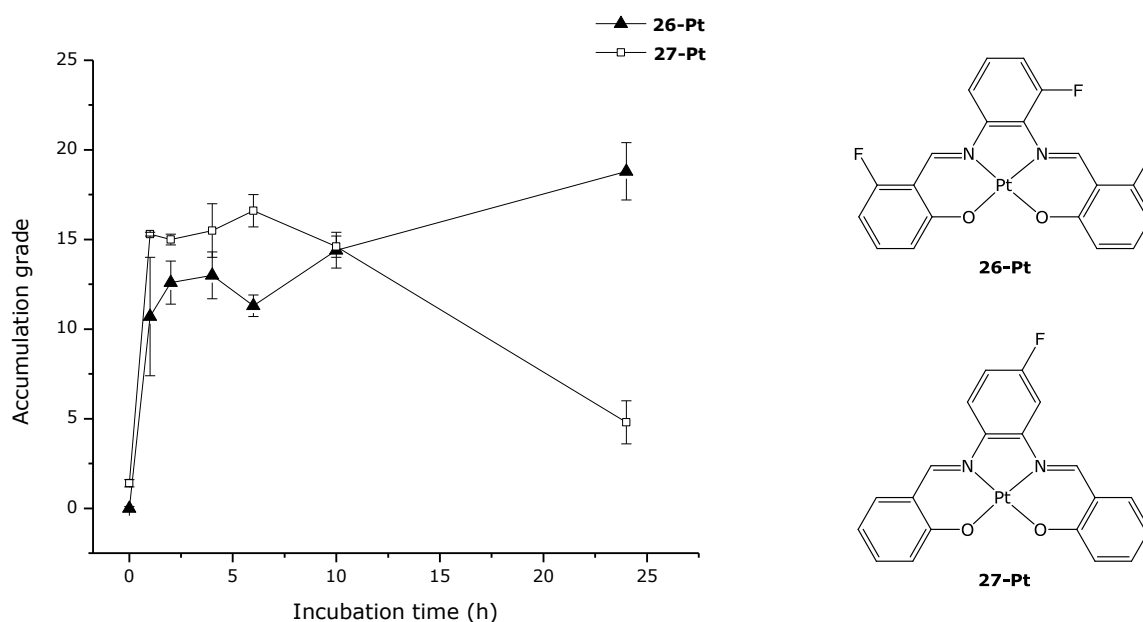


Figure 6.3 Time-dependent accumulation of 0.3 μ M of **26-Pt** (\blacksquare) and **27-Pt** (\square) in MCF-7 cells, and their molecular structure (right).

The differences between accumulation kinetic profiles can be clearly observed. While **26-Pt** showed an apparently non-saturable uptake, **27-Pt** reached a maximum after 6 h incubation and then the accumulation against the medium dropped to approximately one-third the maximum concentration. It is important to emphasize the structural similarities between both complexes (Fig. 6.3 right) and how substituents and their position have a huge impact on the uptake. For example, let us compare **26-Pt** (Fig. 6.3 right above) and **31-Pt** (Fig. 6.2 right middle): the exchange of the fluorine in the

phenylene moiety from R'₄ (**31-Pt**) to R'₃ (**26-Pt**) modified the accumulation kinetic profile from a saturable to a non-saturable one. Moreover, **27-Pt** (Fig. 6.3 below), which in contrast to **31-Pt** presents unsubstituted salicylidene moiety, was the compound which, after having reached the maximum accumulation, reduced the most its intracellular concentration.

Another parameter of interest is the value which represents the enrichment at time zero. Experimentally, the cells were incubated with drug containing medium for only 5 s, before they were collected for the platinum and protein analysis. It is very unlikely that the obtained platinum accumulation after this short drug exposure time represent the real intracellular concentration. As explained before, the plasma membrane is the frontier against exogenous substances, and then membrane bound molecules, lipids and proteins are accessible target molecules for drugs. Thus, the rate of transport and intracellular accumulation of platinum complexes are dependent on their reactivity with membrane structures, and this can depend on the structure of the compounds¹¹¹. The method used to determinate the intracellular accumulation cannot distinguish between binding of the drugs to cell-surface components and true uptake. Therefore, the time zero value may represent membrane-bound or associated platinum complex, instead of intracellular content. Most of the tested platinum(II) complexes presented at time zero, lower concentration of cell associated platinum than the extracellular medium (accumulation grade < 1). An exception was **24-Pt**, which showed at time zero an accumulation grade of 5.6-fold increase (Fig. 6.4).

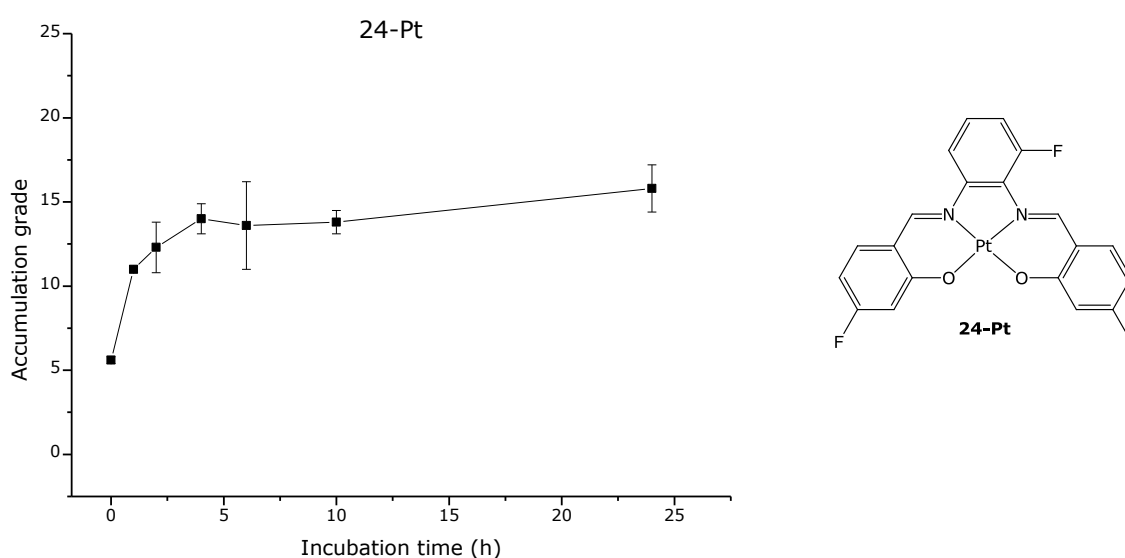


Figure 6.4 Time-dependent accumulation of 0.3 μM of **24-Pt** in MCF-7 cells, and its molecular structure (right).

It is difficult to estimate the impact that this membrane-binding can have on the cellular uptake. On the one hand, the real extracellular concentration of the drug could be reduced due to unspecific binding of the compound to the cellular membrane. As a result, if the complex enters the cell by means of passive diffusion, the uptake rate could be decreased. On the other hand, if the drug binds to membrane proteins that are involved with a specific carrier-mediated uptake mechanism, the enrichment could be enhanced.

In the Appendix the time-dependent accumulation curves for all the [salophene]platinum(II) complexes with an IC_{50} value below 20 μ M are presented.

6.5 Efflux studies

The accumulation of drugs in living cells represents an equilibrium between influx and efflux. From this point of view, and for better understanding of the [salophene]platinum(II) complexes accumulation pattern, the efflux must be investigated. An increased efflux could explain decreased accumulation during the whole drug exposure and/or the strong decrease of intracellular platinum after the maximum have been reached (**15-Pt**, **27-Pt**).

The loss of five compounds (**13-Pt**, **15-Pt**, **18-Pt**, **20-Pt** and **22-Pt**) from MCF-7 cells was determined by measuring the intracellular platinum concentration after incubation with the complexes and subsequent incubation with drug-free medium. The efflux pattern after an initial exposure to 0.3 μ M of **18-Pt** and **15-Pt** is graphically expressed in Fig. 6.5.

Difference between the efflux of **18-Pt** and **15-Pt** can be observed. While in the cells treated with **18-Pt**, the platinum concentration decreased to 70% of the initial value, the cells previously incubated with **15-Pt** showed a very slow efflux. This may explain the differences between the maximum accumulation levels reached by both complexes: 7- and 45-fold for **18-Pt** and **15-Pt** respectively (see Fig. 6.2).

The rest of the tested compounds showed slow and comparable release of platinum. The cells lost 15-25% of the accumulated platinum complex after 2 h. At least, during the time while the efflux was analyzed (2 to 4 h), it represented a considerable influence on the accumulation. These results suggest that reduced drug uptake and increased efflux may explain the accumulation profiles.

In Appendix the efflux curves for **13-Pt**, **15-Pt**, **18-Pt**, **20-Pt** and **22-Pt** are presented.

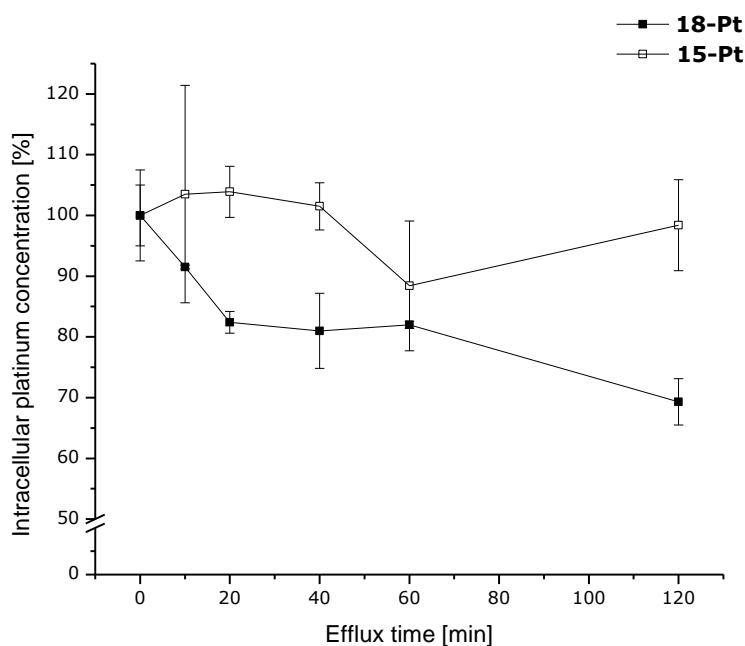


Figure 6.5 Intracellular platinum concentration (%) in MCF-7 cells after 2 h of incubation with **18-Pt** (■) and **15-Pt** (□) and subsequent incubation with drug-free medium. The mean platinum concentration after 2 h incubation was set as 100%.

6.6 Relationship between cellular accumulation and cytotoxicity

Intracellular platinum content is considered to play an important role in cytotoxicity. Although for platinum-based drugs in cancer therapy, DNA platination is the paramount activity parameter, a relationship between the overall intracellular Pt uptake and survival of cells exposed to cisplatin and its metabolites has been reported¹¹². Although previous investigations with gold phosphine complexes¹¹³ showed a relationship between accumulation and growth inhibitory effects under similar test conditions, no relationship was found in the tested platinum(II) complexes. Furthermore, some complexes that were taken up efficiently into cells (as **19-Pt**, which presented after 6 h an accumulation of 26.6-fold), exhibited no cytotoxicity on MCF-7 cells within the tested concentration range (< 20 μM). These results suggest that the uptake of these complexes is not the main reason for their decreased antiproliferative effects.

Since the IC_{50} values were determined after 96 h incubation and the enrichment was analyzed until 24 h, it is difficult to compare the results. Moreover, it has been shown in Section 6.4, that in many cases the accumulation does not reach a plateau. This makes it

difficult to predict the intracellular concentration after longer exposure times than the tested ones (for example 96 h as for IC₅₀ determination).

Anyhow, it is of great interest to make a qualitative comparison between the time-dependent cellular accumulation and cytotoxicity studies. In some cases, the accumulation profile may be an explanation of the observed differences in cytotoxicity as a function of time.

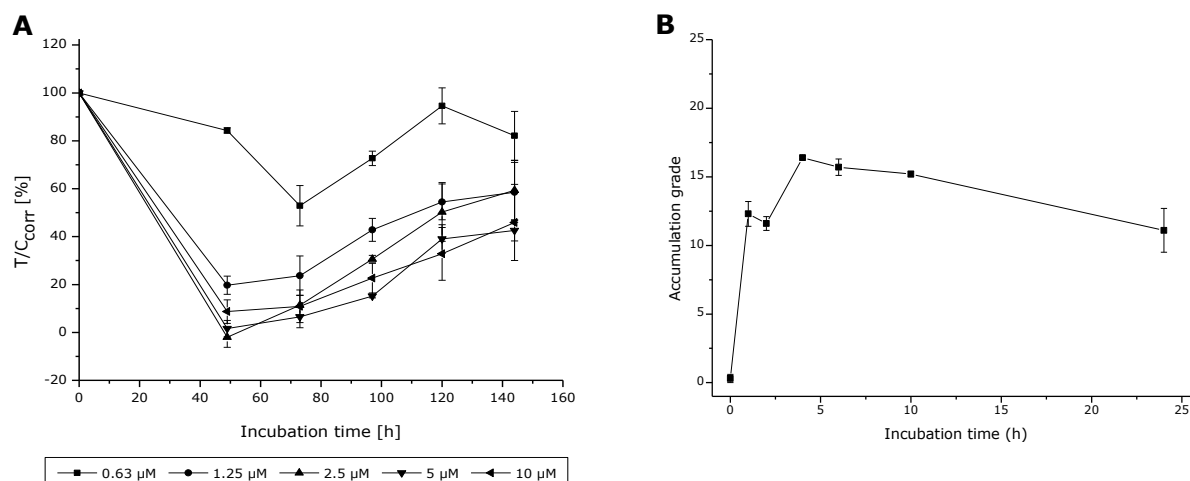


Figure 6.6 Time-dependent cytotoxicity (**A**) and cellular accumulation (**B**) of **13-Pt** in MCF-7 cells.

The time-dependent cytotoxicity and accumulation of **13-Pt** are shown in Fig. 6.6. The complex was taken up fast and reached its maximum at 6 h, followed by a slow decrease of the cellular concentration that continues until the end of the analyzed time (Fig. 6.6 **B**). On the contrary, the cytotoxicity presented a maximum at 48 h and over time the effect seems to decrease (Fig. 6.6 **A**). If the intracellular concentration is related with the antitumour effects, the decrease in the accumulation may explain the reduction of cytotoxicity.

Similar relations between intracellular concentration and cytotoxicity can be predicted for the of other platinum(II) complexes, as for example **18-Pt** and **26-Pt**, whose time-dependent cellular accumulation plots are shown in Figs. 6.2 and 6.3 respectively. As described before, the intracellular concentration of **18-Pt** reached a plateau after 2 h incubation and remained constant until the end of the analysis. Likewise, the cytotoxicity was approximately constant during the time-dependent antiproliferative assay (see Fig. 5.11). The third example is **26-Pt**, whose cellular accumulation increased with the time and so did the cytotoxicity (see Appendix).

6.7 Conclusion on the accumulation studies

In summary, the [salophene]platinum(II) complexes showed rather different degrees of accumulation in MCF-7 cells, and a correlation between the total corresponding cellular accumulations of platinum with the IC_{50} values after 96 h exposure could not be precisely established. Further studies, such as short-term cytotoxicity assays, are needed to compare accumulation and antitumor effects at similar exposure periods.

In most of the analyzed cases, the differences in short-term platinum efflux did not appear to be the only reason of variability in accumulation. Therefore, it is important to consider factors that could decrease the uptake. For example, binding of the platinum(II) complexes to cellular membrane molecules could induce changes in the membrane structure and functions, affect its integrity and viability, and as a consequence modify its permeability.

7 Analysis of physicochemical properties of the [salophene]platinum(II) complexes in relation to their biologic activities

Solubility, degree of ionization and lipophilicity, among other physicochemical properties, are attributes that describe the hydrophilic or hydrophobic characteristics of a drug. They are useful for correlating a drug transport process, its interactions with receptor molecules, and their tendency to cross biological membranes. An appropriate balance between them is needed for drug delivery. The case of cytostatic drugs requires serious attention in this regard: in order to reach its target in the tumour site, they must pass through several membranes in the body, including the cellular membrane to the cytosol. Therefore, the [salophene]- and [saldach]platinum(II) complexes were studied for their lipophilicity and solubility in order to establish a possible relationship between these properties and other biological effects such as cellular uptake and cytotoxicity.

7.1 Lipophilicity

Biomembranes consist primarily in phospholipids arranged in bilayers with embedded proteins. The polar surface and the non-polar core of the membranes, originated by the amphipathic phospholipids, allow them to act as effective barriers to substances.

The permeation of solutes through membranes has been widely studied^{114,115}. Since lipophilicity of drugs is related to the ability of compounds to cross cell membranes by means of passive diffusion, it appears in almost every analysis of physicochemical properties related to absorption and it is recognized as an important parameter in structure-activity relationship studies. Fujita *et al.* proposed first the *octanol-water partition coefficient*, P , where 1-octanol simulates a lipid membrane and water is a model for fluid in and out of cells, constituting a good example for biological partition. Since then, the logarithm of P , ($\log P$), has become the most widely used lipophilicity parameter, which simulates the solubility of compounds in membranes¹¹⁶. For example, a drug with a measured $\log P$ equal to 2 indicates that its concentration is at a 100:1 ratio in 1-octanol to aqueous phase. In contrast, a drug with a $\log P$ equal to -2 indicates that the concentration is at a 1:100 ratio in organic to aqueous phase. Platinum(II) complexes such as cisplatin or carboplatin are hydrophilic, as is usual for small coordination

complexes containing polar coordination bonds, thus their $\log P$ values are negative (-2.27 and -1.63 respectively)¹¹⁷.

7.1.1 Lipophilicity determination: procedure and results

High-performance liquid chromatography (HPLC) provides an easy way to determine the partition properties of compounds based on their retention time. Veith *et al.*¹¹⁸ showed in 1978 a relationship between $\log P$ and the HPLC reverse-phase retention time: the logarithm of the retention factor (k) of substances on a HPLC system, determined from the retention time (t_R) and dead time (t_0)¹¹⁹ as $(t_R - t_0)/t_0$, was found to be linearly related to the $\log P$. Consequently, $\log k$ can be calibrated with the lipophilicity by using average values of $\log P$, obtained from literature¹²⁰, as referenced in Table 7.1. In order to determine the lipophilicity of the [salophene]platinum(II) complexes, a set of six compounds having $\log P$ literature values from 2.13 to 6.30 were selected and used as standards: benzene, naphthalene, biphenyl, anthracene, n-hexylbenzene and n-octylbenzene. The calibration mixture was chromatographed and a calibration curve was constructed daily, in order to avoid differences of flow rate and temperature.

Table 7.1 HPLC retention times and partition coefficients of the organic chemicals used for the calibration.

Compound	t_R (min)	$\log k$	$\log P$ (ref.) ¹²⁰
benzene	5.15	0.010	2.13
naphthalene	8.25	0.350	3.35
biphenyl	10.83	0.512	3.98
anthracene	17.29	0.762	4.50
n-hexylbenzene	29.70	1.028	5.52
n-octylbenzene	64.03	1.383	6.30

The calibration graph in Fig. 7.1 was generated by plotting the $\log P$ vs. $\log k$ values present in Table 7.1, and fitting the data using a linear regression.

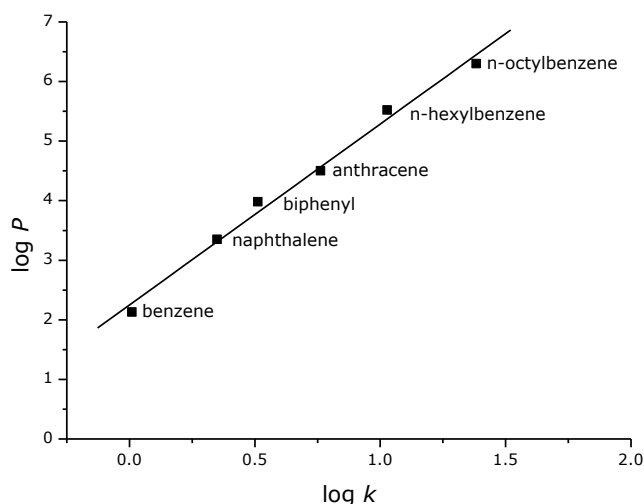


Figure 7.1 HPLC relationship between $\log P$ and HPLC $\log k$ of the calibration mixture, fitted using a linear function.

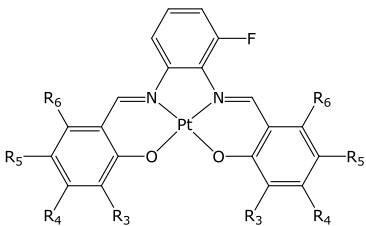
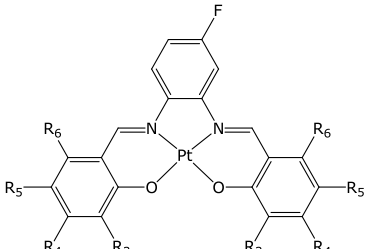
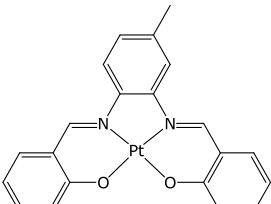
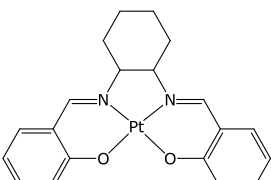
The data in Fig. 7.1 can be summarized with the equation $\log P = 3.037 \log k + 2.249$, with a correlation coefficient of 0.995.

The [salophene]platinum(II) complexes were chromatographed individually in the same conditions as the calibration mixture, and the $\log P$ values were calculated from the regression equation. The compounds are listed in Table 7.2 together with their respective $\log P$, as the mean of two independent experiments.

Table 7.2 Main structures of the different [salophene]platinum(II) complexes and **33-Pt**, with their estimated $\log P$ values.

Structure	R ₃	R ₄	R ₅	R ₆	$\log P$	Compound
	H	H	H	H	4.05 ± 0.01	13-Pt
	OCH₃	H	H	H	4.62 ± 0.11	14-Pt
	H	OCH₃	H	H	4.84 ± 0.01	15-Pt
	H	H	OCH₃	H	4.22 ± 0.01	16-Pt
	H	H	H	OCH₃	6.08 ± 0.01	17-Pt
	F	H	H	H	3.79 ± 0.01	18-Pt
	H	F	H	H	4.59 ± 0.01	19-Pt
	H	H	F	H	4.27 ± 0.01	20-Pt
H	H	H	F	5.84 ± 0.01	21-Pt	

Table 7.2 (cont.)

Structure	R ₃	R ₄	R ₅	R ₆	log <i>P</i>	Compound
	H	H	H	H	5.13 ± 0.07	22-Pt
	F	H	H	H	4.61 ± 0.01	23-Pt
	H	F	H	H	5.56 ± 0.08	24-Pt
	H	H	F	H	5.21 ± 0.08	25-Pt
	H	H	H	F	6.67 ± 0.03	26-Pt
	H	H	H	H	4.19 ± 0.07	27-Pt
	F	H	H	H	3.89 ± 0.01	28-Pt
	H	F	H	H	4.62 ± 0.01	29-Pt
	H	H	F	H	4.33 ± 0.01	30-Pt
	H	H	H	F	5.74 ± 0.01	31-Pt
	-	-	-	-	4.65 ± 0.06	32-Pt
	-	-	-	-	2.69 ± 0.05	33-Pt

The log *P* values of the [salophene]platinum(II) complexes (see Table 7.1) were in the range of 3.79 (**18-Pt**) to 6.67 (**26-Pt**), and was 2.69 for the [saldach]platinum(II) complex, **33-Pt**. Depending on the nature and the position of the substituents present in the complexes, the lipophilicity increased or decreased. Some observations regarding the differences in lipophilicity in relation to the substitution pattern may be noted:

- Insertion of fluorine, methyl or methoxy substituents generally led to compounds with increased lipophilicity when compared to the unsubstituted compound (**13-Pt**).
- Complexes bearing substituted phenylene and unsubstituted salicylidene moieties (**22-Pt**, **27-Pt**, **32-Pt**) were always more lipophilic than **13-Pt**. The lipophilicity increases in the following order: **13-Pt** (R' = H, R = H) < **27-Pt** (R'₄ = F, R = H) < **32-Pt** (R'₄ = CH₃, R = H) < **22-Pt** (R'₃ = F, R = H).

- Additional substitution on the salicylidene moiety enhanced or decreased the lipophilicity depending on the position of the substituent, when the phenylene moiety remained unchanged. While the incorporation of a substituent on position R₃ tends to decrease the lipophilicity, complexes bearing a R₄, R₅ or R₆ substituted moiety enhanced the lipophilicity in the following order: R₅ < R₄ < R₆.
- The most lipophilic compounds were the ones with a R₆ fluorinated position, reaching lipophilicity values of 6.67 in the case of **26-Pt**.

The [saldach]platinum(II) complex, **33-Pt**, demonstrated an unexpected low lipophilicity, with a log *P* value of 2.69. In this case, the replacement of the benzene ring in the phenylene moiety of **13-Pt** (log *P* = 4.05) by a cyclohexane ring (**33-Pt**) resulted in a less lipophilic compound, contrary to expectations, since the log *P* values for benzene and cyclohexane are 2.13 and 3.44 respectively. As a consequence of the observed differences between the expected and the experimental results, the lipophilicity of the salophene (**13**) and saldach (**33**) ligand were investigated. Since the ligands are less lipophilic than the complexes, a different and more appropriate HPLC mobile phase and calibration mixture was used (Table 7.3).

Table 7.3 Organic chemicals used for the calibration, their retention time and literature log *P* values.

Compound	<i>t_R</i> (min)	log <i>P</i> (ref.) ¹²⁰
benzamide	3.64	0.64
acetanilide	4.75	1.16
acetophenone	6.90	1.63
benzene	11.18	2.13
naphthalene	31.11	3.35
biphenyl	56.53	3.98

Surprisingly, the ligands presented very similar log *P* values: 1.64 (± 0.04) for the salophene and 1.63 (± 0.06) for the saldach compound. Since there is no significant difference between these values it may be considered that both ligands have similar lipophilicity. This demonstrates the difficulty to predict the lipophilicity of compounds. With these results it is difficult to explain the difference in the obtained log *P* value of the [salophene]- and [saldach]platinum(II) complex by differential lipophilicity of the ligands.

Many other factors, such as electronic conjugations or conformation influence the lipophilicity of compounds¹²¹. A possible cause for the decreased lipophilicity of the [saldach]platinum(II) complex, is related with the separation of charges originated from the complexation of the ligand with platinum. The exchange of the benzene ring of the salophene complex by a cyclohexane ring decreases the number of conjugated π -electrons, and thus the possibility that the aromatic ring provides to stabilize the separation of charges is eliminated. In this way, the hydrophilic character of the [saldach]platinum(II) complex may be enhanced.

7.1.2 Relationship between lipophilicity and biological properties

Numerous studies have reported that IC_{50} values and uptake rates are linearly related to lipophilicity (the more lipophilic nature of a complex, the lower its IC_{50} value and higher its cellular uptake)^{113,122}. To determine whether the inhibition of cell growth or the cellular uptake had a correlation to lipophilicity, IC_{50} values and the cellular accumulation of the [salophene]platinum(II) complexes were plotted in a logarithmic way against their $\log P$ value (Figs. 7.2 and 7.3 respectively). In the case of the IC_{50} versus $\log P$ graph, Fig. 7.2, only substances with an IC_{50} value under 20 μM were plotted.

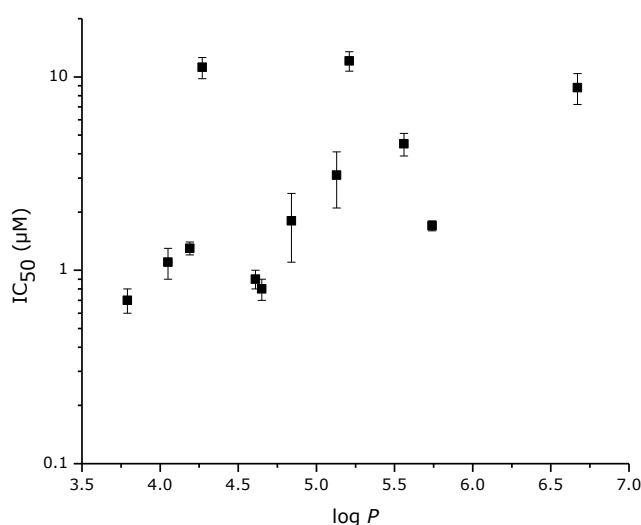


Figure 7.2 Relationship between lipophilicity and growth inhibition of the [salophene]platinum(II) complexes with an IC_{50} value under 20 μM , in MCF-7 tumour cells.

Except **20-Pt** ($IC_{50} = 11.2 \mu\text{M}$) and **25-Pt** ($IC_{50} = 12.1 \mu\text{M}$), whose cytotoxicity may be strongly influenced by factors other than the lipophilicity (such as specific intracellular reactions before reaching the target(s) or modified affinity to the target molecule(s)),

and thus we consider them as outliers, the IC_{50} values show considerable linear dependence on drug lipophilicity, with an R^2 value of 0.75.

In Fig. 7.3 the relationship between the accumulation grade determined at two different times (6 and 24 h) and the lipophilicity are displayed (Figs. 7.3 **A** and **B** respectively).

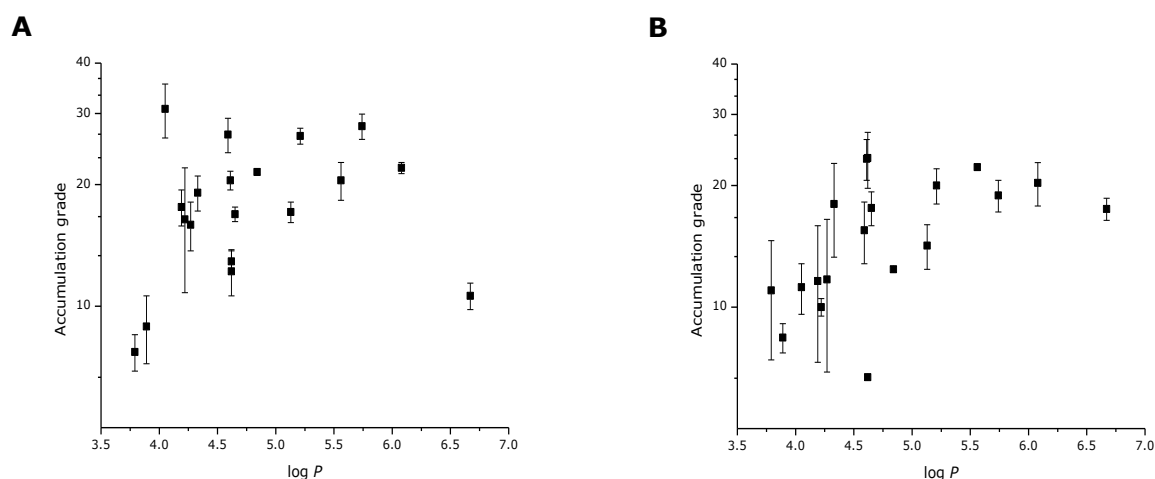


Figure 7.3 Relationship between lipophilicity and cellular uptake (expressed as accumulation grade, see Section 6.2) of the [salophene]platinum(II) complexes in MCF-7 tumour cells. **A** Accumulation grade after 6 h of incubation with the respective tested substance. **B** Accumulation grade after 24 h of incubation with the tested substance.

Although the correlation is not strong, a tendency can be seen: low lipophilicity is related with lower accumulation grades. These results together with the relation between the growth inhibition and lipophilicity suggest that cytotoxicity and cellular uptake are strongly influenced by the lipophilicity of the compounds.

7.2 Aqueous solubility

Aqueous solubility is one of the most fundamental physicochemical properties which characterizes a drug candidate. In the first place, solubility is a key property for the gastrointestinal absorption of orally administered drugs. Unfortunately, compounds with solubility deficiencies are usually found in a drug discovery process, typically due to high lipophilicity. These solubility deficiencies can be overcome by using formulations or delivery systems.

In the second place, solubility limits the concentration of a compound in the activity test solution and therefore, compromises the obtainment of accurate results of biological assays. Hence, solubility measurements can help to interpret activity assay results.

Solubility experiments are mainly based on measuring either the concentration of dissolved compound or the amount of undissolved compound. Several methods are described in literature, such as direct UV absorption¹²³ or nephelometry¹²⁴.

7.2.1 Solubility determination: procedure and results

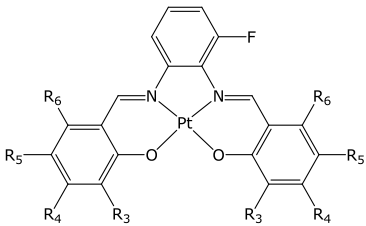
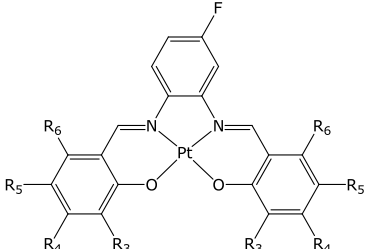
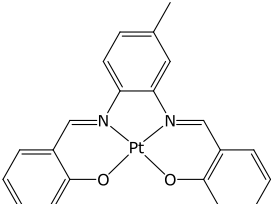
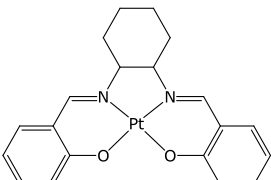
In this work a simplified method was used to determine the aqueous solubility. Our aim was to make a comparison of the solubility of the [salophene]platinum(II) complexes in culture medium, in order to determine a possible relationship between solubility and IC₅₀ values or cellular uptake results. In the assay a solution of 10 mM of the compound in DMF is added to culture medium. The final DMF concentration is kept at 1%, because DMF enhances solubility. First, the solution was mixed for 30 min and then centrifuged at 20.000 *g*¹²⁵ at 37 °C (the same temperature as for biological assays) to decant the undissolved compound. The platinum concentration in the supernatant was measured with AAS, and the solubility of each compound in culture medium was obtained (see data in Table 7.5).

No particular relationship was observed between the solubility and the chemical structure of the tested compounds. The incorporation of substituents in the phenylene or salicylidene moiety produced modifications of the solubility, but in a non systematic way.

Table 7.5 Main structures of the different [salophene]platinum(II) complexes and **33-Pt**, with their solubility values, in culture medium.

Structure	R ₃	R ₄	R ₅	R ₆	Solubility (μM)	Compound
	H	H	H	H	0.33 ± 0.06	13-Pt
	OCH₃	H	H	H	0.70 ± 0.11	14-Pt
	H	OCH₃	H	H	0.34 ± 0.05	15-Pt
	H	H	OCH₃	H	0.28 ± 0.01	16-Pt
	H	H	H	OCH₃	1.20 ± 0.27	17-Pt
	F	H	H	H	1.28 ± 0.02	18-Pt
	H	F	H	H	0.17 ± 0.04	19-Pt
	H	H	F	H	0.30 ± 0.01	20-Pt
	H	H	H	F	0.78 ± 0.25	21-Pt

Table 7.5 (cont.)

Structure	R ₃	R ₄	R ₅	R ₆	Solubility (μM)	Compound
	H	H	H	H	0.91 ± 0.09	22-Pt
	F	H	H	H	1.18 ± 0.16	23-Pt
	H	F	H	H	1.20 ± 0.16	24-Pt
	H	H	F	H	0.60 ± 0.05	25-Pt
	H	H	H	F	0.42 ± 0.01	26-Pt
	H	H	H	H	1.62 ± 0.33	27-Pt
	F	H	H	H	1.54 ± 0.04	28-Pt
	H	F	H	H	0.50 ± 0.02	29-Pt
	H	H	F	H	1.01 ± 0.19	30-Pt
	H	H	H	F	0.96 ± 0.12	31-Pt
			-		0.60 ± 0.03	32-Pt
			-		1.09 ± 0.17	33-Pt

7.2.2 Relationship between solubility and biological properties

As in the case of the lipophilicity, no significant correlation between solubility and IC₅₀ or uptake values were found. The only situation in which a trend could be seen, is in the case of the accumulation grade after 6 h of incubation with the tested compound vs. log *S* plot, where *S* is the solubility in mol/L. This can be seen in the graph drawn in Fig. 7.4.

Although the correlation is not strong, the accumulation is generally reduced by increasing the solubility. The direct reason of this effect could be that an increase in solubility, generally means decrease in lipophilicity, and so the ability of substances to penetrate through biomembranes. Unfortunately, this could not be demonstrated,

because there is no correlation between the solubility and the lipophilicity values of the compounds (see Fig. 7.5). Furthermore, as shown in Fig. 7.3, the accumulation of the compounds in the cells is related with their lipophilicity. However, when the graphs of accumulation grade (6 h) vs. $\log P$ (Fig. 7.3 left) and vs. $\log S$ (Fig. 7.4) are compared, a clear difference between them can be seen. While higher lipophilicity lead generally to higher accumulation grade, high solubility is related to compounds with low intracellular platinum concentration.

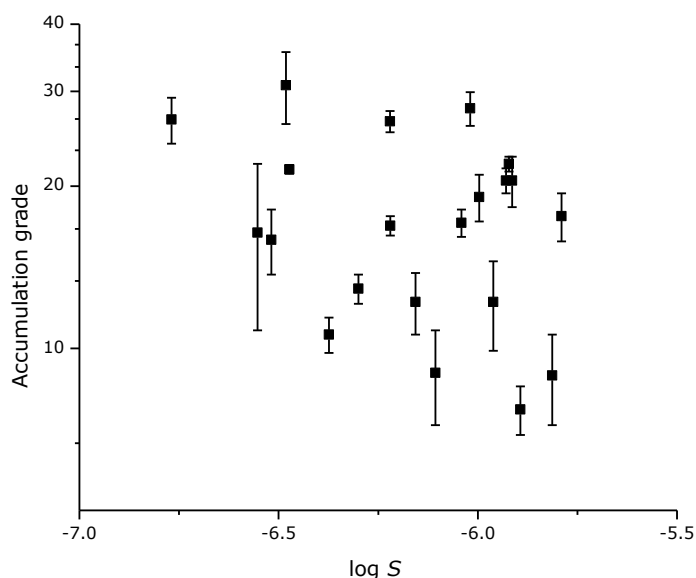


Figure 7.4 Relationship between solubility and cellular uptake (expressed as the accumulation grade, see Section 6.2) of the [salophene]platinum(II) complexes in MCF-7 tumour cells, after 6 h of incubation with the tested substance.

7.3 Conclusion on the solubility and lipophilicity results

The possible relationship between the physicochemical and the biological properties was not observed. Moreover, the inexistent correlation between solubility and lipophilicity was unexpected (Fig. 7.5).

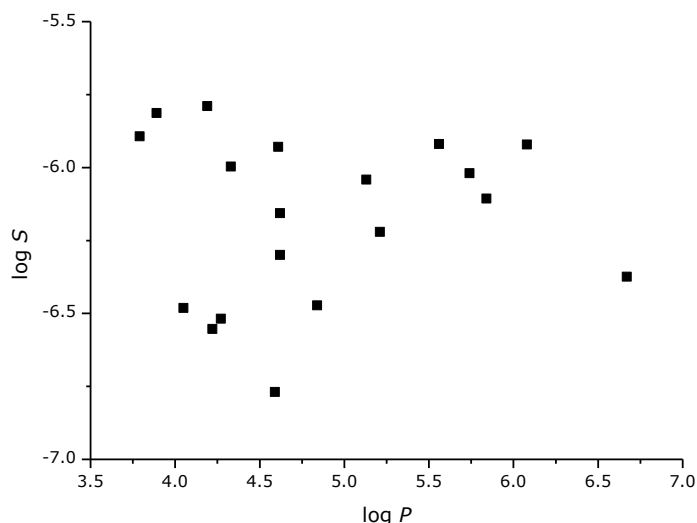


Figure 7.5 Relationship between solubility ($\log S$) and lipophilicity ($\log P$) of the [salophene]platinum(II) complexes.

Many empirical relations between solubility and lipophilicity have been reported over the past fifty years^{126,127}. In 2001, Ran *et al.* proposed a general solubility equation (GSE), in which the correlation between solubility and lipophilicity is influenced by the melting point of each substance¹²⁸. In all these studies, both parameters ($\log S$ and $\log P$) are inversely related, that means that generally, the higher the lipophilicity, the lower the water solubility. This is not the behaviour we observe for the [salophene]platinum(II) complexes. It is possible that the problem lies within the solubility determination. There are number of issues that could have altered the result such as:

- adsorption of the substances to the vial,
- the time spent to achieve the solubility equilibrium (30 min) was not enough,
- substances present in the culture medium (which are not present in water) can modify the solubility of the complexes,
- different dissolution rate between the complexes.

The conditions used to determine the solubility were chosen as similar as possible to those of the cell culture. Therefore, the solubility values, as they were not determined in standard conditions, can only be used to investigate a relationship with the biological results and not to compare with other physicochemical properties like the $\log P$ value. However, from the extremely low determined solubility in culture medium and the high lipophilicity of the compounds, we can predict that the [salophene]platinum(II) complexes are also poorly water soluble compounds.

On the contrary, the lipophilicity was determined following a standard procedure and therefore the results can be compared with literature values. Many guidelines can be found about the optimum $\log P$ values for orally active drugs. In 1997, Lipinski *et al.*, formulated the well known empirical "rule of five"¹¹⁴ which predicts that poor absorption is more likely when more than 5 H-bond donors and 10 H-bond acceptors are present, the molecular weight is greater than 500 and the calculated $\log P$ is greater than 5. If the rule of 5 is implemented to the new [salophene]platinum(II) complexes, which have no H-bond donors, between 4 and 6 H-bond acceptors, molecular weight between 500 and 570 and $\log P$ values mostly between 4 and 6, two parameters are out of range for most of the compounds. This is an alert for possible poor absorption or permeability. The development of drugs with absorption problems is more time and money consuming than for a compound with more suitable properties. Thus, they often have difficulties to get to the market and repay their development costs. Since deficiencies in physicochemical properties may represent the difference between failure and development of a successful oral drug product, the rational optimization of these characteristics of the [salophene]platinum(II) complexes (for example enhancing the solubility by the introduction of hydrophilic substituents) is recommended in order to achieve potential drug candidates.

8 DNA interaction studies of the [salophene] platinum(II) complexes

Platinum-based drugs are among the most active anticancer agents and have been widely used in the treatment of variety of cancers. The anticancer activity of cisplatin and other platinum drugs is believed to arise from their interaction with DNA^{22,129}. Various platinum agents have unique structural and kinetic properties for DNA binding and display different DNA-adduct profiles. Understanding the nature of these platinum adducts is crucial for elucidating how they are recognized and processed by cellular proteins.

8.1 DNA binding modes for metal complexes

Metal complexes can bind with the DNA *via* covalent, non-covalent, or hybrid binding modes. Cisplatin is the best known example of the covalent binders group. It binds to DNA by coordination of the platinum atom to N7 position of two purine bases, either to two guanine bases or to adenine and guanine. Analysis of purified DNA treated with cisplatin or DNA isolated from cisplatin-treated patients demonstrates 1,2-intrastrand d(GpG) cross-link as major adduct (65%)¹³⁰. A small percentage of interstrand cross-links and monofunctional adducts are also present. Biochemical studies demonstrated unwinding and bending as well as destabilization of the duplex induced by the cisplatin lesions¹³¹. Non-covalent modes of binding include: groove binding, intercalation, and insertion (Fig. 8.1).

Groove binders bind DNA in the minor groove at A/T rich regions through electrostatic interactions, hydrogen-bonding, and Van der Waals interaction. In general, these inorganic groove binding drugs are cationic and can adopt a curved structure when bound to DNA, which allows the drug to be closely associated with the minor groove over a span of three to four base-pairs. As an example, Weathe *et al.* have developed multinuclear platinum complexes, linked by flexible 4,4'-dipyrazolymethane, which pre-associates the complex in the DNA minor groove at A/T rich regions. This changes the preference of the dinuclear platinum complexes for guanine residues to adenine residues. Therefore, this pre-covalent binding association could be used to control the site of platination¹³².

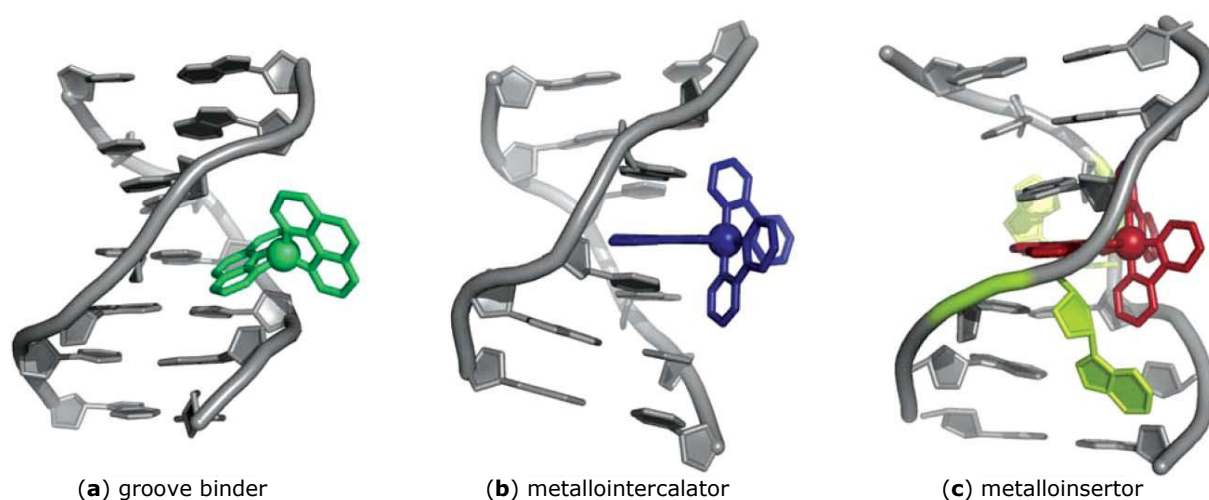


Figure 8.1 The three binding modes of metal complexes with DNA: (a) groove binding, (b) intercalation, and (c) insertion. (Taken from ref. 133)

Metallointercalators are structurally rigid metal complexes with a well-defined symmetry, that bears at least one intercalating ligand. These ligands are small organic molecules that unwind DNA in order to π -stack between two base pairs (Fig. 8.1). They enter the double helix *via* the major groove, with the intercalating ligand acting as a new base pair. There are many examples of platinum complexes that interact with the DNA as metallointercalators. Lippard *et al.* pioneered studies on DNA-metallointercalators using square-planar d^8 platinum(II) complexes¹³⁴. Other new investigations focus on platinum intercalator conjugates. They consist of two specific DNA-recognizing groups connected either by a flexible linker chain (usually a polymethylene chain) or directly bound to the platinum metal centre¹³⁵. Such structures are designed to potentially combine two mechanisms of action: platination and intercalation.

Metalloinsertors contain a planar aromatic ligand that extends into the base-stack upon DNA-binding. While metallointercalators unwind the DNA and insert their planar ligand between two intact base-pairs, metalloinsertors eject the bases of a single base-pair, with their planar ligand acting as a π -stacking replacement in the DNA base stack¹³³. There are only a few examples of metallointercalators. Recently, Barton *et al.* introduced a family of chrysenequinone diimine complexes of rhodium¹³⁶. The main interest in these complexes arises from their ability to selectively bind mismatched sites in DNA and to inhibit cellular proliferation preferentially in mismatch repair (MMR) deficient cells. Considering that deficiencies in MMR are associated with carcinogenesis, mismatched DNA represents a major target.

8.2 Interaction of the platinum(II) complexes with isolated DNA

8.2.1 Circular dichroism studies

Circular dichroism (CD) is a phenomenon originated from interactions of chiral molecules with circularly polarized electromagnetic rays. Absorption of right- (A_r) and left-handed (A_l) circularly polarized light by chiral molecules differs and thus are considered to be "optically active". The difference is called CD ($CD = A_l - A_r$), and is measured as a function of wavelength. The magnitude used to describe this phenomenon is usually expressed in terms of ellipticity, θ , which is measured in degrees. CD is a useful technique for monitoring DNA conformation changes resulting from changes in environmental conditions, such as variations in temperature, pH, or as in this case, interactions between the DNA and the platinum complexes. Most spectral DNA studies employ ultraviolet (UV) light within 180-300 nm range, where DNA bases absorb light¹³⁷. The UV circular dichroic spectrum of calf thymus DNA (CT-DNA) exhibits a positive band at 270 nm due to base stacking and a negative band at 239 nm due to helicity of B-DNA¹³⁸ (Fig. 8.2).

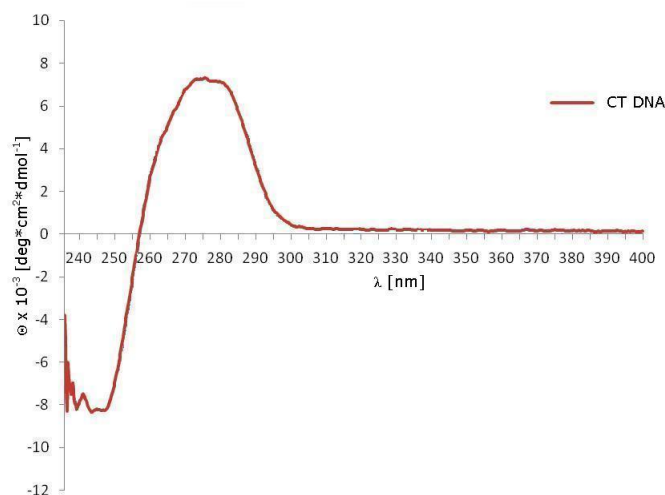


Figure 8.2 CD spectrum of calf thymus DNA (CT-DNA).

These bands are quite sensitive to non-covalent interactions of metal complexes to B-DNA, making this technique useful in diagnosing changes in DNA morphology during drug-DNA interactions. Intercalation enhances the intensities of both bands stabilizing

the right-handed B conformation of *CT-DNA* as observed for the classical intercalator methylene blue¹³⁹.

Therefore, the CD spectra of the interaction of complexes **13-Pt**, **15-Pt** and **17-Pt** with *CT-DNA* have been recorded after 24 h of incubation and for a constant 1:10 complex/[DNA] mixture (Fig. 8.3).

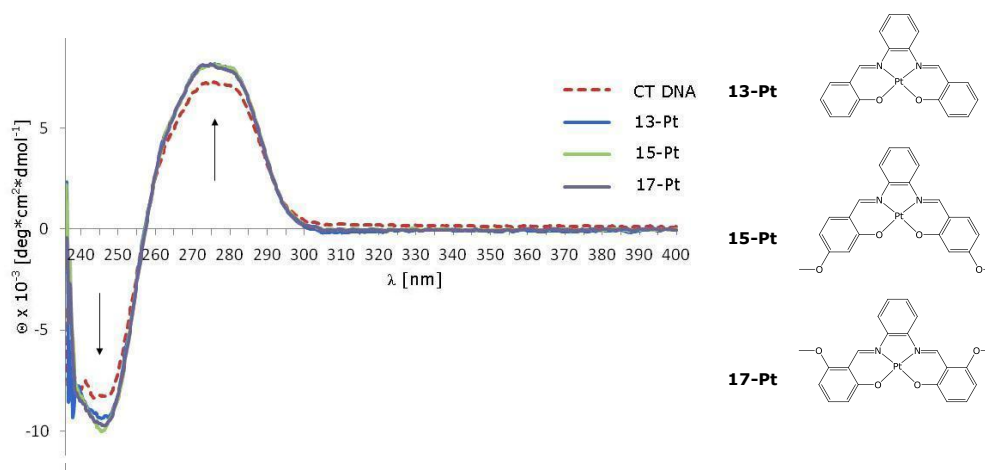


Figure 8.3 CD spectra of **13-Pt** (right above), **15-Pt** (right middle) or **17-Pt** (right below) incubated for 24 h with *CT-DNA* ($r = 1$) in 10 mM phosphate buffer at pH 7.2.

Spectral changes of the positive CD signal at 273 nm might (up arrow in Fig. 8.3) indicate π - π interactions between the nucleobases of the DNA and the π -system of the metal complexes. The three tested substances caused an increase of the intensity of the band in this spectral area. The additional increase of the band at 246 nm (down arrow in Fig. 8.3) in comparison with the band for *CT-DNA* could reflect an alteration in the original B-helical conformation. The absence of any induced CD signal caused by the metal complexes, however, only supports very weak interaction of the platinum complexes with the DNA double helix.

8.2.2 Thermal denaturation studies

By temperature increase the double-stranded DNA progressively denatures: the comparatively stiff DNA double-strand is thereby interrupted by emerging zones of the flexible single-strand. Then, these so-called DNA bubbles grow and merge until the double-strand is fully molten. The melting temperature (T_m) is experimentally defined as the temperature at which half of the strands are in the double-helical state and half are in the "random-coil" state^{140,141} (see Fig. 8.4).

T_m is strictly related to the stability of the double helix, and therefore the interactions of chemicals with DNA can alter it. It is known that the intercalation of small molecules into the DNA results in the stabilization of the double helix due to the stabilizing stacking interactions, increasing the T_m of DNA^{142,143}.

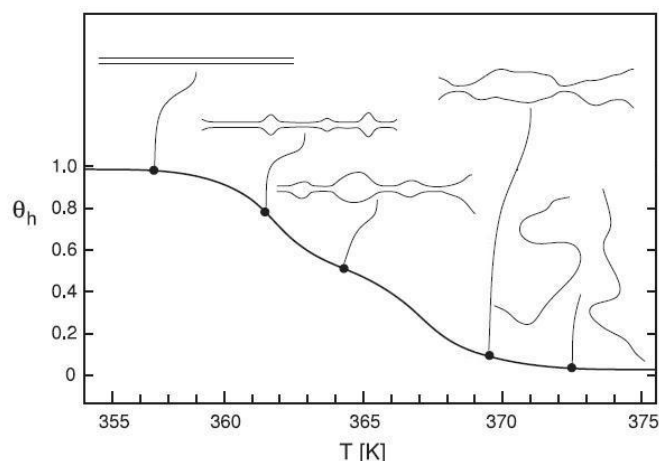


Figure 8.4 Thermal denaturation of double-strand DNA: fraction θ_h of double-helical domains within the DNA as a function of temperature. Schematic representation of θ_h showing the increased formation of bubbles until full denaturation has been reached¹⁴⁰.

The extinction coefficient of DNA bases at 260 nm in the double-helical form is much smaller than in the single-strand form, therefore the melting of the helix leads to an increase in the absorbance at this wavelength. Thus, the T_m can be determined by monitoring the absorbance of the DNA at 260 nm as a function of the temperature. The T_m experiment carried out for *CT-DNA* in the absence of any added complex revealed a T_m of 67 ± 1 °C under our experimental conditions. The ΔT_m after addition of complex **13-Pt**, **15-Pt** or **17-Pt** to DNA ($[DNA]/[complex]=10$) are given in Table 8.1.

Table 8.1 Modification of the T_m of *CT-DNA* in the presence of **13-Pt**, **15-Pt** or **17-Pt**.

Compound	ΔT_m
13-Pt	+ 1
15-Pt	0
17-Pt	+ 1

Addition of complex **13-Pt** or **17-Pt** to DNA showed ΔT_m of + 1 °C for both complexes. It is important to note, however, that these ΔT_m cannot be considered as

significant because they are in the range of the experimental error. On the other side, the melting temperature of *CT-DNA*, after addition of complex **15-Pt**, remained constant (and also within the experimental error). As the expected increase in the temperature at which the helix denaturates in the presence of classical intercalators is much more significant (8-14 °C)¹⁴⁴ than the ones observed here for complexes **13-Pt** and **17-Pt**, we can conclude that the observed changes in T_m are indicative of non-intercalative binding mode.

8.2.3 Viscosity measurements

It is known that the viscosity of DNA increases by complete or partial intercalation of compounds into the DNA base stacking, while electrostatic or covalent binding only lead to mild modifications^{145,146}. Intercalation produces unwinding, lengthening and stiffening of the DNA double helix. These changes are consequence of the untwisting of the helical backbone and base pairs, produced by the incorporation of the intercalator into the double-strand DNA helix.

Therefore, in order to investigate the possible DNA binding mode, viscosity measurements on **13-Pt** and **15-Pt** were carried out. It was impossible to measure the viscosity of DNA in the presence of **17-Pt** due to its low solubility in the used 10 mM phosphate buffer. Figure 8.5 illustrates the dependence of the relative specific viscosity $(\eta/\eta_0)^{1/3}$, where η_0 and η are the specific viscosities of DNA in the absence and presence of the tested compound, respectively, plotted against the [complex]/[DNA] ratio r for complexes **13-Pt** and **15-Pt**, and ethidium bromide (EtBr). As intercalation of molecules increases the length of the DNA helix, and by using the equation of Cohen and Eisenberg, which proposes that $(\eta/\eta_0)^{1/3}$ is proportional to L/L_0 , where L is the length of the intercalated DNA and L_0 is the length of DNA alone¹⁴⁷, it is possible to measure the length increase of the DNA helix resulting from intercalation by viscosimetry. A slope of 1.03 was measured for EtBr, a standard strong intercalator, in the plot of $(\eta/\eta_0)^{1/3}$ vs. r using our experimental setup. This value is in accordance with previous investigations¹⁴⁸.

In the viscosity measurements it was observed that increasing the concentration of **13-Pt** or **15-Pt** only led to a small increase (slopes of 0.33 and 0.16 respectively) of the DNA viscosity, when compared to EtBr (slope of 1.03). The small increase in DNA length in the presence of the tested platinum(II) compounds could possibly be due to covalent or groove binding, but a significant degree of intercalation can be ruled out for both complexes.

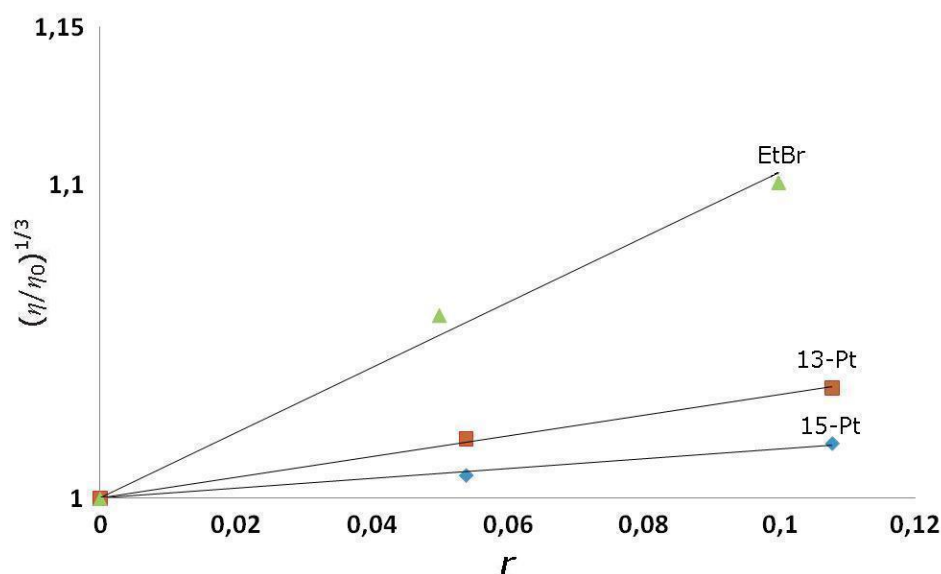


Figure 8.5 Dependence of $(\eta/\eta_0)^{1/3}$ on r $\{r = [\text{complex}]/[\text{DNA}]$ where $[\text{DNA}]$ is given in M (base pairs)} for viscosity measurements of *CT-DNA* with EtBr, **13-Pt** or **15-Pt** in a 10 mM phosphate buffer (pH = 7.2).

8.2.4 Atomic absorption studies

In order to examine the possible interaction of the platinum complexes with DNA, the amount of platinum incorporated into salmon test DNA was determined using the method described by Natarajan *et al.*¹⁴⁹ with some modifications. Thus salmon test DNA was incubated with the platinum complexes for 4 h, followed by precipitation and washing of the DNA-Pt(II) adducts with ethanol. The amount of DNA-bound platinum was measured by AAS and referred to the DNA content, which was determined spectrophotometrically at 260 nm. The lead compound of the [salophene]platinum(II) series (**13-Pt**) and the compounds bearing a methoxy- (**14-Pt**, **15-Pt**, **16-Pt** and **17-Pt**) or fluorine-substituted (**18-Pt**, **19-Pt**, **20-Pt** and **21-Pt**) salicylidene moiety were tested for the binding efficiency. Unfortunately, it was impossible to determine the DNA binding efficiency of **19-Pt** due to low solubility of the compound in ethanol. In Table 8.2 the DNA binding efficiency of the tested platinum complexes in descending order are listed.

Table 8.2 Values of DNA binding efficiency of the platinum complexes expressed as picomol bound compound per microgram DNA (pmol/ μg) also referred to as amount of nucleoside per bound compound (nucleoside/compound).

Compound	pmol/ μg	nucleoside/compound	IC ₅₀ (μM)
21-Pt (R ₆ = F)	236 \pm 113	16 \pm 6	> 20.0
20-Pt (R ₅ = F)	50.3 \pm 10.2	66 \pm 3	11.2 \pm 1.4
18-Pt (R ₃ = F)	42.4 \pm 1.1	77 \pm 2	0.7 \pm 0.1
16-Pt (R ₅ = OCH ₃)	23.0 \pm 5.8	146 \pm 37	> 20.0
17-Pt (R ₆ = OCH ₃)	22.5 \pm 7.5	153 \pm 51	> 20.0
15-Pt (R ₄ = OCH ₃)	20.9 \pm 0.3	156 \pm 2	1.8 \pm 0.7
Cisplatin	14.6 \pm 1.8	230 \pm 22	2.2 \pm 0.1
14-Pt (R ₃ = OCH ₃)	1.8 \pm 0.7	1935 \pm 757	> 20.0
13-Pt	not detected	not detected	1.1 \pm 0.2
19-Pt	not determined	not determined	> 20.0

As shown in Table 8.2, except for **13-Pt** and **14-Pt**, all the compounds bound to DNA (> 20 pmol/ μg), in a more efficient way than cisplatin (< 15 pmol/ μg) under the same experimental conditions. The lead compound **13-Pt** showed no significant binding affinity (the amount of the bound platinum was below the detection limit of the AAS). The methoxy-substituted complexes (with exception of **14-Pt**) showed similar and only average binding efficiency (\sim 22 pmol/ μg). The fluoro-substituted complexes exhibited much higher DNA interactions, reaching values around 230 pmol/ μg for **21-Pt**. Unfortunately, a correlation between the DNA-binding efficiency and the cytotoxicity could not be found (see data in Table 8.2). To the contrary, the compound exhibiting the strongest DNA interaction, **21-Pt**, is not cytotoxic in the tested range of concentrations and **13-Pt**, with an IC₅₀ value of 1.1 (\pm 0.2) μM , showed no significant DNA interaction.

8.3 Conclusion on the results of the interaction of the analyzed [salophene]platinum(II) complexes with isolated DNA

Considering that in most of the cases the cytotoxicity of platinum complexes arises from their interaction with DNA, some of the [salophene]platinum(II) complexes were tested for their capacity to interact with DNA.

On the one hand, the platinum atom in the [salophene]platinum(II) complexes is part of two planar six-membered chelate rings, containing aromatic ligands coplanar with the metal coordination sphere. Therefore, an intercalative process for their mechanism of action was postulated. Unfortunately, the results of CD, thermal denaturation and viscosity studies revealed no significant degree of intercalation with DNA.

On the other hand, if the platinum complexes suffer a chelate-ring opening process, they could possibly bind to DNA in a "cisplatin-like" mechanism (covalent binding to the DNA). Consequently atomic absorption studies were selected to quantify the total amount of DNA bound platinum, indistinctive of the binding mechanism. Even though some complexes revealed strong interaction with DNA, it was impossible to find a correlation with the cytotoxicity. Nevertheless, it is necessary to take into account other factors, such as drug accumulation (see Section 6), that can play a role in cytotoxicity. However, the fact that some compounds with very high cytotoxicity showed no detectable interaction with DNA (**13-Pt**) suggests that DNA may not necessarily be the main target of the [salophene]platinum(II) complexes.

In the past years, many non-genomic biomolecules were reported as potential targets for platinum complexes and other metal-based antitumour drugs, in order to overcome cisplatin disadvantages (see Section 1). Dyson and Sava, proposed in 2006 a post genomic era, involving a wide range of metals and targets¹⁵⁰. In the particular case of platinum-based antitumour drugs, De Pascali *et al.* introduced recently some acetylacetonate platinum(II) complexes¹⁵¹ that are able to activate apoptotic pathways without interacting with DNA. As possible target they suggest amino acid residues in proteins and enzymes involved in the apoptotic induction. Another example consists in the platinum-diethyl[(methylsulfinyl)methyl]phosphonate complexes, developed by Sasanelli *et al.*¹⁵². They inhibit the matrix metalloproteinase activity (besides the interaction with DNA), which is a family of endopeptidases that mediate the homeostasis

of the extracellular matrix. These are only few examples of alternative targets of the platinum complexes.

As the target and the mechanism of cytotoxicity of this promising family of [salophene]platinum(II) complexes has not been completely studied and fully understood, further investigations must be carried out. The mechanism might involve interactions with non-genomic biomolecules, therefore adducts formation with cytoplasm and membrane biochemical systems must be considered and analyzed.

Conclusions

9 Conclusions and outlook

Two series of Schiff base platinum(II) complexes, [diarylsalene]- and [salophene]platinum(II), were synthesized and fully characterized by spectroscopic methods. Ligand modifications of the diarylsalene lead compound (**1-Pt**, $R'_4 = F$) included: *meso* \rightarrow *d,l* stereomerization of the 1,2-diimino-1,2-diarylethane bridge (**2-Pt**), $-OCH_3$ and $-F$ substitution in the salicylidene moiety (**4-Pt** to **7-Pt**, and **8-Pt** to **11-Pt** respectively), as well as $R_5 = NO_2$ (**3-Pt**) and $R'_4 = CF_3$ (**12-Pt**) substitution. Further modification on the lead compound of the [salophene]platinum(II) series (**13-Pt**) involved initially, and in analogy to the [diarylsalene]platinum(II) series, $-OCH_3$ and $-F$ substitution in the salicylidene moiety (**14-Pt** to **17-Pt**, and **18-Pt** to **21-Pt** respectively). Moreover, complexes bearing fluorinated phenylene (**22-Pt** and **27-Pt**) and salicylidene moieties (**23-Pt** to **26-Pt** and **28-Pt** to **31-Pt**) were developed. Other particular modifications included the incorporation of a methyl substituent in the phenylene moiety (**32-Pt**) and the exchange of the aromatic ring of the phenylene moiety by a cyclohexane one (**33-Pt**). NMR spectra of fluorine substituted salophene ligands were especially interesting. Ligands bearing a R'_3 substituted phenylene moiety exhibited a characteristic spin-spin coupling between the fluorine and the azomethine protons ($^5J_{(HF)}$), where the coupling seems to arise as a consequence of the short distance between the *NCH* proton and the R'_3 fluorine. To corroborate this, further studies concerning the sign of the coupling constant⁸⁸ should be made, as well as a theoretical verification¹⁵³.

All compounds were subsequently tested for their anticancer activities. Since some ring-substituted [1,2-diamino-1,2-diarylethane]dichloroplatinum(II) complexes were previously reported to have a selective effect on the hormone-dependent mammary carcinoma¹⁵⁴, three platinum(II) complexes were initially selected and tested *in-vitro* for growth inhibition activity on both hormone dependent MCF-7 (ER +) and hormone independent MDA-MB-231 (ER -) breast cancer cells.

Similar antitumour potency on both breast cancer cell lines lead us to conclude that the activity of [diarylsalene]- and [salophene]platinum(II) complexes was not mediated by the ER system. Further antitumour properties were therefore only investigated on MCF-7 cells. For compounds of both [diarylsalene]- and [salophene]platinum(II) series IC_{50} values in a wide concentrations range were calculated. Outstanding cytotoxic properties demonstrated some [salophene]platinum(II) derivatives, with IC_{50} values less than 1 μM . Anyhow, neither for the diarylsalene nor for the salophene series a structure-

activity relationship could be established. Nevertheless, several observations regarding cytotoxicity can be mentioned.

On the one hand, concerning the [diarylsalene]platinum(II) series, results were in general not very promising. Only one compound (**11-Pt**) produced higher antiproliferative effects than the lead structure (**1-Pt**). The observed low activity of the [diarylsalene]platinum(II) complexes may have several causes, most probably related with specific effects originated by substitution of the diarylsalene structure. For instance, it could be suggested that the incorporation of substituents leads to an increase in steric hindrance, which prevents cellular uptake or the drug-target interaction. Due to the poor antitumour activity of the [diarylsalene]platinum(II) complexes, they were not selected for further investigations.

On the other hand, antitumour effects of the substituted [salophene]platinum(II) were much more encouraging. Although the introduction of substituents produced a marginal increment of the cell growth inhibitory effects only in some cases, the cytotoxic activities were shown to be strongly dependent on the type and position of the substituent. Results suggest that fluorine substituents in the salicylidene moiety, rather than methoxy ones, contribute to the antitumour effects. Moreover, complexes bearing a fluorine substituted phenylene moiety, with or without substituted salicylidene moiety, rarely demonstrated enhanced toxicity. Interestingly, the insertion of fluorine in position R₆ in the salicylidene moiety enhanced the cytotoxicity in the case of the diarylsalene compound, while it abolished the antiproliferative activity of the salophene complex in the tested range of concentrations. Complexes with no detectable antitumour effects were also obtained by main ligand structural changes, such as stereoisomerization of the ethane bridge on the diarylsalene series or exchange of the aromatic ring of the phenylene moiety of the [salophene]platinum(II) complex with a cyclohexane ring. Briefly summarized, substituted salophene complexes exhibited greater cytotoxicity than the diarylsalene substituted ones. Among them, compounds bearing fluorinated ligands showed the most interesting structure-activity characteristics.

Significant differences were also observed on time-dependent cytotoxic effects on MCF-7 cells. Both lead complexes showed time-response curves with a "V-shape" profile, with a fast onset of activity with followed by cell culture recovery. Possible causes for this behaviour were already discussed by Bernhardt *et al.*⁹⁷. Depending on the particularities of the cell line and the target of the compound, they attributed this curve shape to inactivation of the drugs in the culture medium, to the damage of only a subpopulation of cancer cells or to development of secondary resistance. Upon substitution, complexes presented distinct time-activity curves depending again on the substituent and its position. While some compounds maintained the time-dependent cytotoxic profile of the

lead complexes, two additional behaviours were observed. Complexes with a cisplatin-like curve, reaching its maximum effect toward the end of the test, and those which presented an early onset of antiproliferative effects and that then remained almost constant during the test period. It is probable that such differences in the time-activity curve shapes might be due to different factors affecting altogether the final observed cytotoxic activity. Among them, differences in drug accumulation (including cellular uptake and efflux) during the exposure time may modify the real intracellular drug concentration capable of interacting with the drug target and thus enhance or decrease the final antitumour activity. Therefore the accumulation of the [salophene]platinum(II) complexes has been subsequently investigated. Although the complexes demonstrated differences between their intracellular concentrations, a relationship with the antitumour activity could not be established. This suggests that other factors besides distinct accumulation, such as inactivation of the complexes before reaching the drug target or simple differences in the potency of the drugs, may have a stronger influence on the cytotoxicity. It is important to mention that the method used to determinate drug accumulation cannot distinguish between binding of the drugs to cell-surface components and true uptake. It would be interesting, in order to obtain a more accurate value of the intracellular drug concentration, to determine the fraction of platinum complex bound to membrane, as previously described by Buß *et al.*¹⁵⁵. This membrane bound fraction can be then subtracted from the previously obtained accumulation values.

Since the determination of physicochemical properties of drugs is usually part of the early screening for potential new drug candidates, the lipophilicity and solubility of the [salophene]platinum(II) compounds were determined. The complexes generally presented rather high lipophilicity and low solubility, although the two parameters did not demonstrate to be tightly correlated. While the obtained solubility values showed only in a few cases a relationship with the previously analyzed biological properties, lipophilicity seems to be linearly correlated with IC_{50} and accumulation values. Considering that antitumour activity was not directly associated with the intracellular drug concentration, it is not possible to establish the expected direct relationship between drug lipophilicity, cellular accumulation and cytotoxic effect. In other words, although greater lipophilicity normally enhanced accumulation, antineoplastic activity was not increased due to higher cellular drug concentration. Further investigations, regarding for example direct drug-target interactions, are needed in order to understand the influence of lipophilicity on cytotoxicity. Moreover, considering that low solubility is often associated with missinterpretation of biological assays results and, in advanced stages of drug development it can lead to problems related with the successful formulation of a drug product, further drug design strategies should focus on compounds with enhanced

aqueous solubility. We suggest that this could be achieved by introducing hydrophilic groups, such as hydroxy or quaternary ammonium moieties, as substituents in the ligands.

Comparing the obtained cytotoxic effects of methoxy substituted salophene ligands coordinated to platinum(II) (**14-Pt** to **17-Pt**) with those obtained in previous investigations⁶⁴ with iron(III), the influence on antitumour activity of the metal center and its oxidation state quite evident. While most of the methoxy substituted platinum(II) complexes showed no antiproliferative effects within the tested concentration range, iron(III) complexes bearing the same substitution pattern exhibited significant cytotoxic effects at concentrations below 5 μM . Moreover, iron(III) complexes bearing R_4 or $R_6 = \text{OCH}_3$ substituted salophene structures demonstrated cytotoxic effects even at a concentration of 0.5 μM . It is reasonable to suggest that the metal center is related to the mechanism of action of the complexes, as it was already proposed for nickel(II) and iron(III) salophene complexes^{62,65}. Thus, depending on the cellular processing and mechanism of action, substituents may affect in a different mode the activity of the compounds. Since DNA is a likely target for anticancer platinum-based coordination compounds, the [salophene]platinum(II) compounds were analyzed for their interactions with isolated DNA. Surprisingly, neither intercalation nor DNA binding demonstrated to be major mechanisms for the cytotoxic activity of the tested platinum complexes. As discussed in Section 8.3, many other non-genomic targets were reported for platinum anticancer compounds. They include, for example, proteins involved in apoptotic processes or proteins related to the homeostasis of the extracellular matrix.

This work provided a great number of novel platinum-based complexes, potentially active as anticancer agents. It is clear that substituents on the ligand scaffold can modulate the biological properties of the synthesized platinum(II) complexes. Understanding their antitumour mechanism of action and target still remains as an important challenge in order to generate functionalised complexes with optimized physicochemical and biological properties. Therefore, it should be an important area of study in further investigations. For example, apoptotic studies, which can be easily performed with commercially available ready-to-use kits, could clarify the phenomena that occur in the cells after drug exposure and that originate the cytotoxic effects.

Experimental part

10 Materials

10.1 Instrumentation

- Accurate weight: BP 211D, Sartorius AG (Göttingen, Germany)
- Atomic absorption spectrometer: Vario 6, Analytik Jena AG (Jena, Germany)
- Steam autoclave sterilizer: 2540 ELV, Systec GmbH (Wettenberg, Germany)
- Incubator Drying Chamber: B 5060 EK-CO₂, Heraeus Instruments (Hanau, Germany)
- HPLC: 1100 series, Hewlett-Packard (California, USA)
- Inverted microscope: Axiovert 25C, Carl Zeiss (Jena, Germany)
- ¹H-NMR spectrometer: Avance/DPX 400, Burker (Karlsruhe, Germany)
- Microplate reader: Flashscan S12, Analytik Jena AG (Jena, Germany)
- Sterile laminar flow cabinet: Lamin Air HB 2448, Heraeus Instruments (Hanau, Germany)
- X-ray diffractometer: IPDS 2T, STOE (Darmstadt, Germany)
- Counting chamber: Neubauer 0.100 depth, 0.0025 mm², Carl Zeiss (Jena, Germany)
- Mass spectrometer: Agilent 6210 ESI-TOF, Agilent Technologies (Santa Clara, USA)
- Centrifuge: Megafuge 1.0R, Heraeus Instruments (Hanau, Germany); Eppendorf centrifuge 5417R, Eppendorf AG (Hamburg, Germany)
- Spectropolarimeter: J-715, Jasco (Groß-Umstadt, Germany)
- UV-VIS Spectrometer: SPECORD 200, Analytikjena AG (Jena, Germany)
- Viscometer: Cannon-Ubbelohde semi-micro dilution viscometer, Cannon Instrument Co. (State College, U.S.)
- Water bath: W26, Haake (Karlsruhe, Germany)

10.2 Reactants and solutions

All chemicals, reagents and solvents were purchased – if not stated – from Sigma-Aldrich, VWR, Merck, Acros or Alfa Aesar. The laboratory consumables were purchased from Braun, Nunc, Merck and Sarstedt.

- Dulbecco's Modified Eagle Medium with phenol red and 4.5 g/L glucose (DMEM): PAA Laboratories GmbH (Pasching, Austria)
- Fetal calf serum (FCS): Biochrom AG (Berlin, Germany)
- Calf thymus-DNA
- Human serum albumin (HSA)
- Bradford reagent: 250 mg Serva Blue G, 250 mL ethanol (95%), 500 mL H₃PO₄ (86%) and 250 mL distilled H₂O. To perform the assay 1:5 dilution of the Bradford reagent in distilled H₂O
- Phosphate buffered saline (PBS): 0.2 g KH₂PO₄, 8 g NaCl, 1,44 g Na₂HPO₄×2H₂O, and 0,2 g KCl, dissolved in 1 L distilled H₂O
- Glutardialdehyde solution 1%: Glutardialdehyde 25% diluted in PBS
- Trypsin solution: 0.05% trypsin (ICN, Eschwege, Germany) and 0.02% EDTA in PBS. Sterile filtration of the solution using a 0.22 µm filter
- Hexamethylpararosaniline (crystal violet) solution 0.02%.

11 Methods

11.1 Structural analysis and synthesis

11.1.1 General considerations

The solvents were dried according to published procedures¹⁵⁶.

Compounds **12**, **13**, **14**, **15**, **16**, **17** and **33** were kindly supplied by Dr. Annagret Hille.

Reactions were monitored by thin-layer chromatography (TLC), performed on precoated silica gel plates (Silica gel 60 F₂₅₄). Visualization of the TLC was achieved by UV light at 254 and/or 366 nm. Column chromatography was performed with silica gel 60 (0.063-0.200 mm).

The ¹H-NMR spectra were performed on the Avance/DPX 400 spectrometer operating at 400 MHz, using tetramethylsilane (TMS) as an internal standard. The used NMR solvents are detailed in each spectrum. Coupling constants (*J*) are quoted in Herz (Hz) with the following splitting abbreviations: s = singlet, d = doublet, t = triplet, m = multiplet, and dd = double doublet.

Mass spectral data were obtained setting the spectrometer at flow rates of 4 µl/min and spray voltage of 4 kV.

The intensities for the X-ray determinations were collected on the X-ray diffractometer with Mo K_α radiation ($\lambda = 0.71073 \text{ \AA}$) at 200 K. Standard procedures were applied for data reduction and absorption correction.

11.1.2 Synthetic procedures and analytical data

11.1.2.1 Synthesis of *meso*- and *d,l*-3,4-bis(4-fluorophenyl)-1,6-bis(2-hydroxyphenyl)-2,5-diazahexa-1,5-diene

***meso*-1,2-Diamino-*N,N'*-dibenzoyl-1,2-bis(2-hydroxyphenyl)ethane [A1]**

A solution of benzil (50.0 mmol, 10.5 g) in 50.0 mL of ethanol was heated under reflux. Two equivalents of salicylaldehyde (100 mmol, 12.2 g) were added and a low flow of NH₃ was bubbled through the solution for 4 h. The temperature of the reaction must be maintained between 45 and 75 °C. The mixture was allowed to cool to room temperature, the solid was filtered off, washed with ethanol and dried (P₂O₅).

Yield: 16.7 g (36.9 mmol, 74%) yellow crystals.

$C_{28}H_{24}F_2N_2O_4$ (452.50)

1H -NMR (DMSO- d_6): δ = 5.87 (s, 2H, CH); 6.72-6.78 (m, 4H, ArH); 6.98-7.02 (m, 2H, ArH); 7.38-7.43 (m, 4H, ArH); 7.45-7.50 (m, 4H, ArH); 7.60-7.65 (m, 4H, ArH); 8.56 (s, 2H, CONH); 9.94 (s, 2H, ArOH).

***meso-O,O',N,N'*-Tetraacetyl-1,2-diamino-1,2-bis(2-hydroxyphenyl)ethane [A2]**

A suspension of *meso*-1,2-diamino-*N,N'*-dibenzoyl-1,2-bis(2-hydroxyphenyl)ethane (**A1**) (30.7 mmol, 13.9 g) in 50.0 mL of acetic anhydride was heated under reflux for 48 h. The mixture was allowed to cool to room temperature, the precipitate was filtered off, washed with cold acetic anhydride and dried (P_2O_5).

Yield: 7.60 g (18.4 mmol, 60%) white crystals.

$C_{22}H_{24}N_2O_6$ (412.44)

1H -NMR (DMSO- d_6): δ = 1.54 (s, 6H, CH_3CON); 2.28 (s, 6H, CH_3COOAr); 5.67 (s, 2H, CH); 7.02-7.05 (m, 2H, ArH); 7.18-7.29 (m, 4H, ArH); 7.50-7.52 (m, 2H, ArH).

***meso*-1,2-Diamino-1,2-bis(2-hydroxyphenyl)ethane [A3]**

A suspension of *meso-O,O',N,N'*-tetraacetyl-1,2-diamino-1,2-bis(2-hydroxyphenyl)ethane (**A2**) (17.7 mmol, 7.30 g) in 50.0 mL of 47% aqueous HBr solution was heated under reflux for 4 h and then was allowed to cool to room temperature. The diaminoethane dihydrobromide was filtered off and washed with cold water. The product was dissolved in hot water (70 to 80 °C). The hot solution was filtered off and the pH was adjusted to 7-8 with 20% NaOH. In this way, the product will precipitate as the free phenol-base. The precipitate was filtered off and dried (P_2O_5).

Yield: 7.6 g (18.4 mmol, 60%) white crystals.

$C_{22}H_{24}N_2O_6$ (412.44)

1H -NMR (DMSO- d_6): δ = 1.54 (s, 6H, CH_3CON); 2.28 (s, 6H, CH_3COOAr); 5.67 (s, 2H, CH); 7.02-7.05 (m, 2H, ArH); 7.18-7.29 (m, 4H, ArH); 7.50-7.52 (m, 2H, ArH).

***meso*-3,4-Bis(4-fluorophenyl)-1,6-bis(2-hydroxyphenyl)-2,5-diazahexa-1,5-diene [1]**

To a suspension of *meso*-1,2-diamino-1,2-bis(2-hydroxyphenyl)ethane (**A3**) (6.54 mmol, 1.6 g) in acetonitrile (20 mL) was added 2 equivalents of 4-fluorobenzaldehyde (13.08 mmol, 1.6 g). The mixture was stirred at reflux for 5 h. The solvent was reduced by half, and the diimine was subsequently allowed to crystallize. The product was collected, washed with cold diethyl ether and dried over P_2O_5 .

Yield: 2.3 g (5.77 mmol, 88%) yellow crystals.

C₂₈H₂₂F₂N₂O₂ (456.48)

¹H-NMR (DMSO-*d*₆): δ = 5.09 (s, 2H, CH); 6.82-6.92 (m, 4H, ArH-3, ArH-5); 7.10-7.22 (t, ³J=8.81 Hz, 4H, Ar'H-3, Ar'H-5); 7.27-7.41 (m, 8H, ArH-4, ArH-6, Ar'H-2, Ar'H-6); 8.45 (s, 2H, NCH); 13.03 (s, 2H, ArOH).

meso-1,2-Diamino-1,2-bis(4-fluorophenyl)ethane [A4]

A suspension of *meso*-3,4-diaryl-1,6-bis(2-hydroxyphenyl)-2,5-diazahexa-1,5-diene (**1**) (16.9 mmol, 7.7 g) in 50.0 mL of 6 N H₂SO₄ was heated and the forming salicylaldehyde was removed by steam distillation. The hot solution was filtered and made alkaline with 20% NaOH. The precipitated base was extracted with dichloromethane, the organic phase was separated and dried over Na₂SO₄. Finally the organic phase was evaporated under vacuum to remove the solvent.

Yield: 3.8 g (15.3 mmol, 90%) white crystals.

C₁₄H₁₄F₂N₂ (248.27)

¹H-NMR (DMSO-*d*₆): δ = 1.67 (s, 4H, NH₂); 3.92 (s, 2H, CH); 7.01-7.08 (m, 4H, ArH-3, ArH-5); 7.14-7.24 (m, 2H, ArH-2, ArH-6).

meso-1,3,4,6-Tetrakis(4-fluorophenyl)-2,5-diazahexa-1,5-diene [A5]

To a suspension of *meso*-1,2-diamino-1,2-bis(4-fluorophenyl)ethane (**A4**) (13.7 mmol, 3.4 g) in acetonitrile (50 mL) was added 2 equivalents of 4-fluorobenzaldehyde (27.4 mmol, 3.4 g). The mixture was stirred at reflux for 5 h, allowed to cool to room temperature and concentrated to half of the volume. The product was collected, washed with cold diethyl ether and dried over P₂O₅.

Yield: 4.7 g (10.27 mmol, 75%) white crystals.

C₂₈H₂₂F₄N₂ (460.47)

¹H-NMR (DMSO-*d*₆): δ = 4.83 (s, 2H, CH); 7.04-7.11 (t, ³J=8.80 Hz, 4H, Ar'H-3, Ar'H-5); 7.21-7.28 (t, ³J=8.75 Hz, 4H, ArH-3, ArH-5); 7.39-7.43 (m, 4H, Ar'H-2, Ar'H-6); 7.69-7.73 (m, 4H, ArH-2, ArH-6); 8.13 (s, 2H, NCH).

***d,l*-1,2-Diamino-1,2-bis(4-fluorophenyl)ethane [A6]**

9.77 mmol (4.5 g) of *meso*-1,3,4,6-tetrakis(4-fluorophenyl)-2,5-diazahexa-1,5-diene was heated to the melting temperature (210-220 °C) for about 10 min. After cooling and addition of 50 mL 3 N H₂SO₄ steam distillation was performed. After the removal of the forming 4-fluorobenzaldehyde the hot solution was filtered and allowed to cool to room temperature. The crystallized sulfate of **A6** was filtered off and recrystallized in water. Then the crystals were treated with 1 N NaOH and extracted with dichloromethane. The

organic phase was separated, dried over Na_2SO_4 and the solvent was evaporated under vacuum.

Yield: 630.6 mg (2.54 mmol, 26%) white crystals.

$\text{C}_{14}\text{H}_{14}\text{F}_2\text{N}_2$ (248.27)

$^1\text{H-NMR}$ (DMSO- d_6): δ = 2.09 (s, 4H, NH_2); 3.78 (s, 2H, CH); 6.93-6.99 (m, 4H, ArH-3, ArH-5); 7.08-7.18 (m, 2H, ArH-2, ArH-6).

11.1.2.2 General procedure for the synthesis of *meso*- and *d,l*-3,4-diaryl-1,6-bis(2-hydroxyphenyl)-2,5-diazahexa-1,5-diene derivatives

An amount of one equivalent of the respective 1,2-diamino-1,2-diaryl-ethane was suspended in acetonitrile and reacted with the respective salicylaldehyde. The reaction mixture was heated to reflux for 6 h. The solvent was reduced by half, and the diimine was subsequently allowed to crystallize. The crystals were filtered off, washed with diethyl ether, and dried over P_2O_5 .

***d,l*-3,4-Bis(4-fluorophenyl)-1,6-bis(2-hydroxyphenyl)-2,5-diazahexa-1,5-diene [2]**

Was obtained from *d,l*-1,2-diamino-1,2-bis(4-fluorophenyl)ethane (**A6**) (3.98 mmol, 989.0 mg) and salicylaldehyde (7.97 mmol, 972.9 mg).

Yield: 1.3 g (2.85 mmol, 72%) yellow crystals.

$\text{C}_{28}\text{H}_{22}\text{F}_2\text{N}_2\text{O}_2$ (456.48)

$^1\text{H-NMR}$ (DMSO- d_6): δ = 5.11 (s, 2H, CH); 6.81-6.89 (m, 4H, ArH-3, ArH-5); 7.07-7.15 (t, $^3J=8.81$ Hz, 4H, Ar'H-3, Ar'H-5); 7.27-7.38 (m, 8H, ArH-4, ArH-6, Ar'H-2, Ar'H-6); 8.56 (s, 2H, NCH); 13.15 (s, 2H, ArOH).

***meso*-3,4-Bis(4-fluorophenyl)-1,6-bis(2-hydroxy-5-nitrophenyl)-2,5-diazahexa-1,5-diene [3]**

Was obtained from *meso*-1,2-diamino-1,2-bis(4-fluorophenyl)ethane (**A4**) (0.40 mmol, 99.3 mg) and 5-nitrosalicylaldehyde (0.80 mmol, 133.6 mg).

Yield: 185.0 mg (0.34 mmol, 85%) yellow powder.

$\text{C}_{28}\text{H}_{20}\text{F}_2\text{N}_4\text{O}_6$ (546.48)

$^1\text{H-NMR}$ (DMSO- d_6): δ = 5.28 (s, 2H, CH); 6.92-7.02 (d, $^3J=9.26$ Hz, 2H, ArH-3); 7.16-7.30 (t, $^3J=8.76$ Hz, 4H, Ar'H-3, Ar'H-5); 7.38-7.47 (m, 4H, Ar'H-2, Ar'H-6); 8.12-8.20 (dd, $^3J=9.25$ Hz, $^4J=2.78$ Hz, 2H, ArH-4); 8.39-8.46 (d, $^4J=2.79$ Hz, 2H, ArH-6); 8.63 (s, 2H, NCH); 14.22 (s, 2H, ArOH).

***meso*-3,4-Bis(4-fluorophenyl)-1,6-bis(2-hydroxy-3-methoxyphenyl)-2,5-diazahepta-1,5-diene [4]**

Was obtained from *meso*-1,2-diamino-1,2-bis(4-fluorophenyl)ethane (**A4**) (0.35 mmol, 86.0 mg) and 3-methoxysalicylaldehyde (0.69 mmol, 97.0 mg).

Yield: 129.0 mg (0.26 mmol, 75%) light yellow crystals.

C₃₀H₂₆F₂N₂O₄ (516.53)

¹H-NMR (DMSO-*d*₆): δ = 3.77 (s, 6H, OCH₃); 5.08 (s, 2H, CH); 6.76-6.84 (t, 2H, ³J=7.87 Hz, ArH-5); 6.87-6.97 (dd, ³J=7.90 Hz, ⁴J=1.30 Hz, 2H, ArH-4); 7.00-7.08 (dd, ³J=8.00 Hz, ⁴J=1.20 Hz, 2H, ArH-6); 7.12-7.21 (t, ³J=8.81 Hz, 4H, Ar'H-3, Ar'H-5); 7.30-7.44 (m, 4H, Ar'H-2, Ar'H-6); 8.44 (s, 2H, NCH); 13.21 (s, 2H, ArOH).

***meso*-3,4-Bis(4-fluorophenyl)-1,6-bis(2-hydroxy-4-methoxyphenyl)-2,5-diazahepta-1,5-diene [5]**

Was obtained from *meso*-1,2-diamino-1,2-bis(4-fluorophenyl)ethane (**A4**) (0.18 mmol, 44.0 mg) and 4-methoxysalicylaldehyde (0.35 mmol, 53.9 mg).

Yield: 70.0 mg (0.14 mmol, 75%) yellow crystals.

C₃₀H₂₆F₂N₂O₄ (516.53)

¹H-NMR (DMSO-*d*₆): δ = 3.75 (s, 6H, CH₃); 4.98 (s, 2H, CH); 6.36-6.40 (d, ⁴J=2.28 Hz, 2H, ArH-3); 6.40-6.45 (dd, ³J=8.54 Hz, ⁴J=2.36 Hz, 2H, ArH-5); 7.10-7.19 (t, ³J=8.81 Hz, 4H, Ar'H-3, Ar'H-5); 7.19-7.25 (d, ³J=8.57 Hz, 2H, ArH-6); 7.26-7.34 (m, 4H, Ar'H-2, Ar'H-6); 8.32 (s, 2H, NCH); 13.54 (s, 2H, ArOH).

***meso*-3,4-Bis(4-fluorophenyl)-1,6-bis(2-hydroxy-5-methoxyphenyl)-2,5-diazahepta-1,5-diene [6]**

Was obtained from *meso*-1,2-diamino-1,2-bis(4-fluorophenyl)ethane (**A4**) (0.22 mmol, 55.0 mg) and 5-methoxysalicylaldehyde (0.44 mmol, 67.4 mg).

Yield: 90.0 mg (0.17 mmol, 79%) yellow crystals.

C₃₀H₂₆F₂N₂O₄ (516.53)

¹H-NMR (DMSO-*d*₆): δ = 3.67 (s, 6H, CH₃); 5.06 (s, 2H, CH); 6.77-6.83 (d, ³J=8.47 Hz, 2H, ArH-3); 6.90-6.99 (m, 4H, ArH-4, ArH-6); 7.12-7.21 (t, ³J=8.77 Hz, 4H, Ar'H-3, Ar'H-5); 7.30-7.39 (m, 4H, Ar'H-2, Ar'H-6); 8.41 (s, 2H, NCH); 12.41 (s, 2H, ArOH).

***meso*-3,4-Bis(4-fluorophenyl)-1,6-bis(2-hydroxy-6-methoxyphenyl)-2,5-diazahepta-1,5-diene [7]**

Was obtained from *meso*-1,2-diamino-1,2-bis(4-fluorophenyl)ethane (**A4**) (0.54 mmol, 133.0 mg) and 6-methoxysalicylaldehyde (1.07 mmol, 163.2 mg).

Yield: 226.0 mg (0.44 mmol, 83%) yellow crystals.

$C_{30}H_{26}F_2N_2O_4$ (516.53)

1H -NMR (DMSO- d_6): δ = 3.75 (s, 6H, CH_3); 5.16 (s, 2H, CH); 6.37-6.49 (m, 4H, ArH -3, ArH -5); 7.12-7.21 (t, 3J =8.82 Hz, 4H, $Ar'H$ -3, $Ar'H$ -5); 7.23-7.29 (t, 2H, 3J =8.82 Hz, ArH -4); 7.31-7.39 (m, 4H, $Ar'H$ -2, $Ar'H$ -6); 8.70 (s, 2H, NCH); 13.97 (s, 2H, $ArOH$).

***meso*-3,4-Bis(4-fluorophenyl)-1,6-bis(2-hydroxy-3-fluorophenyl)-2,5-diazahexa-1,5-diene [8]**

Was obtained from *meso*-1,2-diamino-1,2-bis(4-fluorophenyl)ethane (**A4**) (0.35 mmol, 86.0 mg) and 3-fluorosalicylaldehyde (0.69 mmol, 97.0 mg).

Yield: 129.0 mg (0.26 mmol, 75%) light yellow crystals.

$C_{28}H_{20}F_4N_2O_2$ (492.46)

1H -NMR (DMSO- d_6): δ = 5.18 (s, 2H, CH); 6.80-6.88 (m, 2H, ArH -5); 7.15-7.23 (m, 6H, ArH -6, $Ar'H$ -3, $Ar'H$ -5); 7.26-7.35 (m, 2H, ArH -4); 7.35-7.44 (m, 4H, $Ar'H$ -2, $Ar'H$ -6); 8.49 (s, 2H, NCH); 13.51 (s, 2H, $ArOH$).

***meso*-3,4-Bis(4-fluorophenyl)-1,6-bis(2-hydroxy-4-fluorophenyl)-2,5-diazahexa-1,5-diene [9]**

Was obtained from *meso*-1,2-diamino-1,2-bis(4-fluorophenyl)ethane (**A4**) (0.41 mmol, 104.0 mg) and 4-fluorosalicylaldehyde (0.84 mmol, 117.4 mg).

Yield: 161.0 mg (0.33 mmol, 80%) light yellow powder.

$C_{28}H_{20}F_4N_2O_2$ (492.46)

1H -NMR (DMSO- d_6): δ = 5.08 (s, 2H, CH); 6.65-6.75 (m, 4H, ArH -3, ArH -5); 7.11-7.21 (t, 3J =8.80 Hz, 4H, $Ar'H$ -3, $Ar'H$ -5); 7.30-7.36 (m, 4H, $Ar'H$ -2, $Ar'H$ -6); 7.39-7.46 (m, 2H, ArH -6); 8.44 (s, 2H, NCH); 13.69 (s, 2H, $ArOH$).

***meso*-3,4-Bis(4-fluorophenyl)-1,6-bis(2-hydroxy-5-fluorophenyl)-2,5-diazahexa-1,5-diene [10]**

Was obtained from *meso*-1,2-diamino-1,2-bis(4-fluorophenyl)ethane (**A4**) (0.34 mmol, 85.0 mg) and 5-fluorosalicylaldehyde (0.68 mmol, 95.9 mg).

Yield: 110.0 mg (0.22 mmol, 66%) dark yellow crystals.

$C_{28}H_{20}F_4N_2O_2$ (492.46)

1H -NMR (DMSO- d_6): δ = 5.09 (s, 2H, CH); 6.85-6.91 (dd, 3J =9.01 Hz, 4J =4.05 Hz, 2H, ArH -3); 7.08-7.23 (m, 6H, ArH -4, $Ar'H$ -3, $Ar'H$ -5); 7.23-7.29 (dd, 3J =8.85 Hz, 4J =3.11 Hz, 2H, ArH -6); 7.29-7.42 (m, 4H, $Ar'H$ -2, $Ar'H$ -6); 8.41 (s, 2H, NCH); 12.68 (s, 2H, $ArOH$).

***meso*-3,4-Bis(4-fluorophenyl)-1,6-bis(2-hydroxy-6-fluorophenyl)-2,5-diazahexa-1,5-diene [11]**

Was obtained from *meso*-1,2-diamino-1,2-bis(4-fluorophenyl)ethane (**A4**) (0.35 mmol, 89.0 mg) and 6-fluorosalicylaldehyde (0.71 mmol, 100.5 mg).

Yield: 75.0 mg (0.15 mmol, 43%) yellow crystals.

C₂₈H₂₀F₄N₂O₂ (492.46)

¹H-NMR (DMSO-*d*₆): δ = 5.28 (s, 2H, CH); 6.62-6.75 (m, 4H, ArH-3, ArH-5); 7.15-7.24 (t, ³J=8.81 Hz, 4H, Ar'H-3, Ar'H-5); 7.32-7.42 (m, 6H, ArH-4, Ar'H-2, Ar'H-6); 8.67 (s, 2H, NCH); 13.70 (s, 2H, ArOH).

***meso*-3,4-Bis(4-trifluoromethylphenyl)-1,6-bis(2-hydroxyphenyl)-2,5-diazahexa-1,5-diene [12]**

C₃₀H₂₂F₆N₂O₂ (556.50)

¹H-NMR (DMSO-*d*₆): δ = 5.29 (s, 2H, CH); 6.84-6.91 (m, 4H, ArH-3, ArH-5); 7.30-7.39 (m, 4H, ArH-4, ArH-6); 7.52-7.57 (d, ³J=7.99 Hz, 4H, Ar'H-2, Ar'H-6); 7.68-7.75 (d, ³J=8.07 Hz, 4H, Ar'H-3, Ar'H-5); 8.52 (s, 2H, NCH); 12.86 (s, 2H, ArOH).

11.1.2.3 Synthesis of 3-fluoro-1,2-phenylenediamine**1,1,1-Trimethylhydrazinium iodide [B1]**

1,1-Dimethylhydrazine (35.0 mmol, 2.1 g) was added dropwise to a solution of methyl iodide (35.0 mmol, 5.0 g) in 30.0 mL of absolute THF at a temperature of 0 °C. After addition of 30 mL of absolute THF, the mixture was stirred for 2 h at room temperature. The precipitate was collected by filtration and washed with THF, and dried (P₂O₅).

Yield: 6.2 g (30.6 mmol, 87%) white crystals.

C₃H₁₁IN (202.04)

¹H-NMR (DMSO-*d*₆): δ = 3.26 (s, 9H, CH₃); 6.08 (s, 2H, NH₂).

2-Fluoro-6-nitroaniline [B2]

1,1,1-Trimethylhydrazinium iodide (30.6 mmol, 6.2 g) was dissolved in a solution of 3-fluoro-nitrobenzene (30.6 mmol, 4.3 g) in dry DMSO. Potassium tert-butoxide was then added in one portion with stirring, after which the solution turned deep red. After 17 h stirring at room temperature, the reaction was quenched with 10% HCl. The fluoro-nitroaniline derivatives were extracted with ethyl acetate, and the products were isolated by silica gel chromatography (9:1 petroleum ether/acetone).

Yield: 1.4 g (8.97 mmol, 29%) yellow crystals.

C₆H₅FN₂O₂ (156.11)

¹H-NMR (DMSO-*d*₆): δ = 6.58-6.68 (m, 1H, ArH); 7.30 (s, 2H, NH₂); 7.40-7.50 (m, 1H, ArH); 7.80-7.87 (m, 1H, ArH).

3'-Fluoro-1,2-phenylenediamine [B3]

To a oven-dried round bottomed flask were added 2-fluoro-6-nitroaniline (8.33 mmol, 1.3 g), SnCl₂·2H₂O (41.6 mmol, 9.4 g) in 30 mL absolute ethanol. The solution was heated at 70 °C under nitrogen. The reaction was controlled by thin layer chromatography. After 2 h the solution was allowed to cool and then poured on ice. The pH was adjusted to 7-8 with 5% aqueous sodium bicarbonate. The reaction mixture was extracted three times with ethyl acetate. The organic phase was extracted with brine and dried over sodium sulphate. Finally, the organic phase was evaporated under vacuum to remove the solvent.

Yield: 0.67 g (5.30 mmol, 63%) black powder.

C₆H₇FN₂ (126.13)

¹H-NMR (DMSO-*d*₆): δ = 4.31 (s, 2H, NH₂); 4.75 (s, 2H, NH₂); 6.23-6.35 (m, 3H, ArH).

11.1.2.4 General procedure for the synthesis of *N,N'*-bis(salicylidene)-1,2-phenylenediamine and derivatives

Two equivalents of the respective salicylaldehyde in ethanol were added dropwise to a solution of one equivalent of 1,2-phenylenediamine in ethanol. The mixture was stirred under reflux for 1-2 h and then allowed to cool down to room temperature. The product was collected, washed with cold ethanol and dried (P₂O₅).

***N,N'*-Bis(salicylidene)-1,2-phenylenediamine [13]**

Was obtained from 1,2-phenylenediamine (0.65 mmol, 70.0 mg) and salicylaldehyde (1.29 mmol, 157.5 mg).

Yield: 174.6 mg (0.55 mmol, 85%) orange powder.

C₂₀H₁₆N₂O₂ (316.35)

¹H-NMR (DMSO-*d*₆): δ = 6.96-7.00 (m, 4H, ArH-3, ArH-5); 7.40-7.48 (m, 6H, ArH-4, Ar'H-3, Ar'H-4, Ar'H-5, Ar'H-6); 7.66-7.68 (dd, ³J=7.60 Hz, ⁴J=1.50 Hz, 2H, ArH-6); 8.94 (s, 2H, NCH); 12.94 (s, 2H, ArOH).

***N,N'*-Bis(3-methoxysalicylidene)-1,2-phenylenediamine [14]**

Dark orange powder.

C₂₂H₂₀N₂O₄ (376.40)

¹H-NMR (DMSO-*d*₆): δ = 3.81 (s, 6H, CH₃); 6.87-6.94 (m, 2H, ArH-5); 7.10-7.16 (dd, ³J=8.02 Hz, ⁴J=1.17 Hz, 2H, ArH-4); 7.22-7.27 (dd, ³J=7.85 Hz, ⁴J=1.25 Hz, 2H, ArH-6);

7.37-7.50 (m, 4H, Ar'H-3, Ar'H-4, Ar'H-5, Ar'H-6); 8.93 (s, 2H, NCH); 13.00 (s, 2H, ArOH).

***N,N'*-Bis(4-methoxysalicylidene)-1,2-phenylenediamine [15]**

Yellow powder.

C₂₂H₂₀N₂O₄ (376.40)

¹H-NMR (DMSO-*d*₆): δ = 3.81 (s, 6H, CH₃); 6.46-6.51 (d, ⁴J=2.32, 2H, ArH-3); 6.52-6.57 (dd, ³J=8.59 Hz, ⁴J=2.37 Hz, 2H, ArH-5); 7.32-7.46 (m, 4H, Ar'H-3, Ar'H-4, Ar'H-5, Ar'H-6); 7.52-7.58 (d, ³J=8.63 Hz, 2H, ArH-6); 8.84 (s, 2H, NCH); 13.52 (s, 2H, ArOH).

***N,N'*-Bis(5-methoxysalicylidene)-1,2-phenylenediamine [16]**

Orange powder.

C₂₂H₂₀N₂O₄ (376.40)

¹H-NMR (DMSO-*d*₆): δ = 3.75 (s, 6H, CH₃); 6.86-6.92 (d, ³J=8.95 Hz, 2H, ArH-3); 7.01-7.08 (dd, ³J=8.93 Hz, ⁴J=3.14 Hz, 2H, ArH-4); 7.27-7.32 (d, ⁴J=3.14 Hz, 2H, ArH-6); 7.37-7.48 (m, 4H, Ar'H-3, Ar'H-4, Ar'H-5, Ar'H-6); 8.91 (s, 2H, NCH); 12.28 (s, 2H, ArOH).

***N,N'*-Bis(6-methoxysalicylidene)-1,2-phenylenediamine [17]**

Orange powder.

C₂₂H₂₀N₂O₄ (376.40)

¹H-NMR (DMSO-*d*₆): δ = 3.85 (s, 6H, CH₃); 6.45-6.56 (m, 4H, ArH-3, ArH-5); 7.34-7.46 (m, 6H, ArH-4, Ar'H-3, Ar'H-4, Ar'H-5, Ar'H-6); 9.08 (s, 2H, NCH); 13.81 (s, 2H, ArOH).

***N,N'*-Bis(3-fluorosalicylidene)-1,2-phenylenediamine [18]**

Was obtained from 1,2-phenylenediamine (0.18 mmol, 20.0 mg) and 3-fluorosalicylaldehyde (0.37 mmol, 51.8 mg).

Yield: 86.0 mg (0.15 mmol, 82%) orange powder.

C₂₀H₁₄F₂N₂O₂ (352.33)

¹H-NMR (DMSO-*d*₆): δ = 6.93-7.00 (m, 2H, ArH-5); 7.37-7.48 (m, 4H, ArH-4, Ar'H-3, Ar'H-6); 7.51-7.56 (m, 4H, ArH-6, Ar'H-4, Ar'H-5); 9.03 (s, 2H, NCH); 13.30 (s, 2H, ArOH).

***N,N'*-Bis(4-fluorosalicylidene)-1,2-phenylenediamine [19]**

Was obtained from 1,2-phenylenediamine (0.28 mmol, 30.6 mg) and 4-fluorosalicylaldehyde (0.56 mmol, 79.0 mg).

Yield: 53.0 mg (0.15 mmol, 54%) yellow powder.

$C_{20}H_{14}F_2N_2O_2$ (352.33)

1H -NMR (DMSO- d_6): δ = 6.76-6.93 (m, 4H, ArH-3, ArH-5); 7.35-7.50 (m, 4H, Ar'H-3, Ar'H-4, Ar'H-5, Ar'H-6); 7.68-7.82 (m, 2H, ArH-6); 8.96 (s, 2H, NCH); 13.56 (s, 2H, ArOH).

***N,N'*-Bis(5-fluorosalicylidene)-1,2-phenylenediamine [20]**

Was obtained from 1,2-phenylenediamine (0.51 mmol, 55.0 mg) and 5-fluorosalicylaldehyde (1.02 mmol, 142.6 mg).

Yield: 197.0 mg (0.36 mmol, 71%) orange powder.

$C_{20}H_{14}F_2N_2O_2$ (352.33)

1H -NMR (DMSO- d_6): δ = 6.95-7.07 (dd, $^3J=9.06$ Hz, $^4J=4.52$ Hz, 2H, ArH-3); 7.24-7.31 (m, 2H, ArH-4); 7.41-7.48 (m, 4H, Ar'H-3, Ar'H-4, Ar'H-5, Ar'H-6); 7.50-7.58 (dd, $^3J=8.99$ Hz, $^4J=3.16$ Hz, 2H, ArH-6); 8.92 (s, 2H, NCH); 12.58 (s, 2H, ArOH).

***N,N'*-Bis(6-fluorosalicylidene)-1,2-phenylenediamine [21]**

Was obtained from 1,2-phenylenediamine (0.31 mmol, 34.0 mg) and 6-fluorosalicylaldehyde (0.63 mmol, 88.1 mg).

Yield: 75.0 mg (0.21 mmol, 69%) orange powder.

$C_{20}H_{14}F_2N_2O_2$ (352.33)

1H -NMR (DMSO- d_6): δ = 6.75-6.86 (m, 4H, ArH-3, ArH-5); 7.41-7.51 (m, 4H, Ar'H-3, Ar'H-4, Ar'H-5, Ar'H-6); 7.54-7.59 (m, 2H, ArH-4); 9.04 (s, 2H, NCH); 13.62 (s, 2H, ArOH).

***N,N'*-Bis(salicylidene)-3'-fluoro-1,2-phenylenediamine [22]**

Was obtained from 3-fluoro-1,2-phenylenediamine (**B3**) (0.79 mmol, 100.0 mg) and salicylaldehyde (1.59 mmol, 193.6 mg).

Yield: 171.0 mg (0.51 mmol, 65%) yellow needles.

$C_{20}H_{15}FN_2O_2$ (334.34)

1H -NMR (DMSO- d_6): δ = 6.86-7.05 (m, 4H, ArH-3, ArH-5); 7.25-7.52 (m, 5H, ArH-4, Ar'H-4, Ar'H-5, Ar'H-6); 7.62-7.71 (m, 2H, ArH-6); 8.89 (s, 1H, NCH); 9.00 (s, 1H, NCH), 12.33 (s, 1H, ArOH); 12.56 (s, 1H, ArOH).

***N,N'*-Bis(3-fluorosalicylidene)-3'-fluoro-1,2-phenylenediamine [23]**

Was obtained from 3-fluoro-1,2-phenylenediamine (**B3**) (0.71 mmol, 90.0 mg) and 3-salicylaldehyde (1.43 mmol, 200.0 mg).

Yield: 131.0 mg (0.35 mmol, 50%) yellow needles.

$C_{20}H_{13}F_3N_2O_2$ (370.32)

1H -NMR (DMSO- d_6): δ = 6.92-7.02 (m, 2H, ArH-5); 7.33-7.49 (m, 5H, ArH-4, Ar'H-4, Ar'H-5, Ar'H-6); 7.50-7.57 (m, 2H, ArH-6); 8.97 (s, 1H, NCH); 9.07 (s, 1H, NCH); 12.61 (s, 1H, ArOH); 12.89 (s, 1H, ArOH).

***N,N'*-Bis(4-fluorosalicylidene)-3'-fluoro-1,2-phenylenediamine [24]**

Was obtained from 3-fluoro-1,2-phenylenediamine (**B3**) (0.79 mmol, 63.0 mg) and 4-salicylaldehyde (1.25 mmol, 175.0 mg).

Yield: 112.0 mg (0.30 mmol, 49%) yellow needles.

$C_{20}H_{13}F_3N_2O_2$ (370.32)

1H -NMR (DMSO- d_6): δ = 6.74-6.90 (m, 4H, ArH-3, ArH-5); 7.28-7.42 (m, 3H, Ar'H-4, Ar'H-5, Ar'H-6); 7.70-7.82 (m, 2H, ArH-6); 8.90 (s, 1H, NCH); 9.01 (s, 1H, NCH); 12.85 (s, 1H, ArOH); 13.21 (s, 1H, ArOH).

***N,N'*-Bis(5-fluorosalicylidene)-3'-fluoro-1,2-phenylenediamine [25]**

Was obtained from 3-fluoro-1,2-phenylenediamine (**B3**) (0.87 mmol, 110.0 mg) and 5-salicylaldehyde (1.75 mmol, 244.4 mg).

Yield: 210.0 mg (0.54 mmol, 58%) brown crystals.

$C_{20}H_{13}F_3N_2O_2$ (370.32)

1H -NMR (DMSO- d_6): δ = 6.93-7.05 (m, 2H, ArH-3); 7.25-7.44 (m, 5H, ArH-4, Ar'H-4, Ar'H-5, Ar'H-6); 7.49-7.68 (m, 2H, ArH-6); 8.87 (s, 1H, NCH); 8.97 (s, 1H, NCH); 11.94 (s, 1H, ArOH); 12.24 (s, 1H, ArOH).

***N,N'*-Bis(6-fluorosalicylidene)-3'-fluoro-1,2-phenylenediamine [26]**

Was obtained from 3-fluoro-1,2-phenylenediamine (**B3**) (0.52 mmol, 65.0 mg) and 6-salicylaldehyde (1.03 mmol, 144.4 mg).

Yield: 125.0 mg (0.34 mmol, 65%) yellow powder.

$C_{20}H_{13}F_3N_2O_2$ (370.32)

1H -NMR (DMSO- d_6): δ = 6.77-6.87 (m, 4H, ArH-3, ArH-5); 7.34-7.54 (m, 5H, ArH-4, Ar'H-4, Ar'H-5, Ar'H-6); 9.04-9.09 (m, 2H, NCH); 13.18 (s, 1H, ArOH); 13.20 (s, 1H, ArOH).

***N,N'*-Bis(salicylidene)-4'-fluoro-1,2-phenylenediamine [27]**

Was obtained from 4-fluoro-1,2-phenylenediamine (0.79 mmol, 100.0 mg) and salicylaldehyde (1.59 mmol, 193.6 mg).

Yield: 121.0 mg (0.36 mmol, 46%) brown needles.

$C_{20}H_{15}FN_2O_2$ (334.34)

¹H-NMR (DMSO-*d*₆): δ = 6.92-7.04 (m, 4H, ArH-3, ArH-5); 7.22-7.31 (m, 1H, Ar'H-5); 7.39-7.47 (m, 3H, ArH-4, Ar'H-3); 7.51-7.56 (dd, ³J=8.80 Hz, ⁴J=5.73 Hz, 1H, Ar'H-6); 7.63-7.71 (m, 2H, ArH-6); 8.93 (s, 1H, NCH); 8.96 (s, 1H, NCH); 12.67 (s, 1H, ArOH); 12.85 (s, 1H, ArOH).

***N,N'*-Bis(3-fluorosalicylidene)-4'-fluoro-1,2-phenylenediamine [28]**

Was obtained from 4-fluoro-1,2-phenylenediamine (0.53 mmol, 67.0 mg) and 3-fluorosalicylaldehyde (1.06 mmol, 148.8 mg).

Yield: 97.0 mg (0.25 mmol, 47%) dark red crystals.

C₂₀H₁₃F₃N₂O₂ (370.32)

¹H-NMR (DMSO-*d*₆): δ = 6.92-7.03 (m, 2H, ArH-5); 7.23-7.35 (m, 1H, Ar'H-5); 7.36-7.46 (m, 2H, ArH-4); 7.47-7.53 (m, 3H, ArH-6, Ar'H-3); 7.57-7.63 (dd, ³J=8.84 Hz, ⁴J=5.58 Hz, 1H, Ar'H-6); 9.00 (s, 1H, NCH); 9.04 (s, 1H, NCH); 12.97 (s, 1H, ArOH); 13.21 (s, 1H, ArOH).

***N,N'*-Bis(4-fluorosalicylidene)-4'-fluoro-1,2-phenylenediamine [29]**

Was obtained from 4-fluoro-1,2-phenylenediamine (0.77 mmol, 97.0 mg) and 4-fluorosalicylaldehyde (1.54 mmol, 215.5 mg).

Yield: 160.0 mg (0.43 mmol, 56%) dark orange powder.

C₂₀H₁₃F₃N₂O₂ (370.32)

¹H-NMR (DMSO-*d*₆): δ = 6.75-6.89 (m, 4H, ArH-3, ArH-5); 7.15-7.33 (m, 1H, Ar'H-5); 7.38-7.46 (dd, ³J=9.91 Hz, ⁴J=2.69 Hz, 1H, Ar'H-3); 7.49-7.58 (dd, ³J=8.81 Hz, ⁴J=5.70 Hz, 1H, Ar'H-6); 7.66-7.79 (m, 2H, ArH-6); 8.92 (s, 1H, NCH); 8.95 (s, 1H, NCH); 13.26 (s, 1H, ArOH); 13.47 (s, 1H, ArOH).

***N,N'*-Bis(5-fluorosalicylidene)-4'-fluoro-1,2-phenylenediamine [30]**

Was obtained from 4-fluoro-1,2-phenylenediamine (0.94 mmol, 119.0 mg) and 5-fluorosalicylaldehyde (1.89 mmol, 264.4 mg).

Yield: 210.0 mg (0.54 mmol, 58%) dark yellow crystals.

C₂₀H₁₃F₃N₂O₂ (370.32)

¹H-NMR (DMSO-*d*₆): δ = 6.95-7.03 (m, 2H, ArH-3); 7.24-7.35 (m, 3H, ArH-4, Ar'H-5); 7.37-7.44 (dd, ³J=9.28 Hz, ⁴J=2.57 Hz, 1H, Ar'H-3); 7.49-7.57 (m, 3H, ArH-6, Ar'H-6); 8.91 (s, 1H, NCH); 8.93 (s, 1H, NCH); 12.29 (s, 1H, ArOH); 12.53 (s, 1H, ArOH).

***N,N'*-Bis(6-fluorosalicylidene)-4'-fluoro-1,2-phenylenediamine [31]**

Was obtained from 4-fluoro-1,2-phenylenediamine (0.79 mmol, 99.0 mg) and 6-fluorosalicylaldehyde (1.57 mmol, 200.0 mg).

Yield: 248.0 mg (0.59 mmol, 75%) dark orange powder.

$C_{20}H_{13}F_3N_2O_2$ (370.32)

1H -NMR (DMSO- d_6): δ = 6.73-6.89 (m, 4H, ArH-3, ArH-5); 7.25-7.34 (m, 1H, Ar'H-5); 7.41-7.53 (m, 2H, ArH-4); 7.54-7.61 (dd, $^3J=9.87$ Hz, $^4J=2.71$ Hz, 1H, Ar'H-3); 7.62-7.68 (dd, $^3J=8.84$ Hz, $^4J=5.67$ Hz, 1H, Ar'H-6); 9.02 (s, 1H, NCH); 9.06 (s, 1H, NCH); 13.40 (s, 1H, ArOH); 13.54 (s, 1H, ArOH).

***N,N'*-Bis(salicylidene)-4'-methyl-1,2-phenylenediamine [32]**

$C_{21}H_{18}N_2O_2$ (330.38)

1H -NMR (DMSO- d_6): δ = 2.40 (s, 3H, CH_3); 6.93-7.01 (m, 4H, ArH-3, ArH-5); 7.20-7.25 (dd, $^3J=8.12$ Hz, $^4J=1.18$ Hz, 1H, Ar'H-5); 7.28-7.30 (m, 1H, Ar'H-3); 7.37-7.45 (m, 3H, ArH-6, Ar'H-6); 7.63-7.71 (m, 2H, ArH-4); 8.93 (s, 1, NCH); 8.94 (s, 1H, NCH); 12.95 (s, 1H, ArOH); 12.94 (s, 1H, ArOH).

***N,N'*-Bis(salicylidene)-*rac-trans*-1,2-cyclohexanediamine [33]**

$C_{20}H_{22}N_2O_2$ (322.40)

1H -NMR (DMSO- d_6): δ = 1.50-1.64 (m, 2H); 1.71-1.91 (m, 6H); 3.64-3.73 (m, 2H); 6.80-6.91 (m, 4H, ArH-3, ArH-5); 7.27-7.34 (m, 2H, ArH-4); 7.39-7.46 (dd, $^3J=7.62$ Hz, $^4J=1.42$ Hz, 2H, ArH-6); 8.58 (s, 2H, NCH); 13.66 (s, 2H, ArOH).

11.1.2.5 General procedure for the synthesis of the [diarylsalene]- and the [salophene]platinum(II) complexes

Two equivalents of K_2CO_3 were dissolved in water, and the resulting solution was added dropwise to a solution of one equivalent of the ligand in dry DMSO. Afterward a solution of one equivalent of potassium tetrachloroplatinate(II) in water was added dropwise. The mixture was heated for 5 h, keeping the temperature of the reaction under 60 °C. The mixture was allowed to cool to room temperature and the solid matter was filtered off.

[*meso*-3,4-Bis(4-fluorophenyl)-1,6-bis(2-hydroxyphenyl)-2,5-diazahexa-1,5-diene]platinum(II) [1-Pt]

Was obtained from *meso*-3,4-bis(4-fluorophenyl)-1,6-bis(2-hydroxyphenyl)-2,5-diazahexa-1,5-diene (**1**) (0.20 mmol, 91.2 mg) and potassium tetrachloroplatinate(II) (0.20 mmol, 82.9 mg).

Yield: 69.0 mg (0.11 mmol, 53%) yellow powder.

$C_{28}H_{20}F_2N_2O_2Pt$ (649.54)

¹H-NMR (DMSO-*d*₆): δ = 5.55 (s, 2H, CH); 6.53-6.63 (t, ³J=7.27 Hz, 2H, ArH-5); 6.95-7.03 (d, ³J=8.53 Hz, 2H, ArH-3); 7.07-7.15 (t, ³J=8.79 Hz, 4H, Ar'H-3, Ar'H-5); 7.20-7.27 (m, 4H, Ar'H-2, Ar'H-6); 7.39-7.52 (m, 4H, ArH-4, ArH-6); 8.26 (s, 2H, NCH).

MS (+)-ESI m/z calc.: 650.1219 [M+H]⁺; 672.1038 [M+Na]⁺; 688.0778 [M+K]⁺; 1517.1302 [2M+K]⁺.

MS (+)-ESI m/z obs.: 650.1179 [M+H]⁺; 672.1001 [M+Na]⁺; 688.0737 [M+K]⁺; 1517.1300 [2M+K]⁺.

[*d,l*-3,4-Bis(4-fluorophenyl)-1,6-bis(2-hydroxyphenyl)-2,5-diazahexa-1,5-diene]platinum(II) [2-Pt]

Was obtained from *d,l*-3,4-bis(4-fluorophenyl)-1,6-bis(2-hydroxyphenyl)-2,5-diazahexa-1,5-diene (**2**) (0.20 mmol, 91.2 mg) and potassium tetrachloroplatinate(II) (0.20 mmol, 82.9 mg).

Yield: 98.0 mg (0.15 mmol, 75%) yellow powder.

C₂₈H₂₀F₂N₂O₂Pt (649.54)

¹H-NMR (DMSO-*d*₆): δ = 5.28 (s, 2H, CH); 6.56-6.67 (t, ³J=7.34 Hz, 2H, ArH-5); 6.93-7.02 (d, ³J=7.41 Hz, 2H, ArH-3); 7.22-7.34 (t, ³J=8.81 Hz, 4H, Ar'H-3, Ar'H-5); 7.40-7.54 (m, 4H, ArH-4, ArH-6); 7.69-7.83 (m, 4H, Ar'H-2, Ar'H-6); 8.52 (s, 2H, NCH).

MS (+)-ESI m/z calc.: 650.1219 [M+H]⁺; 672.1038 [M+Na]⁺; 688.0778 [M+K]⁺; 1517.1302 [2M+K]⁺.

MS (+)-ESI m/z obs.: 650.1185 [M+H]⁺; 672.1004 [M+Na]⁺; 688.0739 [M+K]⁺; 1517.1300 [2M+K]⁺.

[*meso*-3,4-Bis(4-fluorophenyl)-1,6-bis(2-hydroxy-5-nitrophenyl)-2,5-diazahexa-1,5-diene]platinum(II) [3-Pt]

Was obtained from *meso*-3,4-bis(4-fluorophenyl)-1,6-bis(2-hydroxy-5-nitrophenyl)-2,5-diazahexa-1,5-diene (**3**) (0.17 mmol, 93.0 mg) and potassium tetrachloroplatinate(II) (0.17 mmol, 70.6 mg).

Yield: 52.0 mg (0.17 mmol, 41%) red powder.

C₂₈H₁₈F₂N₄O₆Pt (739.54)

¹H-NMR (DMSO-*d*₆): δ = 5.64 (s, 2H, CH); 7.06-7.21 (m, ⁴J=4.81 Hz, 6H, ArH-3, Ar'H-3, Ar'H-5); 7.21-7.35 (m, 4H, Ar'H-2, Ar'H-6); 8.25-8.35 (dd, ³J=9.47 Hz, ⁴J=2.89 Hz, 2H, ArH-4); 8.59 (s, 2H, NCH); 8.63-8.74 (d, ⁴J=2.88 Hz, 2H, ArH-6).

MS (+)-ESI m/z calc.: 762.0740 [M+Na]⁺; 778.0479 [M+K]⁺; 1517.1302 [2M+K]⁺.

MS (+)-ESI m/z obs.: 762.0725 [M+Na]⁺; 778.0475 [M+K]⁺; 1517.1300 [2M+K]⁺.

[*meso*-3,4-Bis(4-fluorophenyl)-1,6-bis(2-hydroxy-3-methoxyphenyl)-2,5-diazahexa-1,5-diene]platinum(II) [4-Pt]

Was obtained from *meso*-3,4-bis(4-fluorophenyl)-1,6-bis(2-hydroxy-3-methoxyphenyl)-2,5-diazahexa-1,5-diene (**4**) (0.19 mmol, 137.0 mg) and potassium tetrachloroplatinate(II) (0.19 mmol, 79.0 mg).

Yield: 79.0 mg (0.11 mmol, 61%) yellow powder.

¹H-NMR (DMSO-*d*₆): δ = 3.82 (s, 6H, OCH₃); 5.54 (s, 2H, CH); 6.48-6.56 (t, 2H, ³J=7.84 Hz, ArH-5); 6.96-7.02 (m, 2H, ArH-4); 7.06-7.25 (m, 10H, ArH-6, Ar'H-2, Ar'H-3, Ar'H-5, Ar'H-6); 8.23 (s, 2H, NCH).

C₃₀H₂₄F₂N₂O₄Pt (709.60)

MS (+)-ESI m/z calc.: 748.0989 [M+K]⁺.

MS (+)-ESI m/z obs.: 748.1033 [M+K]⁺.

[*meso*-3,4-Bis(4-fluorophenyl)-1,6-bis(2-hydroxy-4-methoxyphenyl)-2,5-diazahexa-1,5-diene]platinum(II) [5-Pt]

Was obtained from *meso*-3,4-bis(4-fluorophenyl)-1,6-bis(2-hydroxy-4-methoxyphenyl)-2,5-diazahexa-1,5-diene (**5**) (0.08 mmol, 44.0 mg) and potassium tetrachloroplatinate(II) (0.08 mmol, 35.4 mg).

Yield: 20.0 mg (0.03 mmol, 35%) yellow powder.

C₃₀H₂₄F₂N₂O₄Pt (709.60)

¹H-NMR (DMSO-*d*₆): δ = 3.77 (s, 6H, CH₃); 5.45 (s, 2H, CH); 6.20-6.26 (dd, ³J=8.81 Hz, ⁴J=2.28 Hz, 2H, ArH-5); 6.46-6.50 (d, ⁴J=2.21 Hz, 2H, ArH-3); 7.05-7.13 (t, ³J=8.76 Hz, 4H, Ar'H-3, Ar'H-5); 7.17-7.24 (m, 4H, Ar'H-2, Ar'H-6); 7.27-7.32 (d, ³J=8.88, 2H, ArH-6); 8.05 (s, 2H, NCH).

MS (+)-ESI m/z calc.: 710.1430 [M+H]⁺; 732.1250 [M+Na]⁺; 748.0989 [M+K]⁺.

MS (+)-ESI m/z obs.: 710.1437 [M+H]⁺; 732.1262 [M+Na]⁺; 748.0999 [M+K]⁺.

[*meso*-3,4-Bis(4-fluorophenyl)-1,6-bis(2-hydroxy-5-methoxyphenyl)-2,5-diazahexa-1,5-diene]platinum(II) [6-Pt]

Was obtained from *meso*-3,4-bis(4-fluorophenyl)-1,6-bis(2-hydroxy-5-methoxyphenyl)-2,5-diazahexa-1,5-diene (**6**) (0.10 mmol, 54.0 mg) and potassium tetrachloroplatinate(II) (0.10 mmol, 43.4 mg).

Yield: 25.0 mg (0.03 mmol, 35%) yellow powder.

C₃₀H₂₄F₂N₂O₄Pt (709.60)

¹H-NMR (DMSO-*d*₆): δ = 3.63 (s, 6H, CH₃); 5.53 (s, 2H, CH); 6.89-6.94 (d, ³J=9.23 Hz, 2H, ArH-3); 6.95-6.98 (d, ⁴J=3.14 Hz, 2H, ArH-6); 7.08-7.19 (m, 6H, ArH-4, Ar'H-3, Ar'H-5); 7.19-7.26 (m, 4H, Ar'H-2, Ar'H-6); 8.24 (s, 2H, NCH).

MS (+)-ESI *m/z* calc.: 710.1430 [M+H]⁺; 732.1250 [M+Na]⁺; 748.0989 [M+K]⁺; 1418.2761 [2M+H]⁺; 1440.2580 [2M+Na]⁺; 1457.2398 [2M+K]⁺.

MS (+)-ESI *m/z* obs.: 710.1419 [M+H]⁺; 732.1246 [M+Na]⁺; 748.0984 [M+K]⁺; 1419.2774 [2M+H]⁺; 1441.2575 [2M+Na]⁺; 1457.2315 [2M+K]⁺.

[*meso*-3,4-Bis(4-fluorophenyl)-1,6-bis(2-hydroxy-6-methoxyphenyl)-2,5-diazahexa-1,5-diene]platinum(II) [7-Pt]

Was obtained from *meso*-3,4-bis(4-fluorophenyl)-1,6-bis(2-hydroxy-6-methoxyphenyl)-2,5-diazahexa-1,5-diene (**7**) (0.32 mmol, 163 mg) and potassium tetrachloroplatinate(II) (0.32 mmol, 130 mg).

Yield: 30.0 mg (0.04 mmol, 13%) brown powder.

C₃₀H₂₄F₂N₂O₄Pt (709.60)

¹H-NMR (DMSO-*d*₆): δ = 3.73 (s, 6H, CH₃); 5.42 (s, 2H, CH); 6.13-6.22 (d, ³J=7.91 Hz, 2H, ArH-5); 6.53-6.58 (d, ³J=8.68 Hz, 2H, ArH-3); 7.23-7.30 (t, ³J=8.84 Hz, 4H, Ar'H-3, Ar'H-5); 7.31-7.37 (t, ³J=8.33, 2H, ArH-4); 7.69-7.75 (m, 4H, Ar'H-2, Ar'H-6); 8.75 (s, 2H, NCH).

MS (+)-ESI *m/z* calc.: 732.1250 [M+Na]⁺; 748.0989 [M+K]⁺; 1457.2398 [2M+K]⁺.

MS (+)-ESI *m/z* obs.: 732.1223 [M+Na]⁺; 748.0965 [M+K]⁺; 1457.2325 [2M+K]⁺.

[*meso*-3,4-Bis(4-fluorophenyl)-1,6-bis(2-hydroxy-3-fluorophenyl)-2,5-diazahexa-1,5-diene]platinum(II) [8-Pt]

Was obtained from *meso*-3,4-bis(4-fluorophenyl)-1,6-bis(2-hydroxy-3-fluorophenyl)-2,5-diazahexa-1,5-diene (**8**) (0.19 mmol, 93.0 mg) and potassium tetrachloroplatinate(II) (0.19 mmol, 79.0 mg).

Yield: 79.0 mg (0.11 mmol, 61%) yellow powder.

C₂₈H₁₈F₄N₂O₂Pt (685.53)

¹H-NMR (DMSO-*d*₆): δ = 5.62 (s, 2H, CH); 6.51-6.64 (m, 2H, ArH-5); 7.06-7.19 (t, ³J=8.70 Hz, 4H, Ar'H-3, Ar'H-5); 7.19-7.39 (m, 6H, ArH-6, Ar'H-2, Ar'H-6); 7.38-7.52 (m, 2H, ArH-3); 8.35 (s, 2H, NCH).

MS (+)-ESI *m/z* calc.: 686.1030 [M+H]⁺; 708.0850 [M+Na]⁺; 724.0589 [M+K]⁺; 1408.1520 [2M+K]⁺.

MS (+)-ESI *m/z* obs.: 686.1051 [M+H]⁺; 708.0852 [M+Na]⁺; 724.0606 [M+K]⁺; 1409.1546 [2M+K]⁺.

[*meso*-3,4-Bis(4-fluorophenyl)-1,6-bis(2-hydroxy-4-fluorophenyl)-2,5-diazahexa-1,5-diene]platinum(II) [9-Pt]

Was obtained from *meso*-3,4-bis(4-fluorophenyl)-1,6-bis(2-hydroxy-4-fluorophenyl)-2,5-diazahexa-1,5-diene (**9**) (0.19 mmol, 94.0 mg) and potassium tetrachloroplatinate(II) (0.19 mmol, 79.0 mg).

Yield: 79.0 mg (0.11 mmol, 61%) yellow powder.

C₂₈H₁₈F₄N₂O₂Pt (685.53)

¹H-NMR (DMSO-*d*₆): δ = 5.55 (s, 2H, CH); 6.46-6.54 (m, 2H, ArH-5); 6.73-6.80 (dd, ³J=12.06 Hz, ⁴J=2.27 Hz, 2H, ArH-3); 7.06-7.15 (t, ³J=8.81 Hz, 4H, Ar'H-3, Ar'H-5); 7.18-7.28 (m, 4H, Ar'H-2, Ar'H-6); 7.50-7.58 (m, 2H, ArH-6); 8.26 (s, 2H, NCH).

MS (+)-ESI m/z calc.: 686.1030 [M+H]⁺; 708.0850 [M+Na]⁺; 724.0589 [M+K]⁺; 1408.1520 [2M+K]⁺.

MS (+)-ESI m/z obs.: 686.1033 [M+H]⁺; 708.0866 [M+Na]⁺; 724.0611 [M+K]⁺; 1409.1554 [2M+K]⁺.

[*meso*-3,4-Bis(4-fluorophenyl)-1,6-bis(2-hydroxy-5-fluorophenyl)-2,5-diazahexa-1,5-diene]platinum(II) [10-Pt]

Was obtained from *meso*-3,4-bis(4-fluorophenyl)-1,6-bis(2-hydroxy-5-fluorophenyl)-2,5-diazahexa-1,5-diene (**10**) (0.16 mmol, 77.0 mg) and potassium tetrachloroplatinate(II) (0.16 mmol, 65.0 mg).

Yield: 93.0 mg (0.13 mmol, 82%) dark yellow powder.

C₂₈H₁₈F₄N₂O₂Pt (685.53)

¹H-NMR (DMSO-*d*₆): δ = 5.56 (s, 2H, CH); 6.94-7.03 (dd, ³J=9.27 Hz, ⁴J=4.81 Hz, 2H, ArH-3); 7.07-7.16 (t, ³J=8.82 Hz, 4H, Ar'H-3, Ar'H-5); 7.18-7.25 (m, 4H, Ar'H-2, Ar'H-6); 7.30-7.46 (m, 4H, ArH-4, ArH-6); 8.29 (s, 2H, NCH).

MS (+)-ESI m/z calc.: 686.1030 [M+H]⁺; 708.0850 [M+Na]⁺; 724.0589 [M+K]⁺; 1392.1781 [2M+Na]⁺.

MS (+)-ESI m/z obs.: 686.1087 [M+H]⁺; 708.0853 [M+Na]⁺; 724.0592 [M+K]⁺; 1393.1724 [2M+Na]⁺.

[*meso*-3,4-Bis(4-fluorophenyl)-1,6-bis(2-hydroxy-6-fluorophenyl)-2,5-diazahexa-1,5-diene]platinum(II) [11-Pt]

Was obtained from *meso*-3,4-bis(4-fluorophenyl)-1,6-bis(2-hydroxy-6-fluorophenyl)-2,5-diazahexa-1,5-diene (**11**) (0.13 mmol, 64.0 mg) and potassium tetrachloroplatinate(II) (0.13 mmol, 53.9 mg).

Yield: 48.0 mg (0.07 mmol, 54%) yellow powder.

C₂₈H₁₈F₄N₂O₂Pt (685.53)

¹H-NMR (DMSO-*d*₆): δ = 5.67 (s, 2H, CH); 6.37-6.48 (dd, ³J=10.90 Hz, ⁴J=8.05 Hz, 2H, ArH-5); 6.81-6.90 (d, ³J=8.79 Hz, 2H, ArH-3); 7.08-7.20 (t, ³J=8.73 Hz, 4H, Ar'H-3,

Ar'H-5); 7.20-7.31 (m, 4H, Ar'H-2, Ar'H-6); 7.39-7.50 (m, 2H, ArH-4); 8.46 (s, 2H, NCH).

MS (+)-ESI m/z calc.: 708.0850 [M+Na]⁺.

MS (+)-ESI m/z obs.: 708.0759 [M+Na]⁺.

[*meso*-3,4-Bis(4-trifluoromethylphenyl)-1,6-bis(2-hydroxyphenyl)-2,5-diazahexa-1,5-diene]platinum(II) [12-Pt]

Was obtained from *meso*-3,4-bis(4-trifluoromethylphenyl)-1,6-bis(2-hydroxyphenyl)-2,5-diazahexa-1,5-diene (**12**) (0.10 mmol, 55.6 mg) and potassium tetrachloroplatinate(II) (0.10 mmol, 41.5 mg).

Yield: 38.0 mg (0.05 mmol, 50%) yellow powder.

C₂₀H₂₀F₆N₂O₂Pt (749.56)

¹H-NMR (DMSO-*d*₆): δ = 5.42 (s, 2H, CH); 6.59-6.65 (t, ³J=7.30 Hz, 2H, ArH-5); 6.96-7.02 (d, ³J=8.55 Hz, 2H, ArH-3); 7.41-7.46 (m, 2H, ArH-6) 7.47-7.59 (m, 2H, ArH-4); 7.79-7.88 (d, ³J=8.31 Hz, 4H, Ar'H-2, Ar'H-6); 7.94-8.02 (d, ³J=8.17 Hz, 4H, Ar'H-3, Ar'H-5); 8.61 (s, 2H, NCH).

MS (+)-ESI m/z calc.: 772.0974 [M+Na]⁺; 788.0714 [M+K]⁺; 1538.1792 [2M+K]⁺.

MS (+)-ESI m/z obs.: 772.0978 [M+Na]⁺; 788.0719 [M+K]⁺; 1538.1803 [2M+K]⁺.

[*N,N'*-Bis(salicylidene)-1,2-phenylenediamine]platinum(II) [13-Pt]

Was obtained from *N,N'*-bis(salicylidene)-1,2-phenylenediamine (**13**) (0.19 mmol, 60.0 mg) and potassium tetrachloroplatinate(II) (0.19 mmol, 78.8 mg).

Yield: 75.5 mg (0.15 mmol, 78%) red powder.

C₂₀H₁₄N₂O₂Pt (509.41)

¹H-NMR (DMF-*d*₇): δ = 6.77-6.83 (m, 2H, ArH-5); 7.13-7.19 (d, ³J=8.60 Hz, 2H, ArH-3); 7.45-7.50 (dd, ³J=6.30 Hz, ⁴J=3.25 Hz, 2H, Ar'H-4, Ar'H-5); 7.58-7.64 (m, 2H, ArH-4); 7.91-7.95 (dd, ³J=8.05 Hz, ⁴J=1.53 Hz, 2H, ArH-6); 8.50-8.59 (dd, ³J=6.28 Hz, ⁴J=3.33 Hz, 2H, Ar'H-3, Ar'H-6); 9.65 (s, 2H, NCH).

MS (+)-ESI m/z calc.: 532.0601 [M+Na]⁺; 548.03404 [M+K]⁺; 1041.1304 [2M+Na]⁺; 1057.1043 [2M+K]⁺.

MS (+)-ESI m/z obs.: 532.0615 [M+Na]⁺; 548.0356 [M+K]⁺; 1041.1329 [2M+Na]⁺; 1057.1072 [2M+K]⁺.

[*N,N'*-Bis(3-methoxysalicylidene)-1,2-phenylenediamine]platinum(II) [14-Pt]

Was obtained from *N,N'*-bis(3-methoxysalicylidene)-1,2-phenylenediamine (**14**) (0.10 mmol, 37.0 mg) and potassium tetrachloroplatinate(II) (0.10 mmol, 40.8 mg).

Yield: 10.0 mg (0.02 mmol, 18%) violet powder.

C₂₂H₁₈N₂O₄Pt (569.47)

¹H-NMR (DMSO-*d*₆): δ = 3.85 (s, 6H, CH₃); 6.68-6.81 (m, 2H, ArH-5); 7.11-7.27 (m, 2H, ArH-4); 7.33-7.61 (m, 4H, ArH-6, Ar'H-4, Ar'H-5); 8.39-8.63 (m, 2H, Ar'H-3, Ar'H-6); 9.52 (s, 2H, NCH).

MS (+)-ESI m/z calc.: 592.0812 [M+Na]⁺; 608.0551 [M+K]⁺; 1177.1466 [2M+K]⁺.

MS (+)-ESI m/z obs.: 592.0763 [M+Na]⁺; 608.0541 [M+K]⁺; 1177.1487 [2M+K]⁺.

[N,N'-Bis(4-methoxysalicylidene)-1,2-phenylenediamine]platinum(II) [15-Pt]

Was obtained from *N,N'*-bis(5-methoxysalicylidene)-1,2-phenylenediamine (**15**) (0.10 mmol, 37.0 mg) and potassium tetrachloroplatinate(II) (0.10 mmol, 40.8 mg).

Yield: 50.0 mg (0.09 mmol, 88%) orange powder.

C₂₂H₁₈N₂O₄Pt (569.47)

¹H-NMR (DMSO-*d*₆): δ = 3.84 (s, 6H, CH₃); 6.45-6.50 (dd, ³J=8.92 Hz, ⁴J=2.25 Hz, 2H, ArH-5); 6.60-6.65 (d, ⁴J=2.05 Hz, 2H, ArH-3); 7.37-7.42 (m, 4H, Ar'H-4, Ar'H-5); 7.72-7.77 (d, ³J=9.00 Hz, 2H, ArH-6); 8.33-8.41 (dd, ³J=6.21 Hz, ⁴J=3.37, 2H, Ar'H-3, Ar'H-6); 9.32 (s, 2H, NCH).

MS (+)-ESI m/z calc.: 608.0551 [M+K]⁺.

MS (+)-ESI m/z obs.: 608.0539 [M+K]⁺.

[N,N'-Bis(5-methoxysalicylidene)-1,2-phenylenediamine]platinum(II) [16-Pt]

Was obtained from *N,N'*-bis(5-methoxysalicylidene)-1,2-phenylenediamine (**16**) (0.10 mmol, 37.0 mg) and potassium tetrachloroplatinate(II) (0.10 mmol, 40.8 mg).

Yield: 16.0 mg (0.03 mmol, 29%) dark violet powder.

C₂₂H₁₈N₂O₄Pt (569.47)

¹H-NMR (DMSO-*d*₆): δ = 3.78 (s, 6H, CH₃); 7.03-7.11 (d, ³J=9.26 Hz, 2H, ArH-3); 7.26-7.33 (dd, ³J=9.25 Hz, ⁴J=3.18 Hz, 2H, ArH-4); 7.35-7.39 (d, ⁴J=3.14 Hz, 2H, ArH-6); 7.41-7.48 (dd, ³J=6.26 Hz, ⁴J=3.20 Hz, 2H, Ar'H-4, Ar'H-5); 8.37-8.46 (dd, ³J=6.26 Hz, ⁴J=3.37 Hz, 2H, Ar'H-3, Ar'H-6); 9.51 (s, 2H, NCH).

MS (+)-ESI m/z calc.: 570.0093 [M+H]⁺; 592.0812 [M+Na]⁺; 608.0551 [M+K]⁺; 1161.1726 [2M+Na]⁺; 1177.1466 [2M+K]⁺.

MS (+)-ESI m/z obs.: 516.0992 [M+H]⁺; 592.0825 [M+Na]⁺; 608.0567 [M+K]⁺; 1161.1746 [2M+Na]⁺; 1177.1487 [2M+K]⁺.

[N,N'-Bis(6-methoxysalicylidene)-1,2-phenylenediamine]platinum(II) [17-Pt]

Was obtained from *N,N'*-bis(6-methoxysalicylidene)-1,2-phenylenediamine (**17**) (0.10 mmol, 37.0 mg) and potassium tetrachloroplatinate(II) (0.10 mmol, 40.8 mg).

Yield: 15.0 mg (0.03 mmol, 29%) red powder.

$C_{22}H_{18}N_2O_4Pt$ (569.47)

1H -NMR (DMSO- d_6): δ = 3.94 (s, 6H, CH_3); 6.30-6.37 (m, 2H, ArH-5); 6.68-6.74 (m, 2H, ArH-3); 7.36-7.54 (m, 4H, ArH-4, Ar'H-4, Ar'H-5); 8.21-8.31 (dd, $^3J=6.08$ Hz, $^4J=3.12$ Hz, 2H, Ar'H-3, Ar'H-6); 9.61 (s, 2H, NCH).

MS (+)-ESI m/z calc.: 608.0551 [M+K]⁺; 1161.1726 [2M+Na]⁺; 1177.1466 [2M+K]⁺.

MS (+)-ESI m/z obs.: 608.0577 [M+K]⁺; 1161.1752 [2M+Na]⁺; 1177.1493 [2M+K]⁺.

[*N,N'*-Bis(3-fluorosalicylidene)-1,2-phenylenediamine]platinum(II) [18-Pt]

Was obtained from *N,N'*-bis(3-fluorosalicylidene)-1,2-phenylenediamine (**18**) (0.10 mmol, 35.0 mg) and potassium tetrachloroplatinate(II) (0.10 mmol, 41.3 mg).

Yield: 25.0 mg (0.05 mmol, 50%) dark violet powder.

$C_{20}H_{12}F_2N_2O_2Pt$ (545.40)

1H -NMR (DMSO- d_6): δ = 6.73-6.83 (m, 2H, ArH-5); 7.48-7.58 (m, 4H, ArH-4, Ar'H-4, Ar'H-5); 7.73-7.81 (d, $^3J=8.12$ Hz, 2H, ArH-6); 8.47-8.57 (dd, $^3J=6.06$ Hz, $^4J=3.38$ Hz, 2H, Ar'H-3, Ar'H-6); 9.63 (s, 2H, NCH).

MS (+)-ESI m/z calc.: 546.0593 [M+H]⁺; 568.0412 [M+Na]⁺; 584.0152 [M+K]⁺; 1129.0666 [2M+K]⁺.

MS (+)-ESI m/z obs.: 546.0583 [M+H]⁺; 568.0402 [M+Na]⁺; 584.0144 [M+K]⁺; 1129.0645 [2M+K]⁺.

[*N,N'*-Bis(4-fluorosalicylidene)-1,2-phenylenediamine]platinum(II) [19-Pt]

Was obtained from *N,N'*-bis(4-fluorosalicylidene)-1,2-phenylenediamine (**19**) (0.10 mmol, 35.0 mg) and potassium tetrachloroplatinate(II) (0.10 mmol, 41.3 mg).

Yield: 32.0 mg (0.06 mmol, 56%) dark violet powder.

$C_{20}H_{12}F_2N_2O_2Pt$ (545.40)

1H -NMR (DMSO- d_6): δ = 6.69-6.78 (m, 2H, ArH-5); 6.83-6.94 (dd, $^3J=12.07$ Hz, $^4J=2.17$ Hz, 2H, ArH-3); 7.41-7.50 (dd, $^3J=6.17$ Hz, $^4J=3.13$ Hz, 2H, Ar'H-4, Ar'H-5); 7.88-8.00 (m, 2H, ArH-6); 8.36-8.46 (dd, $^3J=6.11$ Hz, $^4J=3.38$ Hz, 2H, Ar'H-3, Ar'H-6); 9.49 (s, 2H, NCH).

MS (+)-ESI m/z calc.: 568.0412 [M+Na]⁺; 584.0152 [M+K]⁺; 1113.0927 [2M+Na]⁺; 1129.0700 [2M+K]⁺.

MS (+)-ESI m/z obs.: 568.0429 [M+Na]⁺; 584.0172 [M+K]⁺; 1113.0957 [2M+Na]⁺; 1129.0687 [2M+K]⁺.

[*N,N'*-Bis(5-fluorosalicylidene)-1,2-phenylenediamine]platinum(II) [20-Pt]

Was obtained from *N,N'*-bis(5-fluorosalicylidene)-1,2-phenylenediamine (**20**) (0.08 mmol, 29.0 mg) and potassium tetrachloroplatinate(II) (0.08 mmol, 34.2 mg).

Yield: 30 mg (0.06 mmol, 69%) dark violet powder.

C₂₀H₁₂F₂N₂O₂Pt (545.40)

¹H-NMR (DMSO-*d*₆): δ = 7.08-7.17 (dd, ³J=9.37 Hz, ⁴J=4.78 Hz, 2H, ArH-3); 7.44-7.56 (m, 4H, ArH-4, Ar'H-4, Ar'H-5); 7.61-7.70 (dd, ³J=9.37 Hz, ⁴J=4.78 Hz, 2H, ArH-6); 8.35-8.44 (dd, ³J=6.17 Hz, ⁴J=3.34 Hz, 2H, Ar'H-3, Ar'H-6); 9.52 (s, 2H, NCH).

MS (+)-ESI m/z calc.: 568.0412 [M+Na]⁺; 584.0152 [M+K]⁺; 1129.0666 [2M+K]⁺.

MS (+)-ESI m/z obs.: 568.0425 [M+Na]⁺; 584.0172 [M+K]⁺; 1129.0689 [2M+K]⁺.

[*N,N'*-Bis(6-fluorosalicylidene)-1,2-phenylenediamine]platinum(II) [21-Pt]

Was obtained from *N,N'*-bis(6-fluorosalicylidene)-1,2-phenylenediamine (**21**) (0.12 mmol, 42.0 mg) and potassium tetrachloroplatinate(II) (0.12 mmol, 49.5 mg).

Yield: 30.0 mg (0.06 mmol, 46%) dark red powder.

C₂₀H₁₂F₂N₂O₂Pt (545.40)

¹H-NMR (DMSO-*d*₆): δ = 6.58-6.65 (m, 2H, ArH-5); 6.95-6.99 (m, 2H, ArH-3); 7.44-7.48 (m, 2H, Ar'H-4, Ar'H-5); 7.50-7.57 (m, 2H, ArH-4); 8.40-8.51 (dd, ³J=6.05 Hz, ⁴J=2.94 Hz, 2H, Ar'H-3, Ar'H-6); 9.47 (s, 2H, NCH).

MS (+)-ESI m/z calc.: 568.0412 [M+Na]⁺; 584.0152 [M+K]⁺; 1113.0927 [2M+Na]⁺; 1129.0666 [2M+K]⁺.

MS (+)-ESI m/z obs.: 568.0435 [M+Na]⁺; 584.0178 [M+K]⁺; 1113.0957 [2M+Na]⁺; 1129.0645 [2M+K]⁺.

[*N,N'*-Bis(salicylidene)-3'-fluoro-1,2-phenylenediamine]platinum(II) [22-Pt]

Was obtained from *N,N'*-bis(salicylidene)-3'-fluoro-1,2-phenylenediamine (**22**) (0.23 mmol, 76.0 mg) and potassium tetrachloroplatinate(II) (0.23 mmol, 94.0 mg).

Yield: 109.0 mg (0.21 mmol, 90%) dark red powder.

C₂₀H₁₀FN₂O₂Pt (527.41)

¹H-NMR (DMSO-*d*₆): δ = 6.75-6.86 (m, 2H, ArH-5); 7.11-7.19 (m, 2H, ArH-3); 7.35-7.53 (m, 2H, Ar'H-4, Ar'H-5); 7.58-7.64 (m, 2H, ArH-4); 7.81-7.94 (m, 2H, ArH-6); 8.35-8.41 (m, 1H, Ar'H-6); 9.47 (s, 1H, NCH); 9.59 (s, 1H, NCH).

MS (+)-ESI m/z calc.: 528.0687 [M+H]⁺; 550.0506 [M+Na]⁺; 566.0246 [M+K]⁺; 1093.0835 [2M+K]⁺.

MS (+)-ESI m/z obs.: 528.0686 [M+H]⁺; 550.0518 [M+Na]⁺; 566.0256 [M+K]⁺; 1093.0876 [2M+K]⁺.

[*N,N'*-Bis(3-fluorosalicylidene)-3'-fluoro-1,2-phenylenediamine]platinum(II) [23-Pt]

Was obtained from *N,N'*-bis(3-fluorosalicylidene)-3'-fluoro-1,2-phenylenediamine (**23**) (0.20 mmol, 75.0 mg) and potassium tetrachloroplatinate(II) (0.20 mmol, 84.1 mg).

Yield: 21.0 mg (0.04 mmol, 19%) dark violet powder.

$C_{20}H_{11}F_3N_2O_2Pt$ (563.39)

¹H-NMR (DMSO-*d*₆): δ = 6.67-6.82 (m, 2H, ArH-5); 7.40-7.89 (m, 6H, ArH-4, ArH-6, Ar'H-4, Ar'H-5); 8.27-8.38 (m, 1H, Ar'H-6); 9.41 (s, 1H, NCH); 9.56 (s, 1H, NCH).

MS (+)-ESI m/z calc.: 602.0054 [M+K]⁺.

MS (+)-ESI m/z obs.: 602.0067 [M+K]⁺.

[*N,N'*-Bis(4-fluorosalicylidene)-3'-fluoro-1,2-phenylenediamine]platinum(II)

[24-Pt]

Was obtained from *N,N'*-bis(4-fluorosalicylidene)-3'-fluoro-1,2-phenylenediamine (**24**) (0.29 mmol, 108.0 mg) and potassium tetrachloroplatinate(II) (0.29 mmol, 121.1 mg).

Yield: 96.0 mg (0.17 mmol, 59%) dark violet powder.

$C_{20}H_{11}F_3N_2O_2Pt$ (563.39)

¹H-NMR (DMSO-*d*₆): δ = 6.67-6.82 (m, 2H, ArH-5); 6.87-6.98 (m, 2H, ArH-3); 7.34-7.54 (m, 2H, Ar'H-4, Ar'H-5); 7.91-8.05 (m, 2H, ArH-6); 8.27-8.38 (m, 1H, Ar'H-6); 9.41 (s, 1H, NCH); 9.56 (s, 1H, NCH).

MS (+)-ESI m/z calc.: 564.0499 [M+H]⁺; 586.0318 [M+Na]⁺; 1027.0919 [2M+H]⁺; 1149.0719 [2M+Na]⁺; 1165.0458 [2M+K]⁺.

MS (+)-ESI m/z obs.: 564.0496 [M+H]⁺; 586.0323 [M+Na]⁺; 1027.0918 [2M+H]⁺; 1149.0724 [2M+Na]⁺; 1165.0492 [2M+K]⁺.

[*N,N'*-Bis(5-fluorosalicylidene)-3'-fluoro-1,2-phenylenediamine]platinum(II)

[25-Pt]

Was obtained from *N,N'*-bis(5-fluorosalicylidene)-3'-fluoro-1,2-phenylenediamine (**25**) (0.35 mmol, 129 mg) and potassium tetrachloroplatinate(II) (0.35 mmol, 145 mg).

Yield: 149 mg (0.26 mmol, 76%) dark violet powder.

$C_{20}H_{11}F_3N_2O_2Pt$ (563.39)

¹H-NMR (DMSO-*d*₆): δ = 7.10-7.21 (m, 2H, ArH-3); 7.38-7.59 (m, 4H, ArH-4, Ar'H-4, Ar'H-5); 7.68-7.81 (m, 2H, ArH-6); 8.21-8.47 (m, 1H, Ar'H-6); 9.44 (s, 1H, NCH); 9.62 (s, 1H, NCH).

MS (+)-ESI m/z calc.: 602.0054 [M+K]⁺; 1165.0458 [2M+K]⁺.

MS (+)-ESI m/z obs.: 602.0083 [M+K]⁺; 1165.0516 [2M+K]⁺.

[*N,N'*-Bis(6-fluorosalicylidene)-3'-fluoro-1,2-phenylenediamine]platinum(II)

[26-Pt]

Was obtained from *N,N'*-bis(6-fluorosalicylidene)-3'-fluoro-1,2-phenylenediamine (**26**) (0.10 mmol, 37.0 mg) and potassium tetrachloroplatinate(II) (0.10 mmol, 41.5 mg).

Yield: 20.0 mg (0.04 mmol, 36%) dark red powder.

$C_{20}H_{11}F_3N_2O_2Pt$ (563.39)

¹H-NMR (DMSO-*d*₆): δ = 6.59-6.67 (m, 2H, ArH-5); 6.95-7.01 (m, 2H, ArH-3); 7.39-7.49 (m, 2H, Ar'H-4, Ar'H-5); 7.51-7.62 (m, 2H, ArH-4); 8.32-8.39 (m, 1H, Ar'H-6); 9.49 (s, 1H, NCH); 9.72 (s, 1H, NCH).

MS (+)-ESI *m/z* calc.: 564.0499 [M+H]⁺; 586.0318 [M+Na]⁺; 602.0054 [M+K]⁺; 1027.0919 [2M+H]⁺; 1149.0719 [2M+Na]⁺; 1165.0458 [2M+K]⁺.

MS (+)-ESI *m/z* obs.: 564.0508 [M+H]⁺; 586.0330 [M+Na]⁺; 602.0070 [M+K]⁺; 1027.0937 [2M+H]⁺; 1149.0742 [2M+Na]⁺; 1165.0488 [2M+K]⁺.

[*N,N'*-Bis(salicylidene)-4'-fluoro-1,2-phenylenediamine]platinum(II) [27-Pt]

Was obtained from *N,N'*-bis(salicylidene)-4'-fluoro-1,2-phenylenediamine (**27**) (0.26 mmol, 87.0 mg) and potassium tetrachloroplatinate(II) (0.26 mmol, 108.0 mg).

Yield: 93.0 mg (0.18 mmol, 68%) dark red powder.

$C_{20}H_{10}FN_2O_2Pt$ (527.41)

¹H-NMR (DMSO-*d*₆): δ = 6.65-6.91 (m, 2H, ArH-5); 7.11-7.17 (dd, ³*J*=8.60 Hz, ⁴*J*=3.14 Hz, 2H, ArH-3); 7.43-7.50 (m, 1H, Ar'H-5); 7.55-7.65 (m, 2H, ArH-4); 7.85-7.90 (m, 2H, ArH-6); 8.41-8.45 (dd, ³*J*=10.37 Hz, ⁴*J*=2.47 Hz, 1H, Ar'H-3); 8.51-8.56 (dd, ³*J*=9.27 Hz, ⁴*J*=5.23 Hz, 1H, Ar'H-6); 9.50 (s, 1H, NCH); 9.55 (s, 1H, NCH).

MS (+)-ESI *m/z* calc.: 566.0246 [M+K]⁺; 1093.0835 [2M+K]⁺.

MS (+)-ESI *m/z* obs.: 566.0322 [M+K]⁺; 1093.0954 [2M+K]⁺.

[*N,N'*-Bis(3-fluorosalicylidene)-4'-fluoro-1,2-phenylenediamine]platinum(II) [28-Pt]

Was obtained from *N,N'*-bis(3-fluorosalicylidene)-4'-fluoro-1,2-phenylenediamine (**28**) (0.18 mmol, 68.0 mg) and potassium tetrachloroplatinate(II) (0.18 mmol, 76.0 mg).

Yield: 92.0 mg (0.16 mmol, 91%) dark red powder.

$C_{20}H_{11}F_3N_2O_2Pt$ (563.39)

¹H-NMR (DMSO-*d*₆): δ = 6.72-6.83 (m, 2H, ArH-5); 7.44-7.67 (m, 3H, ArH-4, Ar'H-5); 7.67-7.79 (d, ³*J*=8.16 Hz, 2H, ArH-6); 8.41-8.46 (dd, ³*J*=10.22 Hz, ⁴*J*=2.22 Hz, 1H, Ar'H-3); 8.52-8.58 (dd, ³*J*=9.25 Hz, ⁴*J*=5.13 Hz, 1H, Ar'H-6); 9.54 (s, 1H, NCH); 9.59 (s, 1H, NCH).

MS (+)-ESI *m/z* calc.: 602.0054 [M+K]⁺; 1165.0458 [2M+K]⁺.

MS (+)-ESI *m/z* obs.: 602.0056 [M+K]⁺; 1165.0467 [2M+K]⁺.

[*N,N'*-Bis(4-fluorosalicylidene)-4'-fluoro-1,2-phenylenediamine]platinum(II)**[29-Pt]**

Was obtained from *N,N'*-bis(4-fluorosalicylidene)-4'-fluoro-1,2-phenylenediamine (**29**) (0.29 mmol, 108.0 mg) and potassium tetrachloroplatinate(II) (0.29 mmol, 121.1 mg).

Yield: 20.0 mg (0.03 mmol, 12%) red powder.

$C_{20}H_{11}F_3N_2O_2Pt$ (563.39)

1H -NMR (DMSO- d_6): δ = 6.70-6.85 (m, 2H, ArH-5); 6.86-7.01 (m, 2H, ArH-3); 7.45-7.55 (m, 1H, Ar'H-5); 7.89-8.01 (m, 2H, ArH-6); 8.35-8.43 (dd, $^3J=10.32$ Hz, $^4J=2.32$ Hz, 1H, Ar'H-3); 8.45-8.57 (dd, $^3J=9.20$ Hz, $^4J=5.19$ Hz, 1H, Ar'H-6); 9.47 (s, 1H, NCH); 9.52 (s, 1H, NCH).

MS (+)-ESI m/z calc.: 564.0499 [M+H]⁺; 586.0318 [M+Na]⁺; 602.0054 [M+K]⁺; 1165.0458 [2M+K]⁺.

MS (+)-ESI m/z obs.: 564.0525 [M+H]⁺; 586.0363 [M+Na]⁺; 602.0103 [M+K]⁺; 1165.0551 [2M+K]⁺.

[*N,N'*-Bis(5-fluorosalicylidene)-4'-fluoro-1,2-phenylenediamine]platinum(II)**[30-Pt]**

Was obtained from *N,N'*-bis(5-fluorosalicylidene)-4'-fluoro-1,2-phenylenediamine (**30**) (0.25 mmol, 93.0 mg) and potassium tetrachloroplatinate(II) (0.25 mmol, 104.0 mg).

Yield: 134.0 mg (0.24 mmol, 95%) dark red powder.

$C_{20}H_{11}F_3N_2O_2Pt$ (563.39)

1H -NMR (DMSO- d_6): δ = 7.10-7.17 (m, 2H, ArH-3); 7.44-7.66 (m, 5H, ArH-4, ArH-6, Ar'H-5); 8.27-8.34 (dd, $^3J=10.24$ Hz, $^4J=2.36$ Hz, 1H, Ar'H-3); 8.40-8.48 (dd, $^3J=9.32$ Hz, $^4J=5.15$ Hz, 1H, Ar'H-6); 9.45 (s, 1H, NCH); 9.50 (s, 1H, NCH).

MS (+)-ESI m/z calc.: 602.0054 [M+K]⁺; 1165.0458 [2M+K]⁺.

MS (+)-ESI m/z obs.: 602.0058 [M+K]⁺; 1165.0490 [2M+K]⁺.

[*N,N'*-Bis(6-fluorosalicylidene)-4'-fluoro-1,2-phenylenediamine]platinum(II)**[31-Pt]**

Was obtained from *N,N'*-bis(6-fluorosalicylidene)-4'-fluoro-1,2-phenylenediamine (**31**) (0.29 mmol, 108.0 mg) and potassium tetrachloroplatinate(II) (0.29 mmol, 121.1 mg).

Yield: 96.0 mg (0.04 mmol, 19%) dark violet powder.

$C_{20}H_{11}F_3N_2O_2Pt$ (563.39)

1H -NMR (DMSO- d_6): δ = 6.59-6.68 (m, 2H, ArH-5); 6.93-7.00 (d, $^3J=8.74$ Hz, 2H, ArH-3); 7.37-7.47 (m, 1H, Ar'H-5); 7.48-7.61 (m, 2H, ArH-4); 8.43-8.48 (dd, $^3J=10.34$ Hz,

$^4J=2.36$ Hz, 1H, Ar'H-3); 8.49-8.55 (dd, $^3J=9.32$ Hz, $^4J=5.16$ Hz, 1H, Ar'H-6); 9.38 (s, 1H, NCH); 9.44 (s, 1H, NCH).

MS (+)-ESI m/z calc.: 602.0054 [M+K]⁺.

MS (+)-ESI m/z obs.: 602.0031 [M+K]⁺.

[N,N'-Bis(salicylidene)-4'-methyl-1,2-phenylenediamine]platinum(II) [32-Pt]

Was obtained from *N,N'*-bis(salicylidene)-4'-methoxy-1,2-phenylenediamine (**32**) (0.46 mmol, 153 mg) and potassium tetrachloroplatinate(II) (0.46 mmol, 192 mg). Yield: 177 mg (0.34 mmol, 73%) red powder.

C₂₁H₁₆N₂O₂Pt (523.44)

¹H-NMR (DMSO-*d*₆): δ = 2.48 (s, 3H, CH₃); 6.76-6.83 (m, 2H, ArH-5); 7.08-7.14 (m, 2H, ArH-3); 7.29-7.34 (m, 1H, Ar'H-5); 7.53-7.62 (m, 2H, ArH-4); 7.83-7.90 (m, 2H, ArH-6); 8.28-8.36 (m, 3H, Ar'H-3, Ar'H-6); 9.47 (s, 1H, NCH); 9.51 (s, 1H, NCH).

MS (+)-ESI m/z calc.: 524.0938 [M+H]⁺; 546.0757 [M+Na]⁺; 562.0497 [M+K]⁺; 1069.1597 [2M+Na]⁺.

MS (+)-ESI m/z obs.: 524.0946 [M+H]⁺; 546.0766 [M+Na]⁺; 562.0511 [M+K]⁺; 1069.1607 [2M+Na]⁺.

[N,N'-Bis(salicylidene)-rac-trans-1,2-cyclohexanediamine]platinum(II) [33-Pt]

Was obtained from *N,N'*-bis(salicylidene)-1,2-cyclohexanediamine (**33**) (0.14 mmol, 45.0 mg) and potassium tetrachloroplatinate(II) (0.14 mmol, 58.1 mg).

Yield: 40.0 mg (0.08 mmol, 55%) yellow powder.

C₂₀H₂₀N₂O₂Pt (515.46)

¹H-NMR (DMF-*d*₇): δ = 1.20-1.29 (m, 4H); 1.39-1.48 (m, 4H); 3.94-4.04 (m, 2H); 6.59-6.66 (t, $^3J=7.31$ Hz, 2H, ArH-5); 6.88-6.94 (d, $^3J=8.47$ Hz, 2H, ArH-3); 7.40-7.48 (m, 2H, ArH-4); 7.55-7.61 (dd, $^3J=7.86$ Hz, $^4J=1.29$ Hz, 2H, ArH-6); 8.51 (s, 2H, NCH).

MS (+)-ESI m/z calc.: 516.1251 [M+H]⁺; 538.1070 [M+Na]⁺; 554.0810 [M+K]⁺; 1053.2243 [2M+Na]⁺; 1069.1982 [2M+K]⁺.

MS (+)-ESI m/z obs.: 516.1267 [M+H]⁺; 538.1099 [M+Na]⁺; 554.0837 [M+K]⁺; 1053.2281 [2M+Na]⁺; 1069.2018 [2M+K]⁺.

11.2 GF-AAS method

- Instrument: Vario 6 graphite furnace atomic absorption spectrometer
- Company: Analytik Jena AG
- Detection wavelength: 265.9 nm
- Slit width: 0.2 nm
- Background correction: deuterium lamp
- Injection volume: 20 μ L
- GF-AAS temperature program: see Table 11.1

Table 11.1 GF-AAS temperature program for the platinum complexes.

Step	Temp. ($^{\circ}$ C)	Ramp ($^{\circ}$ C/sec.)	Hold (sec.)	Function
1	90	5	20	Drying
2	105	5	20	Drying
3	120	5	10	Drying
4	500	45	20	Pyrolysis
5	1600	250	10	Pyrolysis
6	1600	0	5	
7	2400	1500	4	Atomize
8	2400	500	4	Cleanout

As previously explained in section 3.3, each compound was measured against its own calibration curve, therefore calibration standards were prepared by making serial dilutions from analyte stock solutions in DMF. The number (5 up to 7) and range of calibration points depended on the expected platinum concentration in the samples. Generally, the chosen concentrations were 0.000, 10.000, 25.000, 50.000, 100.000, 200.000, 300.000 and 400.000 μ g/L. Working standard solution were prepared before use with 25 μ L of the concentrated standard solutions, stabilized with 100 μ L Triton X-100 (1%) and 25 μ L of HCl (18%). Each Pt measurement was based on two sequential determinations.

11.3 Cell culture tests

11.3.1 Cell lines and growth conditions

MCF-7 and MDA-MB-231 cells were cultivated as a monolayer culture at 37 °C in a humidified atmosphere (95% air, 5% CO₂) in 25 cm² culture flasks using DMEM supplemented with FCS 5% (V/V) as growth medium. Cell seeding and manipulation was carried out in a sterile laminar flow hood. Medium change was done every few days depending on growth curve of the cells. Passage into a new flask was performed at approximately 70-90% confluency. At this moment, the old medium was removed and the cells were washed with PBS. Trypsin solution was added to detach the cells. After correct distribution of the solution over the surface of the flask it was removed, and the flask was incorporated into the incubator for 2 min. Finally the cells were resuspended in fresh medium and an appropriate aliquot volume of cell suspension (approximately 1/10 dilution) was incorporated into new flasks with fresh medium.

MCF-7

The passage of the cells was carried out once a week, and no medium change was needed.

MDA-MB-231

The passage of the cells was carried out once a week, and medium was changed after 3-4 days of incubation.

11.3.2 *In-vitro* chemosensitivity assays

The *in-vitro* testing of the compounds was carried out on exponentially dividing cancer cells according to a previous published microtiter assay^{97,98}. Exponential cell growth was ensured during the whole time of incubation.

Cell seeding

100 µL of a cell suspension were placed in each well of a 96-well microtiter plate at 7.500 cells/mL of culture medium, after determining the cell concentration in the initial cell suspension using a counting chamber. The plates were incubated at 37 °C in a humidified atmosphere for 3 days.

Addition of the substances

The substances were dissolved in DMF to afford 10 mM stock solutions and then diluted to the chosen concentrations. 10 μL of the metal complex solution or DMF were added to 5 mL of the growth medium. Finally, 100 μL of drug-containing medium were incorporated to the 96-well microtiter plate to achieve the final test concentrations. Four wells were used for each test concentration and for the control which contained the corresponding amount of DMF. Cisplatin was used in each test as a positive control. One extra plate on each test was seeded to determine the initial cell density (t_0 plate).

- “Two-concentrations” assay

Substances were tested initially in the two higher concentrations (20 and 10 μM). Only substances which present a T/C_{corr} value $< 50\%$ at 20 μM (and lower concentration) were tested in further cytotoxicity measurements. The substances were added following the scheme shown in Fig. 11.1. Up to 18 substances (two plates) were tested together in one assay.

DMF	0.1%	DMF	0.1%	substance 4	10
	0.31		0.2%		20
	0.63	substance 1	10	substance 5	10
	1.25		20		20
cisplatin	2.5	substance 2	10	substance 6	10
	5		20		20
	10	substance 3	10	substance 7	10
	20		20		20

Figure 11.1 Pipetting scheme of the 96-wells microtiter plate in the “two-concentrations” test. Concentrations are given in μM .

- IC_{50} determination

To determine the IC_{50} values, solutions of each compound were preparing by diluting the stock solutions. Each compound (which demonstrated T/C_{corr} value $< 50\%$ in the “two-concentrations” determination) was initially tested at five different concentrations, which were added following the scheme in Fig. 11.2. Up to 11 substances (3 plates) were tested together in one assay. In the particular case, that the initial tested concentrations produced strong tumour growth inhibition, even at the lowest concentrations, the test was repeated with less concentrated solutions.

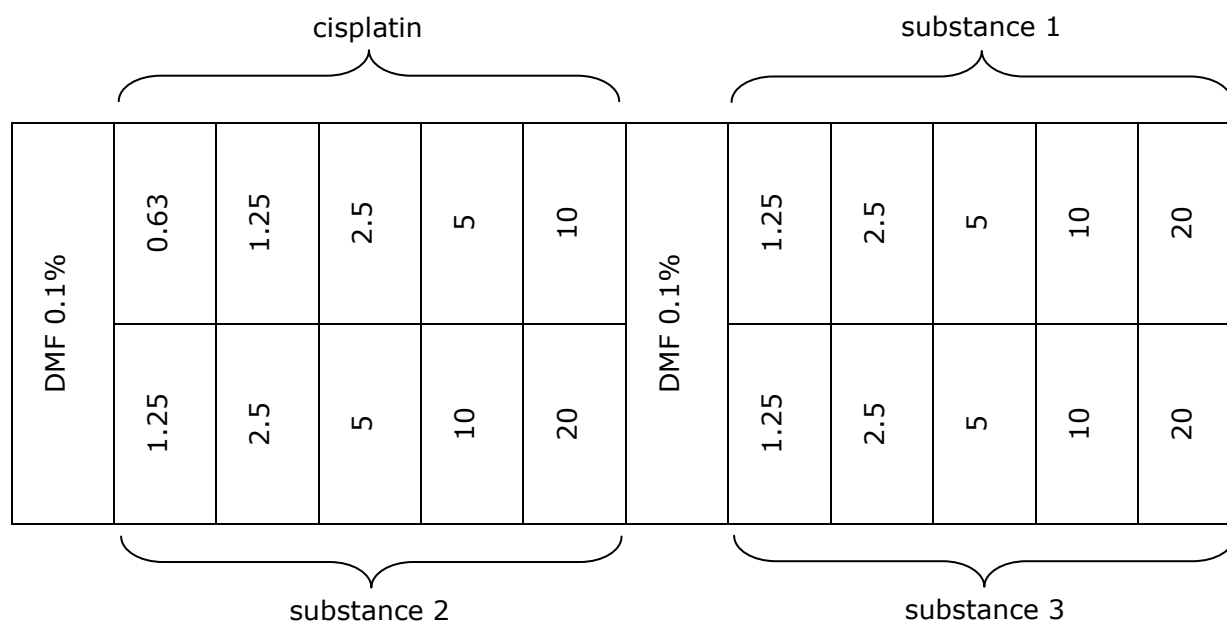


Figure 11.2 Pipetting scheme of the 96-wells microtiter plate in the “IC₅₀ determination” test. Concentrations are given in μM .

- Time- and concentration-dependent cytotoxicity

In this case, the same concentrations and pipetting scheme as in the IC₅₀ determination test was used. The main difference is that each substance was added (with the same concentration pattern) in five different plates, in order to fix the cells at five different times. Up to 11 substances (15 plates) were tested together in one assay.

Cell fixation

After the appropriated incubation time had been reached, the medium was removed and the cells were fixed with 100 μL of glutaraldehyde solution. After 20-30 min of incubation, the solution was shaken off and 180 μL of PBS was added. The plates were stored at 4 $^{\circ}\text{C}$ until staining.

The incubation time in the case of the “two-concentrations” and IC₅₀ determination assay was 96 h. To analyze the time- and concentration-dependent cytotoxicity of the compounds, fixation of the cells was carried out after 48, 72, 96, 120 and 144 h of incubation.

Cell staining and absorption measurement

Cell biomass was determined by means of a crystal violet staining technique^{97,98}. At the end of the experiment, all plates were stained simultaneously with 0.02% aqueous crystal violet solution (100 μL /well) for 30 min. Excess dye was removed by rinsing the

plates with water for 15 min. The stain bound by the cells was redissolved in 70% ethanol (180 μ L/well), while shaking the microplates for 2-4 h. For automatic estimation of the optical density of the crystal violet extract, the absorption at 590 nm was measured using a microplate autoreader.

Calculation of the cytotoxic activity of the complexes

The activity is expressed as corrected T/C_{corr} (%) or τ (%) value according to Eq. 5.1 and 5.2 respectively (see Section 5.2).

11.3.3 Accumulation studies on MCF-7 cells

Cell cultivation and addition of the substances

Cells were cultivated as a monolayer culture at 37 °C in a humidified atmosphere (95% air, 5% CO₂) in 75 cm² culture flasks using DMEM supplemented with FCS 5% (V/V) as growth medium until at least 70% confluency. The substances were prepared as 0.3 mM and 0.15 mM in DMF and then diluted 1:1000 with the cell growth medium. The medium was removed and replaced by 10 mL of drug-containing and FCS-free medium (concentration of drug: 0.3 μ M or 0.15 μ M)

Cell fixation and harvesting

After exposure to drug for 0, 1, 2, 4, 6, 10 or 24 h, the drug-containing medium was removed and the cell monolayer was washed with 5 mL of PBS. The cells were subsequently treated with trypsin (3 mL), resuspended in 10 mL medium and washed twice with PBS. Finally, they were centrifuged (2000 *g*, 4 °C, 5 min) and stored at -18 °C until analysis.

Preparation of the samples for the platinum and protein determination

The cell pellets were homogenized by sonication in 150 μ L Triton X-100 solution (1%) and were adequately diluted for the protein determination and for the platinum analysis (GF-AAS).

Determination of protein concentration

The protein quantification was performed by the Bradford method¹¹⁰. It involves the binding of the dye Coomassie Brilliant Blue G-250 to protein. Three forms of the dye are present in equilibrium at the usual acidic pH of the assay. The red, blue, and green forms have absorbance maxima at 470, 590, and 650 nm respectively¹⁵⁷. The blue is the form that binds the protein, forming a complex that intensely absorbs light at 594 nm¹⁵⁸.

Therefore, it is possible to estimate the concentration of protein directly by measuring the increase in absorbance at 590 nm caused by the presence of the protein. However, as Zor *et al.* showed in 1996 that the accuracy and sensitivity of the assay can be improved about 10-fold by measuring the A_{590}/A_{450} ratio¹⁵⁹, absorbance at both wavelengths was determined and related to the protein content.

The Bradford method is a widely used assay because of its simplicity, ease of performance, rapidity, reproducibility and relative sensitivity (it is possible the quantification of microgram quantities of protein). Another important advantage is that unlike other method, it is less susceptible to interferences by common laboratory reagents, which may be present in the protein samples. The only components that give excessive interfering colour are detergents such as sodium dodecyl sulphate (SDS) or Triton X-100¹¹⁰.

Bradford protein assay procedure

The Bradford reagent (see section 9.1.2) was prepared by diluting 1 volume of the dye stock with 4 volumes of distilled H₂O (1:5). The protein standards were prepared using HSA in distilled H₂O. The chosen concentrations were 0.000, 0.025, 0.050, 0.075, 0.100, 0.125, 0.150 and 0.175 µg/mL. As the protein samples were resuspended in Triton X-100 (1%), which is a known interfering substance, it was added in the same amount to the protein standards and to the protein solutions.

The cell pellets, previously resuspended in 150 µL in Triton X-100 (1%), were diluted 1:80 or 1:100 in distilled H₂O.

200 µL of the diluted Bradford reagent were placed in each well of a 96-well microtiter plate. 20 µL of either the protein standard solutions or cell sample solutions were added into the wells containing Bradford reagent, and the content of each well was gently mixed using pipette-mixing. Three wells were used for each standard or sample. Finally, the absorbance at 450 and 590 nm was recorded in a microplate autoreader and the calibration curve was constructed, as exemplified in Fig. 11.3.

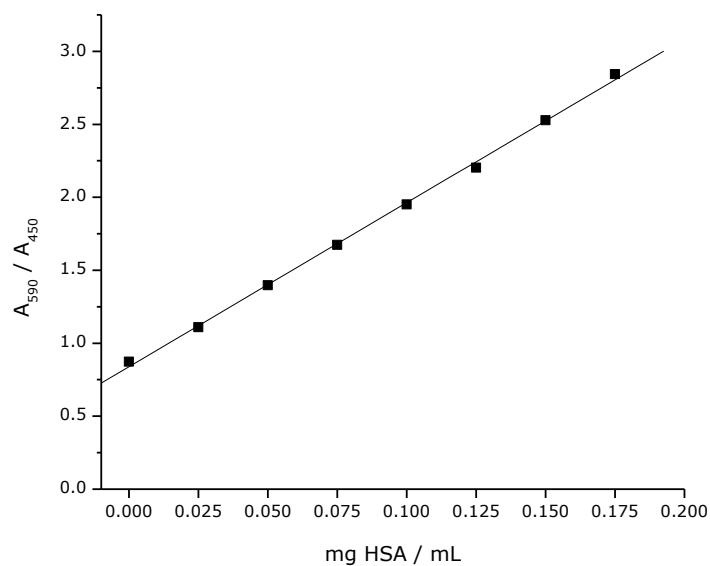


Figure 11.3 Representative standard curve of the relation between the A_{590}/A_{450} ratio and the HSA concentration. Each point represents the mean of each HSA standard, added in triplicate. Values were fitted using the linear regression model ($R^2 = 0.9986$).

The protein concentration in the sample dilutions were predicted by interpolation of their A_{590}/A_{450} ratio on the respective calibration regression curve. Finally, the initial protein concentration was calculated multiplying the interpolated value by the dilution factor (1:80 or 1:100).

Determination of platinum concentration

To 100 μL of the cell suspension, 25 μL HCl (18%) and 25 μL DMF were added for the GF-AAS platinum analysis. The calibration curve and the measurement procedure are described in Section 11.2

Calculation of cellular uptake

The cellular platinum content was calculated as pmol Pt per μg cellular protein. Furthermore, it was possible to estimate the intracellular platinum concentration using the protein-volume relation (1.0 ng cellular protein corresponds to a cellular volume of 8.85 (MCF-7) pL), described by Eq. 6.1 in Section 6.2. Dividing the intracellular concentration of the drug by the concentration in the extracellular medium, the accumulation grade was obtained. Results were expressed as means from two independent experiments.

11.3.4 Drug efflux studies

In order to characterize the efflux of platinum, MCF-7 cells were cultivated as described in Section 11.3.3. Approximately at 70% confluency, cells incubated with 0.3 μM platinum complexes for 2 h. A part of the cells was collected as described above. The other part of the cells was washed twice with 5 mL PBS and incubated for 10, 20, 40, 60 and 120 min with drug-free medium. Afterwards, the cells were collected and analyzed for their protein and platinum concentration as previously described (see Section 11.3.3).

11.4 DNA binding studies

11.4.1 Circular dichroism spectroscopy

CD-spectra were recorded with a JASCO J-715 instrument in the range 220–400 nm for 1:10 complex/DNA mixtures [complex = 20 μM , DNA concentration in M (based on nucleotide number) = 200 μM] in a 10 mM phosphate buffer at pH 7.2 with CT-DNA at 25 $^{\circ}\text{C}$ after an incubation time of 24 h. About 1% DMF was added to ensure solubility of all substances.

11.4.2 Thermal denaturation studies

The thermal denaturation temperatures T_m of 1:10 complex/DNA mixtures 1:10 complex/DNA mixtures [complex = 20 μM , DNA concentration in M (based on nucleotide number) = 200 μM] in a 10 mM phosphate buffer at pH 7.2. DMF (1%) was added to ensure solubility of all substances. Melting curves were recorded in 2 $^{\circ}\text{C}$ steps in the range 50–85 $^{\circ}\text{C}$ at 260 nm with an SPECORD 200 spectrometer connected to a Peltier temperature controller. T_m values were calculated by determining the midpoints of melting curves from the first-order derivatives. The experimental ΔT_m values in Table 6.1 are estimated to be accurate to within ± 1 $^{\circ}\text{C}$. The concentrations of CT-DNA were determined spectrophotometrically using the molar extinction coefficient $\epsilon_{260} = 6.600 \text{ M}^{-1} \text{ cm}^{-1}$ ¹⁶⁰.

11.4.3 Viscosity measurements

Viscosities for complex/sonicated DNA mixtures were determined using a Cannon-Ubbelohde Semi-micro dilution viscometer held at a constant temperature of 25 $^{\circ}\text{C}$ in a

water bath. Reduced viscosities η were calculated by literature methods¹⁴⁷ and plotted as $(\eta/\eta_0)^{1/3}$ (η_0 = reduced viscosity of the DNA solution in the absence of complex) against r { $r = [\text{complex}]/[\text{DNA}]$ where [DNA] is given in M (base pairs)}.

11.4.4 Atomic absorption studies

Precipitation of drug DNA adducts was performed according to a described method¹⁶¹ with some modifications: salmon testes DNA was dissolved in phosphate-buffered saline pH 7.4 and drugs were added as stock solutions in DMF. The final solutions contained 40 μM drug and 250 $\mu\text{g/mL}$ salmon testes DNA. After vortexing, the solutions were incubated at 37 °C in a water bath for 4 h. Aliquots of 200 μL were mixed with 100 μL of 0.9 M sodium acetate and three volumes of ice cold ethanol. Samples were stored at -20 °C for 30 min. The pellets were isolated by centrifugation (5000 U/min, 10 min, 4 °C) and resuspended in 300 μL of 0.3 M sodium acetate. 900 μL of ice cold ethanol were added, and the precipitate was collected after centrifugation (5000 U/min, 10 min, 4 °C). Samples were washed twice with ice cold ethanol and were stored at -20 °C. The pellets were dissolved in 500 μL of water (twice distilled), and the DNA content was determined by absorption reading at 260 nm in a UV-microplate reader. Salmon testes DNA dissolved in water (twice distilled) was used for calibration purposes. The chosen concentrations were 0, 20, 50, 75, 100 and 200 $\mu\text{g/mL}$. Samples (25 μL) for GF-AAS platinum determination were stabilized by 25 μL of Triton X-100 (4%), followed by addition of 25 μL HCl (18%), 25 μL DMF and 50 μL H₂O (twice distilled). The amount of drug bound to DNA was expressed as pmol of drug per μg of DNA and as amount of nucleoside per bound compound (nucleoside/compound). Results were expressed as means from at least two independent experiments.

11.5 HPLC-Lipophilicity

- Instrument: 1100 series
- Company: Agilent/Hewlett-Packard (California, USA)
- Detector: diode array Detector (DAD)
- Stationary phase: Eurospher 100-5 C18, 250 x 4 mm.
- Mobile phase: complexes, Methanol:H₂O (70/30); ligands, Methanol:H₂O (60/40).
- Injection volume: 5 μL
- Flow rate: 0.800 mL/min

Six chemicals for which $\log P$ has been reported, were used to calibrate the elution time in units of $\log P$. In order to determine the lipophilicity of the [salophene]platinum(II) complexes the selected calibration standards included benzene, naphthalene, biphenyl, anthracene, n-hexylbenzene and n-octylbenzene. Since the ligands are less lipophilic than the complexes the selected calibration substances were benzamide, acetanilide, acetophenone, benzene, naphthalene and biphenyl. The $\log P$ values were obtained from J. Sangster¹²⁰. As only the retention time, which is independent of concentration in dilute solutions, was used in this method, the quantity of individual chemicals in the solution was adjusted to give easily detectable chromatographic peaks. Therefore, to determine the calibration line, the standards were dissolved together and in different concentrations in ethanol HPLC grade and introduced into the HPLC system at the beginning and end of each run. To determine the calibration regression curve, $\log P$ values were plotted against the average $\log k$ values, and the data were fitted using a linear regression.

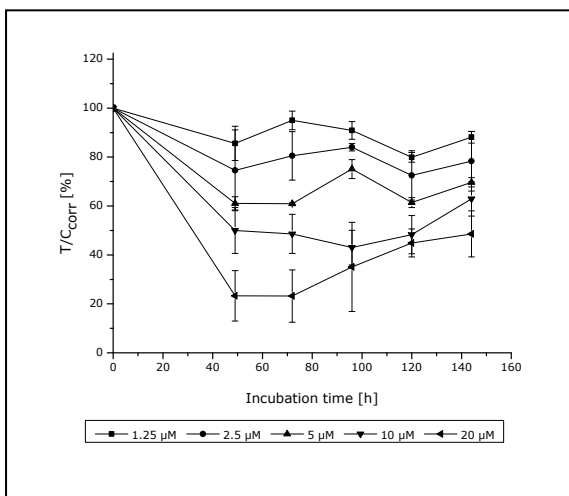
Platinum complexes and ligands were prepared as 1 mM stock solutions in DMF. 30 μL were diluted in 1.470 mL H_2O (twice distilled) and chromatographed individually. Their $\log P$ values were obtained by interpolation of their $\log k$ on the respective calibration regression curve. Results were expressed as means from at least two independent experiments.

11.6 Solubility

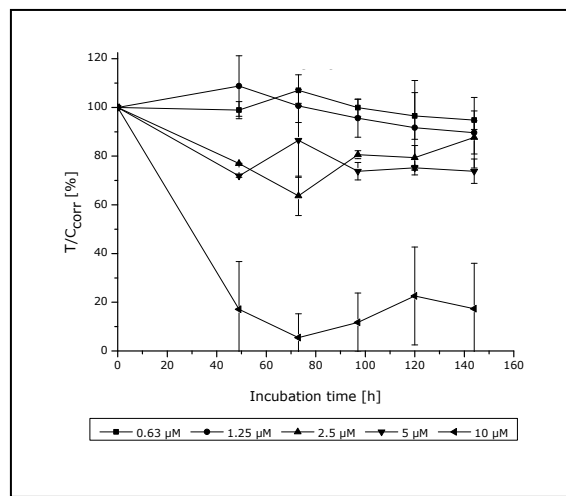
10 μL of a 10 mM platinum complex stock solution were added to 990 μL of culture media at 37 °C. The samples were shaken and placed into an ultrasonic bath for 30 min. After the sonication the samples were centrifugated at 20.000 g and 37 °C for 30 min. Samples (25 μL) for GF-AAS platinum determination were stabilized by 25 μL of Triton X-100 (4%), followed by addition of 25 μL HCl (18%), 25 μL DMF and 50 μL H_2O (twice distilled). Results were expressed as means from at least two independent experiments.

Appendix

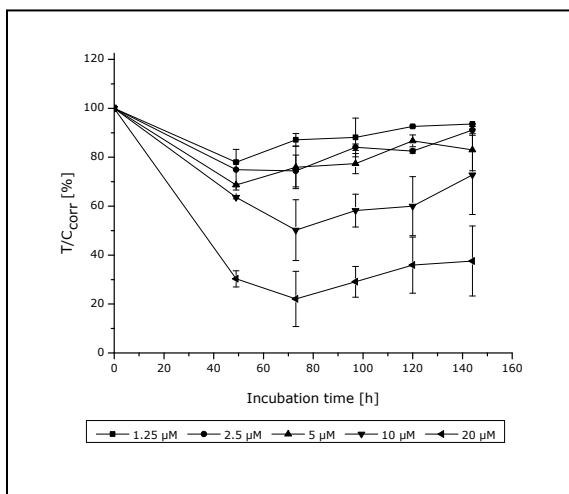
A. Time- and concentration-dependent cytotoxicity diagrams



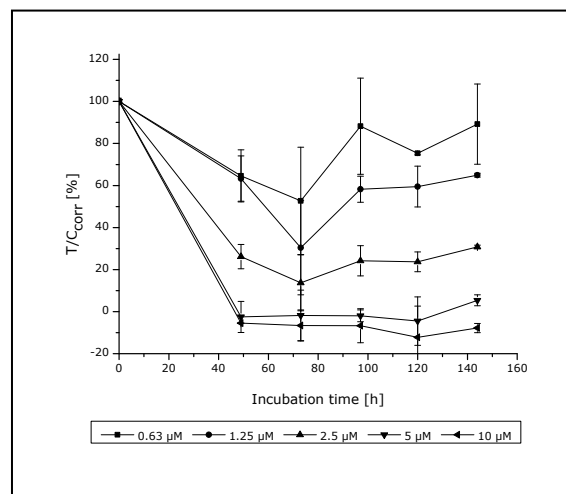
1-Pt



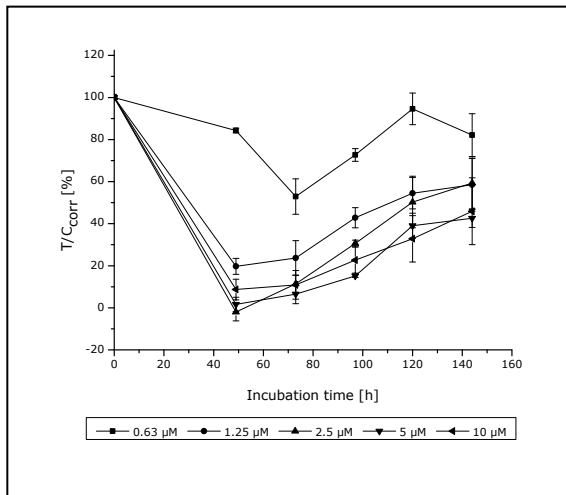
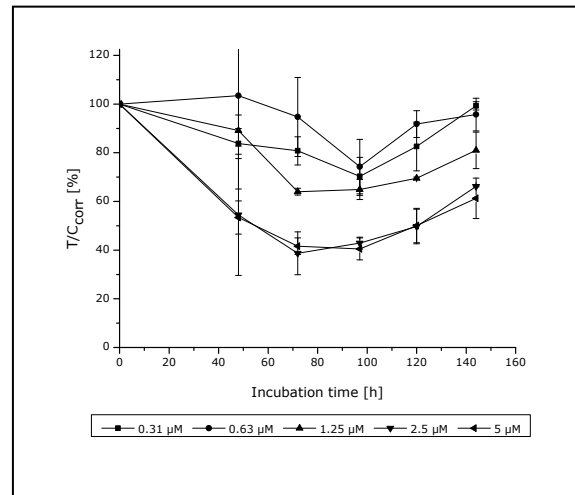
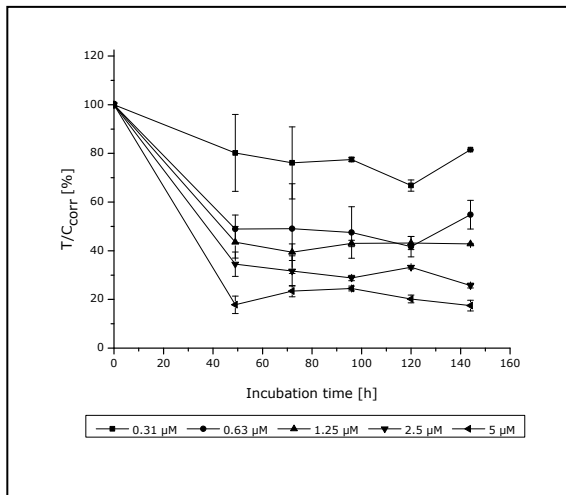
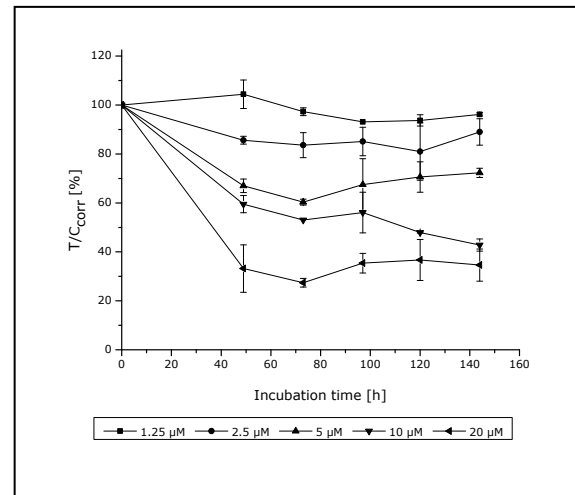
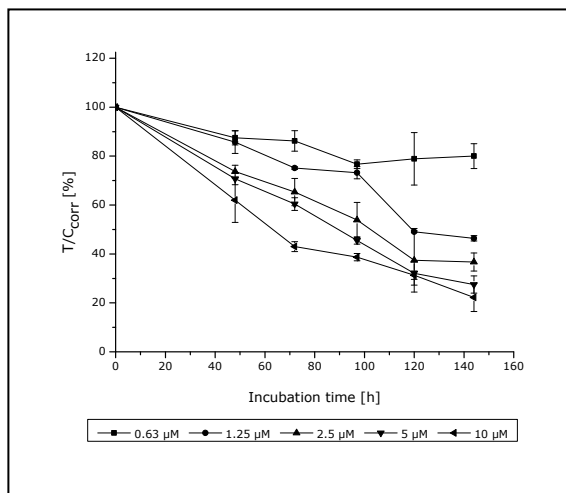
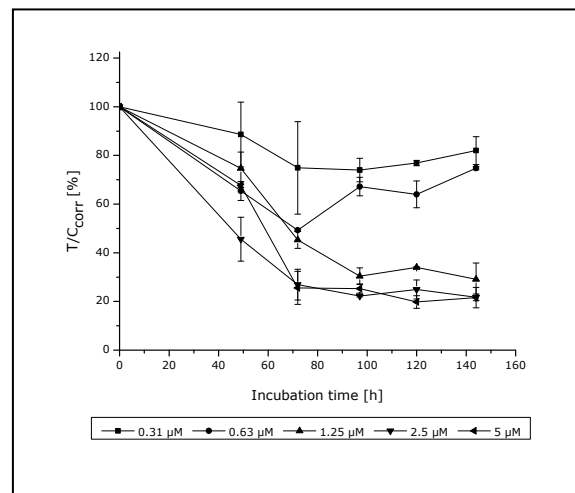
9-Pt

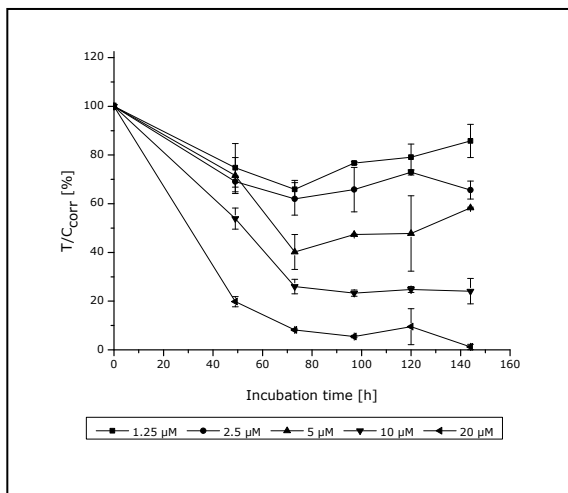


10-Pt

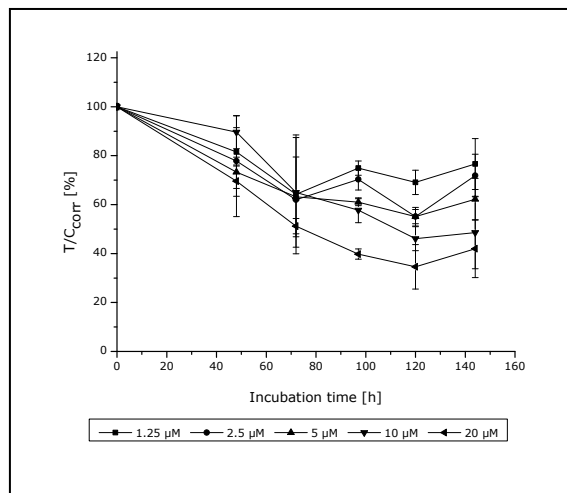


11-Pt

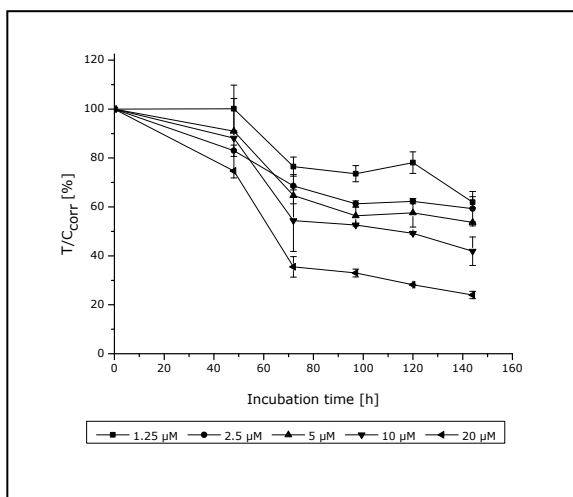
**13-Pt****15-Pt****18-Pt****20-Pt****22-Pt****23-Pt**



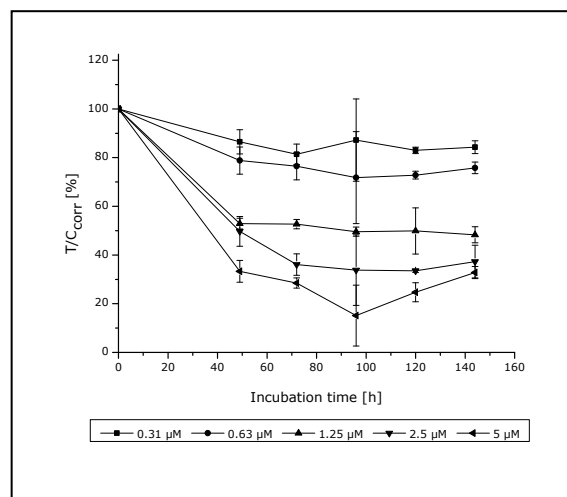
24-Pt



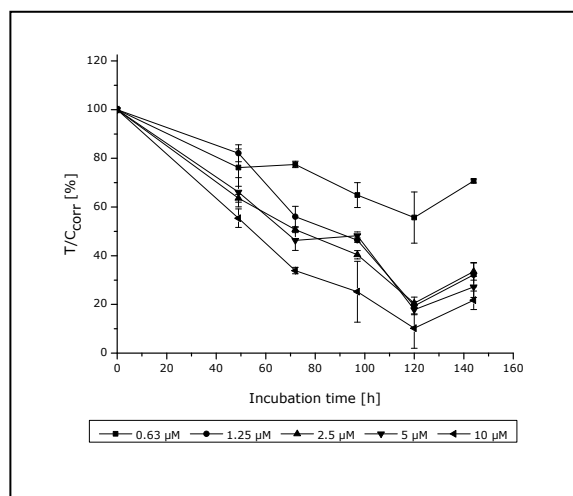
25-Pt



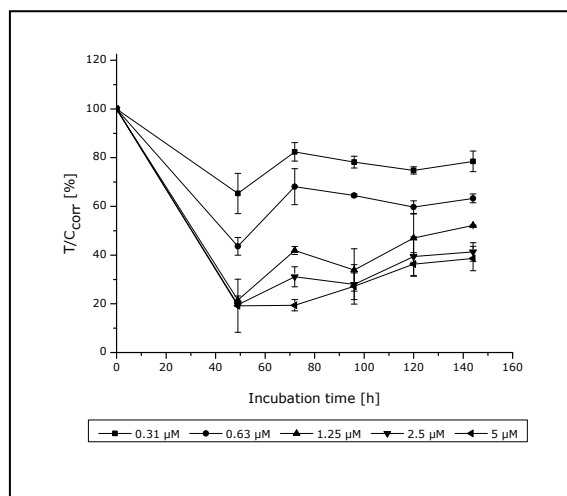
26-Pt



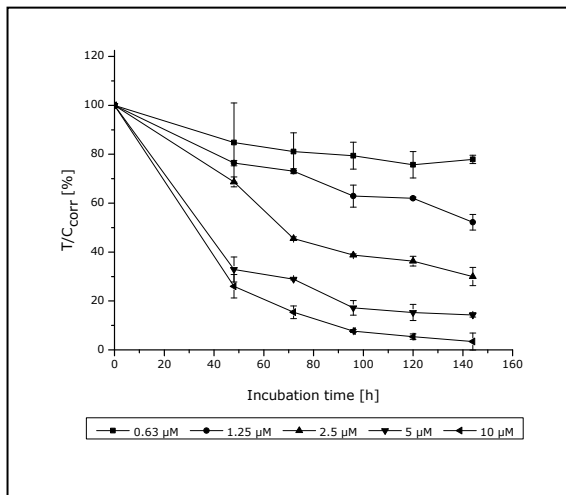
27-Pt



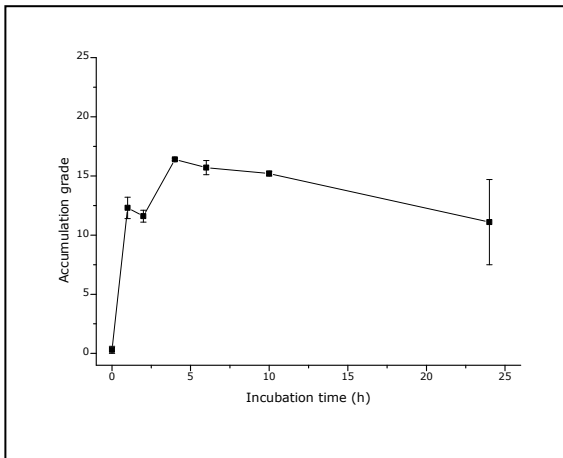
31-Pt



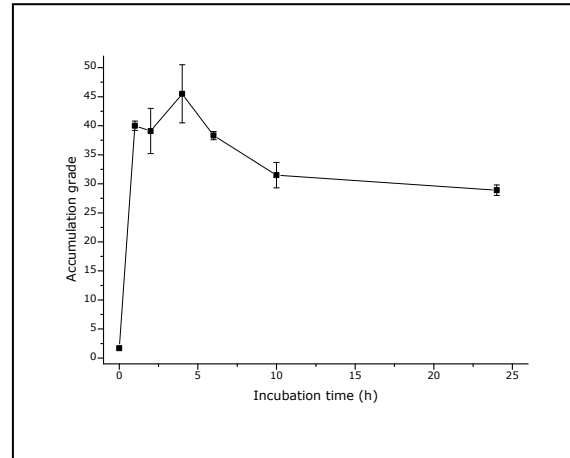
32-Pt

**Cisplatin**

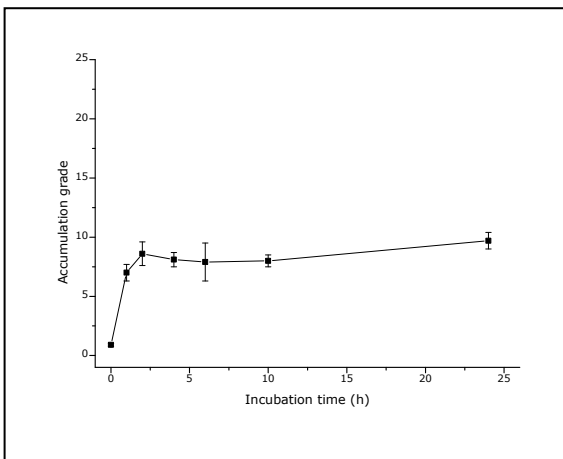
B. Time-dependent cellular accumulation diagrams



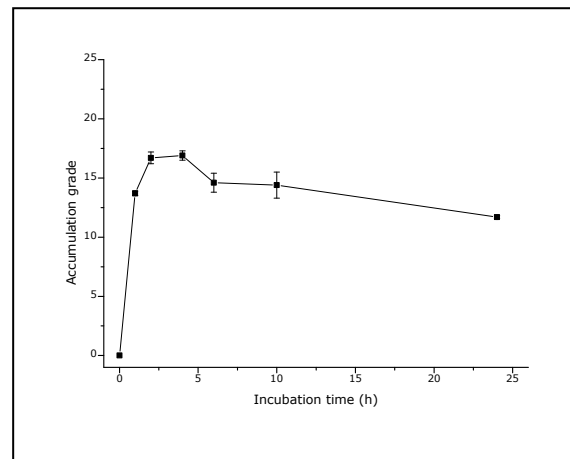
13-Pt



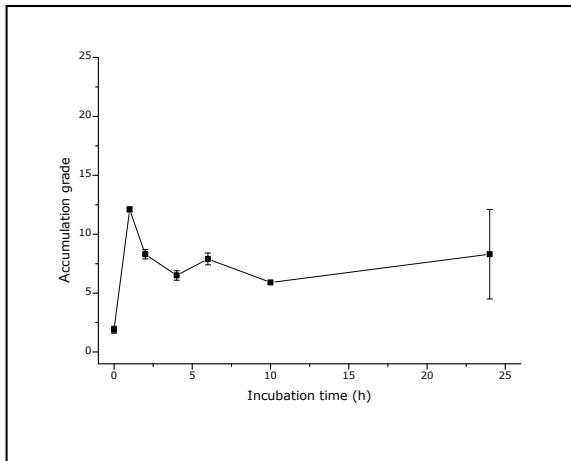
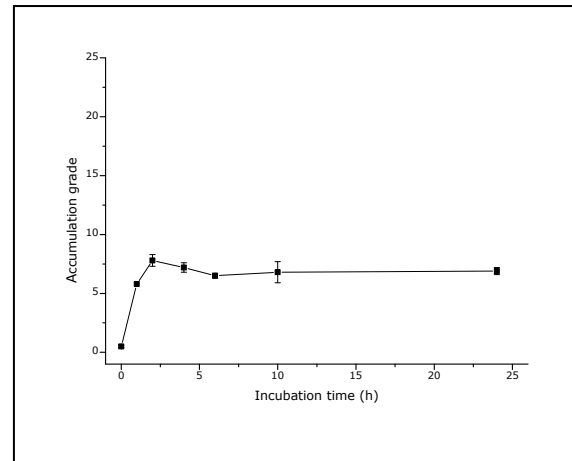
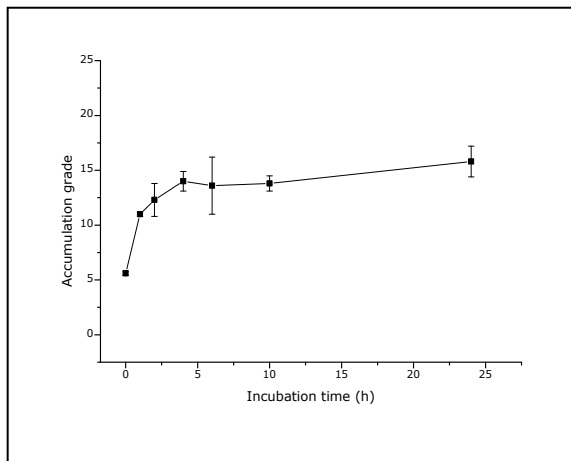
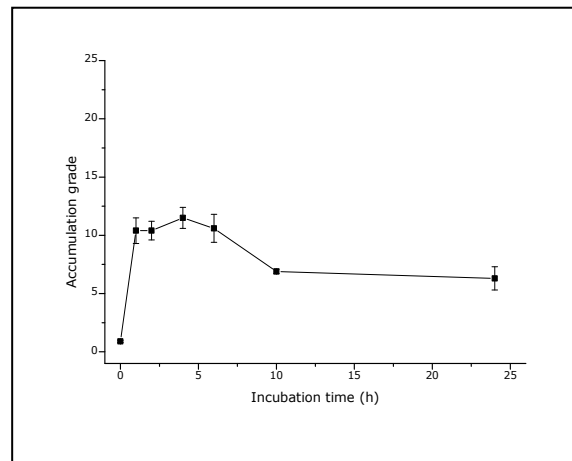
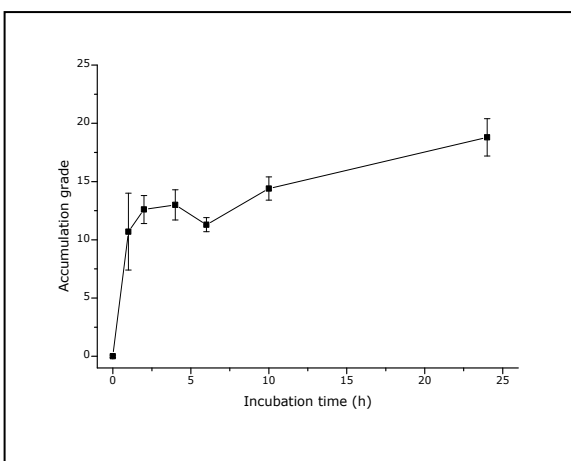
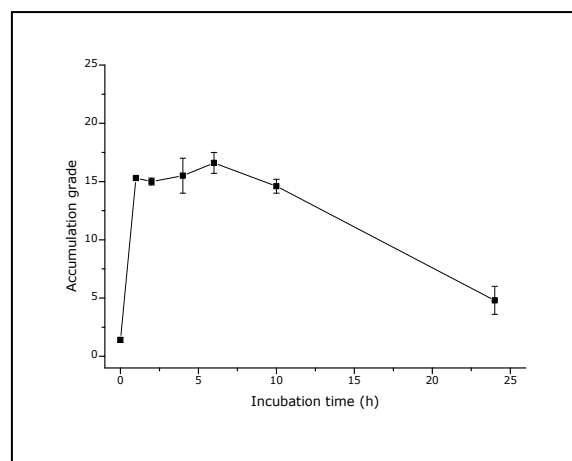
15-Pt

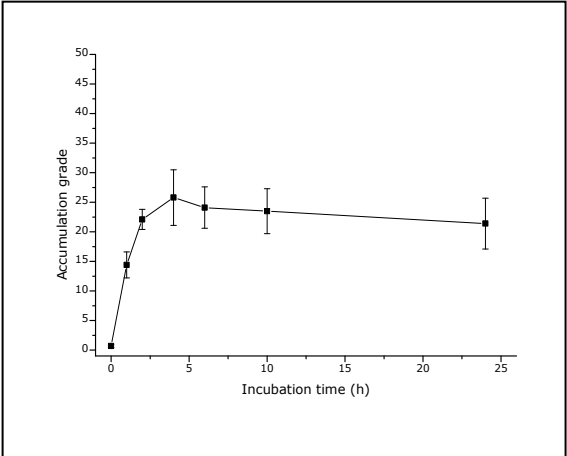


18-Pt

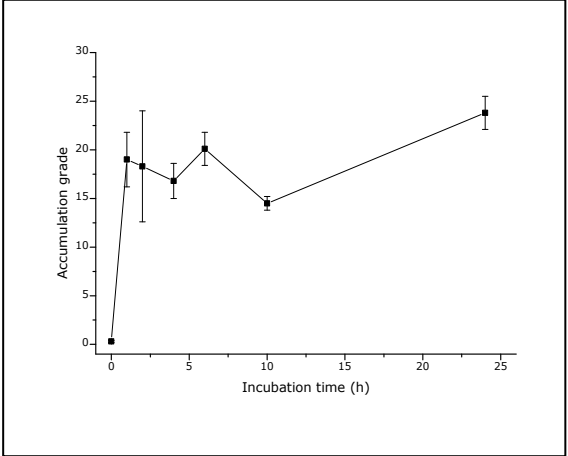


20-Pt

**22-Pt****23-Pt****24-Pt****25-Pt****26-Pt****27-Pt**

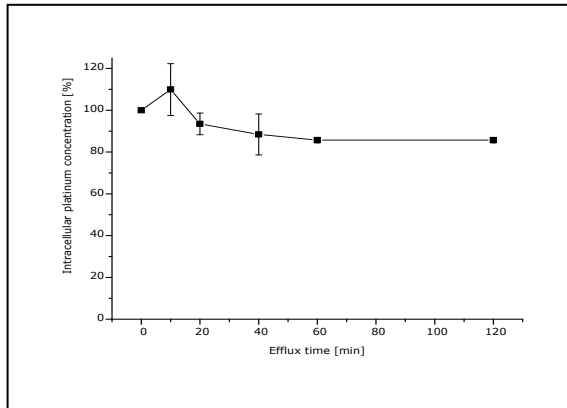
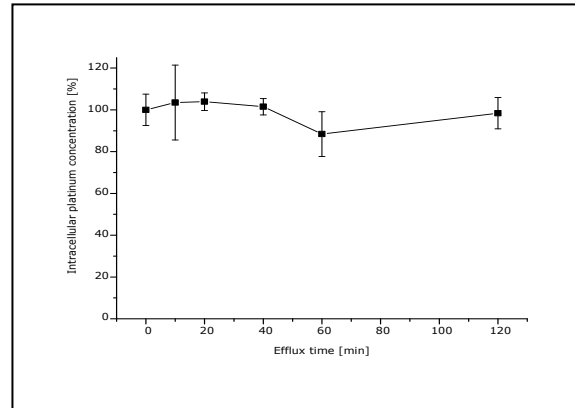
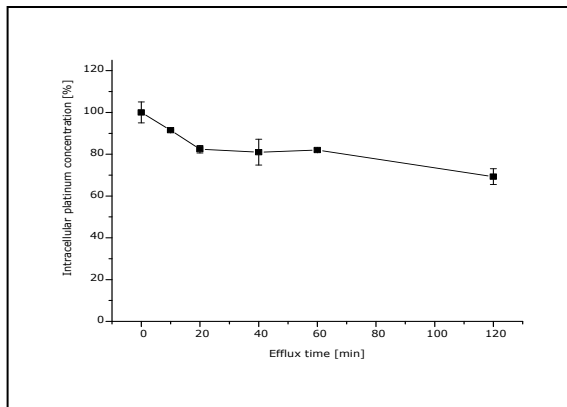
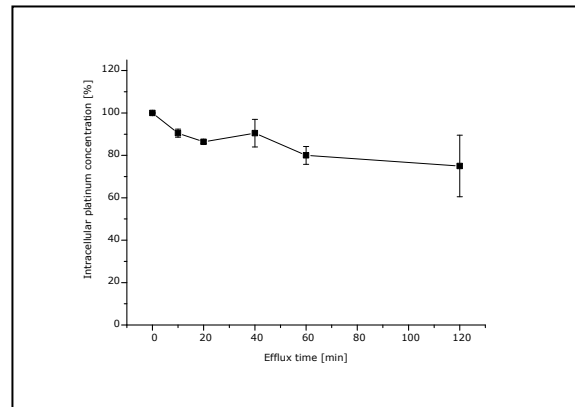
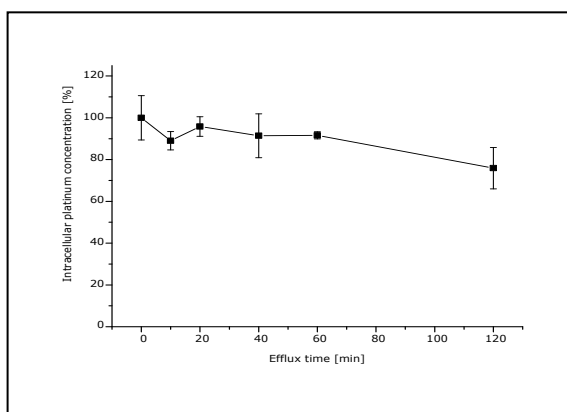


31-Pt



32-Pt

C. Efflux diagrams

**13-Pt****15-Pt****18-Pt****20-Pt****22-Pt**

D. Summary

This thesis presents the synthesis and characterization of antitumour active platinum(II) complexes as well as their physicochemical and biological properties under *in-vitro* conditions.

Two compounds, [*meso*-3,4-bis(4-fluorophenyl)-1,6-bis(2-hydroxyphenyl)-2,5-diaza-hexa-1,5-diene]platinum(II) and [*N,N'*-bis(salicylidene)-1,2-phenylenediamine]platinum(II), were chosen as lead substances for the design of [diarylsalene]- and [salophene]platinum(II) derivatives (see Fig. D.1). Ligands with structural differences or bearing different substitutions patterns were prepared in order to investigate the influence of the ligand structure on the antitumour activity.

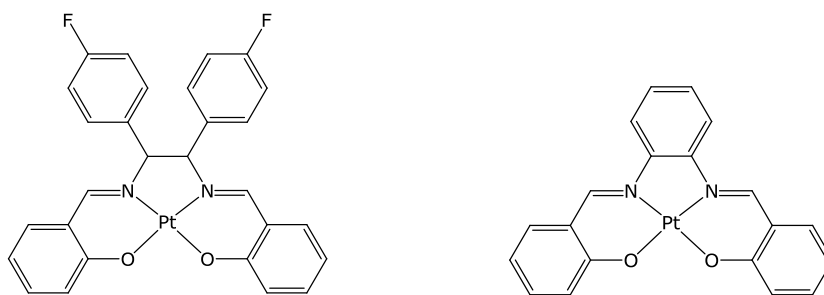


Figure D.1 Structure of the lead compounds of the [diarylsalene]- (left) and [salophene]platinum(II) (right) series.

The cytotoxicity was evaluated mainly in MCF-7 human breast cancer cells and is presented as IC_{50} values. Moreover, active substances ($IC_{50} < 20 \mu\text{M}$) were tested for their cytotoxic activity in a time- and concentration-dependent manner. For compounds of both [diarylsalene]- and [salophene]platinum(II) series IC_{50} values in a wide concentrations range were calculated. Outstanding cytotoxic properties demonstrated some [salophene]platinum(II) derivatives, with IC_{50} values less than $1 \mu\text{M}$. Anyhow, neither for the diarylsalene nor for the salophene series a structure-activity relationship has been found. Concerning the [diarylsalene]platinum(II) series, results were in general not very promising since only one compound produced higher antiproliferative effects than the lead structure. Therefore, further investigations were carried out only with the [salophene]platinum(II) derivatives.

In an attempt to explain the differences in cytotoxicity between the [salophene]platinum(II) derivatives, their cellular accumulation was analyzed. All the

complexes were satisfactorily taken up into the tumour cells. Although a correlation between accumulation grade and cytotoxicity could not be precisely established, the intracellular drug concentration demonstrated to be strongly influenced by the nature and the position of the ligand substituents.

Physicochemical analysis included the determination of the lipophilicity and aqueous solubility of the compounds. The complexes generally presented rather high lipophilicity and low solubility. While the obtained solubility values showed only in a few cases a relationship with the analyzed biological properties, lipophilicity seems to be linearly correlated with IC_{50} and accumulation values. Considering that antitumour activity was not directly associated with the intracellular drug concentration, it is not possible to establish the expected direct relationship between drug lipophilicity, cellular accumulation and cytotoxic effect. This suggests that it would be interesting to investigate a possible direct influence of lipophilicity on the drug-target interaction.

Since DNA is a likely target for anticancer platinum-based coordination compounds, the [salophene]platinum(II) compounds were analyzed for their interactions with isolated DNA. Surprisingly, neither intercalation nor DNA binding demonstrated to be major mechanisms for the cytotoxic activity of the tested platinum complexes. This suggests that it is possible to exclude DNA as the main target of the [salophene]platinum(II) complexes. Non-genomic structures, such as proteins involved in apoptotic processes or proteins related to the homeostasis of the extracellular matrix, are proposed as possible targets.

Overall, this work provided a great number of novel platinum-based complexes, potentially active as anticancer agents. It is clear that substituents on the ligand scaffold can modulate the biological properties of the synthesized platinum(II) complexes. Understanding their antitumour mechanism of action and target still remains as an important challenge in order to generate functionalised complexes with optimized physicochemical and biological properties.

E. Zusammenfassung

Diese Arbeit stellt die Synthese und Charakterisierung von antitumor-aktiven Platin(II)-Komplexen sowie deren physikochemischen und biologischen Eigenschaften unter *in-vitro* Bedingungen vor.

Zwei Verbindungen, [*meso*-3,4-Bis(4-fluorphenyl)-1,6-bis(2-hydroxyphenyl)-2,5-diazahexa-1,5-dien]platin(II) und [*N,N'*-Bis(salicyliden)-1,2-phenylendiamin]platin(II), wurden jeweils als Leitsubstanzen für die [Diarylsalen]- und [Salophen]platin(II)-Derivate (siehe Abb. E.1) ausgewählt. Liganden mit strukturellen Unterschieden oder verschiedenen Substitutionsmustern wurden vorbereitet, um den Einfluss ihrer Struktur auf die Antitumor-Aktivität zu untersuchen.

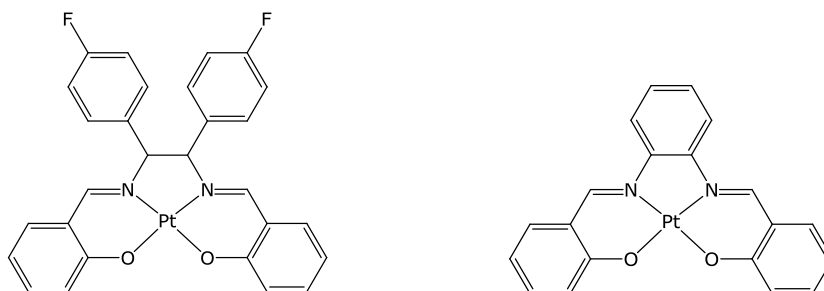


Abbildung E.1 Aufbau der Leitstrukturen der [Diarylsalen]- (links) und [Salophen]platin(II) (rechts) Derivate.

Die Zytotoxizität wurde vor allem in MCF-7 Brustkrebszellen ausgewertet und als IC_{50} -Werte präsentiert. Darüber hinaus wurden – in Abhängigkeit von Zeit und Konzentration – Wirkstoffe ($IC_{50} < 20 \mu M$) auf ihre zytotoxische Aktivität geprüft. In beiden Serien, der [Diarylsalen]- und der [Salophen]platin(II)-Serie, wurden Verbindungen mit IC_{50} -Werten in einem großen Konzentration-Bereich nachgewiesen. Besonders einige [Salophen]platin(II)-Derivate wiesen herausragende zytotoxische Eigenschaften auf, mit IC_{50} -Werten von weniger als $1 \mu M$. Es wurde jedoch weder für die Diarylsalen- noch für die Salophen-Serie eine Struktur-Wirkungs-Beziehung gefunden.

In Bezug auf die [Diarylsalen]platin(II)-Serie waren die Ergebnisse generell nicht sehr vielversprechend, da nur eine Verbindung eine signifikante Erhöhung der antiproliferativen Effekte im Vergleich zu der Leitstruktur bewirkte. Daher wurden weitere Untersuchungen nur mit den [Salophen]platin(II)-Derivaten durchgeführt.

Um die Unterschiede in der Zytotoxizität zwischen den [Salophen]platin(II)-Derivaten zu erklären, wurde ihre zelluläre Akkumulation analysiert. Alle Komplexe erwiesen sich

als in den Tumorzellen gut aufnehmbar. Obwohl eine Korrelation zwischen Akkumulations-Werten und Zytotoxizität nicht genau festgestellt werden konnte, wurde aufgezeigt, dass die intrazelluläre Wirkstoffkonzentration stark von der Natur und der Position der Liganden-Substituenten beeinflusst wird.

Mittels physikochemischer Analyse wurden Lipophilie und Wasserlöslichkeit der Verbindungen bestimmt. Die Komplexe wiesen grundsätzlich ziemlich hohe Lipophilie und eine geringe Löslichkeit auf. Während die Löslichkeitswerte nur in wenigen Fällen einen Zusammenhang mit den analysierten biologischen Eigenschaften zeigten, scheint Lipophilie linear mit IC_{50} und Akkumulation korreliert zu sein. In Anbetracht dessen, dass Antitumor-Aktivität mit der intrazellulären Wirkstoffkonzentration nicht unmittelbar assoziiert war, lässt sich kein direkter Zusammenhang zwischen Lipophilie, zellulärer Akkumulation und zytotoxischer Wirkung begründen. Weiterführend wäre es interessant, einen möglichen unmittelbaren Einfluss der Lipophilie auf die „Drug-Target“-Wechselwirkung zu untersuchen.

Da die DNA als ein Ziel für Platin-basierte Anti-Krebs-Wirkstoffe galt, wurden die [Salophen]platin(II)-Verbindungen auf ihre Wechselwirkungen mit isolierten DNA analysiert. Überraschenderweise erwiesen sich weder Interkalation noch DNA-Bindung als wesentliche Mechanismen für die zytotoxische Aktivität der untersuchten Platin-Komplexe. Dies bedeutet, dass die DNA als Hauptziel der [Salophen]platin(II)-Komplexe ausgeschlossen werden kann. Stattdessen werden nicht-genomische Strukturen, wie in apoptotischen Prozessen beteiligte Proteine oder Proteine im Zusammenhang mit der Homöostase der extrazellulären Matrix vorgeschlagen.

Insgesamt wurde in dieser Arbeit eine große Anzahl von neuen Platin-Komplexen, als potentielle Antikrebs-Wirkstoffe identifiziert. Substituenten am Liganden-Gerüst können die biologischen Eigenschaften der synthetischen Platin(II)-Komplexe modulieren. Es bleibt als große Herausforderung, ihren Antitumor-Wirkungsmechanismus und ihre Target zu verstehen, um funktionalisierte Komplexe mit optimierten physikochemischen und biologischen Eigenschaften zu generieren.

F. Curriculum Vitae

For reasons of data protection,
the curriculum vitae is not included in the online version

References

- ¹ <http://www.who.int/cancer/en/> **2001**.
- ² Globocan 2008, Cancer fact sheet, *IARC*, **2010**.
- ³ World Cancer Report 2008, *IARC*, **2008**.
- ⁴ Airley, R. Cancer chemotherapy: basic science to the clinic. *Wiley-Blackwell*, **2009**, p. 67-111.
- ⁵ Jones, C.J.; Thornback, J. Medical applications of coordination chemistry. *Royal Society of Chemistry*, **2005**.
- ⁶ Orvig, C.; Abrams, M.J. Medicinal inorganic chemistry: introduction. *Chem. Rev.* **1999**, *99*, 2201-2203.
- ⁷ Lloyd, N.C.; Morgan, H.W.; Nicholson, B.K.; Ronimus, R.S. The composition of Ehrlich's salvarsan: resolution of a century-old debate. *Angew. Chem. Int. Ed. Engl.* **2005**, *44*, 941-944.
- ⁸ Shaw III, C.F. Gold-based therapeutic agents. *Chem. Rev.* **1999**, *99*, 2589-2600.
- ⁹ Birch, N.J. Inorganic pharmacology of lithium. *Chem. Rev.* **1999**, *99*, 2659-2682.
- ¹⁰ Butler, A.R.; Megson, I.L. Non-heme iron nitrosyls in biology. *Chem. Rev.* **2002**, *102*, 1155-1165.
- ¹¹ Leyland-Jones, B. Treating cancer-related hypercalcemia with gallium nitrate. *J. Support. Oncol.* **2004**, *2*, 509-516.
- ¹² Carr, H.S.; Wlodkowski, T.J.; Rosenkranz, H.S. Silver sulfadiazine: in vitro antibacterial activity. *Antimicrob. Agents Chemother.* **1973**, *4*, 585-587.
- ¹³ Yang, N.; Sun, H. Biocoordination chemistry of bismuth: recent advances. *Coord. Chem. Rev.* **2007**, *251*, 2354-2366.
- ¹⁴ Waldo, J.H.; Shonle, H.A.; Powell, H.M. The bacteriological evaluation of some new water soluble organo-mercury compounds. *J. Bacteriol.* **1931**, *21*, 323-329.
- ¹⁵ Marshall, M.S. The merthiolate - a new antiseptic. *Cal. West. Med.* **1931**, *35*, 43-44.
- ¹⁶ Yu, S-B.; Watson, A.D. Metal-based X-ray contrast media. *Chem. Rev.* **1999**, *99*, 2353-2377.

- ¹⁷ Rosenberg, B.; Van Camp, L.; Krigas, T. Inhibition of cell division in *Escherichia coli* by electrolysis products from a platinum electrode. *Nature*, **1965**, *205*, 698-699.
- ¹⁸ Wheate, N.J.; Walker, S.; Craig, G.E.; Oun, R. The status of platinum anticancer drugs in the clinic and in clinical trials. *Dalton Trans.* **2010**, *39*, 8113-8127.
- ¹⁹ Kelland, L. The resurgence of platinum-based cancer chemotherapy. *Nat. Rev. Cancer* **2007**, *7*, 573-584.
- ²⁰ Reedijk, J. Metal-ligand exchange kinetics in platinum and ruthenium complexes *Platinum Met. Rev.* **2008**, *52*, 2-11.
- ²¹ Ott, I.; Gust R. Medizinische Chemie der Platinkomplexe. *Pharm. Unserer Zeit* **2006**, *35*, 124-133.
- ²² Jung, Y.; Lippard, S.J. Direct cellular responses to platinum-induced DNA damage. *Chem. Rev.* **2007**, *107*, 1387-1407.
- ²³ Wang, D.; Lippard, S.J. Cellular processing of platinum anticancer drugs. *Nature Rev. Drug Discov.* **2005**, *4*, 307-320.
- ²⁴ Kostova, I. Platinum complexes as anticancer agents. *Rec. Pat. Anti-Cancer Drug Discov.* **2006**, *1*, 1-22.
- ²⁵ Siddik, Z.H. Cisplatin: mode of cytotoxic action and molecular basis of resistance. *Oncogene* **2003**, *22*, 7265-7279.
- ²⁶ Puckett, A.; Ernst, R.J.; Barton, J.K. Exploring the cellular accumulation of metal complexes. *Dalton Trans.* **2010**, *39*, 1159-1170.
- ²⁷ Hall, M.D.; Okabe, M.; Shen, D-W.; Liang, X-J.; Gottesman, M.M. The role of cellular accumulation in determining sensitivity to platinum-based chemotherapy. *Annu. Rev. Pharmacol. Toxicol.* **2008**, *48*, 495-535.
- ²⁸ Jamieson, E.R.; Lippard, S.J. Structure, recognition, and processing of cisplatin-DNA adducts. *Chem. Rev.* **1999**, *99*, 2467-2498.
- ²⁹ Baik, M-H.; Friesner, R.A.; Lippard, S.J. Theoretical study of cisplatin binding to purine bases: why does cisplatin prefer guanine over adenine?. *J. Am. Chem. Soc.* **2003**, *125*, 14082-14092.
- ³⁰ Kartalou, M.; Essigmann, J.M. Recognition of cisplatin adducts by cellular proteins. *Mutat. Res.* **2001**, *478*, 1-21.

- ³¹ Kasparikova, J.; Vojtiskova, M.; Natile, G.; Brabec, V. Unique properties of DNA interstrand cross-links of antitumour oxaliplatin and the effect of chirality of the carrier ligand. **2008**, *14*, 1330-1341.
- ³² Choy, H.; Park, C.; Yao, M. Current status and future prospects for satraplatin, an oral platinum analogue. *Clin. Cancer Res.* **2008**, *14*, 1633-1638.
- ³³ Holford, J.; Sharp, S.Y.; Murrer, B.A.; Abrams, M.; Kelland, L.R. In vitro circumvention of cisplatin resistance by the novel sterically hindered platinum complex AMD473. *Br. J. Cancer* **1998**, *77*, 366-373.
- ³⁴ Sharp, S.Y.; O'Neill, C.F.; Rogers, P.; Boxall, F.E.; Kelland, L.R. Retention of activity by the new generation platinum agent AMD0473 in four human tumour cell lines possessing acquired resistance to oxaliplatin. *Eur. J. Cancer* **2002**, *38*, 2309-2315.
- ³⁵ Ott, I.; Gust, R. Non platinum metal complexes as anti-cancer drugs. *Arch. Pharm. (Weinheim)* **2007**, *340*, 117-126.
- ³⁶ Clarke, M.J. Ruthenium Metallopharmaceuticals. *Coord. Chem. Rev.* **2002**, *232*, 69-93.
- ³⁷ Antonarakis, E.; Emadi, A. Ruthenium-based chemotherapeutics: are they ready for prime time? *Cancer Chemother. Pharmacol.* **2010**, *66*, 1-9.
- ³⁸ Schluga, P.; Hartinger, C.G.; Egger, A.; Reisner, E.; Galanski, M.; Jakupec, M.A.; Keppler, B.K. Redox behavior of tumor-inhibiting ruthenium(III) complexes and effects of physiological reductants on their binding to GMP. *Dalton Trans.* **2006**, *14*, 1796-1802.
- ³⁹ Sava, G.; Capozzi, I.; Clerici, K.; Gagliardi, G.; Alessio, E.; Mestroni, G. Pharmacological control of lung metastases of solid tumours by a novel ruthenium complex. *Clin. Exp. Metastasis* **1998**, *16*, 371-379.
- ⁴⁰ Sava, G.; Zorzet, S.; Turrin, C.; Vita, F.; Soranzo, M.; Zabucchi, G.; Cocchietto, M.; Bergamo, A.; DiGiovine, S.; Pezzoni, G.; Sartor, L.; Garbisa, S. Dual Action of NAMI-A in inhibition of solid tumor metastasis: selective targeting of metastatic cells and binding to collagen. *Clin. Cancer Res.* **2003**, *9*, 1898-1905.
- ⁴¹ Vacca, A.; Bruno, M.; Boccarelli, A.; Coluccia, M.; Ribatti, D.; Bergamo, A.; Garbisa, S.; Sartor, L.; Sava, G. Inhibition of endothelial cell functions and of angiogenesis by the metastasis inhibitor NAMI-A. *Br. J. Cancer* **2002**, *86*, 993-998.

- ⁴² Kapitza, S.; Pongratz, M.; Jakupec, M.A.; Heffeter, P.; Berger, W.; Lackinger, L.; Keppler, B.K.; Marian, B. Heterocyclic complexes of ruthenium(III) induce apoptosis in colorectal carcinoma cells. *J. Cancer. Res. Clin. Oncol.* **2005**, *131*, 101–110.
- ⁴³ Scolaro, C.; Bergamo, A.; Brescacin, L.; Delfino, R.; Cocchietto, M.; Laurency, G.; Geldbach, T.J.; Sava, G.; Dyson, P.J. In vitro and in vivo evaluation of ruthenium(II)-arene PTA complexes. *J. Med. Chem.* **2005**, *48*, 4161–4171.
- ⁴⁴ Bergamo, A.; Masi, A.; Dyson, P.J.; Sava, G. Modulation of the metastatic progression of breast cancer with an organometallic ruthenium compound. *Int. J. Oncol.* **2008**, *33*, 1281–1289.
- ⁴⁵ Schilling, T.; Keppler, K.B.; Heim, M.E.; Niebch, G.; Dietzfelbinger, H.; Rastetter, J.; Hanauske, A.R. Clinical phase I and pharmacokinetic trial of the new titanium complex budotitane. *Invest. New Drugs* **1996**, *13*, 327–332.
- ⁴⁶ Lümnen, G.; Sperling, H.; Luboldt, H.; Otto, T.; Rübber, H. Phase II trial of titanocene dichloride in advanced renal-cell carcinoma. *Cancer Chemother. Pharmacol.* **1998**, *42*, 415–417.
- ⁴⁷ Kröger, N.; Kleeberg, U.R.; Mross, K.; Edler, L.; Saß, G.; Hossfeld, D.K. Phase II clinical trial of titanocene dichloride in patients with metastatic breast cancer. *Onkologie* **2000**, *23*, 60–62.
- ⁴⁸ Toney, J.H.; Marks, T.J. Hydrolysis chemistry of the metallocene dichlorides $M(\eta^5\text{-C}_5\text{H}_5)_2\text{Cl}_2$ $M = \text{Ti, V, Zr}$. Aqueous kinetics, equilibria, and mechanistic implications for a new class of antitumor agents. *J. Am. Chem. Soc.* **1985**, *107*, 947–953.
- ⁴⁹ Sweeney, N.J.; Mendoza, O.; Müller-Bunz, H.; Pampillón, C.; Rehmann, F.-J.K.; Strohsfeldt, K.; Tacke, M. Novel benzyl substituted titanocene anti-cancer drugs. *J. Organomet. Chem.* **2005**, *690*, 4537–4544.
- ⁵⁰ Hart, M.M.; Adamson, R.H. Antitumor activity and toxicity of salts of inorganic group IIIa metals: aluminum, gallium, indium, and thallium. *Proc. Natl. Acad. Sci. USA* **1971**, *68*, 1623–1626.
- ⁵¹ Collery, P.; Keppler, B.; Madoulet, C.; Desoize, B. Gallium in cancer treatment. *Crit. Rev. Oncol. Hematol.* **2002**, *42*, 283–296.
- ⁵² Timerbaev, A.R. Advances in developing tris(8-quinolinolato)gallium(III) as an anticancer drug: critical appraisal and prospects. *Metallomics* **2009**, *1*, 193–198.

- ⁵³ Hillard, E.; Vessières, A.; Thouin, L.; Jaouen, G.; Amatore, C. Ferrocene-mediated proton-coupled electron transfer in a series of ferrocifen-type breast-cancer drug candidates. *Angew. Chem. Int. Ed. Engl.* **2006**, *118*, 291-296.
- ⁵⁴ Hillard, E.; Vessières, A.; Le Bideau, F.; Plazuk, D.; Spera, D.; Huché, M.; Jaouen, G. A series of unconjugated ferrocenyl phenols: prospects as anticancer agents. *ChemMedChem.* **2006**, *1*, 551-559.
- ⁵⁵ Hill, K.E.; McCollum, G.W.; Boeglin, M.E.; Burk, R.F. Thioredoxin reductase activity is decreased by selenium deficiency. *Biochem. Biophys. Res. Commun.* **1997**, *234*, 293-295.
- ⁵⁶ Gromer, S.; Arscott, L.D.; Williams, C.H.; Schirmer, R.H.; Becker, K. Human placenta thioredoxin reductase. Isolation of the selenoenzyme, steady state kinetics, and inhibition by therapeutic gold compounds. *J. Biol. Chem.* **1998**, *273*, 20096-20101.
- ⁵⁷ Gust, R.; Schönenberger, H. Third generation antitumor platinum(II) complexes of the [1-(fluoro/difluorophenyl)-2-phenylethylenediamine]platinum(II) type. *Arch. Pharm. (Weinheim)* **1995**, *328*, 595-603.
- ⁵⁸ Gust, R.; Ott, I.; Posselt, D.; Sommer, K. Development of cobalt(3,4-diarylsalen) complexes as tumor therapeutics. *J. Med. Chem.* **2004**, *47*, 5837-5846.
- ⁵⁹ Ott, I.; Gust, R. Preclinical and clinical studies on the use of platinum complexes for breast cancer treatment. *Anti-cancer Agents Med. Chem.* **2007**, *7*, 95-110.
- ⁶⁰ Köckerbauer, R.; Bednarski, P.J. Unusual reactivity of cisplatin analogs that bear o-phenylenediamine ligands: insights for the design of more effective cytotoxic agents. *J. Inorg. Biochem.* **1996**, *62*, 281-298.
- ⁶¹ Hansch, C.; Venger, B.H.; Panthanickal, A. Mutagenicity of substituted (o-phenylenediamine)platinum dichloride in the Ames test. A quantitative structure-activity analysis. *J. Med. Chem.* **1980**, *23*, 459-461.
- ⁶² Hille, A.; Ott, I.; Kitanovic, A.; Kitanovic, I.; Alborzina, H.; Lederer, E.; Wölfl, S.; Metzler-Nolte, N.; Schäfer, S.; Sheldrick, W.S.; Bischof, C.; Schatzschneider, U.; Gust, R. [N,N'-Bis(salicylidene)-1,2-phenylenediamine]metal complexes with cell death promoting properties. *J. Biol. Inorg. Chem.* **2009**, *14*, 711-725.

- ⁶³ Lee, S-Y.; Hille, A.; Kitanovic, I.; Jesse, P.; Henze, G.; Wöfl, S.; Gust, R.; Prokop, A. [Fe(III)(salophene)Cl], a potent iron salophene complex overcomes multiple drug resistance in lymphoma and leukemia cells. *Leuk. Res.* **2011**, *35*, 387-393.
- ⁶⁴ Hille, A.; Gust, R. Influence of methoxy groups on the antiproliferative effects of [Fe^{III}(salophene-OMe)Cl] complexes. *Eur. J. Med. Chem.* **2010**, *45*, 5486-5492.
- ⁶⁵ Lee, S-Y.; Hille, A.; Frias, C.; Kater, B.; Bonitzki, B.; Wöfl, S.; Scheffler, H.; Prokop, A.; Gust, R. [Ni^{II}(3-OMe-salophene)]: a potent agent with antitumor activity. *J. Med. Chem.* **2010**, *53*, 6064-6070.
- ⁶⁶ Wu, P.; Ma, D-L.; Leung, C-H.; Yan, S-C.; Zhu, N.; Abagyan, R.; Che, C-M. Stabilization of G-quadruplex DNA with platinum(II) Schiff base complexes: luminescent probe and down-regulation of c-myc oncogene expression. *Chemistry* **2009**, *15*, 13008-13021.
- ⁶⁷ Patel, D.J.; Phan, A.T.; Kuryavyi, V. Human telomere, oncogenic promoter and 5'-UTR G-quadruplexes: diverse higher order DNA and RNA targets for cancer therapeutics. *Nucleic Acids Res.* **2007**, *35*, 7429-7455.
- ⁶⁸ Vögtle, F.; Goldschmitt, E. Die Diaza-Cope-Umlagerung. *Chem. Ber.* **1976**, *109*, 1-40.
- ⁶⁹ Vögtle, F.; Goldschmitt, E. [3,3]-Sigmatropic reactions in the N,N'-dimethyleneethylenediamine system. *Angew. Chem., Int. Ed. Engl.* **1973**, *12*, 767-768.
- ⁷⁰ Chin, J.; Mancin, F.; Thavarajah, N.; Lee, D.; Lough, A.; Chung, D.S. Controlling diaza-Cope rearrangement reactions with Resonance-Assisted Hydrogen Bonds. *J. Am. Chem. Soc.* **2003**, *125*, 15276-15277.
- ⁷¹ Kim, H.; Nguyen, Y.; Yen, C.P.; Chagal, L.; Lough, A.J.; Kim, B.M.; Chin, J. Stereospecific synthesis of C₂ symmetric diamines from the mother diamine by Resonance-Assisted Hydrogen-Bond directed diaza-Cope rearrangement. *J. Am. Chem. Soc.* **2008**, *130*, 12184-12191.
- ⁷² Gilli, P.; Bertolasi, V.; Ferretti, V.; Gilli, G. Evidence for intramolecular N-H...O Resonance-Assisted Hydrogen Bonding in β -Enaminones and related heterodienes. A combined Crystal-Structural, IR and NMR Spectroscopic, and Quantum-Mechanical investigation. *J. Am. Chem. Soc.* **2000**, *122*, 10405-10417.
- ⁷³ Filarowski, A.; Koll, A.; Glowiak, T. Low barrier hydrogen bonds in sterically modified Schiff bases. *J. Chem. Soc., Perkin Trans. 2* **2002**, 835-842.

- ⁷⁴ Vögtle, F.; Goldschmitt, E. Dynamic stereochemistry of the degenerate diaza-Cope Rearrangement. *Angew. Chem., Int. Ed. Engl.* **1974**, *13*, 480-482.
- ⁷⁵ Charushin, V.N.; Chupakhin, O.N. Nucleophilic aromatic substitution of hydrogen and related reactions. *Mendeleev Commun.* **2007**, *17*, 249-254.
- ⁷⁶ Makosza, M.; Wojciechowski, K. Nucleophilic substitution of hydrogen in heterocyclic chemistry. *Chem. Rev.* **2004**, *104*, 2631-2666.
- ⁷⁷ Pagoria, P.; Mitchell, A.; Schmidt, R. 1,1,1-Trimethylhydrazinium Iodide: a novel, highly reactive reagent for aromatic amination via Vicarious Nucleophilic Substitution of Hydrogen. *J. Org. Chem.* **1996**, *61*, 2934-2935.
- ⁷⁸ Omietanski, G.M.; Sisler, H.H. The reaction of chloramine with tertiary amines. 1,1,1-Trisubstituted Hydrazinium salts. *J. Am. Chem. Soc.* **1956**, *78*, 1211-1213.
- ⁷⁹ Harries, C.; Haga, T. Über die Methylierung des Hydrazinhydrats. *Ber. Dtsch. Chem. Ges.* **1898**, *31*, 56-64.
- ⁸⁰ Sisler, H.H.; Omietanski, G.M.; Rudner, B. The chemistry of quaternized hydrazine compounds. *Chem. Rev.* **1957**, *57*, 1021-1047.
- ⁸¹ Bellamy, F.D.; Ou, K. Selective reduction of aromatic nitro compounds with stannous chloride in non acidic and non aqueous medium. *Tetrahedron Lett.* **1984**, *25*, 839-842.
- ⁸² IUPAC. *Compendium of Chemical Terminology.* **1995**, *67*, 1364.
- ⁸³ Dominiak, P.M.; Grech, E.; Barr, G.; Teat, S.; Mallinson, P.; Wozniak, K. Neutral and ionic hydrogen bonding in Schiff Bases. *Chem. Eur. J.* **2003**, *9*, 963-970.
- ⁸⁴ Tong, W.L.; Lai, L.M.; Chan, M.C.W. Platinum(II) Schiff Base as versatile phosphorescent core component in conjugated oligo(phenylene-ethynylene)s. *Dalton Trans.* **2008**, 1412-1414.
- ⁸⁵ Jacobsen, N.E. NMR spectroscopy explained: simplified theory, applications and examples for organic chemistry and structural biology. **2007**, p. 61.
- ⁸⁶ Afonin, A.V. Through space spin-spin coupling ^{19}F - ^1H as the base for comparative analysis of conformational equilibrium in fluorine-substituted aryl vinyl selenides and sulfides. *Russ. J. Org. Chem.* **2010**, *46*, 1313-1316.

- ⁸⁷ Scuseria, G.E.; Contreras, R.H. Ab initio calculations of through-space nuclear spin-spin coupling constants with the IPPP method. *Intern. J. Quant. Chem.* **1986**, *30*, 603–612.
- ⁸⁸ Rae, I.D.; Weigold, J.A.; Contreras, R.H.; Yamamoto, G. Signs of ^{19}F - ^1H and ^{19}F - ^{13}C spin-spin coupling constants mainly transmitted through space. *Magn. Reson. Chem.* **1992**, *30*, 1047-1050.
- ⁸⁹ IUPAC. *Compendium of Chemical Terminology*. **1994**, *66*, 1077.
- ⁹⁰ Bovey, F.A. Nuclear magnetic resonance spectroscopy. *Academic Press*, **1969**, p. 64.
- ⁹¹ The alpha (α) position refers to the first substituting group of atoms that attaches to a functional group in the molecule. By extension, the second position is the beta (β) position, and so on.
- ⁹² Haswell, S.J. Atomic absorption spectrometry: theory, design and applications. *Elsevier*, **1991**, p. 1-77.
- ⁹³ Che, C.-M.; Kwok, C.-C.; Lai, S.-W.; Rausch, A.F.; Finkenzeller, W.J.; Zhu, N.; Hartmut, Y. Photophysical properties and OLED applications of phosphorescent platinum(II) Schiff base complexes. *Chem. Eur. J.* **2010**, *16*, 233-247.
- ⁹⁴ Sawodny, W.; Thewalt, U.; Potthoff E.; Ohl, R. [N,N' -Bis(salicylidene) ethylenediaminato- N,N',O,O']platinum(II). *Acta Cryst.* **1999**, *C55*, 2060-2061.
- ⁹⁵ Che, C.-M.; Chan, S.-C.; Xiang, H.-F.; Chan, M.C.W.; Liu, Y.; Wang, Y. Tetradentate Schiff base platinum(II) complexes as a new class of phosphorescent materials for high-efficiency and white-light electroluminescent devices. *Chem. Comm.* **2004**, 1484-1485.
- ⁹⁶ Brooks, S.; Locke, E.; Soule, H. Estrogen receptor in a human cell line (MCF-7) from breast carcinoma. *J. Biol. Chem.* **1973**, *248*, 6251-6253.
- ⁹⁷ Bernhardt, G.; Reile, H.; Birnböck, H.; Spruss, T.; Schönenberger, H. Standardized kinetic microassay to quantify differential chemosensitivity on the basis of proliferative activity. *J. Cancer Res. Clin. Oncol.* **1992**, *118*, 35-43.
- ⁹⁸ Reile, H.; Birnböck, H.; Bernhardt, G.; Spruss, T.; Schönenberger, H. Computerized determination of growth kinetic curves and doubling times from cells in microculture. *Anal. Biochem.* **1990**, *187*, 262-267.

⁹⁹ Please note that the error bars as shown only display *half* of the total error, with the lower half hidden behind the symbols.

¹⁰⁰ Gust, R.; Schnurr, B.; Krauser, R.; Bernhardt, G.; Koch, M.; Schmid, B.; Hummel, E.; Schönenberger, H. Stability and cellular studies of [*rac*-1,2-bis(4-fluorophenyl)-ethylenediamine][cyclobutane-1,1-dicarboxylato]platinum(II), a novel, highly active carboplatin derivative. *J. Cancer Res. Clin. Oncol.* **1998**, *124*, 585–597.

¹⁰¹ Gately, D.P.; Howell, S.B. Cellular accumulation of the anticancer agent cisplatin: a review. *Br. J. Cancer.* **1993**, *67*, 1171–1176.

¹⁰² Mistry, P.; Kelland, L.R.; Loh, S.Y.; Abel, G.; Murrer, B.A.; Harrap, K.R. Comparison of cellular accumulation and cytotoxicity of cisplatin with that of tetraplatin and amminedibutyratodichloro(cyclohexylamine)platinum(IV) (JM221) in human ovarian carcinoma cell lines. *Cancer Res.* **1992**, *52*, 6188-6193.

¹⁰³ Binks, S.P.; Dobrota, M. Kinetics and mechanism of uptake of platinum based pharmaceuticals by rat small intestine. *Biochem. Pharmacol.* **1990**, *40*, 1329-1336.

¹⁰⁴ Dornish, J.M.; Pettersen, E.O. Requirement of a reactive aldehyde moiety for aldehyde-mediated protection against *cis*-dichlorodiammineplatinum-induced cell inactivation. *Biochem. Pharmacol.* **1990**, *39*, 309-318.

¹⁰⁵ Dornish, J.M.; Pettersen, E.O.; Oftebro, R. Modifying effect of cinnamaldehyde and cinnamaldehyde derivatives on cell inactivation and cellular uptake of *cis*-diamminedichloroplatinum(II) in human NHIK 3025 cells. *Cancer Res.* **1989**, *49*, 3917-3921.

¹⁰⁶ Howell, S.B.; Safaei, R.; Larson, C.A.; Sailor, M. Copper transporters and the cellular pharmacology of the platinum-containing cancer drugs. *Mol. Pharmacol.* **2010**, *77*, 887-894.

¹⁰⁷ Burger, H.; Zoumaro-Djayoon, A.; Boersma, A.W.M.; Helleman, J.; Berns, E.M.J.J.; Mathijssen, R.H.J.; Loos, W.J.; Wiemer, E.A.C. Differential transport of platinum compounds by the human organic cation transporter hOCT2 (hSLC22A2). *B. J. Pharmacol.* **2010**, *159*, 898-908.

¹⁰⁸ Reile, H.; Bernhardt, G.; Koch, M.; Schönenberger, H.; Holstein, M.; Lux, F. Chemosensitivity of human MCF-7 breast cancer cells to diastereoisomeric diaqua(1,2-diphenylethylenedimaine)platinum(II) sulfates and specific platinum accumulation. *Cancer Chemo. Pharmacol.* **1992**, *30*, 113–122.

- ¹⁰⁹ Zou, J.; Yang, X.G.; Li, R.C.; Lu, J.F.; Wang, K. The chirality selectivity in the uptake of platinum (II) complexes with 1,2-cyclohexanediamine isomers as carrier ligands by human erythrocytes. *BioMetals* **1997**, *10*, 37-43.
- ¹¹⁰ Bradford, M.M. A rapid and sensitive method for the quantitation of microgram quantities of protein utilizing the principle of protein-dye binding. *Anal. Biochem.* **1976**, *72*, 248-254.
- ¹¹¹ Wang, K.; Lu, J.; Li, R. The events that occur when cisplatin encounters cells. *Coord. Chem. Rev.* **1996**, *151*, 53-88.
- ¹¹² Shirazi, F.H.; Molepo, J.M.; Stewart, D.J.; Ng, C.E.; Raaphorst, G.P.; Goel, R. Cytotoxicity, accumulation, and efflux of cisplatin and its metabolites in human ovarian carcinoma cells. *Tox. Appl. Pharmacol.* **1996**, *140*, 211-218.
- ¹¹³ McKeage, M.J.; Berners-Price, S.J.; Galettis, P.; Bowen, R.J.; Brouwer, W.; Ding, L.; Zhuang, L.; Baguley, B.C. Role of lipophilicity in determining cellular uptake and antitumour activity of gold phosphine complexes. *Cancer Chemother. Pharmacol.* **2000**, *46*, 343-350.
- ¹¹⁴ Lipinski, C.A.; Lombardo, F.; Dominy, B.W.; Feeney, P.J. Experimental and computational approaches to estimate solubility and permeability in drug discovery and development settings. *Adv. Drug Del. Rev.* **2001**, *46*, 3-26.
Note that the name of the rule is because the cutoffs for each of the four parameters were all close to 5 or a multiple of 5.
- ¹¹⁵ Lambert, W.J. Modeling oil-water partitioning and membrane permeation using reversed-phase chromatography. *J. Chromatogr. A.* **1993**, *656*, 469-484.
- ¹¹⁶ Fujita, T.; Iwasa, J.; Hansch, C. A new substituent constant, π , derived from partition coefficients. *J. Am. Chem. Soc.* **1964**, *86*, 5175-5180.
- ¹¹⁷ Platts, J.A.; Oldfield, S.P.; Reif, M.M.; Palmucci, A.; Gabano, E.; Osella, D. The RP-HPLC measurement and QSPR analysis of log $P_{o/w}$ values of several Pt(II) complexes. *J. Inorg. Biochem.* **2006**, *100*, 1199-1207.
- ¹¹⁸ Veith, G.D.; Austin, N.M.; Morris, R.T. A rapid method for estimating log P for organic chemicals. *Water Res.* **1979**, *13*, 43-47.
- ¹¹⁹ Kazakevich, Y.; LoBrutto, R. HPLC for pharmaceutical scientists. *John Wiley & Sons*, **2007**, p. 15-16.

- ¹²⁰ Sangster, J. Octanol-water partition coefficients of simple organic compounds. *J. Phys. Chem. Ref. Data* **1989**, *18*, 1111-1229.
- ¹²¹ Testa, B.; Carrupt, P.A.; Gaillard, P.; Billois, F.; Weber, P. Lipophilicity in molecular modelling. *Pharm. Res.* **1996**, *13*, 335-343.
- ¹²² Reithofer, M.R.; Bytzek, A.K.; Valiahdi, S.M.; Kowol, C.R.; Groessl, M.; Hartinger, C.G.; Jakupec, M.A.; Galanski, M.; Keppler, B.K. Tuning of lipophilicity and cytotoxic potency by structural variation of anticancer platinum(IV) complexes. *J. Inorg. Biochem.* **2010**, *105*, 46-51.
- ¹²³ Kerns, E.H.; Di, L. Physicochemical profiling: overview of the screens. *Drug Discovery Today: Technol.* **2004**, *1*, 343-348.
- ¹²⁴ Bevan, C.; Lloyd, R.S. A high-throughput screening method for the determination of aqueous drug solubility using laser nephelometry in microtiter plates. *Anal. Chem.* **2000**, *72*, 1781-1787.
- ¹²⁵ *g* refers to the acceleration of gravity, which is equal to 9.81 m/s².
- ¹²⁶ Hansch, C.; Quinlan, J.E.; Lawrence, G.L. Linear free-energy relationship between partition coefficients and the aqueous solubility of organic liquids. *J. Org. Chem.* **1968**, *33*, 347-350.
- ¹²⁷ Isnard, P.; Lambert, S. Aqueous solubility and n-octanol/water partition coefficients correlations. *Chemosphere*, **1989**, *18*, 1837-1853.
- ¹²⁸ Ran, Y.; Jain, N.; Yalkowski, S.H. Prediction of aqueous solubility of organic compounds by the General Solubility Equation (GSE). *J. Chem. Inf. Comput. Sci.* **2001**, *41*, 1208-1217.
- ¹²⁹ Fuertes, M.A.; Castilla, J.; Alonso, C.; Perez, J.M. Biochemical modulation of cisplatin mechanisms of action: enhancement of antitumor activity and circumvention of drug resistance. *Curr. Med. Chem.* **2003**, *103*, 646-662.
- ¹³⁰ Kartalou, M.; Essigmann, J.M. Mechanisms of resistance to cisplatin. *Mutat. Res.* **2001**, *478*, 23-43.
- ¹³¹ Cohen, G.L.; Bauer, W.R.; Barton, J.K.; Lippard, S.J. Binding of *cis*- and *trans*-dichlorodiammineplatinum(II) to DNA: Evidence for unwinding and shortening of the double helix. *Science* **1979**, *203*, 1014-1016.

- ¹³² Collins, J.G.; Wheate, N.J. Potential adenine and minor groove binding platinum complexes. *J. Inorg. Biochem.* **2004**, *98*, 1578-1584.
- ¹³³ Zeglis, B.M.; Pierre, V.C.; Barton, J.K. Metallointercalators and metalloinsertors. *Chem. Comm.* **2007**, *44*, 4565-4579.
- ¹³⁴ Howe-Grant, M.; Lippard, S.J. Binding of platinum(II) intercalation reagents to deoxyribonucleic acid. Dependence on base-pair composition, nature of the intercalator, and ionic strength. *Biochem.* **1979**, *18*, 5762-5769.
- ¹³⁵ Baruah, H.; Barry, C.G.; Bierbach, U. Platinum-intercalator conjugates: from DNA-targeted cisplatin derivatives to adenine binding complexes as potential modulators of gene regulation. *Curr. Top. Med. Chem.* **2004**, *4*, 1537-1549.
- ¹³⁶ Ernst, R.J.; Song, H.; Barton, J.K. DNA mismatch binding and antiproliferative activity of rhodium metalloinsertors. *J. Am. Chem. Soc.* **2009**, *131*, 2359-2366.
- ¹³⁷ Kypr, J.; Kejnovska, I.; Renciuik, D.; Vorlickova, M. Circular dichroism and conformational polymorphism of DNA. *Nuc. Ac. Res.* **2009**, *37*, 1713-1725.
- ¹³⁸ Garrett, H.G.; Grisham, C.H. Biochemistry. *Brooks/Cole, Cengage learning*, **2010**, p. 321-323.
- ¹³⁹ Norden, B.; Tjerneld, F. Structure of methylene blue-DNA complexes studied by linear and circular dichroism spectroscopy. *Biopolymers* **1982**, *21*, 1713-1734.
- ¹⁴⁰ Metzler, R.; Ambjörnsson, T.; Hanke, A.; Fogedby, H.C. Single DNA denaturation and bubble dynamics. *J. Phys.: Condens. Matter*, **2009**, *21*, 034111.
- ¹⁴¹ SantaLucia, J.Jr. A unified view of polymer, dumbbell, and oligonucleotide DNA nearest-neighbor thermodynamics. *Proc. Natl. Acad. Sci. USA* **1998**, *95*, 1460-1465.
- ¹⁴² LePecq, J.B.; Paoletti, C. A fluorescent complex between ethidium bromide and nucleic acids. Physical-chemical characterization. *J. Mol. Biol.* **1967**, *27*, 87-106.
- ¹⁴³ Kelly, J.M.; Tossi, A.B.; Mc Connel, D.J.; OhUigin, C. A study of the interactions of some polypyridylruthenium(II) complexes with DNA using fluorescence spectroscopy, topoisomerisation and thermal denaturation. *Nucl. Ac. Res.* **1985**, *13*, 6017-6034.
- ¹⁴⁴ Neyhart, G.A.; Grover, N.; Smith, S.R.; Kalsbeck, W.A.; Fairley, T.A.; Cory, M.; Thorp, H.H. Binding and kinetics studies of oxidation of DNA by oxoruthenium(IV). *J. Am. Chem. Soc.* **1993**, *115*, 4423-4428.

- ¹⁴⁵ Lerman, L.S. Structural considerations in the interaction of DNA and acridines. *J. Mol. Biol.* **1961**, *3*, 18-30.
- ¹⁴⁶ Yang, G.; Wu, J.Z.; Wang, L.; Ji, L.N.; Tian, X. Study of the interaction between novel ruthenium(II)-polypyridyl complexes and calf thymus DNA. *J. Inorg. Biochem.* **1997**, *66*, 141-144.
- ¹⁴⁷ Cohen, G.; Eisenberg, H. Viscosity and sedimentation study of sonicated DNA-proflavine complexes. *Biopolymers* **1969**, *8*, 45-55.
- ¹⁴⁸ Bieda, R.; Ott, I.; Gust, R.; Sheldrick, W.S. Cytotoxic rhodium(III) polypyridyl complexes containing the tris(pyrazolyl)methane coligand: Synthesis, DNA binding properties and structure-activity relationships. *Eur. J. Inorg. Chem.* **2009**, 3821-3831.
- ¹⁴⁹ Natarajan, G.; Malathi, R.; Holler, E. Increased DNA-binding activity of cis-1,1-cyclobutanedicarboxylatodiammineplatinum(II) (carboplatin) in the presence of nucleophiles and human breast cancer MCF-7 cell cytoplasmic extracts: activation theory revisited. *Biochem. Pharmacol.* **1999**, *58*, 1625-1629.
- ¹⁵⁰ Dyson, P.J.; Sava, G. Metal-based antitumour drugs in the post genomic era. *Dalton Trans.* **2006**, 1929-1933.
- ¹⁵¹ De Pascali, S.A.; Lugoli, F.; De Donno, A.; Fanizzi, F.P. Mutagenic tests confirm that new acetylacetonate Pt(II) complexes induce apoptosis in cancer cells interacting with nongenomic biological targets. *Metal-Based Drugs*, **2011**, *2011*, 1-10.
- ¹⁵² Sasanelli, R.; Boccarelli, A.; Giordano, D.; Laforgia, M.; Arnesano, F.; Natile, G.; Cardelicchio, C.; Capozzi, M.A.M.; Coluccia, M. Platinum complexes can inhibit matrix metalloproteinase activity: platinum-diethyl[(methylsulfinyl)methyl]phosphonate complexes as inhibitors of matrix metalloproteinases 2, 3, 9 and 12. *J. Med. Chem.* **2007**, *50*, 3434-3441.
- ¹⁵³ Contreras, R.H.; Gotelli, G.; Ducati, L.C.; Barbosa, M.; Tormena, C.F. Analysis of canonical molecular orbitals to identify Fermi contact coupling pathways. 1. Through-space transmission by overlap of ³¹P lone pairs. *J. Phys. Chem. A* **2010**, *114*, 1044-1051.
- ¹⁵⁴ Karl, J.; Gust, R.; Spruss, T.; Schneider, M.R.; Schönenberger, H.; Engel, J.; Wrobel, K.H.; Lux, F.; Haeblerlin, S.T. Ring-substituted [1,2-bis(4-hydroxyphenyl)ethylenediamine]dichloroplatinum(II) complexes: compounds with a selective effect on the hormone-dependent mammary carcinoma. *J. Med. Chem.* **1988**, *31*, 72-83.

- ¹⁵⁵ Buss, I.; Garmann, D.; Galanski, M.; Weber, G.; Kalayda, G.V.; Keppler, B.K.; Jaehde, U. Enhancing lipophilicity as a strategy to overcome resistance against platinum complexes? *J. Inorg. Biochem.* **2011**, *105*, 709-717.
- ¹⁵⁶ Armarego, W.L.S.; Chai, C.L.L. Purification of laboratory chemicals, *6th edition*, Elsevier Inc., Oxford, **2009**.
- ¹⁵⁷ Chial, H.J.; Thompson, H.B.; Splittgerber, A.G. A spectral study of the charge forms of Coomassie blue G. *Anal. Biochem.* **1993**, *209*, 258-266.
- ¹⁵⁸ Compton, S.J.; Jones, C.G. Mechanism of dye response and interference in the Bradford protein assay. *Anal. Biochem.* **1985**, *151*, 369-374.
- ¹⁵⁹ Zor, T.; Selinger, Z. Linearization of the Bradford protein assay increases its sensitivity: theoretical and experimental studies. *Anal. Biochem.* **1996**, *236*, 302-308.
- ¹⁶⁰ Liu, H-Q.; Peng, S-M.; Che, C.M. Interaction of a luminescent platinum(II) complex of substituted 2,2'-bipyridine with DNA. Spectroscopic and photophysical studies. *J. Chem. Soc., Chem. Commun.* **1995**, 509-510.
- ¹⁶¹ Ott, I.; Schmidt, K.; Kircher, B.; Schumacher, P.; Wiglenda, T.; Gust, R. Antitumor-active cobalt-alkyne complexes derived from acetylsalicylic acid: studies on the mode of drug action. *J. Med. Chem.* **2005**, *48*, 622-629.